

https://dspace.org/

An evaluation of the effects of metal complexes on cell death signalling networks in breast cancer cell lines

Myeza, Nonzuzo

2025
University of the Witwatersrand, Johannesburg
https://hdl.handle.net/10539/50016

Myeza, Nonzuzo. (2025). An evaluation of the effects of metal complexes on cell death signalling networks in breast cancer cell lines [PhD thesis, University of the Witwatersrand, Johannesburg]. WIReDSpace. https://hdl.handle.net/10539/50016

Downloaded from a DSpace repository. https://dspace.org/

An evaluation of the effects of metal complexes on cell death signalling networks in breast cancer cell lines.



WITS
UNIVERSITY

Nonzuzo Myeza

(1038710)

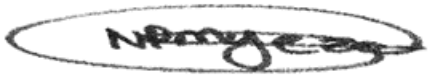
Supervised by **Dr. Leonie Harmse**

A dissertation submitted to the Faculty of Health Sciences, University of the Witwatersrand, Johannesburg, in fulfilment of the requirements for the degree of Doctor of Philosophy (Pharmacology)

September 2025

DECLARATION

I declare that this thesis is my own, unaided work. It is being submitted for the Degree of Doctor of Philosophy at the University of the Witwatersrand, Johannesburg. It has not been submitted before for any degree or examination at any other University.



_____

(Nonzuzo Praiseworth Myeza)

On this day_____10/09/2025_____

Dedication

This thesis is dedicated to my son, Lulama, and my daughter, Thingolwenkosazana.

“So, we DO NOT LOSE HEART.

Though our outer self is wasting away,

our inner self is being renewed day by day”.

2 Corinthians 4:16

Abstract

Despite the successful treatment of breast cancer, the prognosis for patients with triple-negative breast cancer (TNBC) remains poor. This type of breast cancer is characterised by the absence of receptors for oestrogen, progesterone, and the human epidermal growth factor receptor-2, rendering targeted therapies ineffective and highlighting the need for alternative treatment options. Alternative metal-based complexes, including copper and gold complexes, have been investigated for their potential anticancer properties. This study explored the efficacy of a small library of phenanthroline- and theophylline-based copper complexes, an 8-aminoquinoline-naphthyl copper complex, and gold(I) ferrocenyl-substituted 1,2,3-triazol-5-ylidene complexes, against a triple-negative breast cancer cell line compared to a mammary epithelial cell line. Doxorubicin and staurosporine were used as positive controls throughout the study.

MDA-MB-231 breast cancer cells and MCF-10A mammary cells were grown in culture, and the cytotoxicity of the metal complexes with and without haemoxygenas-1 inhibitor, OB24,(1-[[2-[2-(4-Bromophenyl)ethyl]-1,3-dioxolan-2-yl]methyl]-1H-imidazolehydrochloride) was evaluated using a spectrophotometric method based on the reduction of a tetrazolium salt to a formazan product by viable cells. Morphological changes were assessed with fluorescent microscopy to rule out necrosis. Mitochondrial function was determined by measuring the level of the reactive oxygen species and mitochondrial membrane potential. Apoptosis-related assays such as annexin V binding, caspase-3/7, caspase-8, and caspase-9 activity confirmed apoptotic cell death. Changes in the expression levels of apoptosis regulatory proteins were identified using an apoptotic proteome array profiler. Immunofluorescence detected the expression and localization of phosphorylated p53 serine 15 (phospho-p53(s15)), the cyclin-dependent kinase inhibitor p21, nuclear factor-kappa B-inducing kinase (NIK), and haemoxygenase-1 (HMOX-1). The Western blot assay validated HMOX-1 expression and its molecular weight.

$AuPPh_3$(trz-Fc-Dipp), $CuPhenTh_2$, and Cu8AqN complexes were most potent with IC_{50} values below 5 μM in MDA-MB-231 cells. $CuPhenTh_2$ and Cu8AqN showed selectivity toward MDA-MB-231 cells compared to the MCF-10A cells, as indicated by their lower IC_{50} values.

Doxorubicin was less potent in MDA-MB-231 cells, with an IC_{50} value of 8.75 ± 0.88 μM, and was cytotoxic to MCF-10A cells with an IC_{50} value of 2.99 ± 0.88 μM.

The copper and gold complexes caused nuclear condensation and fragmentation, consistent with apoptosis. Excessive generation of reactive oxygen species indicated oxidative stress. Increased annexin V binding to phosphatidylserine and activation of caspase-3/7 confirmed apoptotic cell death. The activation of caspase-9 and caspase-8 indicated the involvement of both the intrinsic and extrinsic apoptosis pathways, respectively. Mitochondrial membrane depolarisation suggested mitochondrial dysfunction and supported the intrinsic pathway of apoptosis.

$CuPhenTh_2$ and Cu8AqN, which were selective to cancer cells reduced the expression of inhibitor of apoptosis proteins like cIAP1, survivin, and XIAP. The expression level of Fas/CD95 was decreased indicative of inhibition of canonical nuclear factor kappa B (NF-κB) signalling and the increased expression of NIK suggested the activation of the non-canonical NF-κB pathway. Increased nuclear phospho-p53(s15) and p21 expression indicated oxidative stress. Highly expressed HMOX-1 provided additional evidence for oxidative stress. Varied expression of hypoxia inducing factor-1α levels suggested complex modulation of HMOX-1, and its involvement in treatment response. Western blots confirmed the high expression of full length HMOX-1 with a molecular weight of 32 kDa. Inhibition of HMOX-1 enzymatic activity using OB24 decreased the IC_{50} value of Cu8AqN and increased that of $CuPhenTh_2$, indicating that HMOX-1 plays an important role in treatment response in TNBC. Given the aggressive nature of TNBC and its resistance to standard therapies, these copper and gold complexes emerge as promising candidates with partial selectivity compared to conventional chemotherapeutic agents like doxorubicin and worthy of further preclinical evaluation. Future work assessing HMOX-1 expression by other transcriptional factors, like Nrf2, and HMOX-1 gene expression at the mRNA level would provide comprehensive evidence of HMOX-1 modulation to better understand its role in TNBC treatment and improve treatment outcomes.

Keywords: Breast cancer, copper and gold complexes, oxidative stress, apoptosis, haemoxygenase-1

Acknowledgements

To God Almighty, thank you for your grace and for the gift of life.

I would like to express my sincere gratitude to the following individuals who have played a significant role in my journey toward completing this thesis:

- **Dr. Leonie Harmse**, my supervisor: Thank you for welcoming me into your laboratory and for the opportunity to conduct research in cancer pharmacology. Your guidance, encouragement, and support have been invaluable. This thesis would not have been possible without your constructive criticism, insightful advice, and patience. I am deeply grateful for the opportunities you've provided, which have contributed to my growth as a scientist and emerging academic.
- **My family**, to my parents and siblings: thank you for your constant love, support, and prayers. *Mama*, your words of encouragement and faith carried me through. *Lungisile, sis wami*, thank you for opening your home to me, for your advice, motivation, and belief in my potential.
- **Rhulani Hlungwani**, Myen'wam': thank you for being my source of strength, sanity, and unwavering support. Your presence has meant the world to me.
- **Zandile and Tebogo**, my dearest friends: thank you for walking this journey with me, for listening, supporting, and sharing countless memories. In you, I have found sisters.
- **Fellow postgraduate students** in the Cancer Research Group: thank you for the good working environment and scientific discussions. I wish you success.
- **Funding:** This study would have not been possible without final support from the following entities. I would like to thank The McGill Bequest to the Wits Department of Pharmacology and The University of the Witwatersrand Faculty Research Committee for research funds. I would like to extend my gratitude to The University of the Witwatersrand Postgraduate Merit Award and The National Research Foundation and DAAD In-Country Innovation Scholarship for PhD studies.

Research output

Publications

- Myeza N, Slabber C, Munro OQ, Sookai S, Zacharias SC, Martins-Furness C, Harmse L. An 8-aminoquinoline-naphthyl copper complex causes apoptotic cell death by modulating the expression of apoptotic regulatory proteins in breast cancer cells. European Journal of Pharmacology (2024). https://doi: 10.1016/j.ejphar.2024.176764.
- Gordon A, Abosede O, Ntsimango S, Hosten E, Myeza N , van Eyk A., Harmse L., Ogunlaja, A. Synthesis and anticancer evaluation of copper (II)- and manganese (II)- theophylline mixed ligand complexes. Polyhedron (2022). https://doi.org/10.1016/j.poly.2022.115649.

Conferences contributions

International conferences

Nonzuzo Myeza, Cathy Slabber, Orde Munro, Adeniyi Olugunlaja and Leonie Harmse. Copper complexes induce apoptosis and suppress the expression of Inhibitor of Apoptosis proteins: Poster presentation at the European Association of Cancer Researchers. Seville, Spain. *19- 22 June 2022.*

Nonzuzo Myeza, An apoptotic effect of metal complexes in MDA-MB-231 triple negative breast cancer cells. Oral Presentation at Kenya Society for Basic and Applied Pharmacology: All African Congress for Pharmacology 2021. Nairobi, Kenya (Online). *15-17 September 2021.*

National conferences

Nonzuzo Myeza, Slabber C, Munro OQ, Martins-Furness C, Harmse L. An 8-aminoquinoline-naphthyl copper complex causes apoptotic cell death by modulating the expression of apoptotic regulatory proteins in breast cancer cells. Poster presentation at Wits Faculty of Health Sciences Wits Health Science Campus, Johannesburg, South Africa. *5 September 2024.*

Nonzuzo Myeza, Orde Munro, Adeniyi Olugunlaja and Leonie Harmse**.** Copper complexes induce apoptosis and increase haem-oxygenase-1 expression in triple negative breast cancer cells. Poster

presentation at Faculty of Heath Sciences Postgraduate Research expo held at Wits Education Campus, Johannesburg, South Africa. *5 September 2023.*

Nonzuzo Myeza, Orde Munro, Adeniyi Olugunlaja and Leonie Harmse. Metal complexes induce apoptosis in MDA-MB-231 triple negative breast cancer cells. Poster presentation at School of Therapeutic Sciences Biennial Research Day. Virtual: Whova Platform. 15 *September 2022.*

Nonzuzo Myeza, Cathy Slabber, Orde Munro, Adeniyi Olugunlaja and Leonie Harmse. Copper complexes induce apoptosis and suppress the expression of Inhibitor of Apoptosis proteins. Poster presentation at the South African Society for Basic and Clinical Pharmacology. Virtual: Whova platform. *12-13 October 2022.*

Nonzuzo Myeza, Orde Munro, Adeniyi Olugunlaja and Leonie Harmse. Metal complexes induce apoptosis in MDA-MB-231 triple negative breast cancer cells. Poster presentation at the School of Therapeutic Sciences Biennial Research Day. Virtual: Microsoft Teams *September 2021*.

Nonzuzo Myeza, Metal complexes cause apoptosis in MDA-MB-231 triple negative breast cancer cells. Poster presentation at Wits Faculty of Health Sciences Virtual Research Day and postgraduate expo. Whova platform. *15 October 2020*.

Table of contents

Abstract ..... **iii**
Research output ..... **vi**
Table of contents ..... **viii**
Abbreviations ..... **xiv**
Latin letters ..... **xvii**
Unit of measurements ..... **xvii**
List of Tables ..... **xviii**
List of Figures ..... **xix**
Chapter One: Introduction And Literature Review **1**
1.0 Breast cancer origin and epidemiology **1**
1.1 Molecular classification of breast cancer subtypes **2**
1.2 Triple negative breast cancer **3**
1.2.1 Molecular subtypes of triple negative breast cancer 4
1.2.2 Triple negative breast cancer risk factors 4
1.2.3 The hallmarks of cancer 6
1.3 Breast cancer management **6**
1.3.1 Chemotherapy 6
1.3.2 Food and drug administration approved targeted therapies. 7
1.3.2.1 Poly (adenosine diphosphate -ribose) polymerase inhibitors: Olaparib and Talazoparib 8
1.3.2.2 Checkpoint Inhibitors: Pembrolizumab and Atezolizumab 8
1.3.2.3 Antibody–Drug Conjugate: Sacituzumab Govitecan 9
1.4 Mechanisms of cell death **9**
1.4.1 Unregulated cell death: Necrosis 10
1.4.2 Regulated cell death 10
1.4.2.1 Ferroptosis 11
1.4.2.2 Cuproptosis 11
1.4.2.3 Autophagic cell death 12
1.4.2.4 Apoptotic cell death 12

1.5 Proteins involved in the regulation of apoptosis. 15
1.5.1 Tumour suppressor p53 16
1.5.2 The B cell lymphoma-2 protein family 18
1.5.3 Nuclear factor-kappa B signalling 19
1.5.4 Cyclin-dependant kinase inhibitor, p21 20
1.5.5 Regulation by inhibitors of apoptosis proteins 20
1.5.6 Heat shock proteins 21
1.5.7 Haem oxygenase 22
1.6 Novel anti-cancer drugs 23
1.6.1 Metal-based complexes 24
1.6.1.1 Gold complexes 24
1.6.1.2 Copper complexes 25
1.7 *In vitro* models of TNBC and mammary epithelial cells 26
1.7.1 TNBC cell model: MDA-MB-231 26
1.7.2 Mammary epithelial cell model: MCF-10A cells 26
1.8 Problem statement 27
1.9 Aim 27
1.10 Objectives 27
Chapter Two: Methods And Materials 29
2.0 Introduction 29
2.1 Metal complexes 29
2.2 Cell culture techniques 30
2.2.1 Cell lines and ethical clearance 30
2.2.2 Cell propagation and maintenance 30
2.2.3 Cell sub-culturing and cryopreservation 31
2.2.4 Cell cryopreservation 31
2.2.5 Cell counting 32
2.3 Cell viability assay: MTT assay 32
2.3.1 MTT assay procedure 32
2.4 Determination of cell death mechanisms 33
2.4.1 Assessment of cell morphology 33
2.4.2 Determination of the generation of reactive oxygen species 35

2.4.3 Detection of apoptosis with annexin V binding assay 35
2.4.4 Assessment of the mitochondrial membrane potential (ΔΨm) 36
2.4.5 Determination of caspase-9 activity.....37
2.4.6 Determination of caspase-8 activity.....37
2.4.7 Assessment of caspase-3/7 activity assay. 38
2.5 Evaluation of apoptosis-related regulatory proteins 39
2.5.1 Proteome profiler human apoptosis array 39
2.5.2 Protein concentration quantification: Bradford assay 41
2.5.3 Antibody based immunofluorescence assays.....42
2.5.4 Western blot assay 43
2.6 Data analysis..... 44
Chapter Three: Results 45
PART 1: Cytotoxicity of the metal complexes..... 45
3.1 Cytotoxic effects of the metal complexes on breast cancer and mammary epithelial cell lines..... 45
3.1.1 The effects of the metal complexes and ligands on cell viability of MDA-MB-231 breast cancer cells 45
3.1.2 IC_{50} values of the active metal complexes on MDA-MB-231 breast cancer cells.....47
3.1.3 Selection of the metal complexes for further evaluation 50
3.1.4 The effects of selected active metal complexes on the viability of MCF-10A mammary epithelial cells 50
3.1.5 IC_{80} Concentrations of the metal complexes in MDA-MB-231 and MCF-10A cells.....51
3.2 The effects of the metal complexes on the cell morphology of MDA-MB-231 and MCF-10A cells 51
3.2.1 The effects of metal complexes on the cell morphology of MDA-MB-231 breast cancer cells 53
3.2.2 The effects of the metal complexes on the morphology of MCF-10A mammary epithelial cells 55
3.2.3 Cell line selection for the mechanisms of cell death assays.....57
3.3 Evaluation of cell death mechanisms in MDA-MB-231 breast cancer cells..... 58
3.3.1 The effects of the metal complexes on reactive oxygen species.....58
3.3.1.1 Measurement of ROS in MDA-MB-231 breast cancer cells 58
3.3.2 The effects of metal complexes on the exposure of phosphatidyl serine.....62

3.3.2.1 The effects of the metal complexes on phosphatidyl serine in MDA-MB-231 breast cancer cells 62

3.3.3 The investigation of effects of the metal complexes on mitochondrial membrane *(ΔΨm)* potential in MDA-MB-231 breast cancer cells 65

3.3.3.1 Determination of effects of the metal complexes on ΔΨm in MDA-MB-231 breast cancer cells 65

3.3.4 Evaluation of the effects of the metal complexes on caspase-9 activity 68

3.3.4.1 Assessment of the effects of the metal complexes on caspase-9 activity in MDA-MB-231 breast cancer cells 70

3.3.5. Assessment of caspase-8 activity 71

3.3.5.1 Determination of caspase-8 activity in MDA-MB-231 breast cancer cells……72

3.3.6 The effect of the metal complexes on caspse-3/7 activity 74

3.3.6.1 The effect of the metal complexes on caspase-3/7 activity in MDA-MB-231 cells after treatment 74

3.4 Proteome profiler human apoptosis array 78

3.4.1 The effects of copper complexes and doxorubicin on apoptotic regulatory proteins in MDA-MB-231 breast cancer cells 80

3.4.2 The effects of copper complexes on the expression levels of phosphorylated p53 species in MDA-MB-231 breast cancer cells 82

3.4.3 The effects of copper complexes on expression levels of the Bcl-2 family 83

proteins in MDA-MB-231 breast cancer cells 83

3.4.4 The effects of the copper complexes and doxorubicin on the expression levels of cytochrome c, Smac/DIABLO and HtrA2 in MDA-MB-231 breast cancer cells 84

3.4.5 The effects of the copper complexes and doxorubicin on the expression of death receptor proteins in MDA-MB-231 breast cancer cells 85

3.4.6 The effects of copper complexes and doxorubicin on the expression levels of p21/Cip1, p27Kip1 and phospho-Rad17 in MDA-MB-231 breast cancer cells 86

3.4.7 The effects of copper complexes on the expression levels of IAPs: cIAP-1, cIAP-2, livin, survivin and XIAP in MDA-MB-231 breast cancer cells 87

3.4.8 The effects of the copper complexes on the expression of heat shock proteins: HSP27, HSP60, HSP70 and PON2 in MDA-MB-231 breast cancer cells 88

3.4.9 The effects of copper complexes on the expression of HIF-1α, HMOX-1, and HMOX-2 in MDA-MB-231 breast cancer cells. 89

3.5 Detection of NIK, phospho-p53(s15), p21, and HMOX-1 by immunofluorescence90

3.5.0 Introduction 90

3.5.1 The effects of copper complexes and doxorubicin on the expression of NIK in MDA-MB-231 breast cancer cells. 90

3.5.2 The effects of copper complexes on the expression levels of phospho-p53(s15) in MDA-MB-231 breast cancer cells 93

3.5.3 The effects of copper complexes and doxorubicin on the expression levels of p21 in MDA-MB-231 breast cancer cells 96

3.5.4 The effects of the copper complexes on the expression levels of HMOX-1 in MDA-MB-231 breast cancer cells 98

3.6 Determination of HMOX-1 expression using the western blot assay 100

3.6.1 Assessing molecular weight of HMOX-1 in MDA-MB-231 breast cancer cells 101

3.6.2 Assessing the efficacy of Cu8AqN and $CuPhenTh_2$ in the presence of HMOX-1 inhibitor in MDA-MB-231 breast cancer cells 102

Chapter Four: Discussion 104

4.0 Brief overview of the study 104

4.1 Copper and gold complexes preferentially inhibit the proliferation of MDA-MB-231 cells compared to MCF-10A cells 105

4.1.1 Cytotoxicity of the gold(I) complexes and 1,2,3-triazolylidene (trz) ligand 105

4.1.2 Cytotoxicity of the copper complexes and ligands 106

4.2 Copper and gold metal complexes caused changes to the morphology of MDA-MB-231 breast cancer and MCF-10A mammary epithelial cells 109

4.3 Copper and gold metal complexes caused the accumulation of reactive oxygen species (ROS) in MDA-MB-231 breast cancer cells 111

4.4 Copper and gold metal complexes disrupt mitochondrial membrane potential (ΔΨm) in MDA-MB-231 breast cancer cells 113

4.5 Copper and gold metal complexes induced apoptotic cell death by increasing annexin V binding and activating caspase-3/7 in MDA-MB-231 breast cancer cells 114

4.5.1 Annexin V binding 114

4.5.2 Caspase-3/7 activation 115

4.6 The copper and gold metal complexes activate both caspase-8 and caspase-9 in MDA-MB-231 breast cancer cells 117

4.6.1 Caspase-9 activation 117

4.6.2 Caspase-8 activation 118

4.7 Copper complexes cause changes to apoptosis regulatory proteins 119

4.7.1 The effect of the copper complexes and doxorubicin on phosphorylated p53 species 120

4.7.2 Copper complexes decreased the expression of Bad in MDA-MB-231 breast cancer cells 122

4.7.3 Copper complexes decreased the inhibitor of apoptosis proteins (IAPs) in MDA-MB-231 breast cancer cells 123

4.7.3.1 cIAP1 expression prevents caspase-8 activation....125
4.7.3.2 cIAP1 supressed the canonical nuclear factor kappa B pathway....125
4.7.4 Copper complexes decreased the expression of Smac /DIABLO, and HtrA2/Omi in MDA-MB-231 breast cancer cells....126
4.7.5 Copper complexes caused insignificant changes in the highly expressed cleaved caspase-3 in MDA-MB-231 breast cancer cells....127
4.7.6 Copper complexes decreased the expression of the Fas/ CD95 receptor in MDA-MB-231 breast cancer cells....128
4.7.7 Copper complexes decreased the expression of cell cycle regulators, p21, p27 and phospho-RAD179 (s635) in MDA-MB-231 breast cancer cells....129
4.7.8 Copper complexes decreased paraoxonase-2 and heat shock proteins in MDA-MB-231 breast cancer cells....130
4.7.9 Copper complexes increased the expression of haem oxygenase-1 in MDA-MB-231 breast cancer cells....131
4.8 Immunofluorescence of NIK, phospho-p53(s15) and HMOX-1....133
4.8.1 Copper complexes caused nuclear expression of NF-κB-inducing kinase (NIK) in MDA-MB-231 breast cancer cells....133
4.8.2 Copper complexes increased the expression of nuclear phospho-p53(s15) in MDA-MB-231 breast cancer cells....134
4.8.3 Copper complexes increased the expression of nuclear HMOX-1 in MDA-MB-231 breast cancer cells....135
4.8.4 The efficacy of copper complexes in the presence of HMOX-1 inhibitor, OB24. 136
4.9 Study limitations....137
Chapter Five: Conclusion....138
References....142
Appendix A: Ethics waiver certificate....186
Appendix B: Doxorubicin concentration selection supplementary images....187
Appendix C: MCF-10A cell morphology supplementary image....188
Appendix D: Standard curves....189
D1 Standard curve for proteome array and western blot assay....189
D2 Standard curve for molecular weight markers....189
Appendix E: Western blot membranes....190
Appendix F: Turn-It-In report....191
Appendix G: Figure copyright permission....192

Abbreviations

AIF	Apoptosis-inducing factor
AO	Acridine orange
AP-1 and 2	Activator protein 1 and 2
APAF-1	Apoptotic protease-activating factor-1
Au	Gold metal
Bad	Bcl-2-associated agonist of cell death
Bak	Bcl-2 antagonist/killer
Bax	Bcl-2-associated X protein
BC	Breast cancer
Bcl-2 family	B-cell lymphoma 2 family
Bcl-2	B-cell lymphoma 2
Bcl-xL	B-cell lymphoma-extra-large
BH	Bcl-2 homology
BIR	Baculovirus IAP Repeat
BRCA1	Breast Cancer susceptibility gene 1
CDKIs	Cyclin-dependent kinase inhibitors
cIAP1/2	cellular Inhibitor of apoptosis1/ 2
Cu	Copper metal
DIABLO	Direct IAP-binding protein
DISC	Death-inducing signalling complex.
DMSO	Dimethyl sulfoxide
DNA	Deoxyribose nucleic acid
ER	Estrogen receptor.

FADD	Fas-associated death domain
Fas	First Apoptosis Signal receptor
HER2	Human epidermal growth factor receptor 2
HIF-1α	Hypoxia inducing factor 1- alpha.
HMOX-1	Haem oxygenase-1
HO	Hoechst 33342
HSP	Heat shock proteins
IAPs	inhibitors of apoptosis proteins
IC_{50}	50 % inhibitory concentration
IC_{80}	80 % inhibitory concentration
IKK	IκB kinase
JaCoP	Just another Co-localization
JC-1	dye-5,5′,6,6,6,6-tetrachloro-1,1′,3,3,3,3-tetraethylbenzimi-dazolylcarbocyanine iodide.
MCF-10A	Michigan Cancer Foundation-10A
MDA-MB-231	MD Anderson Metastatic Breast- 231
MDM2	Mouse Double Minute 2 homolog
MOMP	Mitochondrial outer membrane permeabilization
MTT assay	3-(4,5-dimethylthiazol-2-yl)-2,5-diphenyl tetrazolium bromide
NF-κB	Nuclear factor-kappa B
NIK	NF-κB-inducing kinase.
Nrf2	Nuclear factor erythroid 2-related factor-2
OB24	(1-[[2-[2-(4-Bromophenyl)ethyl]-1,3-dioxolan-2-yl]methyl]-1H-imidazolehydrochloride)
Omi/HtrA2	Temperature requirement protein A
p21	Cyclin-Dependent Kinase Inhibitor 1A (CDKN1A)

p27	Cyclin-Dependent Kinase Inhibitor 1B (CDKN1B)
PARP	Poly (ADP-ribose) polymerase.
PCC	Pearson Correlation Coefficient
PD-1	Programmed cell death protein.
p53	Tumor suppressor protein
Phospho-p53(s15)	Phosphorylated p53 serine 15
Phospho-p53(s392)	Phosphorylated p53 serine 392
Phospho-p53(s46)	Phosphorylated p53 serine 46
Phospho-RAD17	phosphorylated form of radiation sensitive 17
PI	Propidium iodide
PON2	Paraoxonase 2
PR	Progesterone receptor
ROS	Reactive oxygen species
RPM	Rotations per minute
SI	Selectivity index
Smac	Second mitochondria-derived activator of caspases
tBHP	Tert-butyl hydroperoxide
TBST	tris-buffered saline with Tween 20
TNBC	Triple-Negative Breast Cancer
TNF R1	Tumour Necrosis Factor Receptor 1
TP53 gene	Tumour Protein 53
TRAF1/2	TNF receptor-associated factors1/2
TRAIL	TNF-related apoptosis-inducing ligand
TrxR	Thioredoxin reductase
XIAP	X-linked inhibitor of apoptosis protein
ΔΨm	mitochondrial membrane potential

Latin letters

α	Alpha
β	Beta
γ	Gamma
σ	Sigma

Unit of measurements

µg	Microgram
µg/ml	Grams per millilitre
µl	Microlitres
µM	Micromolar
cm^2	square centimetre
h	Hours
min	Minutes
ml	Millilitres
mg/ ml	Milligram per millilitre
ng/ ml	Nanogram per millilitre
nm	Nanometre
V	Volts
%	Percent
^0C	Degree Celsius

List of Tables

Chapter One

Table 1.1: Breast cancer subtypes, prognosis, and molecular markers 3

Chapter Three

Table 3.1: IC_{50} values, and chemical structures of active metal complexes 48

Table 3.2: IC_{50} values and selectivity indices of selected metal complexes 51

Table 3.3: IC_{80} values of selected metal complexes 53

Table 3.4: Cell percentage of early and late apoptotic MDA-MB-231 cells 65

Table 3.5: Target proteins and their corresponding coordinates membrane array 79

Table 3.6: The grading scale of pixel density used to classify the expression level 80

Table 3.7: Percentage change in the expression of apoptosis related proteins 81

Table 3.8: Percentage of MDA-MB-231 cells expressing p21 97

Table 3.9: IC_{50} values of Cu8AqN and $CuPhenTh_2$ after OB24 HMOX-1 inhibition 103

Chapter Four

Table 4.1: Structure activity relationship of the gold-1,2,3-triazolylidene complexes 106

Table 4.2: Structure activity relationship of the copper complexes and ligands 108

List of Figures

Chapter One

Fig. 1.1 An illustration of eight Hallmarks of Cancer. 6

Fig. 1.2 Diagram showing the extrinsic and intrinsic apoptotic pathways 13

Fig. 1.3 Mechanisms of inactivation of the tumour suppressive activity of p53 16

Chapter Three

Fig. 3.1 MDA-MB-231 cell viability after treatment with complexes and ligands 46

Fig. 3.2 Representative dose-response curves of the active metal complexes 49

Fig. 3.3 Fluorescent micrographs showing apoptotic nuclei changes 52

Fig. 3.4 Fluorescent micrographs of MDA-MB-231 cell morphology changes 54

Fig. 3.5 Fluorescent micrographs of MCF-10A cells cell morphology changes 56

Fig. 3.6 Photomicrographs of MDA-MB-231 cells showing ROS formation 60

Fig. 3.7 Bar graphs showing ROS fold increase measurement 61

Fig. 3.8 Fluorescent micrographs showing annexin-V binding 63

Fig. 3.9 Fluorescent micrographs of MDA-MB-231 with $\Delta\Psi m$ changes 67

Fig. 3.10 Quantitative analysis of JC-1 aggregates and monomers 68

Fig. 3.11 Fluorescent micrographs of MDA-MB-231 cells with caspase-9 activity 69

Fig. 3.12 Quantitative presentation of capaspe-9 activity 71

Fig. 3.13 Photomicrographs of caspase-8 positive MDA-MB-231 72

Fig. 3.14 Bar graphs showing percentage of cells with caspase-8 activation 73

Fig. 3.15 Photomicrographs showing caspase -3/7 activity in MDA-MB-231 cells 76

Fig. 3.16 Bar graphs showing percentage of cells positive for active caspase-3/7 77

Fig. 3.17 Coordinates for the human apoptosis array 78

Fig. 3.18 Chemiluminescent signals on nitrocellulose membrane arrays 80

Fig. 3.19 Expression levels of phosphorylated p53 species in MDA-MB-231 cells 82

Fig. 3.20 Expression of Bcl-2 family proteins in MDA-MB-231 breast cancer cells 83

Fig. 3.21 Expression levels of cytochrome c, Smac/DIABLO, and HtrA2 in the cells 84

Fig. 3.22 Expression of death receptor proteins in MDA-MB-231 breast cancer cells 85

Fig. 3.23 Expression of /Cip1, p27Kip1 and phosho-RAD17 (s653) 86

Fig. 3.24 Expression levels of AIPs in MDA-MB-231 breast cancer cells 87

Fig. 3.25 The expression levels of HSP and PON2 in MDA-MB-231 breast cells 88

Fig. 3.26 The expression levels of HIF-1 α, HMOX-1 and HMOX-2 89

Fig. 3.27 The expression of NIK in MDA-MB-231 breast cancer cells 91

Fig. 3.28 NIK intensity and correlation measurement in MDA-MB-231 92

Fig. 3.29 The expression and colocalization of phospho-p53(s15) 94

Fig. 3.30 Bar graphs showing phospho-p53(s15) expression and PCC 95

Fig. 3.31 The effects of copper complexes and doxorubicin on p21 expression 96

Fig. 3.32 Photomicrograph showing HMOX-1 expression 99

Fig. 3.33 Quantification of HMOX-1 expression and correlation in MDA-MB-231 100

Fig. 3.34 Western blots and bar graphs showing HMOX-1 expression 101

Fig. 3.35 The effects of OB24 on MDA-MB-231 cell viability 102

Chapter Five

Fig. 5.1 Mechanism of cell death of copper complexes in MDA-MB-231 cells 139

Chapter One: Introduction And Literature Review

1.0 Breast cancer origin and epidemiology

Breast cancer develops in the epithelial cells lining the milk ducts and less frequently in the lobules of the breast tissue. Cancer that occurs in the ducts is referred to as ductal carcinoma, whereas breast cancer developing in the lobules is called lobular carcinoma (Medina *et al.*, 2020). This type of cancer appears as a lump or mass in the breast tissue (Makki, 2015; Menon *et al*. 2024). The four common histological subtypes of breast cancer are invasive or in situ ductal carcinoma (IDC/ DCIS) and invasive or in situ lobular carcinoma (ILC/ LCIS), which are classified based on their invasive potential and site of origin (Howlader *et al.,* 2014; Watkins, 2019, Menon *et al.,* 2024). IDC, the most prevalent form of invasive breast cancer, is characterised as dense, irregular masses and accounts for 80 % of all breast cancer cases. It is caused by malignant epithelial cells infiltrating from the milk ducts into the surrounding stroma (Watkins, 2019, Menon *et al.,* 2024).

Ductal carcinoma in situ (DCIS) is non-invasive, non-infiltrating and confined in mammary ducts. When untreated, DCIS have a risk of progressing to IDC (Wang *et al.,* 2024). Conversely, ILC is characterised by single cancer cells that invade and spread without forming cohesive growth pattern and contributes 15 % of ILC. Due to its growth pattern, ILC is diagnosed at a more advanced stage or larger tumour size (Oesterreich *et al.,*2022; Batra *et al.,* 2023). Lobular carcinoma in situ (LCIS), is non-invasive counterpart of ILC, originating from the terminal duct–lobular parts of the breasts. ILC expresses high oestrogen receptor, lacks HER2 and spreads to the peritoneum and gastrointestinal tract (Batra *et al.,* 2023). Breast cancer is commonly diagnosed in women worldwide (Watkins, 2019). In 2022, approximately 2.3 million new breast cancer cases were reported globally, accounting for 23.8 % of all cancer cases in women. It was the first leading cause of cancer-related deaths, contributing 15.5 % in all cancer mortalities (Giaquinto *et al.,* 2022; Bray *et al.,* 2024).

In South Africa, breast cancer accounted for 26.2 % of all new cancer cases in women and was the second leading cause of cancer-related deaths (15.5%), after cervical cancer (Giaquinto *et al.,* 2022). According to GLOBOCAN 2022, South Africa reported high breast cancer mortality rates despite having a lower incidence, in comparison to a country in Europe like the United Kingdom (GLOBOCAN, 2022; Giaquinto *et al*., 2022). Higher mortality rates in South Africa are attributable to poor/late diagnosis, inadequate breast cancer screening programs, unequal healthcare access, and limited treatment options (Hamdi *et al.,* 2021; Omotoso *et al.,* 2023).

In South Africa, access to treatment facilities remains limited for patients in underdeveloped or rural areas. For example, some patients travel over 400 km to receive treatment at Charlotte Maxeke Academic Hospital. This disparity highlights the need to explore alternative and potentially more accessible treatment options (Personal Interviews). Alternative treatment methods such as metal-based complexes, offer promising anticancer potential and could complement existing treatment regimens. Their development and integration into treatment protocols could expand therapeutic options and efficacy, for all cancer patients including patients facing challenges accessing centralised cancer treatment facilities. This highlights the need for novel treatment approaches, particularly in regions where access to facilities with standard therapies is limited.

1.1 Molecular classification of breast cancer subtypes

Breast cancer is a heterogeneous disease and is classified into molecular subtypes based on the expression of hormone receptors (oestrogen receptor (ER), progesterone receptor (PR)) and human epidermal growth factor receptor 2 (HER2). The main subtypes are luminal A, luminal B, HER2-enriched, and Triple-Negative/Basal-like breast cancer (TNBC) (Bianchini *et al.*, 2016; Shaath *et al.*, 2021; Almansour, 2022). Luminal A subtype accounts for approximately 40 % of breast cancer cases. It expresses ER and PR, lacks HER2 and has low Ki-67 (proliferation protein) levels (Bianchini *et al.*, 2016). Luminal A tumours are considered to have good prognosis and a lowest risk of recurrence (Shaath *et al.*, 2021). Luminal B subtype has an intermediate prognosis and represents 20 % of breast cancers. This subclass is characterized by ER positivity with varying levels of PR and HER2 expression, and high Ki-67 levels indicating high proliferative profile (Miah *et al.*, 2019).

HER2-positive tumours contribute 15 % of all breast cancer cases and are defined by HER2 overexpression with absence of the hormone receptors. Although they have an aggressive clinical profile, targeted anti-HER2 therapies have improved outcomes (Bianchini *et al.*, 2016; Shaath *et al.*, 2021; Almansour, 2022). Finally, TNBC constitutes 25 % of all breast cancer cases. This subtype lacks the expression of ER, PR, and HER2, does not respond to hormone and HER2-targeted therapies and associated with poor outcomes, Table 1.1 (Lehmann *et al.*, 2011; Bianchini *et al.*, 2016; Almansour, 2022).

Table 1.1: Breast cancer subtypes, prognosis, and molecular markers, adapted from (Bianchini *et al.*, 2016; Almansour, 2022).

Subtype	Prevalence	Prognosis	Molecular markers
Luminal A	40 %	Good prognosis; low recurrence	ER+, PR+, HER2−, low Ki-67
Luminal B	20 %	Intermediate prognosis; higher proliferation	ER+, PR±, HER2±, high Ki-67
HER-2 positive	15 %	Poorer prognosis but improved with HER2-targeted therapies	ER−, PR−, HER2+
TNBC/Basal	25 %	Poor prognosis; aggressive; limited targeted therapy	ER−, PR−, HER2−

1.2 Triple negative breast cancer

TNBC is an aggressive form of breast cancer defined by the absence of ER, PR, and HER2 expression. It primarily affects younger women, particularly those under 40 years of age, and is more prevalent among African and Hispanic women (DeSantis *et al.*, 2016; Wright *et al.*, 2018). Unlike hormone receptor-positive or HER2-positive subtypes, TNBC lacks specific targeted therapies, making treatment more challenging to treat (Xiong *et al.*, 2024).

Its metastatic behaviour also differs; TNBC commonly metastasize to visceral organs such as the lungs, brain, and liver contributing to poor prognosis (Yousefi *et al.*, 2018; Lv *et al.*, 2021). TNBC tumours tend to be high grade, with rapid proliferation, and are often larger at the time of diagnosis.

A high risk of recurrence, within the first three years after diagnosis is common (Alkabban and Ferguson, 2023). Five-year survival rates vary depending on the stage of the disease: approximately 65 % for *in situ* disease and only 11 % for distant metastases (Denkert *et al.*, 2017; Gonçalves *et al.*, 2018).

1.2.1 Molecular subtypes of triple negative breast cancer

TNBC is a heterogenous disease with multiple subtypes. Lehmann *et al.*(2011) have proposed molecular classification as a guide for subtype-specific therapies in TNBC. There are six subtypes of TNBC namely (1) Basal-like-1: Characterized by elevated expression of genes involved in cell cycle and DNA damage response such as cyclin-dependent kinases, *Ki-67* which is a marker of proliferation and checkpoint kinases for cell cycle arrest upon DNA damage. These tumours are highly proliferative and may be sensitive to DNA-damaging agents (Badve *et al.*, 2011). (2) Basal-like-2: Enriched in growth factor signalling and metabolic pathways. (3) Mesenchymal: Marked by genes involved in epithelial–mesenchymal transition (E-cadherin), cell motility (Matrix metalloproteinases: Degrade extracellular matrix), and differentiation (Lamouille *et al.*, 2014). (4) Mesenchymal stem-like: Shares characteristics with the mesenchymal subtype but with stemness features and immune suppression. (5) Immunomodulatory: Defined by the presence of immune cell processes, suggesting potential responsiveness to immunotherapy. (6) Luminal Androgen Receptor: Expresses androgen receptor and hormone-regulated pathways, with possible sensitivity to hormone-targeted therapy (Lehmann *et al.*, 2016; Almansour, 2022).

1.2.2 Triple negative breast cancer risk factors

There are multiple factors that contribute to the development of TNBC, including genetic, environmental, and lifestyle factors. While many of these risks are non-modifiable, understanding them can help in early detection and prevention (Yao *et al.*, 2019). Early menstruation (before the age 12) or late menopause (after the age of 55) increases the risk due to prolonged exposure to oestrogen (Travis and Key, 2003). Having a first child after the age 30, not breastfeeding, or never having given birth is associated with a higher risk of TNBC (Ma *et al.,* 2017). Lifestyle-related factors such as alcohol consumption, obesity, particularly after menopause, and a lack of physical activity all increases the risk of breast cancer development (Yao *et al.*, 2019; McCarthy *et al.*, 2021).

One of the main risk factors for breast cancer is having a family history of the disease. This is often associated with inherited mutations in the breast cancer susceptibility genes BRCA1 and BRCA2, which are tumour suppressor genes involved in the repair of DNA double-strand breaks through homologous recombination (Starita and Parvin, 2003). Mutations in these genes impair DNA repair, leading to genomic instability and an increased risk of developing breast and other cancers. Women with a BRCA1 mutation have a 55 – 65 % lifetime risk of developing breast cancer, while those with a BRCA2 mutation have about a 45 % lifetime risk . These mutations also increase the risk of ovarian cancer and, to a lesser extent, other cancers (Kuchenbaecker *et al.*, 2017). Genetic testing is often recommended for individuals with a strong family history of breast or ovarian cancer, especially at a young age (Pogoda *et al.*, 2020; Almansour, 2022).

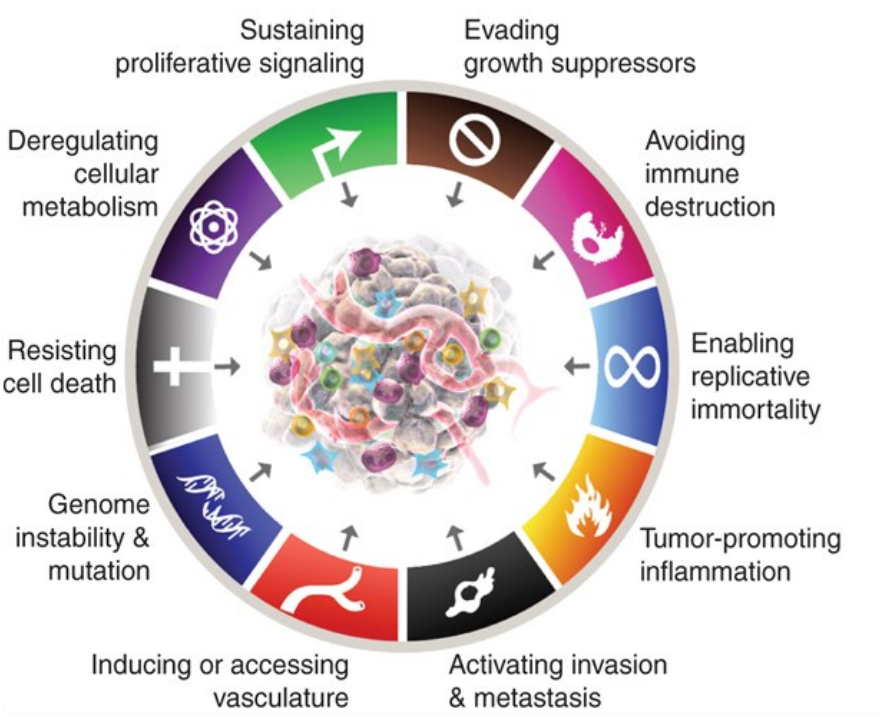


Fig. 1.1 An illustration of eight Hallmarks of Cancer. Eight hallmark capabilities have been elucidated and include sustaining proliferative signalling, evading growth inhibitors, resisting cell death, enabling replicative immortality, inducing angiogenesis, activating invasion and metastasis, reprogramming cellular metabolism, and avoiding immune destruction adapted from (Hanahan, 2022; License Number: 6093000188204).

1.2.3 The hallmarks of cancer

During the transformation from normal cellular state to malignant state, cancer cells acquire capabilities that enables growth and metastasis as proposed by Hanahan and Weinberg (Hanahan and Weinberg, 2011; Hanahan, 2022). To date, eight hallmark capabilities have been elucidated and include (Fig 1.1) sustaining proliferative signalling, evading growth inhibitors, resisting cell death, enabling replicative immortality, inducing angiogenesis, activating invasion and metastasis, reprogramming cellular metabolism, and avoiding immune destruction. Characteristics like genomic instability and tumour promoting inflammation intersect to activate these capabilities (Hanahan and Weinberg, 2011). Cancer drugs are being developed to block one or more of these capabilities, specifically disrupting pathways that sustain proliferation, promote immune evasion, or enable metastatic progression (Hanahan and Weinberg, 2011)

1.3 Breast cancer management

Breast cancer management includes surgery, radiation, and chemotherapy (Shah *et al.*, 2014). Breast conservation surgery is used to remove regional and localized breast tumours (Litière *et al.*, 2012). Before surgery, neoadjuvant chemotherapy is administered to reduce tumour size thus decreasing the extent of surgery. This is followed by adjuvant chemotherapy to reduce the risk of recurrence and metastasis (Lim *et al.*, 2014). Radiation therapy exposes the tumour to high levels of radiation to kill cancer cells. It is used before and after surgery to either shrink the tumour or to eradicate remaining tumour cells (Whelan *et al.*, 2015).

1.3.1 Chemotherapy

The main treatment for TNBC is conventional chemotherapy, however, this treatment is associated with drug resistance and adverse drug reactions (Wahba and El-Hadaad, 2015). Anthracycline-taxane based regimens with doxorubicin constitute the standard care for triple negative breast cancer. The anthracyclines interact with DNA through intercalation, causing a direct inhibition of the DNA replication and repair. Anthracyclines form a tripartite complex with the DNA through guanine bases in both strands of the DNA and inhibits topoisomerase II enzyme activity (Wellstein and Sausville, 2023). Topoisomerase II enzyme is an enzyme that binds to DNA to unwind/uncoil the coiled structure of DNA, and it forms double-strand breaks on 3’phosphate backbone.

After DNA uncoiling the topoisomerase II enzyme re-ligates the DNA strand for the repair and replication of the molecule. Anthracycline tripartite complex blocks the re-ligation of the uncoiled DNA resulting in apoptosis (Wellstein and Sausville, 2023).

Anthracyclines cause severe hepatic and cardiac adverse effects and are commonly used in combination with taxanes or vinca alkaloids. Paclitaxel and docetaxel are examples of taxanes (Wellstein and Sausville, 202). This class of drugs prevents the depolymerization of microtubules by binding to the beta (β) subunit of tubulin in microtubules on the second gap phase/ mitotic phase (G2/M phase) of the cell cycle (Wellstein and Sausville, 2023). This results in inhibition of cell cycle progression by causing acentrosomal impairment and preventing the disassembly of tubulin. This causes microtubule bundles and damaged structures to appear in the mitotic phase of the cell cycle, which in turn inhibit mitosis and induce apoptosis.

On the other hand, vinca alkaloids (vincristine and vinblastine) are microtubule-targeting agents, which binds strictly to β-tubulin and block the polymerization with α tubulin in microtubules. In the presence of vinca alkaloids the microtubules dissolve and results in crystals and prevent formation of spindles. This cause cell cycle arrest at the metaphase. The chromosomes fail to align on the division plate as a result they are scattered in the cytoplasm or form group of clumps. The cells that are blocked during mitosis then display apoptotic features. The vinca alkaloids results in serious side effects such as myelosuppression, neurotoxicity and alopecia (Ritter *et al.*, 2008; Wellstein and Sausvill, 2023).

1.3.2 Food and drug administration approved targeted therapies.

Despite being one of the most aggressive breast cancer subtypes, TNBC lacks the molecular targets targeted in hormone receptor-positive or HER2-enriched subtype (DeSantis *et al.*, 2016). In recent years, several targeted therapies have gained Food and drug administration approval for specific molecular subtypes of TNBC. These include poly (adenosine diphosphate-ribose) polymerase (PARP) inhibitors, immune checkpoint inhibitors, and antibody–drug conjugate targeting trophoblast cell-surface antigen 2 (Trop-2) *(*Sun *et al.,* 2015; Lord and Ashworth, 2017; Turner *et al.*, 2019). While these therapies have made progress in TNBC management, they are each associated with significant limitations that minimize their clinical use.

1.3.2.1 Poly (adenosine diphosphate -ribose) polymerase inhibitors: Olaparib and Talazoparib

Olaparib (inhibitor of PARP1,-2, and 3) and talazoparib (inhibitor of PARP1 and PARP2) are FDA-approved PARP inhibitors indicated for TNBC patients with germline mutations in BRCA1 or BRCA2 (Robson *et al.,* 2019). PARP1 is a nuclear protein that transfers ADP-ribose from NAD+ to target proteins, functions in the repair of single-strand breaks in DNA and is commonly inactivated in human cancer. Poly(ADP-ribosyl)ation (or PARylation) of nuclear proteins by PARP1 has an important role in the DNA damage response (Tallis *et al.,* 2014). Inactive PARP1 joins chromatin and helps to form a compact chromatin structure in the nucleosome. DNA damage mobilizes the enzyme, promoting PARP-mediated PARylation, with result of chromatin relaxation at the damaged area. PARylation of PARP1 itself and of histones and other chromatin-associated proteins, yields branching chains that provide docking centres for specific recruitment of PAR binding factors, DNA repair enzymes and proteins that assist in the maintenance of inactive environment in the open chromatin area while the damaged DNA is being repaired (Wellstein and Giaccone, 2023).

These drugs inhibit PARP enzymes responsible for repairing single-strand deoxyribonucleic acid (DNA) breaks through base excision repair. In BRCA-mutated cells, the homologous recombination repair pathway is impaired, making them dependant on PARP for DNA repair. Inhibition of PARP causes the accumulation of DNA double-strand breaks during replication, genomic instability, and cell death (Turner *et al.,* 2019). While effective in BRCA-mutated TNBC, PARP inhibitors have limited use in other TNBC subtypes, and other cancers. Moreover, resistance to PARP inhibition can develop rapidly through restoration of homologous recombination via secondary mutations in BRCA1/2 or upregulation of alternative repair pathways (Li *et al*., 2020). Additionally, adverse effects such as fatigue, nausea, and anaemia may limit tolerability in some patients (Lord and Ashworth, 2017; Turner *et al.*, 2019).

1.3.2.2 Checkpoint Inhibitors: Pembrolizumab and Atezolizumab

Checkpoint inhibitors used in TNBC include humanized monoclonal IgG4κ antibody, pembrolizumab (anti–programmed cell death protein (PD-1)) and IgG1 monoclonal antibody called atezolizumab (anti– programmed cell death protein 1-ligand (PD-L1)) (Almansour, 2022).

PD-1 is an inhibitory receptor expressed on activated CD4 and CD8 T lymphocytes (T-cells), as well as the B cells and macrophages, while PDL-1 is a ligand expressed on cancer cells and antigen presenting cells and form a receptor-ligand system (Sun *et al.*, 2015). In the tumour microenvironment, when PD-1 binds to PDL-1, it inhibits the anti-tumour immune response, allowing the cancer cells to evade immune surveillance (Topalian *et al.*, 2016). By inhibiting this interaction, these therapies restore T-cell activity by allowing the T-cells to recognise cancer and promote immune-mediated apoptosis (Chen and Han, 2015). These agents have shown survival benefits in PD-L1-positive metastatic TNBC, particularly when combined with chemotherapy. However, only a subset of TNBCs is immunogenic, and most patients are limited or do not benefit. In addition, immune-related adverse events such as colitis, pneumonitis, and thyroid dysfunction can lead to treatment discontinuation. The response is also highly dependent on the tumour microenvironment, which in many TNBC cases is characterized by immunosuppression (Almansour, 2022).

1.3.2.3 Antibody–Drug Conjugate: Sacituzumab Govitecan

Sacituzumab govitecan is an antibody–drug conjugate that targets Trop-2, which is overexpressed in most TNBCs (Chapdelaine and Sun, 2023). The antibody is conjugated to 7-ethyl-10-hydroxycamptothecin via hinge cysteine residues (SN-38) and is an active metabolite of the topoisomerase I inhibitor, camptothecin. Upon binding to Trop-2, the complex is internalized, and SN-38 is released inside the cells, where it inhibits topoisomerase I, causing DNA damage and apoptotic cell death. Although Sacituzumab govitecan has demonstrated significant improvements in overall survival in metastatic TNBC, its use is associated with considerable hematologic and gastrointestinal toxicity, including neutropenia, diarrhoea, and fatigue (Rugo *et al.,* 2022). Resistance may also arise through Trop-2 downregulation or impaired internalization (Chapdelaine and Sun, 2023).

1.4 Mechanisms of cell death

Cell death occurs through a variety of mechanisms categorized as regulated or unregulated**.** Understanding cell death mechanisms is essential in cancer research because the ability of cancer cells to evade death is a hallmark of tumour progression and treatment resistance (Hanahan and

Weinberg, 2011; Fouad and Aanei, 2017). In TNBC, where conventional therapies often fail due to the absence of hormone receptors and HER2 expression, investigating how cancer cells may die, or resist death provides knowledge on signalling pathways that can be targeted by novel therapies.

1.4.1 Unregulated cell death: Necrosis

Necrosis is a form of cell death marked by cytoplasmic swelling (oncosis), rupture of the plasma membrane, and organelle swelling, resulting in the uncontrolled release of intracellular contents. Morphologically, it contrasts with apoptosis by lacking chromatin condensation and showing cell lysis rather than fragmentation (Kroemer *et al.*, 2005, 2009). Necrosis involves adenosine triphosphate depletion, mitochondrial dysfunction, lysosomal membrane permeabilization, and the generation of reactive oxygen species (ROS). It may also involve regulated mechanisms, such as receptor-interacting protein kinase 1 kinase-dependent necroptosis (Nicotera and Melino, 2004).

A key hallmark of necrosis is a loss of membrane integrity, often assessed by propidium iodide (PI) staining, which enters and binds DNA in dead cells. Lactate dehydrogenase (LDH) release into the medium is another biochemical marker, its presence outside the cell reflects membrane rupture (Nicotera and Melino, 2004). Together, PI positivity and LDH leakage confirm necrotic cell death. Necrosis is often pro-inflammatory due to the release of damage-associated molecular patterns (DAMPs) (Kroemer *et al.*, 2005; Galluzzi *et al.*, 2012), which trigger immune activation and tissue damage, making it an undesirable mode of cell death.

1.4.2 Regulated cell death

Programmed cell death has an important role in physiological homeostasis of tissues and is dysregulated in cancer cells causing the survival of cells that carry oncogenic mutations (Galluzzi *et al.*, 2007). Based on distinctive morphological and biochemical features, there are multiple regulated cell death mechanisms including; necroptosis, pyroptosis, ferroptosis, autophagy, and apoptosis (Elmore, 2007; Tait and Green, 2010; Galluzzi *et al.*, 2018). In cancer treatment, apoptotic cell death is preferred, since it does not trigger an inflammatory response (Galluzzi *et al.*, 2018).

1.4.2.1 Ferroptosis

Ferroptosis is a regulated form of non-apoptotic cell death, morphologically, characterised by reduced mitochondria with increased mitochondrial membrane densities, reduction of mitochondria crista, outer mitochondrial membrane rupture and a normal nucleus (Dixon *et al.*, 2012; Li *et al .,* 2020). Biochemically, there is a depletion of intracellular glutathione (GSH) and decreased activity of glutathione peroxidase 4 (GPX4), leading to an inability to metabolise lipid peroxides through GPX4-catalyzed reduction. Additionally, iron oxidises lipids in a Fenton-like reaction, resulting in the generation of ROS, which facilitates ferroptosis (Gao *et al.*, 2019). Ferroptosis is gaining relevance as many cancers, particularly those resistant to apoptosis, remain susceptible to factors that trigger ferroptosis suggesting its therapeutic potential in resistant tumours, including triple-negative breast cancer. Moreover, ferroptosis intersects with tumour immunity and may either enhance or suppress anti-tumour responses depending on the immunity profile of the tumour (Friedmann Angeli *et al.*, 2014).

1.4.2.2 Cuproptosis

Cuproptosis is a recently characterized form of regulated cell death that is strictly dependent on intracellular copper and mitochondrial metabolism. Unlike apoptosis, necroptosis, or ferroptosis, cuproptosis is triggered by the accumulation of reduced copper ions (Cu^{+}) in the cells, particularly in those with active tricarboxylic acid (TCA) cycle (Tsvetkov *et al.*, 2022). Copper binds directly to lipoylated components of the mitochondrial pyruvate dehydrogenase complex, mainly the dihydrolipoamide S-acetyltransferase (DLAT), leading to protein oligomerization, destabilization of iron-sulphur cluster proteins, and proteotoxic stress causing cell death (Tsvetkov *et al.*, 2022; Xie *et al.*, 2023). Biochemically, it is characterized by DLAT accumulation, reduced iron-sulphur cluster stability, and increased proteotoxic stress without ROS accumulation (Tsvetkov *et al.*, 2022). Cuproptosis is implicated in oncology since the cancer cells have high metabolic rates making them more susceptible to this form of cell death (Feng *et al.,* 2024). This has caused interest in copper ionophores like elesclomol and disulfiram as potential therapeutic agents, either alone or in combination with other treatments to exploit cuproptosis sensitivity in cancer cells (Xie *et al.,* 2023).

1.4.2.3 Autophagic cell death

Autophagic cell death (ACD) is characterized by extensive autophagic vacuolization of the cytoplasmic organelles without chromatin condensation, distinguishing it morphologically from apoptosis. Hallmark features include the accumulation of double-membraned autophagosomes, conversion of microtubule-associated protein 1 light chain 3-I (LC3-I to LC3-II), and accumulation of autophagy related proteins such as Atg5, Atg7and Atg12 (Galluzzi *et al.,* 2012). Autophagy often promotes cell survival under stress, and in most instances, the inhibition of autophagy promotes cell death rather than preventing cell death (Kroemer and Jäättelä, 2005; Galluzzi *et al.*, 2012).

1.4.2.4 Apoptotic cell death

Apoptosis is a regulated form of cell death where damaged and redundant cells are killed in a controlled manner (Su *et al.*, 2015). Dysregulation/evasion of apoptosis is an important feature of tumour transformation. Apoptosis is inhibited because of mutated p53, reduced expression of pro-apoptotic proteins and enhanced expression of anti-apoptotic proteins commonly referred to as inhibitors of apoptosis proteins (IAPs). Cancer cells also have impaired death receptor signalling pathways caused by reduced expression of death receptors. The extrinsic death receptor pathway (Fig 1.2 Left) and the intrinsic mitochondrial pathway (Fig 1.2 Right) are two main apoptotic pathways (Tait *et al.*, 2014; Lopez and Tait, 2015). In cancer therapy, apoptosis is a preferred mode of cell death because it occurs in an orderly, non-inflammatory manner. Apoptotic cells are efficiently cleared by phagocytic cells, such as macrophages, thereby preventing the release of intracellular contents that could trigger inflammation. This process also reduces the risk of tumour lysis syndrome, a potentially life-threatening complication associated with the rapid death of cancer cells (Vaidya and Acevedo, 2015).

1.4.2.4.1Extrinsic/ death receptor apoptotic pathway

Tumour necrosis factor-related apoptosis-inducing ligand (TRAIL) triggers apoptosis by binding to its death receptors DR4 (TRAIL-R1) and DR5 (TRAIL-R2), which contain cytoplasmic death domains (DDs), Fig. 1.2 on the left, (Su *et al.*, 2015). Ligand binding promotes trimerization of these receptors, facilitating the recruitment of the adaptor protein Fas-associated death domain

(FADD). FADD, through its death effector domain (DED), then recruits initiator procaspases 8 and 10 to form the death-inducing signalling complex (DISC) (Liu *et al.*, 2017).

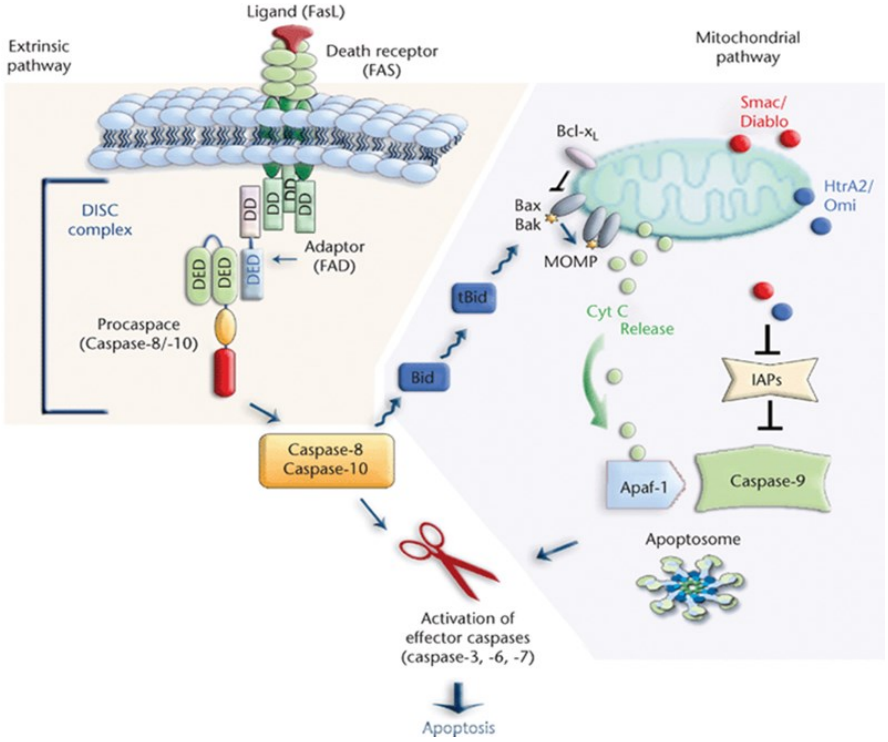


Fig. 1.2 Diagram showing the extrinsic (LEFT) and intrinsic (RIGHT) apoptotic pathways. FasL binding to the Fas receptor activates the extrinsic apoptosis pathway (LEFT) via intracellular death domain (DD) interacts with FADD, and TRADD, which also have DD motifs. FADD recruits procaspase-8 and -10 using its death effector domain (DED) while Fas uses the DD, forming a death inducing signalling complex (DISC) which is required for caspase-8 activation. Caspase-8 then cleaves downstream effector caspases and truncates Bid, a pro-apoptotic Bcl-2 family member. tBid converges on the extrinsic and the intrinsic pathways. tBid activates Bax and Bak, which antagonises Bcl-2 and Bcl-xL, to enhance mitochondrial outer membrane permeabilization (MOMP). MOMP releases apoptogenic mitochondrial components including cytochrome c, Smac/Diablo, and HtrA2/Omi. The release of cytochrome c initiates the intrinsic apoptotic pathway (RIGHT). Cytochrome *c* recruits procaspase-9 and oligomerizes Apaf-1 to form an apoptosome, which activates caspase-9. Caspase-9 then cleaves effector caspases. While Smac and HtrA2 neutralise IAPs which inhibit caspases. This causes apoptosis execution (Cairrao and Domingos, 2010; License Number: 6093001483503).

Within DISC, procaspases 8/10 are activated via dimerization and autocatalytic cleavage. Activated caspase-8/10 directly cleaves and activates executioner caspases-3, -6, and -7, leading to cell death (Pimentel *et al.*, 2023). Additionally, caspase-8 cleaves the B cell lymphoma-2 (Bcl-2) homology 3 protein (BH3), BH3-interacting domain protein (Bid) into its truncated form (tBid), which translocate to mitochondria and activates Bcl-2-associated X protein (Bax)/ Bcl-2 antagonist/killer (Bak), inducing mitochondrial outer membrane permeabilization (MOMP). This pathway is tightly regulated by cellular FLICE-like inhibitory protein (c-FLIP), a catalytically inactive caspase-8 homolog, can be recruited to DISC and block procaspase-8 activation resulting to the inhibition of the extrinsic apoptotic pathway (Weinlich *et al.*, 2013). Importantly, TRAIL-induced apoptosis involves both extrinsic (DISC-mediated) and intrinsic (mitochondrial) pathways, and it is dependent on the balance between the pro- and anti-apoptotic proteins (Pimentel *et al.*, 2023).

1.4.2.4.2 The intrinsic/ mitochondrial pathway

In the mitochondrial pathway, the internal stimuli like DNA damage, hypoxia, oxidative stress, and anti-tumour drugs cause an increase in mitochondrial permeability causing the release of cytochrome c to the cytoplasm, Fig. 1.2 on the right, (Galluzzi *et al.*, 2018). The release of cytochrome c stimulates the formation of the apoptosome which consists of cytochrome *c*, apoptotic protease-activating factor-1 (APAF-1), deoxyadenosine triphosphate and procaspase-9 (Tait and Green, 2010). Inside the apoptosome, procaspase-9 is activated into active caspase-9 which in turn activates the executioner caspases-3 and -7. The executioner caspases cleaves proteins and cause cell death (Tait and Green, 2010; Galluzzi *et al.*, 2018).

The mitochondrial membrane may release pro-apoptotic proteins such as apoptosis-inducing factor (AIF), second mitochondria-derived activator of caspases/ direct inhibitor of apoptosis protein-binding protein with low pI (Smac/DIABLO) and temperature requirement protein A (Omi/HtrA2) (Lopez and Tait, 2015)(Lopez and Tait, 2015). Smac/DIABLO mediates caspase-3 and caspase-9 activation by binding to inhibitor of apoptosis proteins (IAPs): x-linked inhibitor of protein (XIAP) and cellular inhibitor of apoptosis 1 and 2 (cIAP1, and cIAP2) (Galluzzi *et al.*, 2018). Omi/HtrA2, when released from the mitochondria, cause IAP degradation via binding to IAP-binding motif,

causing ubiquitination and proteasomal degradation, thereby blocking the inhibitory effects of IAPs, Fig 1.2 right, (Lopez and Tait, 2015; Galluzzi *et al.*, 2018).

1.4.2.4.3 Regulation of apoptosis by the caspases

Apoptosis is tightly regulated by a family of proteases known as caspases (cysteine-aspartic proteases), which exist as inactive zymogens and are activated in response to specific apoptotic signals (Cavalcante *et al.*, 2019). Caspases are classified into initiator caspases such as caspase-2, caspase-8, caspase-9, and caspase-10, and executioner or effector caspases, including caspase-3, caspase-6, and caspase-7 (Sebbagh *et al.,* 2001). Initiator caspases function at the upstream apoptotic pathways and are activated through dimerization within large multiprotein complexes such as apoptosome or DISC. Once activated, they cleave and activate executioner caspases, which then mediate the execution phase of apoptosis by targeting structural and regulatory proteins (Walsh *et al.,* 2008; Olsson and Zhivotovsky, 2011). Executioner caspases such as caspase-3 and caspase-7 play important roles in the execution phase of apoptosis. Once activated, caspase-3 cleaves a host of cellular substrates to trigger the morphological and biochemical characteristics of apoptosis. One of its most important targets is the inhibitor of caspase-activated DNase (ICAD); cleavage of ICAD releases CAD, which translocate to the nucleus and fragments DNA (Jänicke *et al.*, 1998; Slee *et al.*, 2001; Walsh *et al.*, 2008; Olsson and Zhivotovsky, 2011).

Caspase-3 and caspase-7 cleaves cytoskeletal proteins, including gelsolin, leading to cell shrinkage, membrane blebbing, and formation of apoptotic bodies (Coleman *et al.*, 2001; Sebbagh *et al.*, 2001). These morphological changes facilitate the recognition and clearance of apoptotic cells by phagocytes. Overall, caspases constitute the central regulation of apoptosis, integrating signals from both the intrinsic and extrinsic pathways and executing the orderly dismantling of the cell. Their regulation ensures that apoptosis occurs in a controlled manner, preventing inflammation and maintaining tissue homeostasis (Cavalcante *et al.*, 2019).

1.5 Proteins involved in the regulation of apoptosis.

Apoptosis is a tightly controlled process and multiple transcriptional proteins such as p53, nuclear factor kappa B (NF-κB), haem oxygenase-1(HMOX-1) enzyme and the Bcl-2 family of proteins have significant roles in the modulation of apoptosis.

1.5.1 Tumour suppressor p53

The tumour suppressor protein p53, also known as "*the Guardian of the Genome"*, is a transcription factor that regulates genes involved in DNA repair, cell cycle progression, senescence, and apoptosis (Helton & Chen, 2007; Tait & Green, 2010; Dolan *et al.,* 2015; Marvalim *et al.,* 2023a). These regulatory functions are activated in response to intra- and extracellular stress stimuli, including hypoxia, ROS, DNA damage, and chemotherapeutic agents (Madan *et al.,* 2019; Wang *et al.,* 2019; Mancikova *et al.,* 2023).When activated, p53 translocate to the nucleus and trigger the transcription of genes involved in cell cycle regulation, such as p21 (Georgakilas *et al.*, 2017; Duffy *et al.*, 2022). p53 promotes the intrinsic apoptotic pathway by upregulating pro-apoptotic genes for Bax, phorbol-12-myristate-13-acetate-induced protein 1 (Noxa), AIF-1, Puma, and Bid. The transcription of tumour necrosis factor receptor family like as fibroblast-associated cell-surface antigen (Fas), DR5, and TRAIL, which are involved in extrinsic apoptotic signalling are regulated by p53, as show in Fig 1.3 left panel (Tait and Green, 2010; Chen, 2016; Marvalim *et al.*, 2023).

The function of p53 is modulated by multiple post translation modifications (PTM) including phosphorylation which is the most common PTM (Sankunny and Eng, 2018; Liu *et al.*, 2021; Xin Li *et al.*, 2022). Phosphorylation is required for p53 stabilization, accumulation, and translocation to the nucleus, where it activate or regress its target genes. Phosphorylation of p53 at serine residues is a primary modification in response to DNA damage (Xin Li *et al.,* 2022). Tumour suppressor p53 is phosphorylated at specific serine amino acid residues including s15, s46 and s392. This is necessary for p53 physiological function (Abuetabh *et al.*, 2022). The levels of p53 are attenuated back to normal or kept low due to proteasomal degradation regulated by E3 ubiquitin ligase MDM2. MDM2 attaches to p53 and degrade it via ubiquitination (Haupt *et al.*, 1997; Yue *et al.*, 2017).

The *TP53* gene encodes for p53, however, in many cancers, including TNBC the p53 gene is mutated, as a result, the p53 tumour suppressive functions are lost (Bae *et al.*, 2014). Mutant p53 accumulate in cancer cells to disrupts the functions of wild-type p53 and promotes gain-of-function (GOF) mechanisms and engages with transcription factors to modulate genes that facilitate cancer progression and survival, Fig. 1.3 Right panel (Hui *et al.*, 2006; Yue *et al.*, 2017). Studies have

reported that 70 - 80 % of TNBC cases display *TP53* mutations, contributing to the tumour aggressiveness, poor prognosis, and chemoresistance (Olivier *et al.*, 2002; Curtis *et al.*, 2012; Meric-Bernstam *et al.*, 2018).

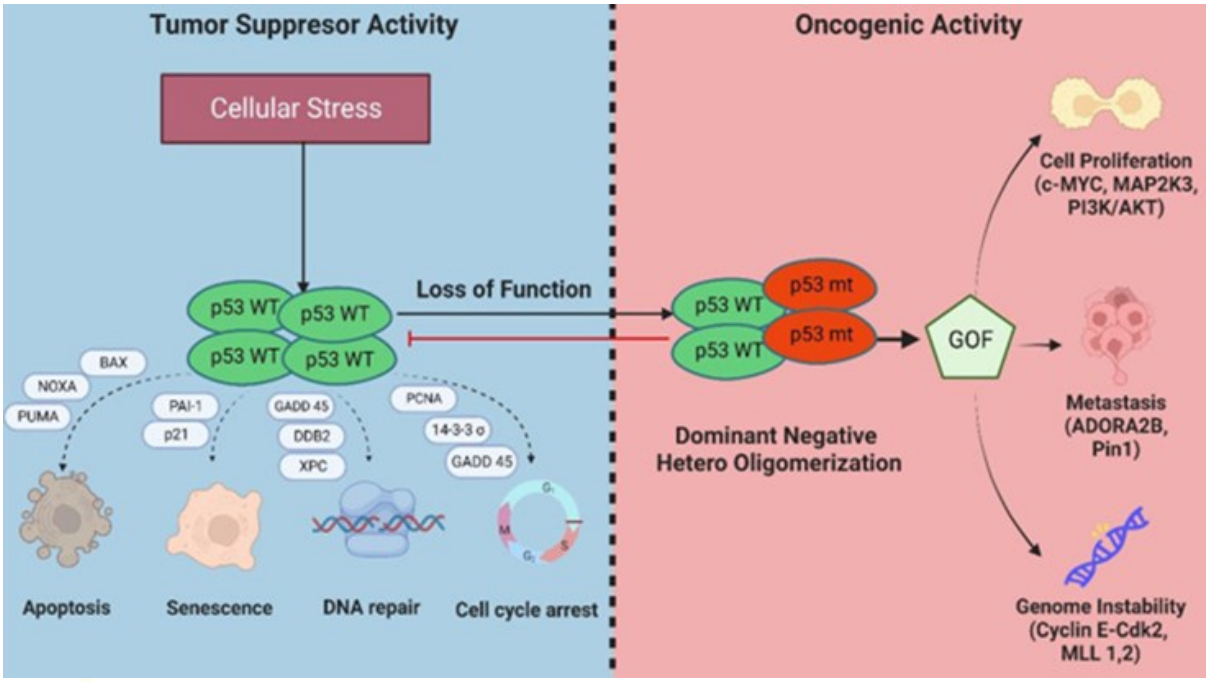


Fig. 1.3 Mechanisms of inactivation of the tumour suppressive activity of wild-type p53 and GOF activities in mutant p53-bearing breast tumours. Wild type p53 tumour suppressor activity (blue panel on the left) is initiated upon cellular stress, causing the translocation of p53 into the nucleus and triggering the transcription of pro-apoptotic genes such as Bax, NOXA, and PUMA to promote the intrinsic apoptotic pathway. Senescence is regulated by transcription of cyclin-dependent kinase inhibitor 1A (p21) and plasminogen activator inhibitor-1. DNA repair mechanisms are initiated after the transcription of growth arrest and DNA damage-inducible genes (GADD45), damage-specific DNA-binding protein 2 (DDB2), and xeroderma pigmentosum, complementation group C (XPC). Activated p53 also promotes the transcription of genes involved in cell cycle regulation, such as proliferating cell nuclear antigen (PCNA), 14-3-3σ (stratifin), and GADD45. Mutant p53 (red panel on the right) may exhibit dominant-negative activity or acquire oncogenic gain-of-function (GOF) properties that destruct wild-type p53 functions. Mutant p53 drives the transcription of genes involved in cell proliferation, including cellular myelocytomatosis oncogene (c-MYC), mitogen-activated protein kinase 3 (MAPK3), and phosphoinositide 3-kinase/AKT (PI3K/AKT). It also interacts with the adenosine A2b receptor and Pin1 to promote metastasis. Genomic instability is facilitated through modulation of cyclin E–CDK2 activity and DNA methyltransferases 1 and 2 (DNMT1 and DNMT2), as described by Marvalim *et al.,* (2023); CC-BY Licence: https://creativecommons.org/licenses/by/4.0/)

1.5.2 The B cell lymphoma-2 protein family

The intrinsic apoptotic pathway is primarily regulated by the bcl-2 family of proteins, which control the mitochondrial outer membrane permeability and determines cell survival or death (Singh *et al.*, 2019). These proteins are characterized by conserved bcl-2 homology (BH) domains that enable protein-protein interactions which is important in apoptosis regulation. Anti-apoptotic members such as Bcl-2, B-cell lymphoma-extra-large (Bcl-xL), Myeloid cell leukaemia 1 (Mcl-1), and B-cell lymphoma-w (Bcl-w) possess BH1– 4 domains and function to maintain mitochondrial integrity by sequestering pro-apoptotic proteins (Eom *et al.*, 2016).

Conversely, the pro-apoptotic group includes BH3-only proteins like BH3-interacting domain death agonist (Bid), Bcl-2-interacting mediator of cell death (Bim), and p53 upregulated modulator of apoptosis (Puma) (activators), Bcl-2-associated agonist of cell death (Bad) and noxa (sensitizers), and pore-forming effectors such as Bcl-2-associated X protein (Bax) and Bcl-2 antagonist/killer (Bak). These proteins facilitate MOMP, a point of no return in apoptosis. Dysregulation of Bcl-2 family protein expression particularly the overexpression of anti-apoptotic members is frequently observed in breast cancer and is associated with apoptotic evasion, chemoresistance, and disease progression (Czabotar *et al.*, 2014; Eom *et al.*, 2016; Singh *et al.*, 2019).

Among the pro-apoptotic effectors, Bad, a BH3-only sensitizer, promotes apoptosis by displacing Bax from Bcl-2/Bcl-xL complexes, a process tightly regulated by phosphorylation via kinases including protein kinase A (PKA), mitogen-activated protein kinase (MAPK), and protein kinase B (AKT) (Wen *et al.*, 2019). When phosphorylated, Bad is sequestered in the cytoplasm, rendering it inactive and promoting cell survival. Overexpression of Bcl-2 and Bcl-xL in breast cancer inhibits these pro-apoptotic interactions, contributing to tumour aggressiveness and resistance to therapy. Therapeutic strategies targeting Bcl-2 family members such as venetoclax and Abbott Laboratories compound 737 (ABT-737), which mimic BH3-only proteins are under development to restore apoptosis sensitivity and overcome treatment resistance (Datta *et al.*, 2000; Wen *et al.*, 2019; D'Aguanno and Del Bufalo, 2020).

1.5.3 Nuclear factor-kappa B signalling

Nuclear factor-kappa B (NF-κB) is a transcription factor that is translocated from the cytoplasm to the nucleus following phosphorylation of the inhibitor of NF-κB proteins (IκB). In the canonical pathway, NF-κB dimers are governed by inhibitory molecules of the IκB family, which prevents their translocation into the nucleus (Gambhir *et al.*, 2015). Extracellular stimuli such as pro-inflammatory cytokines; bacterial toxin; viral products; and cell death stimuli (free oxygen radicals, UV light, gamma (γ)-radiation) activates the IκB kinase (IKK) complex (IKK, IKK beta (β), and IKKγ), which phosphorylates and mediates the ubiquitination of IκB and its subsequent degradation by the proteasome (Cetraro *et al.*, 2022; Siegmund *et al.*, 2022). This results in translocation of NF-κB into the nucleus and initiation of target gene expression. In the non-canonical pathway, IκB is absent (Gambhir *et al.,* 2015; Siegmund *et al.,* 2022).

Signalling from cluster of differentiation 40 ligand (CD40L), lymphotoxin β receptor (LTβR), and B cell-activating factor receptor (BAFFR) leads to NF-κB-inducing kinase (NIK) activation, Activated NIK phosphorylate and activate the homodimer IKKα/IKKα, which transfers the phosphate group to the C-terminal residues of p100 facilitating ubiquination and processing to p52. p52, which dimerizes with v-rel avian reticulo endotheliosis viral oncogene homolog B (RelB) translocate to the nucleus and cause activation of NF-κB target genes involved in cell survival and proliferation (Gambhir *et al.*, 2015; Siegmund *et al.*, 2022). NF-κB activation has been linked to the inhibition of apoptosis. This is achieved by modulating anti-apoptotic genes and genes that promote cancer cell survival (Rovillain *et al.*, 2011).

In the nucleus, NF-κB transcribes for genes encoding for cell cycle regulatory proteins like cyclin D1, proteins that stabilize membrane of the mitochondria, Bcl2-related protein A1 (BFL-1) and Bcl-xL, caspase suppressors cIAP1/2, and TNF receptor-associated factors, TRAF1 and TRAF2. These proteins inhibit apoptosis by blocking caspase 8 activation and directly binding to downstream mediators causing inhibition of their effects (Rovillain *et al.*, 2011; Gambhir *et al.*, 2015; Siegmund *et al.*, 2022). Exploring cell-specific pathways of NF-κB, will aid in the unravelling of cell death signalling networks and the identification of specific targets of the copper complexes.

1.5.4 Cyclin-dependant kinase inhibitor, p21

Cyclin-dependant kinase inhibitor, p21, belongs to the family of cyclin-dependent kinase inhibitors (CDKIs), which regulate cell cycle progression and stress response. The activity of p21 regulate cyclin-CDK complexes, specifically CDK2 and CDK1, causing cell cycle arrest in the gap phase 1 and 2/mitotic phase (G1 and G2/M phases). Cell cycle arrest creates a window for DNA repair, ensuring genomic stability when cells are exposed to genotoxic compounds (Abbas and Dutta, 2010). The function, localization, protein-protein interaction, stability, and degradation of p21 is regulated by transcriptional factors such as, posttranscriptional regulators like microRNAs (miRNAs) and phosphorylation. p21, which is primarily regulated by the tumour suppressor p53, is rapidly increased in response to cellular stress and DNA damage (Katner *et al.*, 2002; Abbas and Dutta, 2010).

Subcellular distribution and localisation have significant roles on the physiological functions of p21. In the nucleus, p21 cause cell cycle arrest and contribute to cellular senescence, acting as tumour suppressors (Dolan *et al.*, 2015). In the nucleus, p21 binds to proliferating cell nuclear antigen (PCNA) and inhibits PCNA-dependent DNA replication and repair processes, ensuring inhibition of uncontrolled cell division (Georgakilas *et al.*, 2017). Cytoplasmic p21 has been shown to interact with apoptotic regulators such as caspase-3, caspase-8, and apoptosis signal-regulating kinase 1 (ASK1), suppressing apoptosis and promoting cell survival, especially in p53-deficient cells, where the anti-apoptotic activity of p21 may contribute to cancer development (Kreis *et al.*, 2019). The functional results of p21 are context dependant, influenced by cellular localisation, upstream regulatory signals, and specific cellular stressors, making it a potential target in cancer treatment.

1.5.5 Regulation by inhibitors of apoptosis proteins

The inhibitor of apoptosis proteins (IAPs) is a family of anti-apoptotic regulators, defined by baculovirus IAP repeat (BIR) domains, which are zinc-coordinating regions essential for mediating protein-protein interactions (Finlay *et al.*, 2017). IAPs, include well-studied members such as X-linked inhibitor of apoptosis protein (XIAP) also called BIRC4, cellular Inhibitor of apoptosis 1 (cIAP1) also termed BIRC2, cellular Inhibitor of apoptosis 2 (cIAP2) alternatively

referred as BIRC3, survivin, and livin directly bind to and inhibit the activation of caspases-3,-7,and -9, thus promoting cancer cell survival (Fulda, 2014; Finlay *et al.*, 2017; Albadari and Li, 2023).

These proteins contain the RING domain, which confers E3 ubiquitin ligase activity, allowing them to ubiquitinate target proteins for degradation, further enhancing their anti-apoptotic function in various cancers, where they contribute to tumour progression, metastasis, increased morbidity and chemoresistance (Finlay *et al.*, 2017). In addition to the inhibition of caspase-3 and -7, cIAP1 and cIAP2 regulate survival pathways by modulating the NF-κB signalling pathway, which is implicated in inflammation and cell survival through interactions with TNFR-associated factor 1and 2 (TRAF1 and TRAF2) (Varfolomeev *et al.*, 2008; Zheng *et al.*, 2010; Dumétier *et al.*, 2023).

XIAP, livin and survivin are often upregulated in haematological malignancies and solid tumours, aiding in immune evasion and increasing the ability of the tumours to resist apoptosis induced by chemotherapeutic agents. All three proteins bind to and inhibit caspase-3, -7 and -9 to inhibit apoptosis, as reviewed in (Fulda, 2014; Lalaoui and Vaux, 2018). Notably, survivin is highly expressed in breast cancer, serves as a prognostic marker and therapeutic target due to its role in inhibiting caspase activation and promoting mitotic cell division (Albadari and Li, 2023). Found in both the cytoplasm and nucleus, survivin associates with other IAPs, like XIAP, to enhance their stability (Soleimanpour and Babaei, 2015; Albadari and Li, 2023). Upregulation of IAPs in breast cancer make them a target of interest for therapies aiming to restore apoptosis in resistant tumours.

1.5.6 Heat shock proteins

Heat shock proteins (HSP), including the major kinds HSP27, HSP60, HSP70, and HSP90, function as molecular chaperones, ensuring normal protein folding and preventing misfolded protein aggregation. Stressors like heat, oxidative damage, and anticancer therapies all induce their expression. Hight levels of HSP27 in breast cancer cells are associated with proliferation, invasion and drug resistance (Wang *et al.*, 2020; Bi *et al.*, 2023). The role of HSP60 in the cells in dependent on the location. In the mitochondria, HSP60 inhibit apoptosis by binding to mitochondrial p53 and promote cell survival (Ghosh *et al.*, 2008).

When expressed in the endoplasmic reticulum, HSP60 inhibit the expression of XIAP and allow for apoptosis to occur (Arya *et al.*, 2015). Expression of HSP60 on the cell membranes promotes breast cancer metastasis by interacting with α3β1 integrin (Cappello *et al.*, 2014). HSP70 is a marker for poor prognosis and promotes cell proliferation, migration and tumorigenesis (Mawatari *et al.*, 2015; Chanteloup *et al.*, 2020). HSPs have important roles in cellular survival in cancer, where they may promote tumour progression by increasing stress tolerance and suppressing cell death pathways.

1.5.7 Haem oxygenase

Haem oxygenase enzymes, particularly the isoforms haem oxygenase-1 (HMOX-1) and haem oxygenas-2 (HMOX-2), are essential in the degradation of haem to biliverdin, carbon monoxide, and free iron (Tenhunen *et al.*, 1968). Biliverdin is converted into bilirubin by biliverdin reductase, bilirubin acts as a potent antioxidant, scavenging reactive oxygen species (ROS). Carbon monoxide acts as a signalling molecule that can reduce inflammation and inhibit apoptosis. Free iron though potentially toxic, is sequestered by ferritin, a storage protein, minimizing its pro-oxidant effects and contributing to iron homeostasis (Su *et al.*, 2022).

HMOX-1 also called HSP32, is an inducible 32 kDa oxidative stress response protein, whereas HMOX-2 is constitutively expressed with a molecular weight of around 36 kDa. HMOX-1 primarily localizes in the smooth endoplasmic reticulum (sER) but can translocate to the nucleus and mitochondria under stress conditions, while HMOX-2 is predominantly found in the sER and brain tissue, where it plays a role in maintaining basal haem homeostasis, ensuring continuous production of protective byproducts like CO and bilirubin (Gandini *et al.*, 2019; Mascaró *et al.*, 2021). Both HMOX-1 and HMXO-2 have roles in cellular defence against oxidative stress, both enzymes produce bilirubin and CO, which neutralize ROS and prevent oxidative damage. By alleviating oxidative stress and inflammation, these enzymes promote cell survival in conditions of oxidative or inflammatory stress (Wu *et al.*, 2021).

The transcription of the HMOX-1 gene is regulated by various transcription factors including hypoxia inducing factor 1- alpha (HIF-1α), NFκB, nuclear factor erythroid 2-related factor-2 (Nrf2), and activator protein 1 and 2(AP-1) (Podkalicka *et al.*, 2017).

HMOX-1 is expressed in many cancers, including breast cancer (Podkalicka *et al.*, 2017; Gandini *et al.*, 2019), but the exact role of HMOX-1 in breast cancer, whether promoting cancer cell survival or cell death remains unclear (Noh et al., 2013; Luu-Hoang et al., 2021). HMOX-1 may be colocalized in the nucleus and, or cytoplasm depending on stimuli and function ((Noh *et al.*, 2013; Biswas *et al.*, 2014; Gandini *et al.*, 2019).

In cancer cells subjected to oxidative stress, HMOX-1 may translocate from the ER to the nucleus, where it can engage in gene transcription as a cofactor, independently of its enzymatic function. Nuclear HMOX-1 is a truncated form, enzymatically inactive and associated with more aggressive tumours (Hwang *et al.*, 2009). In contrast, cytoplasmic HMOX-1 is assumed to be enzymatically active and required for the normal cell survival response to oxidative stress (Gandini *et al.*, 2019). In breast cancer HMOX-1 expression correlates with poorer prognoses, influencing the tumour microenvironment, promoting angiogenesis, and enabling immune evasion. These attributes mark HMOX-1 as a potential target for cancer therapy (Chen *et al.*, 2022; Su *et al.*, 2022).

1.6 Novel anti-cancer drugs

The discovery of platinum-based compounds such as cisplatin, oxaliplatin and carboplatin, as potent anti-cancer chemotherapeutic drugs has led to the investigation of other metal-based drugs such as copper, ruthenium, and gold, (Oun *et al.*, 2018). Platinum agents are cytotoxic DNA damaging agents leading to DNA strand breaks and apoptosis (Silver *et al.*, 2010). Several clinical trials have investigated platinum agents as a treatment option in TNBC patients. Some studies indicated platinum agents as good anticancer drugs while other studies proved otherwise (Guan *et al.*, 2015). Based on current breast cancer guidelines, the use of platinum agents to standard neoadjuvant chemotherapy in unselected TNBC patients is not recommended while its use may be considered in breast cancer patients harbouring BRCA mutations since their mechanism of action is suitable for cells with DNA repair deficiency (Oun *et al.*, 2018). Furthermore, the use of platinum-based drugs is associated with drug resistance and adverse drug reactions such as nephrotoxicity, myelosuppression, and neurotoxicity, cardiotoxicity and pain (Oun *et al.*, 2018). The search for new drugs with improved, wider efficacy and selectivity is warranted.

1.6.1 Metal-based complexes

1.6.1.1 Gold complexes

The application of gold (I) in medicine was first reported in the treatment of rheumatoid arthritis, with auranofin, an oral gold (I) compound, being approved by the FDA for rheumatoid arthritis (Kean and Kean, 2008). Auranofin has shown potential anticancer activity in various cancer cells including breast cancer cells. It has been reported to act by inhibiting thioredoxin reductase (TrxR), thereby increasing oxidative stress in cancer cells, leading to mitochondrial dysfunction and apoptosis (Valko *et al.*, 2016; Hatem *et al.*, 2019; Momose *et al.*, 2021). Auranofin lacks selectivity causing limitation to its therapeutic efficacy in breast cancer.

Based on the chemical structure of Auranofin, researchers have explored modifications to enhance its anticancer activity and selectivity. One approach involves incorporating ferrocenyl and triazolylidene ligands into gold complexes, further optimizing their pharmacological potential. The ferrocenyl moiety contributes to redox reactivity, improving intracellular bioavailability and facilitating electron transfer reactions, which may enhance cytotoxicity (Perez *et al.*, 2015). Triazolylidene ligands are strong sigma (σ)-donors that stabilize the gold centre, allowing for targeted interactions with cysteine and selenocysteine residues in proteins (Aucamp *et al.*, 2018). A variety of gold complexes have been synthesized and tested for anticancer activity as reviewed in (Porchia *et al.*, 2018).

Anticancer properties of triphenylphosphine gold chloride, [AuCl(PPh3)], and its ability to stimulate autophagy have given insights into the biological properties of this class of gold complexes. In another study gold ferrocenyl-substituted N-heterocyclic carbene was shown to inhibit cell proliferation of A549 cells at low micromolar concentrations and increase ROS by inhibition of thioredoxin reductase (TxR). Gold complexes have been shown to cause apoptotic cell death mediated by oxidative stress and activation of the caspases (Porchia *et al.*, 2018; Reddy *et al.*, 2018; Gorini *et al.*, 2021; Olelewe *et al.*, 2022). Aucamp *et al.* (2018) reported that gold (i)-ferrocenyl-1,2,3-triazol-5-ylidene inhibited cell proliferation in lung cancer cells at sub-micromolar IC_{50} values. Additionally, the study showed that the most active gold complex caused cell morphology changes associated with apoptotic cell death (Aucamp *et al.*, 2018).

1.6.1.2 Copper complexes

Copper is an essential trace element that plays key roles in cellular respiration, antioxidant defence, and connective tissue formation. In the human body, copper is predominantly bound to proteins and enzymes such as cytochrome c oxidase, superoxide dismutase, and ceruloplasmin where it is oxidized between Cu(I) and Cu(II) oxidation states to mediate redox reaction important for cellular metabolism. Copper is perceived to have lower toxicity in normal cells compared to platinum-based complexes These observations have motivated for the development of copper complexes as anticancer agents. Copper complexes of different ligand scaffolds have been shown to have antiproliferative effects in a variety of cancer cells as reviewed in (Tisato *et al.*, 2010; Marzano *et al.*, 2012; Santini *et al.*, 2014; Gordan *et al.,* 2022).

1,10-Phenanthroline (Phen) is a chelating ligand that has been shown to inhibit matrix metalloproteinases *in vitro* (Bencsik *et al.,* 2017). 1,10-phenanthroline scaffolds intercalate between guanine–cytosine base pairs through the main groove and achieve stable intercalation in adenine–thymine base pairs when carbon–hydrogen/ π-hydrogen bond (CH/π) interactions are improved by a methyl substitution (Sánchez-González & Gil, 2021a). Theophylline, a 1,3-dimethylxanthine, is a naturally occurring alkaloid in the xanthine family. Theophylline is used clinically for the management of asthma (Barnes, 2013). Studies have theophylline to display anti-breast-cancer properties in MCF-7 cells by supressing serine/arginine-rich splicing factor 3, altering p53α to p53β, and inducing apoptosis and G2/M arrest (Chang *et al.,* 2017). The 8-aminoquinoline ligand is metal a chelating ligand with a rigid structure (Facchetti *et al.,* 2019; Ali *et al.,* 2021).

While naphthyl ligands, such as 1,8-naphthalimides, originate from the naphthalene-imide function as planar DNA intercalators and topoisomerase inhibitors (Zhang *et al.,* 2024). Several Cu(I) and Cu(II) complexes co-ordinated in different ligands have been shown to inhibit the 26S proteasome, and subsequent activation of endoplasmic reticulum stress responses and paraptosis-like cell death which is caspase-independent mechanism characterized by cytoplasmic vacuolization (Gandin *et al.*, 2012; Ng *et al.*, 2014; Li *et al.*, 2019). In addition, the generation of ROS, leading to oxidative DNA damage, lipid peroxidation, and mitochondrial dysfunction has been linked to the cytotoxicity of copper complexes (Ng *et al.*, 2014; Li *et al.*, 2019).

Some copper complexes selectively inhibit thioredoxin reductase (TrxR), disrupting redox homeostasis and inducing apoptosis or non-apoptotic death (Santini *et al.*, 2011; Gandin *et al.*, 2014). Studies from our research group have reported that chelating copper complexes bearing different ligands were cytotoxic with IC_{50} values below 5 μM and induced oxidative stress mediated intrinsic apoptotic cell death, evidenced by increased ROS and HMOX-1expression in colorectal and pancreatic cancer cells (Harmse *et al.*, 2019; Ismail *et al.,* 2022; Jhetam *et al.*, 2025). These mechanisms show that copper complexes could be useful as alternative therapy, especially in aggressive cancers like TNBC that resist treatment or do not respond to cell death signals.

1.7 *In vitro* models of TNBC and mammary epithelial cells

Cell lines are immortalized populations grown under controlled laboratory conditions to study cellular behaviour, disease mechanisms, and therapeutic responses. These models have proven to be important in cancer research due to their reproducibility, cost-effectiveness, and adaptability. While they cannot fully replicate the clinical tumour microenvironment, they offer a simplified and manipulable model to dissect molecular pathways, and drug responses in tumour progression (Kathryn *et al.*, 2012).

1.7.1 TNBC cell model: MDA-MB-231

The MD Anderson Metastatic Breast- 231 (MDA-MB-231) cell line is one of the most extensively studied models of triple-negative breast cancer. It was derived from a pleural effusion of a Caucasian female with metastatic breast cancer in the 1970s, MDA-MB-231 cells are classified as basal B subtype, display a mesenchymal phenotype, and grow as elongated, spindle shaped cells. These cells harbour mutant *TP53*, and demonstrate increased migration and invasive properties (Huang *et al.*, 2020).

1.7.2 Mammary epithelial cell model: MCF-10A cells

The Michigan Cancer Foundation-10A (MCF-10A) is a model used to study the behaviour of normal human breast epithelial cells. It originates from benign proliferative breast tissue and spontaneously immortalized, without the addition of defined oncogenic factors (Martin and Leder, 2001).

These cells are non-tumorigenic and lack oestrogen receptor expression. They are characterized by the loss of the chromosomal region containing the *p16* and *p14ARF* genes which are the regulators of cellular senescence and lack the accumulation of the *Myc* oncogene (Soule *et al.,* 1973; Martin and Leder, 2001).

1.8 Problem statement

TNBC is an aggressive subtype of breast cancer that lacks the expression of ER, PR and HER2, causing poor responsiveness to hormone and HER2-targeted therapies. Consequently, patients with TNBC have limited treatment options, contributing to poor prognosis, with high rates of recurrence and metastasis. Conventional chemotherapy remains the standard of care treatment, but its efficacy is reduced by systemic toxicity and the occurrence of drug resistance. These limitations show the need for the formulation of alternative therapeutic agents with improved selectivity and reduced adverse effects. This study seeks to evaluate the antiproliferative effects and the mechanisms of cell death induced by active copper and gold complexes in MDA-MB-231 TNBC cells, with the aim of contributing to the development of alternative therapeutic strategies.

1.9 Aim

Evaluate the efficacy, mechanism of cell death and modulation of cell death signalling networks of copper and gold complexes using MDA-MB-231 TNBC cells.

1.10 Objectives

- Identify active complexes by exposing the MDA-MB-231 cells to a small library of copper, and gold complexes, and a manganese complex
- Determine IC_{50} values of the active metal complexes in MDA-MB-231.
- Determine the IC_{50} values of the active metal in MCF-10A to assess selectivity.
- Evaluate the effects of the active metal complexes on cell morphology of MDA-MB-231 and MCF-10A cells to preliminary determine the mode of cell death.
- Determine the ability of the active metal complexes to cause ROS.
- Evaluate the effects of the active metal complexes on mitochondrial integrity of MDA-MB-231 breast cancer cell lines.

- Investigate if the active metal complexes cause apoptosis by assessing apoptosis markers such as annexin V binding and caspase-3/7 activation in MDA-MB-231 breast cancer cells.
- Evaluate the type of apoptotic pathway activated either the intrinsic apoptotic pathway identified by caspase-9 activation or extrinsic apoptotic pathway by assessing caspase-8 activation.
- Evaluate the effects of the copper complexes apoptosis-related proteins using a human apoptosis proteome array.
- Investigate the effects of copper complexes on the expression and subcellular location of NIK, phospho-p53(s15), p21, and HMOX-1 in MDA-MB-231 cells using immunofluorescence.
- Determine the effects of copper complexes on the expression and molecular size of HMOX-1
- Evaluate the effects of efficacy of the copper complexes in the presence of HMOX-1 inhibitor

Chapter Two: Methods And Materials

2.0 Introduction

This chapter describes the methods and materials used to evaluate the cytotoxicity, mechanisms of cell death and effects on apoptosis related proteins of metal-based complexes on the MDA-MB-231 breast cancer cell line. In addition, the cytotoxicity of the metal complexes was compared to that of a normal mammary epithelial cell line, MCF-10A.

2.1 Metal complexes

A small library of eight metal complexes comprised of copper(II)- and manganese(II)- and gold(I) complexes were evaluated for biological activity. This included phenathroline theophylline mixed ligand complexes with copper and manganese; $CuTh_2$, $CuPhenTh_2$, $MnTh_2$**,** an 8-aminoquinolone-naphthyl copper complex **(**Cu8AqN**)**, and gold(I) ferrocenyl substituted 1,2,3-triazol-5-ylidene complexes; AuCl(trz-Fc-Dipp), AuPh(trz-Fc-Dipp), $AuPPh_3$(trz_Fc-Dipp), $AuPPh_3$(trz-Ph-Dipp**).** All complexes and their ligands were synthesized, characterized, and structures confirmed with X-ray diffraction crystallography or spectroscopic methods as described by Gordon *et. al.,* 2022; Myeza *et. al.,* 2024; and Aucamp *et.al.* 2018, respectively.

The Cu8AqN, and AuCl(trz-Fc-Dipp), AuPh(trz-Fc-Dipp), $AuPPh_3$(trz-Fc-Dipp), $AuPPh_3$(trz-Fc-Dipp) were synthesized by the researchers in the School of Chemistry at the University of the Witwatersrand. $CuTh_2$, $CuPhenTh_2$, $MnTh_2$ were prepared by the researchers at Nelson Mandela University. Doxorubicin and staurosporine (Sigma) were used as positive controls and all results were compared to untreated cells as negative controls. The Metal complexes were dissolved in culture grade dimethyl sulfoxide (DMSO, PanReac) at stock concentrations of 10 mM for $CuTh_2$, $CuPhenTh_2$, $MnTh_2$, AuCl(trz-Fc-Dipp), AuPh(trz-Fc-Dipp), $AuPPh_3$(trz-Fc-Dipp), $AuPPh_3$(trz-Ph-Dipp). Cu8AqN was prepared at a stock concentration of 3 mM and staurosporine at 1.25 mM. DMSO concentration was less than 1 %. Doxorubicin was prepared in 70 % ethanol at 10mM. The metal complexes were stored at 4 ^{0}C until used. All buffers and solutions were prepared in sterile Milli-Q water.

2.2 Cell culture techniques

Cell culture techniques were used to grow and maintain the cell cultures under controlled laboratory conditions, providing a reliable model for *in vitro* experiments. Strict aseptic procedures were followed throughout to prevent microbial contamination and preserve cell integrity.

2.2.1 Cell lines and ethical clearance

The effects of the metal complexes were evaluated against the MDA-MB-231 triple negative breast cancer cell line and in normal mammary epithelial cells line MCF-10A. Both cell lines were obtained from the American Type Culture Collection (ATCC). The cell lines were tested for authenticity by Iqaba Biotech, SA, using Short Tandem Repeat (STR) profiling. All cell lines were regularly checked for mycoplasma infection with Hoechst 33342. An ethics waiver for the use of the cell lines was obtained from the University of the Witwatersrand Human Research Ethics Committee: W-CBP-190923-01 (Appendix A).

2.2.2 Cell propagation and maintenance

Cells were maintained under aseptic conditions with the use of a laminar flow cabinet (Esco). Cells from the cryovial storage were thawed at 37 º C (Incotherm: Labotec) and transferred to 25 cm^2 culture flasks (Greiner Bio-One) containing 8 ml of culturing media. MDA-MB-231 breast cancer cells were thawed in 1:1 Dulbecco modified eagle medium (DMEM)/ Ham's Nutrient Mixture F-12 (Ham's F12) media (Gibco) supplemented with 20 % heat inactivated fetal bovine serum (FBS) (Gibco), 1 % of L-glutamine, sodium pyruvate, non-essential amino acids, and penicillin-streptomycin (Thermo Fisher). Once the cells were confluent, they were transferred to a 75cm^2 flasks and maintained in 25 ml of the same media formulation, but with the fetal bovine serum concentration reduced to 10 %. MCF-10A cells were thawed as described above but in a different media formulation. Cells were cultured in basal serum-free media for mammary epithelium cells containing human epidermal growth factor (20 ng/ ml), cholera toxin (100 ng/ ml), insulin (0.01mg/ ml), hydrocortisone (500 ng/ ml), bovine pituitary extract (25 mg), and isoproterenol transferrin (Thermo Fisher).

For both cell lines, the culture medium was replaced every three days to remove cell debris and ensure the constant supply of nutrients. The cells were viewed daily to monitor proliferation and check for contamination using the phase contrast viewing method with an inverted microscope (Olympus CK41) Once the cells had reached 80 % confluency, they were sub-cultured by trypsinization.

2.2.3 Cell sub-culturing and cryopreservation

Upon reaching logarithmic growth phase, the cells were passaged with 0.25 % trypsin ethylenediamine tetraacetate (trypsin-EDTA) solution (Sigma-Aldrich) to maintain a desired density for growth. Trypsin is a proteolytic enzyme that is used to hydrolyse proteins at the carboxyl terminal of lysine and arginine amino acids to detach and dislodge the cells from their culture environment and produce a single cell suspension (Rick, 1974). The cells were trypsinized by discarding the media and washing the cells with 5 ml of phosphate-buffered saline (PBS)(137 mM NaCl, 10 mM Na_2HPO_4, 2.7 mM KCl and 1.8 mM KH_2PO_4, pH 7.4) thrice. Thereafter, trypsin (5 ml) was added, the flasks were incubated at 37 ^{0} C/ for 3-5 minutes (min). Trypsin was neutralized with 8 ml of culture media, and the cells were gently resuspended to loosen any aggregated cells. Cell suspension was collected into 15 ml centrifuge tubes (Nest) and centrifuged at 250 x *g* (Thermo^{TM} Scientific Heraeus Megafuge 40) for 5 min to pellet the cells. At this point, the cells were either returned to the flask and /or used for experiments.

2.2.4 Cell cryopreservation

The cells were cryopreserved to prevent transformation. To do this, the supernatant was removed, and the cell pellet was resuspended in 8 mL of freezing medium, which consisted of HAM/DMEM supplemented with 20 % FBS and 5 % DMSO. After mixing the cells gently with a pipette, 1 ml of the cell suspension was aliquoted to 1.5 ml cryogenic vials (Greiner Bio-One). The vials were labelled with the name of the cell line, date, and the passage number, then placed in Cool Cell freezing container (Thermo Scientific) to ensure a controlled freezing process of 1 ^{0} C/ min at -70 ^{0} C.

2.2.5 Cell counting

Cell counting was performed to ensure consistent seeding densities for the experiments. The cell counting was performed with a haemocytometer and trypan blue dye was used to assess the percentage of healthy cells (Sigma-Aldrich). The trypan blue is a dye which permeates the cell membrane of dead cells, staining them blue while living cells remain unstained (Tennant, 1964). To count cells, one part of 0.2 % trypan blue solution was mixed with one part of the single cell suspension (1:1) in a one ml micro-centrifuge tube. Thereafter, ten µl of the solution was added on each side of a haemocytometer and stained or unstained cells were counted using a haemocytometer.

2.3 Cell viability assay: MTT assay

Cell viability was performed according to the method of Mosmann, which uses the reagent 3-(4,5-dimethylthiazol-2-yl)-2,5-diphenyl tetrazolium bromide (MTT), commonly referred to as the MTT assay. MTT calorimetric method was used to assess the effects of the metal complexes on the cancer cells and to determine IC_{50} values for the active metal complexes. The MTT reagent (Thermo Fisher) is a yellow tetrazolium salt, bearing a positive charge and can permeate cell and inner mitochondrial membranes. In the mitochondria of viable cells, nicotinamide adenine dinucleotide (NADH) is reduced to NAD^+ by a mitochondrial dehydrogenase enzyme, and metabolically active cells convert the MTT to purple-blue water insoluble formazan crystals (Mosmann, 1983). The quantity of formazan crystals is directly proportional to the number of viable cells. The formazan crystals were solubilized prior to the measurement of the absorbances. This method was selected as the best method to assess cytotoxicity because it does not involve multiple washings steps, which is likely to cause cell loss.

2.3.1 MTT assay procedure

The assay was performed in both cell lines as described by (Mosmann, 1983) with minor modifications as described below. Cells were plated in 96 well plates at 10 000 cells/well in 100 µl of culture media (Nest) and allowed to adhere over-night. On the next day, the cells were treated with 100 µl of the complexes at double the final concentration. Initially, the cells were treated with 5 and 50 µM to determine which complexes and positive controls were active.

Then the IC_{50} of each active metal complex was determined by treating the cells with a range of concentrations. Each concentration was performed in quadruplicate. The metal complexes were tested between 0.124 to 100 µM, doxorubicin was tested at concentrations between 0.124 to 200 µM. Staurosporine is highly active and was tested at low micromolar concentrations between 0.01-6 µM. in MDA-MB-231 cells,

The cells were treated for a total incubation period of 48 hours (h), at 44 h of treatment period, 40 µl of MTT solution (5 mg/ml in PBS) was added to each well and the plates were incubated for additional 4 h. At the end of 48 h, the plates were centrifuged at 250 *x g* (Thermo^{TM} Scientific Heraeus Megafuge 40) for 5 min to ensure sedimentation of the formazan crystals. Thereafter, the supernatant was carefully removed. The formazan crystals were dissolved in 200 µl of DMSO and the plate was agitated for 5 min at 800 RPM using the MRC thermo-shaker (Thermo Fisher). The absorbance of the solubilized formazan crystals was measured at 540 nm and 690 nm (reference) using a Labsystems iEMS plate reader (Thermo Lab systems). The percentage of viable cells was determined with Microsoft 365 Excel. GraphPad Prizm version 9.5 was used to obtain the IC_{50} values and construct sigmoidal dose response curves and evaluate statistical significance of IC_{50} values of the active complexes alone and IC_{50} values of OB24 combinations. Statistical differences were determined using *Student's t test* and $p < 0.05$ was considered significant.

2.4 Determination of cell death mechanisms

Fluorescent microscopy using the Olympus BX41 microscope (Olympus) was used to assess the mechanisms of cell death. The cells were seeded on sterile glass coverslips (Lasec) at a density of 300 000 cells in 400 µl culture media per coverslip and allowed to adhere for 30 min at room temperature, thereafter, 1.6 ml of culture media was added in the plates. The plates were incubated overnight in a humidified incubator at 37 ^{0} C with 5 % CO_2 prior to treatment with the metal complexes and positive control.

2.4.1 Assessment of cell morphology

Changes to cell morphology identifies biological activity at early stages of drug development and discovery process (Ziegler *et al.*, 2021). Fluorescent microscopy was used to evaluate morphological changes caused by the active metal complexes and positive controls in MDA-MB-

231 breast cancer cells and to assess the effects of the active complexes on the morphology of the MCF-10A cells.

The fluorochromes acridine orange (Invitrogen), propidium iodide (Molecular probes) and Hoechst 33342 (Sigma Aldrich) detect morphological changes caused by the active metal complexes and positive controls in the treated cells. Acridine orange (AO) is a fluorescent dye that easily permeates cell membranes of the live and dead cells, staining the nuclei green and lysosomes (acidic compartments) orange/yellow. The fluorochrome emits green fluorescence at 526 nm and has an excitation wavelength of 500 nm (Pierzyńska-Mach *et al.*, 2014). Propidium iodide (PI) is a fluorescent dye that intercalates into DNA and stains the nucleus of the cells with compromised cell membranes (Crowley *et al.*, 2016). This dye emits red light between 600 and 700 nm wavelength. The fluorochrome stains the nucleus orange-red and is an indicator of necrotic cell death. Hoechst 33342 (HO) is a DNA binding dye that visualizes the nuclei of the cells. Nuclei of living cells display a homogenous blue colour while apoptotic nuclei are fragmented, therefore show globular structures with an increase in blue fluorescence at an emission between 460 and 490 nm (Ribble *et al.*, 2005). The assay was performed as previously described by (Harmse *et al.*, 2019).

The cells were seeded onto glass coverslips placed in six well plates and treated with the metal complexes and the positive controls at concentrations equivalent to 80 % inhibitory concentration (IC_{80}) for 18 h. The IC_{80} represents the concentration at which 80 % of the cell population is inhibited and was selected because previous studies showed maximum cell death at this concentration. After the treatment period, the media was discarded, and the coverslips were gently rinsed twice with 1 ml of PBS. The cells were then incubated with 500 µl staining mixture for 20 min in the dark at room temperature. The staining mixture consisted of 5 µg/ ml HO, 10 µg/ ml of PI and AO in PBS. Following incubation, the cells were rinsed with one ml PBS to remove the staining concoction and minimize background noise, thereafter the coverslips were mounted on microscope slides (Lasec) and the cells were viewed on an Olympus BX41 epifluorescent microscope, using the following Olympus filter cubes sets; U-MNIB3 for AO, U-MWIG2 for PI and U-MWU2 for HO. Images were captured with an Olympus DP72 camera and analysed with the Olympus CellSens Software.

2.4.2 Determination of the generation of reactive oxygen species

ROS production was measured by CellROX Deep Red Reagent fluorogenic probe (Molecular Probes). CellROX Deep Red Reagent fluorogenic probe is an oxidative stress reagent formulated to measure ROS in live and formaldehyde fixed cells. This cell-permeable reagent is non-fluorescent or poorly fluorescent while in a reduced state and upon oxidation, it displays a strong red signal in the cytoplasm of the cells. In this study, ROS was measured in live treated and untreated MDA-MB-231 cells using fluorescent microscopy. Tert-butyl hydroperoxide (tBHP) was used as a positive control for ROS at a concentration of 20 μM. tBHP is an organic peroxide commonly used to study oxidative stress in cells and tissues. It induces oxidative stress by generating peroxyl and alkoxyl radicals and by interacting with the glutathione peroxidase enzyme (Zhao *et al.,* 2017).

The cells were plated on six coverslips in six well plates and incubated overnight. The cells were treated with copper and gold complexes at concentrations equivalent to IC_{80} with 2.5 μM of the CellROX Deep Red Reagent (Invitrogen) and incubated for 2, 6 and 18 h. At the end of the incubation period, the treatment media was removed, and the cells were washed with PBS. After the wash step, the coverslips were mounted on microscope slides for viewing with an Olympus BX41 microscope, using the U-MWIG2 filter cube for ROS signal (excitation/emission of 640/665 nm). Pixel intensity was measured in 3 separate fields using Fiji: ImageJ software (National Institutes of Health), and data was presented as a fold increase.

2.4.3 Detection of apoptosis with annexin V binding assay

Annexin-V conjugated with fluorescein isothiocyanate, and PI staining detected early apoptotic events using the Annexin-V-FLUOS Staining Kit (Roche). In early apoptosis, phosphatidyl serine (PS) translocate from the inner leaflet to the outer leaflet of the cell membranes. Annexin V is a phospholipid protein with a high affinity for PS and can identify apoptotic cells by binding to the exposed PS on the cell membrane (Vermes *et al.*, 1995). Propidium iodide is impermeant to cells with intact cell membrane and stains late apoptotic and necrotic cells (Crowley *et al.*, 2016). Annexin V only staining detected early apoptotic cells, annexin V and PI staining, determined late apoptotic cells and PI only detected necrosis.

MDA-MB-231 cells were grown on coverslips in six well plates and allowed to adhere overnight in a humidified incubator with 5 % CO_2. The next day, the cells were treated with copper and gold complexes at concentrations equivalent to IC_{80} treated for 6 and 18 h. At the end of each treatment period, the culture media was removed, and the coverslips were gently rinsed with 1 ml PBS. The coverslips were incubated with 40 µl of the Annexin-V-FLOUS and PI working solution in the dark for 15 min. Thereafter, the slides were viewed, and images were captured with the Olympus DP72 camera using the U-MNIB3 filter cube for annexin V and U-MWIG2 for PI. In all microscopic experiments, images were analysed with the Olympus CellSens Software using the basic *Process* menu and ImageJ basic menu. The percentage of annexin V binding on the cells was measured by counting the number of annexin V or annexin V/PI positive cells relative to the number of cells in the corresponding phase contrast image. Three separate fields were counted on each coverslip, and the experiment was repeated three times.

2.4.4 Assessment of the mitochondrial membrane potential (ΔΨm)

Changes in Δψm were detected with 5,5′,6,6,6,6-tetrachloro-1,1′,3,3,3,3-tetraethylbenzimidazolylcarbocyanine iodide (JC-1 dye). JC-1 (Abcam) is a mitochondrial membrane potential-dependent lipophilic dye. In healthy cells with normal mitochondrial function, a high membrane potential is maintained due to active electron transport and proton pumping across the inner mitochondrial membrane, creating a strongly negative potential in the matrix. This high negative membrane potential facilitates JC-1 dye entrapment and accumulation as red-fluorescent JC-1 aggregates. When the ΔΨ is decreased, a shift from red/orange fluorescence to green-fluorescent monomers is observed in the cells. The membrane potential becomes less negative, and insufficient to accumulate the high concentration of JC-1 needed to form aggregates. Instead, the dye remains in the monomeric form which fluoresces green and is an indicator of mitochondrial function (Reers *et al.*, 1995; Pendergrass *et al.*, 2004).

MDA-MB-231 cells were plated on coverslips in six well plates and treated with copper and gold complexes at concentrations equivalent to IC_{80} and doxorubicin for 6 and 18 h. Following treatment, the cells were rinsed gently with 2 ml of PBS and then incubated in the dark for 20 min. at 37 °C with 500 µl of a 5 µg/ml JC-1 reagent. After removing the reagent, the coverslips were washed and mounted on the microscope slides.

The signal was observed on an Olympus BX41 epifluorescence microscope at 400 X magnification using the Olympus U-MWIG2 filter cube for JC-1 aggregates and U-MNIB3 filter cube for JC-1 monomers. Images were captured with an Olympus DP72 camera and analysed using the *Process* menu in Olympus CellSens Software package and ImageJ.

2.4.5 Determination of caspase-9 activity

The caspase-9 (active) FITC staining kit (ab65615) (Abcam) detected caspase-9 activity. The assay uses caspase-9 inhibitor leucyl-glutamyl-histidyl-aspartic-fluoromethyl ketone (LEHD-FMK) conjugated to fluorescein isothiocyanate (FITC). FITC-LEHD-FMK is a non-toxic, cell permeable fluorescent marker which irreversibly binds to active caspase-9 in apoptotic cells and emits bright green fluorescence.

MDA-MB-231 cells were plated on coverslips in six well plates and incubated overnight for the cells to adhere. The next day, the cells were treated with metal complexes at concentrations equivalent to IC_{80} for 18, 24 and 48 h. At the end of the treatment, the media was discarded, and the coverslips were rinsed with PBS. Thereafter, each coverslip was incubated for 45 min. with 3 µl FITC-LEHD-FMK in 900 µl of caspase-9 buffer (proprietary composition) in a humidified incubator at 37 ^{0} C with 5 % CO_2. The coverslips were gently rinsed with the caspase-9 buffer, mounted on microscope slides, and viewed with an Olympus BX41 microscope at a 400X magnification, using the U-MNIB3 filter cube. The images were captured with Olympus DP72 camera and processed with the Olympus CellSens Software and basic ImageJ menu. The percentage of caspase-9 positive cells was measured by counting the number of caspase-9 positive cells relative to the number of cells in the corresponding phase contrast image. Three separate fields were counted on each coverslip, and the experiment was repeated three times.

2.4.6 Determination of caspase-8 activity

The effects of the complexes on the activation of caspase-8 were detected with the Caspase-8 staining kit from (Abcam). The assay uses a caspase-8 inhibitor benzyloxycarbonyl-isoleucyl-glutamyl-threonyl-aspartic acid fluoromethyl ketone (IETD-FMK) conjugated to sulfo-rhodamine (Red-IETD-FMK).

The conjugate is a non-toxic, cell-permeant fluorescent marker that irreversibly binds to activated caspase-8 in apoptotic cells and has bright red fluorescent signal at excitation/ emission of 540/570 nm.

MDA-MB-231 cells were grown on coverslips in six-well plates and treated as described before for 18, 24 and 48 h. At the end of each treatment period, the media was removed, and the cells were washed with PBS. Thereafter, the cells were incubated for 60 min. at 37 ^{0} C / 5 % CO_2 with 3 µl Red-IETD-FMK peptide in 900 µl of caspase-8 proprietary buffer. Post incubation, the cells were rinsed with the same buffer and mounted on microscope slides for viewing with an Olympus BX41 microscope at 400 X magnification, using the U-MWIG2 filter cube. The photographs were captured and analysed as described previously.

2.4.7 Assessment of caspase-3/7 activity assay

Caspase-3/7 activity was assessed with the CellEvent^{TM} Caspase-3/7 live cell green detection reagent (Invitrogen). This is a cell permeable four amino acid (Aspartic acid (Asp) – Glutamic acid (Glu) – Valine (Val) – Aspartic acid (Asp)) peptide-based substrate (DEVD) co-joined to a nucleic acid binding dye. The DEVD peptide sequence acts as a cleavage site for caspase-3 and caspase-7 and the conjugated dye is non-fluorescent, only emitting fluorescence once it is separated from the peptide and attached to DNA. In the presence of apoptotic cells with activated caspase-3/7, the DEVD peptide bond is cleaved, allowing for the dye to bind to the DNA and produce a bright green fluorescence with excitation/emission of 502/530 nm, detectable with the U-MNIB3 filter cube.

The cells were grown on coverslips in six-well plates and incubated overnight. The following day, the cells were treated with copper and gold complexes at concentrations equivalent to IC_{80} for 24 h and 48 h. At the end of each experiment, culture media was collected in 5 mL tubes to harvest any cells that have detached from the growth surface by centrifugation at 250 *x g* (Thermo^{TM} Scientific Heraeus Megafuge 40). The cells were washed with PBS, subsequently, incubated with 5 µM of CellEvent^{TM} Caspase-3/7 detection reagent for 30 min at 37 ^{0} C. The fluorescent signal was detected with an Olympus BX41 microscope, using the U-MNIB3 filter cube for Caspase-3/7 activity.

Images were captured with an Olympus DP72 camera and analysed with the Olympus CellSens Software using the *Process* menu for image modification and overlay. The percentage of caspase-3/7 positive cells was measured by counting the number of caspase-3/7 positive cells relative to the number of cells in the corresponding phase contrast image. Three separate fields were counted on each coverslip, and the experiment was repeated three times.

2.5 Evaluation of apoptosis-related regulatory proteins

Apoptosis related regulatory proteins were evaluated to determine the target proteins and get a better understanding of the molecular pathways involved in cell death. This was achieved by using a human proteome array profiler, immunofluorescence, and western blot analysis.

2.5.1 Proteome profiler human apoptosis array

The proteome profiler human apoptosis array (R and D systems) is an antibody-based array, useful to evaluate the expression of 35 apoptosis-related proteins simultaneously. The proteome array detects proteins associated with the execution and regulation of apoptosis, thereby providing a better understanding of the effects of the copper complexes on apoptosis. The array is validated for analyte detection in cell lysates. This essay evaluated the effects of copper complexes and doxorubicin.

Assay principle

In the proteome profiler human apoptosis array the nitrocellulose membranes are pre-spotted with duplicate capture antibodies, which selectively bind target proteins in the sample. Biotinylated detection antibodies then identify the captured proteins and amplify the signal, which is finally detected by horseradish peroxidase (HRP) conjugated secondary antibodies. The chemiluminescent signals are captured on the membranes as a pair of duplicate spots representing each apoptosis-associated protein. The signal intensity correlates with the quantity of the bound analyte. The assay was performed in MDA-MB-231 cells following the instruction of the manufacturer.

Assay procedure

Step one: Treatment of the cells

Seven million MDA-MB-231 cells per flask were seeded in four 75 cm^2 culture flasks with 20 ml culture media and incubated overnight. The following day, the media was decanted, and the cells were treated with the metal complexes at concentrations equivalent to their IC_{60} values; Cu8AqN (3.1 μM), $CuPhenTh_2$ (2.3 μM) and doxorubicin (10.0 μM). The untreated control flask received 20 ml of fresh media. These concentrations were selected since preliminary results showed no obvious changes in the gross morphology of the treated cells after an 18-h treatment period and the intention was to evaluate changes in apoptotic protein prior to cell death.

Step two: Cell lysate preparation

After an 18 h treatment period, before any visible changes were observed using phase-contrast microscopy, media from all four flasks was collected into four separate 50 ml centrifuge tubes (Corning) to harvest any cells that may have detached form the growth surface, this prevented cell loss. The cells in each flask were harvested with a cell scraper in 5 ml of cold PBS, and the PBS-cell suspensions were added to their respective 50 ml tubes and kept on ice. The tubes were centrifuged at 250 *x g* for 5 min to harvest the cells. After centrifugation, the supernatant was discarded, and the cell pellet was resuspended in 1.2 ml of cold PBS. The cell suspensions were transferred to 2 ml microcentrifuge tubes and centrifuged again, followed by discarding the supernatant. The harvested cells were then lysed in the propriety lysis buffer 17, containing Complete™, mini, EDTA free protease inhibitor cocktail tablet (Millipore Sigma) to prevent protein degradation. To minimize viscosity, the cells were vigorously resuspended with a narrow-gauge needle fitted onto a 5 ml syringe in lysis buffer to prevent DNA aggregation during lysate preparation. The microcentrifuge tubes were subsequently incubated in a cold room at 4 °C for 30 min while being agitated on a rotating platform. This was followed by centrifuging with a Sorvall LYNX 4000 centrifuge, (Thermo Fisher) at 14000 *x g* for 5 min. The supernatants were transferred to new 1.5 ml eppendorf tubes and kept on ice.

Step three: Membrane preparation

The nitrocellulose membranes were incubated with array buffer 1 for 60 min in 4 well multi dishes to block non-specific binding of the proteins. The required volume of cell lysate for each sample was calculated to provide 400 ug of protein per lysate and prepared in lysis buffer 17 . The membranes with the lysates were incubated overnight at 4 ^{0} C on a rocking platform. On the following day, a total of 3 washes for 10 mins per wash and 20 ml of wash buffer was performed on each membrane. Thereafter, the membranes were incubated for one h in a rocking platform at room temperature with 15 µl of detection-biotinylated antibody cocktail diluted in 1.5 ml of 1X array buffer 2/3. This was followed by three wash steps as described above. Horseradish peroxidase conjugated streptavidin (1:2000) amplified the biotinylated detection antibodies signal and this was incubated with the membranes at room temperature for 30 min on a rocking platform. After this step, the membrane arrays were washed again as described previously. The membranes were then simultaneously exposed to Chemi-Reagent Mix for 1 min. and the chemiluminescent signals captured using the BioRad Chemidoc MP Imager. The data was analysed using BioRad Image Lab software version V (Bio-Rad Laboratories) and the intensity of the dots were presented as pixel density.

2.5.2 Protein concentration quantification: Bradford assay

The total protein concentration of the lysates was determined for the lysates of the proteome array and the lysates prepared for western blot assay. Protein concentration in each lysate was determined with the Thermo^{TM} Scientific Pierce^{TM} Detergent Compatible Bradford assay reagent (Thermo Scientific). The assay is based on Bradford assay principle. Binding of the protein molecules to Coomassie brilliant blue G-250 dye under acidic conditions causes colour change from green to blue. The blue colour change is measured at 595 nm with a spectrophotometer, and the absorbance is proportional to the amount of protein present in a sample.

The assay was performed in a 96-well plate. The standard curve was prepared with bovine serum albumin (1 mg/ml) (Thermo Fisher) as a standard. The working concentration range 0.05-1 mg/ml of the standards was used for the extrapolation of the concentration of the unknown samples. The standards and samples were diluted with MilliQ water, at a dilution factor of 1:10.

In duplicates, 10 µl of each standard and unknown sample was added into microplate wells, thereafter, Thermo^{TM} Scientific Pierce^{TM} Detergent Compatible Bradford assay reagent (300 µl) was added in each well containing the standards and unknown samples. The plate was incubated for 10 min at room temperature. Absorbance was measured at 595 nm with the Thermo Scientific Multiskan GO microplate spectrophotometer. The standard curve of protein the concentration vs absorbance was constructed (Appendix D), and the concentration of the samples was determined in Prism Software version 9.5.

2.5.3 Antibody based immunofluorescence assays

Immunofluorescence provides a measure of the expression level and subcellular location of specific proteins in cells. Hoechst 33342 was used to counterstain the nucleus of the treated and untreated cells. The effects of copper complexes on the expression and subcellular location of NIK (Abcam), phospho-p53(s15), p21, and HMOX-1 (Invitrogen) in MDA-MB-231 cells was determined with fluorescent microscopy. The cells were treated Cu8AqN at 3.1 µM, $CuPhenTh_2$ at 2.3 µM and doxorubicin at 10.0 µM. The untreated negative control cells incubated without the primary antibody were the primary antibody negative control for the immunofluorescence assay to determine secondary antibody specificity. The untreated control cells incubated with the primary antibody were the treatment negative control to compare with the treated cells.

Cells were grown on coverslips in six well plates and treated with copper complexes and doxorubicin for 18 h. Following treatment, the cells were rinsed with PBS or harvested if they were detached form the growth surface and fixed for 20 min in 3 % formaldehyde in PBS. This was followed by washing and permeabilization for 20 min with 0.25 % Triton X100 in PBS containing 0.5 % bovine serum albumin (BSA). After permeabilization, the cells were washed as described before and blocked with 0.5 % BSA in PBS for 60 min. The cells were washed again and incubated at 4 °C overnight with 1:200 dilution of each specific primary antibodies in PBS with 0.5 % BSA. The primary antibodies were polyclonal rabbit anti-NIK antibody, phospho-p53(s15) mouse monoclonal antibody, p21 rabbit polyclonal, and polyclonal rabbit anti-HMOX-1 antibody. On the next day, the cells were washed and incubated with 1:800 dilution of an appropriate secondary antibody conjugated to the Alexa fluor 488^{TM} or Alexa fluor 594^{TM} (ThermoFisher) and Hoechst 33342 for 1 h.

Following a washing step with PBS, the coverslips were mounted on microscope slides using Fluoromount^{TM} mounting media (Sigma) and allowed to dry before viewing with an Olympus BX41 epifluorescence microscope. Images were captured with an Olympus DP72 camera, and the images were processed with CellSens Software and ImageJ. Intensity measurement was measured using ImageJ. The plugin "Just another co-localization" (JaCoP) in ImageJ software was used to measure the extend to nuclear colocalization and results were expressed as a Pearson correlation coefficient (PCC). A coefficient of one indicated 100 % nuclear co-localization

2.5.4 Western blot assay

Cell lysates of the control, Cu8AqN, CuPhenTh_2 and doxorubicin were denatured in Laemmli buffer. Proteins were separated by SDS-PAGE using a discontinuous buffer system. The stacking gel (4 % acrylamide) was prepared in stacking buffer composed of 0.125 M Tris-HCl (pH 6.8), while the separating gel (12 % acrylamide) used separating buffer containing 0.375 M Tris-HCl (pH 8.8). In separate lanes, the molecular weight markers (5 µl: Bio-Rad) and the samples containing the same concentration of protein were separated on a discontinuous 12 % SDS-PAGE gel in running (tank) buffer consisting of 25 mM Tris, 192 mM glycine, and 0.1 % SDS (pH ~8.3).

The Mini-PROTEAN Tetra system (Bio-Rad, USA) was used for electrophoresis set at 150 volts (V) until the marker dye tuns off the plates. After electrophoresis, proteins were transferred from the gel to PVDF membranes using a transfer buffer composed of 25 mM Tris, 192 mM glycine, and 20 % methanol (v/v), pH ~8.3. This buffer facilitates the transfer of proteins from the gel onto the membrane during the electrotransfer. The proteins were transferred using PowerPac^{TM} 3000 Universal system (Bio-Rad) and Bio-Rad Mini Trans-Blot system at 100 V for 1 h. The transfer of proteins was assessed by staining the gels with Coomassie blue dye (Thermo Fisher Scientific). The membranes were blocked for 1 h with 5 % BSA in tris-buffered saline with Tween 20 (TBST) and subsequently washed with TBST. The polyclonal rabbit anti-HMOX-1 (1:2000) prepared in 10 ml TBST with 20 µl of β tubulin (reference protein) was added onto membranes and incubated overnight at 4 ^{0}C. The next day, the membranes were subjected to 5 washes (10 min each with gentle agitation) using TBST.

The membranes were incubated with 10 ml HRP-conjugated secondary antibody prepared in TBST with streptactin at room temperature for 1 h Streptactin is a streptavidin analogue that binds specifically to the Strep-tag II peptide. This component was included to enhance detection sensitivity. After the washing step, the membranes were incubated with freshly prepared Pierce^{TM} ECL Western blotting substrate (Thermo Scientific) for 5 min and chemiluminescent signals were detected with the BioRad Chemidoc (Bio-Rad). The data was analysed using Biorad Image Lab software version 4 (Bio-Rad Laboratories). Data was presented as a fold increase relative to the untreated control.

2.6 Data analysis

All experiments were performed at least three times and data is presented as a mean and ± standard error of means (SEM) where appropriate. Data and statistical significance were analysed with GraphPad Prism version 9.5. The significance and *p*-value between the IC_{50} values of the complexes and doxorubicin was determined with *Student's t-test*. Unless otherwise stated, results from the fluorescent microscopy were expressed as the percentage of cells with positive fluorescence relative to the total number of cells in the accompanying phase contrast image, and three separate fields were counted for each treatment, and all experiments were repeated three times. Analysis and statistical significance of fluorescent microscopy data, proteome array data and western blot were determined by analysis with a one-way ANOVA followed by Dunnett's multiple comparison test. The results were considered statistically significant for a p-value ≤ 0.05.

Chapter Three: Results

PART 1: Cytotoxicity of the metal complexes

3.1 Cytotoxic effects of the metal complexes on breast cancer and mammary epithelial cell lines

3.1.1 The effects of the metal complexes and ligands on cell viability of MDA-MB-231 breast cancer cells

The cytotoxic effects of eight metal complexes were tested against MDA-MB-231 breast cancer cells. The complexes included gold(I)ferrocenyl-1,2,3-triazol-5-ylidene complexes AuCl(trz-Fc-Dipp), AuPh(trz-Fc-Dipp), $AuPPh_3$(trz-Fc-Dipp), $AuPPh_3$(Ph-trz-Dipp), copper(II) and manganese(II) complexes with theophylline-phenanthroline ligands ($CuTh_2$, $CuPhenTh_2$, $MnTh_2$), and a copper complex with 8-aminoquinolone-naphthyl ligand (Cu8AqN). The ligands were tested to determine their contribution on the cytotoxicity of the complexes. Doxorubicin and gemcitabine were used as positive controls, while untreated cells were a negative control. The cells were treated with 5 and 50 μM of the metal complexes and their respective ligands for 48 h. The metal complexes that reduced cell viability to less than 50 % at 5 μM were considered active, indicating that they can kill cancer cells at low micromolar, clinically relevant concentrations and these complexes were studied further.

The ferrocenyl-1,2,3-triazoly-5-lidene ligand was poorly active, with cell viability above 90 % at both tested concentrations, as shown in Fig. 3.1. The gold-trz complexes decreased the viability of MDA-MB-231 cells. Cell viability was 43.5 % in cells treated with AuCl(trz-Fc-Dipp) and 20.2 % in those treated with $AuPPh_3$(trz-Fc-Dipp) at 5 μM. The AuPh(trz-Fc-Dipp) and $AuPPh_3$(trz-Ph-Dipp) complexes were less active, with cell viability of 90.2 % and 68.1 % , respectively at 5 μM. At 50 μM, all complexes were highly effective and decreased cell viability to below 15 %, with $AuPPh_3$(trz-Ph-Dipp) significantly decreasing cell survival to 2.3 % , Fig. 3. 1.

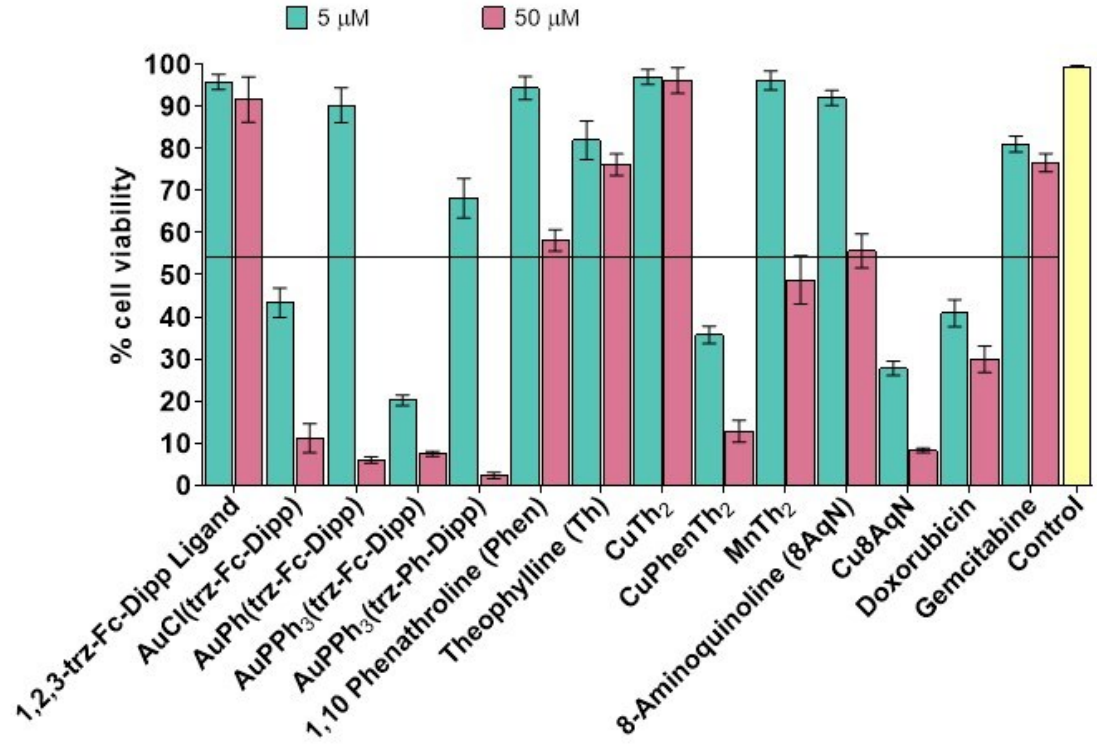


Fig. 3.1 The effects of metal complexes and ligands on the cell viability of MDA-MB-231 breast cancer cells. The cells were treated with metal complexes and ligands at 5 and 50 µM for 48 h. Results were expressed as a mean ± standard error of the mean (SEM) of at least three independent experiments.

The 1,10-phenanthroline (Phen) ligand was poorly active at 5 µM and the treated cells had a cell viability of 80 %, which was decreased to 55 % at 50 µM concentration. Theophylline (Th) ligand was even less active at both tested concentrations and reduced cell viability by more than 70 %. $CuTh_2$, and $MnTh_2$ were poorly active with 80 % cell viability at 5 µM and showed more than 48 % cell viability at 50 µM, which disqualified them for further investigation. In contrast, $CuPhenTh_2$ (copper complexed to phenanthroline and theophylline) was the most potent complex with cell viability of 39.56 % at 5 µM and 15 % at 50 µM, warranting for further exploration. The copper free-8-aminoquinoline (8AqN) naphthyl ligand was poorly active with 80 % cell viability at 5 µM and moderately active, with 55 % cell viability at 50 µM. In contrast, Cu8AqN, copper coordinated to 8-aminoquinoline naphthyl ligand was highly active with cell viability of 28.50 % at 5 µM which decreased to 10 % at 50 µM. Among the positive controls, gemcitabine was poorly active with cell viability of more than 70 % at both tested concentrations, whereas

doxorubicin showed moderate activity, and reduced cell viability to 48.10 % at 5 μM and 30 % at 50 μM, presented in Fig. 3.1.

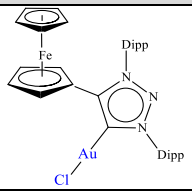
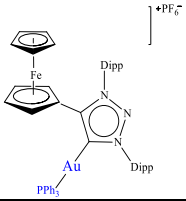
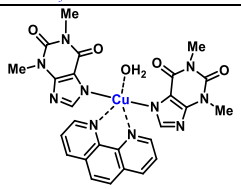
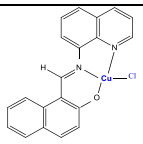
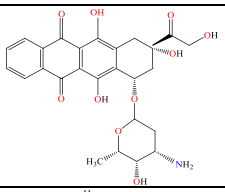
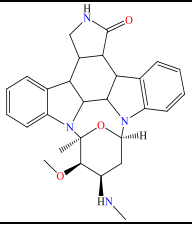
3.1.2 IC_{50} values of the active metal complexes on MDA-MB-231 breast cancer cells

The active metal complexes identified in 3.1.1 and positive control, doxorubicin were tested to determine their IC_{50} and potency. IC_{50} represents concentration where 50 % of the cell population is inhibited. Doxorubicin is an anthracycline, that intercalates into DNA strands, blocking DNA replication and transcription, and causes reactive oxygen species and apoptotic cell death (Wellstein and Sausville, 2023). It is clinically used in the treatment of triple negative breast cancer.

The cells were treated with concentrations of the metal complexes ranging between 0.124 and 50 μM, and doxorubicin between 0.124 and 100 μM. Staurosporine, a highly toxic and non-selective protein kinase inhibitor known for its ability to induce apoptosis (Ōmura *et al.*, 2018), was included as an additional positive control for the evaluation of apoptosis. Staurosporine has shown activity at low nanomolar concentrations, and in this study, it was tested at concentrations between 0.05 and 6 μM. The cells were treated for 48 h, and sigmoidal dose-response curves were generated with GraphPad Prism version 9.5.

The IC_{50} values were determined on the data from at least five independent experiments using the MTT cytotoxicity assay. Each data point in each experiment was determined in quadruplicate. Metal complexes with the IC_{50} values lower than 5 μM were considered good lead candidates for this study based on the criteria reviewed by (Robles-Bañuelos *et al.*, 2024) and were evaluated for the mechanism of cell death. The active metal complexes decreased the viability of MDA-MB-231 cells in a dose-dependent manner after a 48-h treatment period. The results shown in Table 3.1 and Fig. 3.2 indicate that the gold complex, AuCl(trz-Fc-Dipp) was less effective and had a higher IC_{50} value of 7.75 ± 0.70 μM compared to the other gold complex, $AuPPh_3$(trz-Fc-Dipp). The IC_{50} value of $AuPPh_3$(trz-Fc-Dipp) was 2.00 ± 0.39 μM. Copper complex, $CuPhenTh_2$ was the most potent with the IC_{50} values of 1.89 ± 0.14 μM while Cu8AqN was less potent with the IC_{50} value of 3.31 ± 0.06 μM.

Table 3.1: IC_{50} values, and chemical structures of active metal complexes in MDA-MB-231 breast cancer cells after 48-h treatment.

Treatment	IC_{50} values (µM)	Chemical structures
AuCl(trz-Fc-Dipp) 1,3-Bis(2,6-diisopropylphenyl)-4-ferrocenyl-1,2,3-triazol-5-ylidene gold(I) chloride	7.75 ± 0.70	
$AuPPh_3$(trz-Fc-Dipp) 1,3-Bis(2,6-diisopropylphenyl)-4-ferrocenyl-1,2,3-triazol-5-ylidene gold(I) triphenylphosphine	2.00 ± 0.39	
$CuPhenTh_2$ Copper(theophylline)$_2$phenanthroline (H_2O) ·$5H_2O$	1.89 ± 0.14	
Cu8AqN 8-aminoquinoline-naphthyl copper	3.31 ± 0.06	
Doxorubicin (7S,9S)-7-[(2R,4S,5S,6S)-4-amino-5-hydroxy-6-methyloxan-2-yl]oxy-6,9,11-trihydroxy-9-(2-hydroxyacetyl)-4-methoxy-8,10-dihydro-7H-tetracene-5,12-dione	8.75 ± 0.88	
Staurosporine (5S,6R,7R,9R)-6-methoxy-5-methyl-7-(methylamino)-6,7,8,9,15,16-hexahydro-17-oxa-4b,9a,15-triaza-5,9-methano dibenzo[b,h]cyclonona[jkl]cyclopenta[e]-as-indacen-14(5H)-one	0.06 ± 0.001	

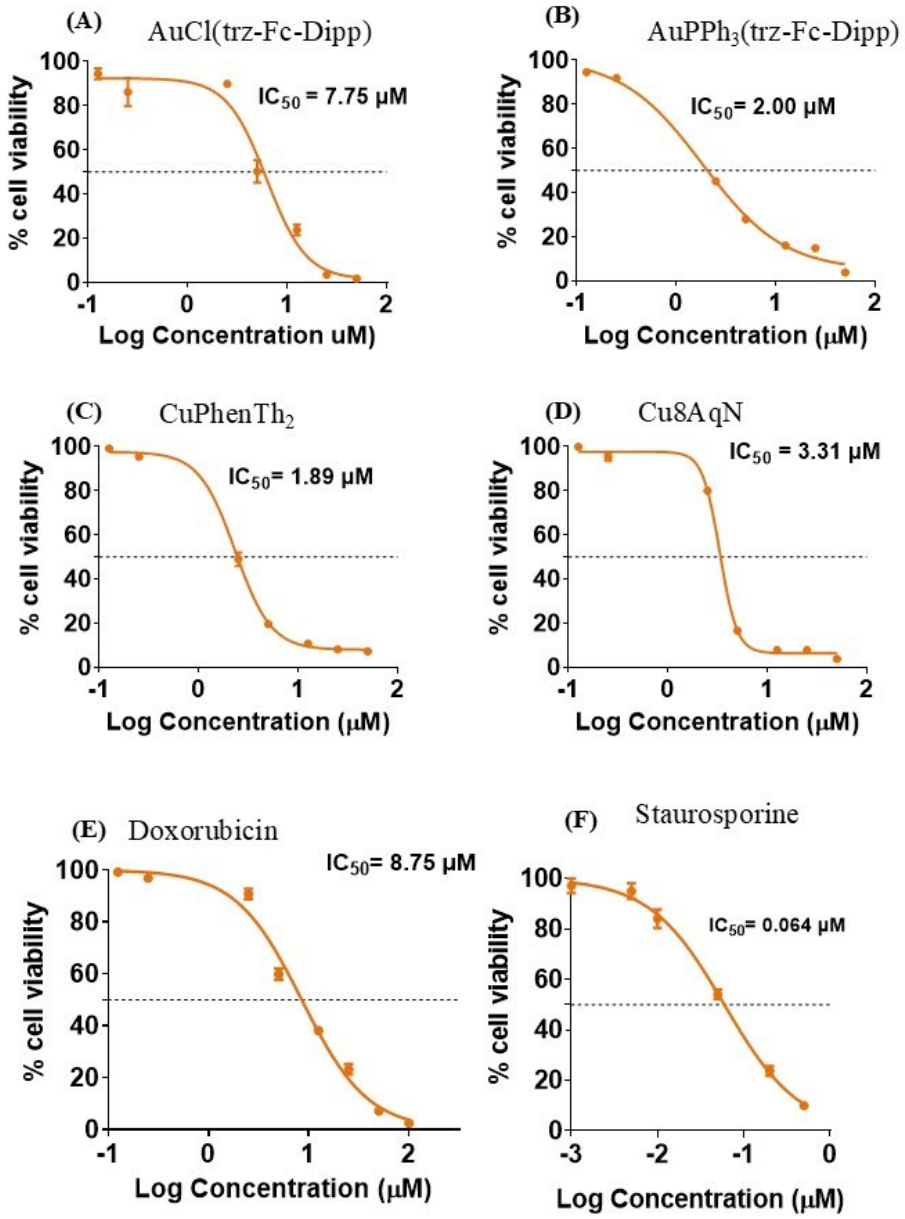


Fig. 3.2 Representative dose-response curves of the active metal complexes in MDA-MB-231 cells. The cells were treated with metal complexes at concentrations between 50 µM and 0.124 µM. Doxorubicin between 100 µM and 0.124 µM while Staurosporine was tested at concentrations between 6. µM and 0.05 µM for 48 h. Curves A-E shows sigmoid dose- response curves for (A) AuCl(trz-Fc-Dipp), (B) $AuPPh_3$(trz-Fc-Dipp), (C) $CuPhenTh_2$, (D) Cu8AqN, (E) doxorubicin and (F) staurosporine, respectively. Each data point indicates the cell viability at each log concentration, with error bars representing the standard error of the mean (SEM). Legend: dotted line= 50 % cell growth inhibition, µM= micromolar concentration, IC_{50}=50 % inhibitory concentration.

The IC_{50} value of doxorubicin was 8.75 ± 0.88 µM, which was higher than the tested metal complexes, indicating a reduced activity in MDA-MB-231 breast cancer cells. Staurosporine had a lowest IC_{50} value of 0.06 ± 0.001 µM compared to the metal complexes and doxorubicin, confirming its high cytotoxic potency. The IC_{50} values of $AuPPh_3$(trz-Fc-Dipp), $CuPhenTh_2$, Cu8AqN, and staurosporine were significantly different from that of doxorubicin, while the IC_{50} value of AuCl(trz-Fc-Dipp) showed no significant difference (p = 0.98). AuCl(trz-Fc-Dipp) had an IC_{50} value above 5 µM and was not investigated further. Representative dose response curves of the metal complexes and the positive controls are shown in Fig. 3.2 with their corresponding IC_{50} values and chemical structures.

3.1.3 Selection of the metal complexes for further evaluation

Based on their IC_{50} values, three metal complexes $AuPPh_3$(trz-Fc-Dipp), $CuPhenTh_2$, and Cu8AqN) and two positive controls (doxorubicin and staurosporine) were selected for further evaluation, as shown in Table 3.2. Further studies included the evaluation of their cytotoxic effects on a normal mammary epithelial cell line, MCF-10A cells and mechanisms of cell death in MDA-MB-231 triple negative breast cancer cells.

3.1.4 The effects of selected active metal complexes on the viability of MCF-10A mammary epithelial cells

The copper and gold metal complexes were tested against the MCF-10A cells to determine the toxicity by measuring IC_{50} values and selectivity of the complexes. The cells were treated with concentrations of the metal complexes ranging between 0.124 and 50 µM; doxorubicin between 0.124 and 100 µM. Staurosporine between 0.05 and 6 µM for 48 h. The IC_{50} values of the metal complexes in MCF-10A cells were used to determine the selectivity index (SI) using the formula: $SI = \frac{\boldsymbol{IC50\ of\ normal\ cells}}{\boldsymbol{IC50\ of\ cancer\ cells}}$. where the complexes with SI > 2 at 48 h were considered selective to cancer cells according to (Olar *et al.*, 2022). The results in Table 3.2 show that the $AuPPh_3$(trz-Fc-Dipp) gold complex, was toxic to the MCF-10A cells and had an IC_{50} value of 3.33 ± 0.4 µM with SI of 1.66 which was lower than 2, indicative of poor selectivity. The IC_{50} values of $CuPhenTh_2$ and Cu8AqN were 5.76 ± 1.96 µM and 9.52 ± 0.03 µM, respectively, indicating that they were less toxic against the normal cell line compared to the gold complex.

Selectivity indices observed for the copper complexes were 3.04 for $CuPhenTh_2$ and 2.88 for Cu8AqN, which were above 2 indicating some selectivity toward MDA-MB-231 cancer cells. The IC_{50} value of doxorubicin was 2.99 ± 0.17 (SI = 0.34) while the IC_{50} value of staurosporine was 0.22 ± 0.0032 (SI= 3.67) in these cells.

Table 3.2: IC_{50} values and selectivity Indices of selected metal complexes in MDA-MB-231 breast cancer and MCF-10A mammary epithelial cells at 48 h

Treatment	IC_{50} values (µM)		Selectivity index
	MDA-MB-231 cells	MCF-10A Cells	
$AuPPh_3$(trz-Fc-Dipp)	2.00 ± 0.39	3.33 ± 0.40	1.67
$CuPhenTh_2$	1.89 ± 0.14	5.76 ± 1.96	3.04
Cu8AqN	3.31 ± 0.06	9.51 ± 0.03	2.88
Staurosporine	0.06 ± 0.001	0.22 ± 0.003	3.67
Doxorubicin	8.75 ± 0.88	2.99 ± 0.88	0.34

3.1.5 IC_{80} Concentrations of the metal complexes in MDA-MB-231 and MCF-10A cells

For preliminary determination of the mechanism of cell death, both cell lines were treated with metal complexes and staurosporine at concentrations equivalent to 80 % inhibitory concentration IC_{80} for each cell line. The determined IC_{80} for doxorubicin in MDA-MB-231 cells was 24.3 µM, but exploratory results showed extensive red innate fluorescence in the nucleus at this concentration which interfered with nuclear binding dyes like Hoechst 33342 (HO) and propidium iodide (PI) (Appendix B**)**, and for this reason, doxorubicin was used at 10 µM in MDA-MB-231 cells, which was proven active with minimal innate fluorescence. The treatment concentrations are shown in Table 3.3 below.

3.2 The effects of the metal complexes on the cell morphology of MDA-MB-231 and MCF-10A cells

Cell morphology assessment provided preliminary indication of the possible mechanisms of cell death and importantly, indicated whether the tested copper and gold complexes caused necrosis

or not. Dying or damaged cells undergo a sequence of nuclear changes, especially in apoptosis, to indicate the mechanism of cell death, Fig. 3.3 below (Earnshaw, 1995).

The MDA-MB-231 and MCF-10Acells were treated with $AuPPh_3$(trz-Fc-Dipp), $CuPhenTh_2$, Cu8AqN, doxorubicin and staurosporine for 18 h at IC_{80} in Table 3.3. IC_{80} was selected because previous studies showed that this concentration caused optimum cell death in leukemic cells (Ismail *et al.,* 2022). The cells were then stained with a dye combination which consisted of HO, PI and acridine orange (AO,) as described in section 2.5.2. Cells were observed with an Olympus BX41 microscope using the Olympus U-MWU2 filter cube for HO, the U- MNIBA3 filter cube for AO and the U-MWIG2 for PI detection. Images were captured with an Olympus DP72 camera.

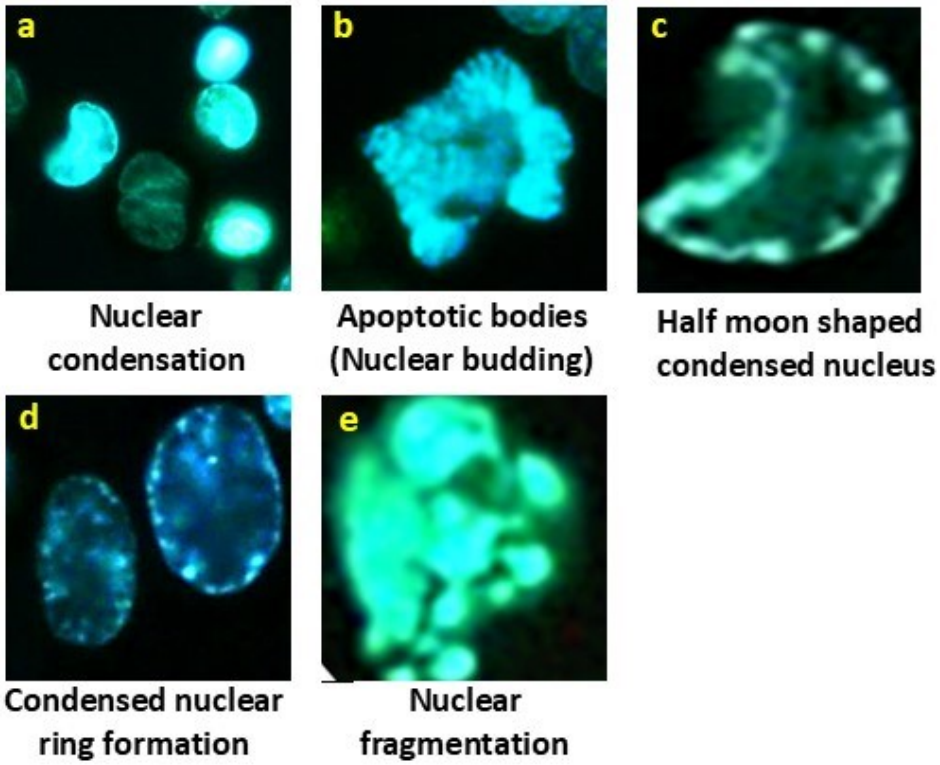


Fig. 3.3 Fluorescent micrographs showing apoptotic nuclei changes stained by HO (A) shows bright blue, fluorescent cells as an indication of nuclear condensation. (B) Illustrates cluster of budding nuclei, (C) shows half-moon shaped condensed and fragmented apoptotic nucleus. (D) Indicates typical nuclear ring formation commonly seen in doxorubicin treated cells (E) shows nuclear fragmentation. Images were viewed on an Olympus BX41 epifluorescence microscope, captured with an Olympus DP72 camera and analysed with *Process* menu on Olympus CellSens Software.

Table 3.3: IC_{80} values of selected metal complexes and positive controls in MDA-MB-231 and MCF-10A cells

Treatment	IC_{80} values (µM)	
	MDA-MB-231 cells	MCF-10A Cells
$AuPPh_3$(trz-Fc-Dipp)	5.81 ± 0.32	6.07 ± 0.25
$CuPhenTh_2$	5.63 ± 0.10	10.23 ± 0.20
Cu8AqN	4.19 ± 0.10	16.56 ±0.05
Staurosporine	0.25 ± 0.006	2.04 ± 0.07
Doxorubicin	10	11

3.2.1 The effects of metal complexes on the cell morphology of MDA-MB-231 breast cancer cells

Representative results of changes in the morphology of MDA-MB-231 cells are shown in Fig. 3.4. Untreated MDA-MB-231 control cells indicated adherent monolayered, spindle-like shaped cells with oval, uniformly HO-stained nuclei which was simultaneously observed in AO staining, as shown by a white arrow, (Fig. 3.4, panel a, b and c). The treatment of the cells with the metal complexes and the positive controls changed the morphology of the cells.

In all the treated cells, the lack of PI staining on the nuclei indicated the absence of necrotic cell death and that cell membranes were intact. The cells treated with $AuPPh_3$(trz-Fc-Dipp) appeared rounded, with a few showing perinuclear vacuoles (yellow arrow, panel d), which presented as small white vesicles around the nuclei. HO staining showed numerous cells with fragmented nuclei, as indicated by green arrows suggesting apoptotic cell death (Fig. 3.4, panel d and e).

The AO/HO merge image had an increase in lysosome formation around the nuclei, which appeared as bright yellow globular structures (red arrows) indicative of cellular stress or autophagy (Fig. 3.4, panel f). Treatment with $CuPhenTh_2$ caused the cells to detach from the growth surface, form vacuoles (yellow arrows) and assume a round shape with apoptotic nuclei (Fig. 3.4, panel g).

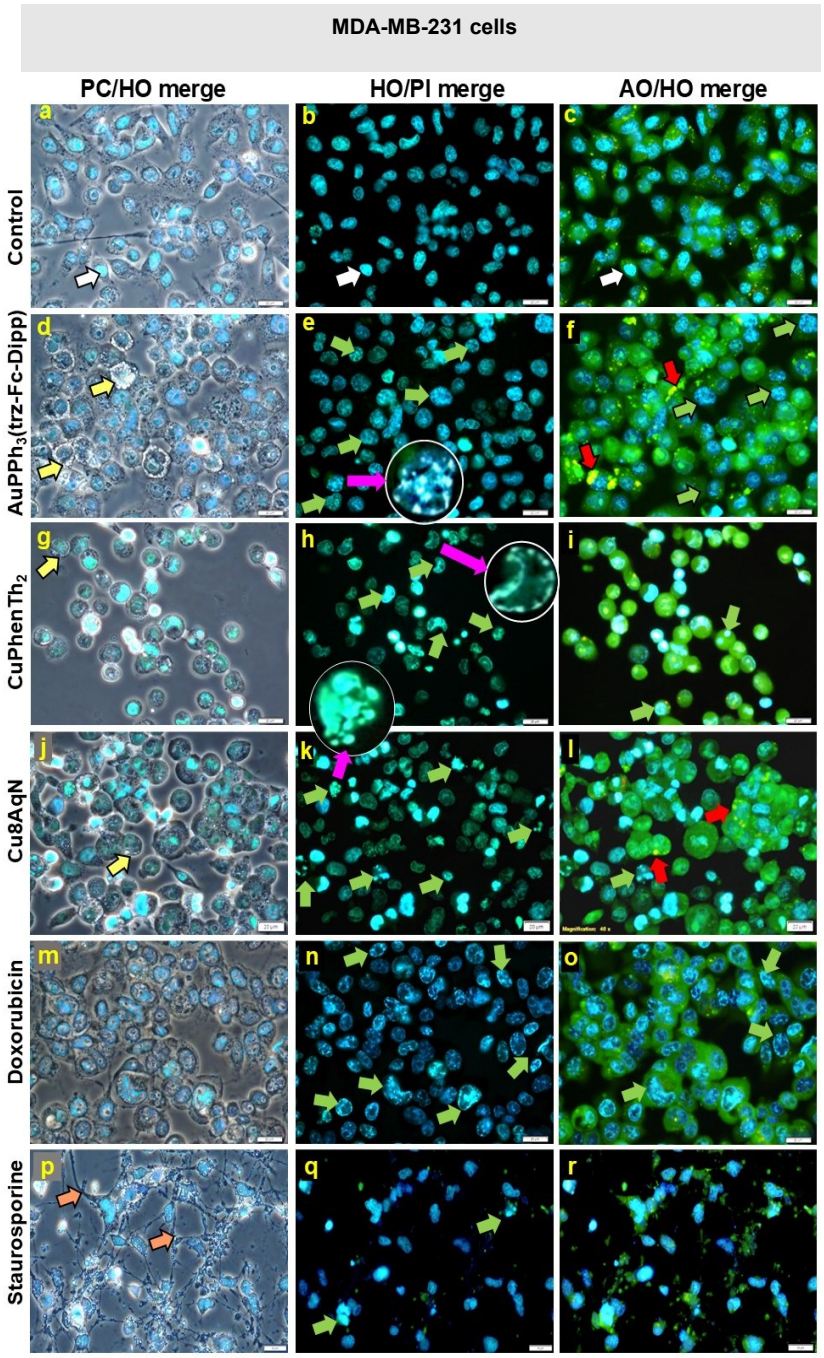


Fig. 3.4 Photomicrographs showing the effects of the metal complexes and positive controls on MDA-MB-231 cell morphology. The MDA-MB-231 cells were treated with 5.8 µM of $AuPPh_3$(trz-Fc-Dipp), 5.6 µM $CuPhenTh_2$, 4.2 µM Cu8AqN, doxorubicin at 10 µM and 0.25 µM of staurosporine for 18 h. Cell were viewed with an Olympus BX41 epifluorescence microscope at 400 x magnification. Images were captured with an Olympus DP72 camera and analysed with the '*Process*' menu in Olympus CellSens Software. Scalebar: 20 µm. Legend: white arrows= nucleus, yellow arrow= vacuoles, green arrow= apoptotic cell, purple arrow = nuclear fragmentation, red arrow= lysosomes, orange arrow=fibrils, PC=phase contrast, HO=Hoechst 33324, PI=propidium iodide, AO=acridine orange.

The nuclei were half-moon shaped, with concomitant condensation and fragmentation observed as globular structures with increased HO fluorescence, features of apoptosis, as shown by green and purple arrows, (Fig. 3.4, panel h and i). Low numbers of acidic granules were evident in the cells when compared to $AuPPh_3$(trz-Fc-Dipp), (Fig. 3.4, panel i). Few cells that were treated with Cu8AqN showed vacuoles (Fig. 3.4, panel j), cells were rounded up, had nuclear fragmentation and condensation, as illustrated by green arrow, and these features were again associated with apoptosis, (Fig. 3.4, panel k and l). In some cells, Cu8AqN caused lysosome formation (red arrows), indicative of cellular stress (Fig. 3.4, panel l).

Doxorubicin treated cells appeared slightly round (Fig. 3.4, panel m). Many nuclei were fragmented with nuclear ring, /necklace formation suggesting apoptosis as indicated by HO staining in Fig. 3.4, panel n and o. AO staining was observed around and in the cells with no evidence of cell stress. Treatment of the cells with staurosporine caused the formation of fibrils, keeping the cells together and adherent (Fig.3.4, panel p). The green arrows in HO-stained cells showed nuclear fragmentation, characteristic of apoptotic cells (Fig.3.4, panel q). The absence or the lack of AO in some cells suggested extensive cell damage around the nucleus, since AO stains the cytoplasm and the nuclei (Fig. 3.4, panel r).

3.2.2 The effects of the metal complexes on the morphology of MCF-10A mammary epithelial cells

The effects of the copper complexes and the positive controls on the morphology of MCF-10A cells were assessed. The cells were treated with copper and gold metal complexes at the IC_{80} obtained on MCF-10A cells. These results are shown in Fig. 3.5. Untreated MCF-10A cells had normal morphology, characterized by large, cuboidal cells in (Fig. 3.5, panel a) with evenly blue stained round nuclei, indicated by white arrow in Fig. 3.5 panel a, b and c. The absence of PI staining on the nuclei of the cells treated with the metal complexes and the positive controls suggested the absence of necrosis, and intact cell membrane.

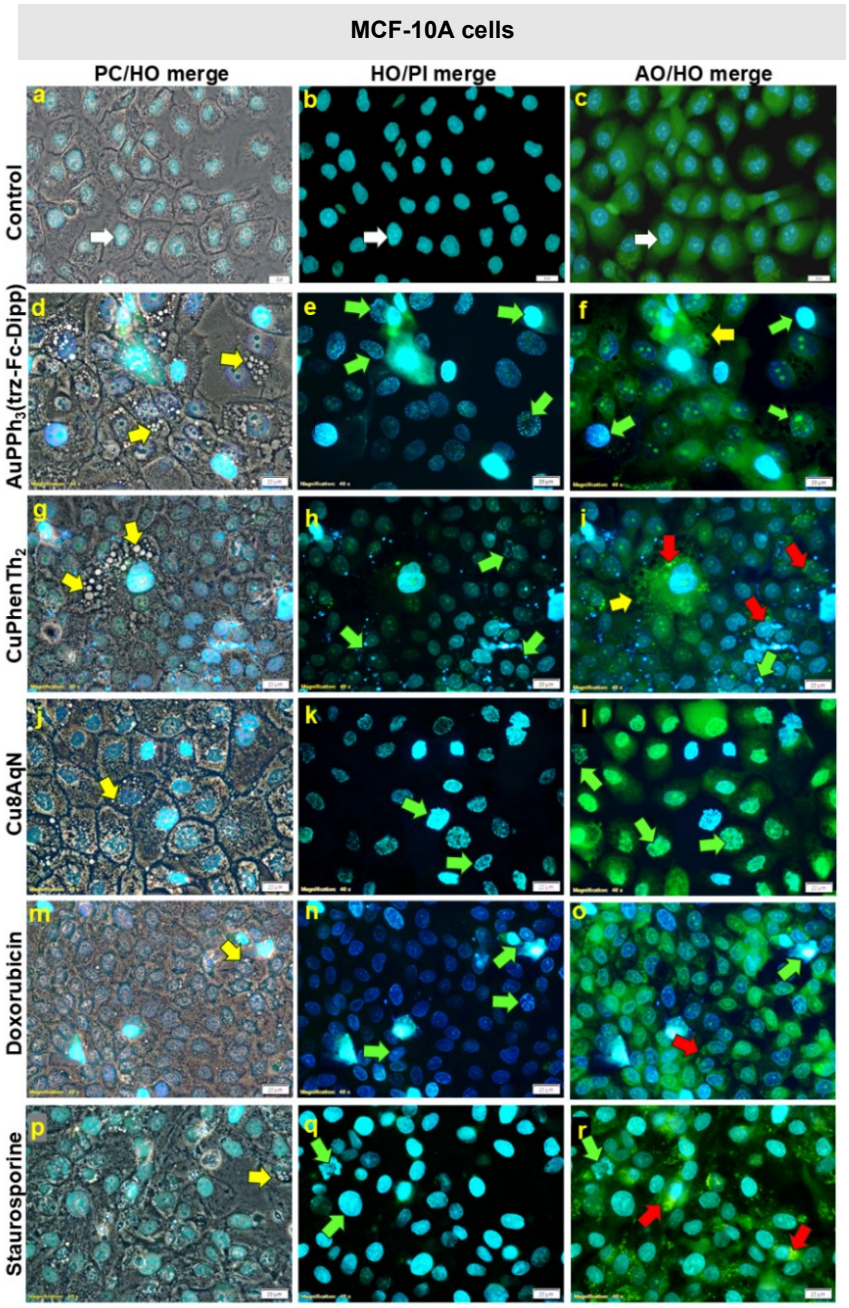


Fig. 3.5 Photomicrographs showing the effects of the metal complexes and positive controls on the morphology of MCF-10A cells. The MCF-10A cells were treated with 6.07 µM $AuPPh_3$(trz-Fc-Dipp), 10.23 µM of $CuPhenTh_2$, 16.56 µM of Cu8AqN, 11 µM of doxorubicin and 2.04 µM of staurosporine, for 18 h and viewed with an Olympus BX41 epifluorescence microscope at 400 x magnification. Images were photographed with Olympus DP72 camera and analysed with the Olympus CellSens Software using the '*Process"* menu and ImageJ software. Scalebar: 20 µm. Legend: white arrows= nucleus, yellow arrow= vacuoles, green arrow= apoptotic cell, red arrow= lysosomes, PC=phase contrast, HO= Hoechst 33324, PI=propidium iodide, AO=acridine orange.

Extensive perinuclear vacuole formation indicated by yellow arrows in the cells treated with $AuPPh_3$(trz-Fc-Dipp) were observed (Fig. 3.5, panel d, e, and f). In AO-stained cells, cytoplasmic vacuoles lacked green fluorescence, and no lysosomal accumulation was evident (Fig. 3.5, panel f).

$CuPhenTh_2$ treatment caused cytoplasmic vacuolization in the cells indicated by a yellow arrow (Fig. 3.5, panel g). HO panel presented apoptotic nuclei shown by half-moon shaped nuclei with increased HO fluorescence, (Fig.3.5, panel h). Some cells had lysosomal formation indicated by bright yellow fluorescence around the nuclei after being stained with AO (Fig.3.5, panel i). Few perinuclear vacuoles as shown by yellow arrow, were present in the cells treated with Cu8AqN compared to $AuPPh_3$(trz-Fc-Dipp) and $CuPhenTh_2$ (Fig.3.5, panel j). HO increased fluorescence, indicative of apoptotic nuclei (Fig. 3.5, panel k), which was seen in AO/HO merged image in panel l, (Fig. 3.5, panel l).

Doxorubicin-treated cells were round and attached to the growth surface (Fig. 3.5, panel m). Green arrows in HO-stained cells show apoptotic nuclei presented by fragmentation and condensation (Fig. 3.5, panel n and o). AO staining showed few cells with lysosomes (Fig. 3.5, panel o), when compared to $CuPhenTh_2$. Cells treated with staurosporine had some vacuoles, presence of apoptotic nuclei shown by nuclear budding (green arrow) and extensive granular yellow fluorescing acidic compartments (red arrows) were visible on the cells when stained with AO, (Fig. 3.5, panels p, q and r).

3.2.3 Cell line selection for the mechanisms of cell death assays

MDA-MB-231breast cancer and MCF-10A mammary epithelial cells showed comparable results, displaying apoptotic and some autophagic characteristics following treatment with $AuPPh_3$(trz-Fc-Dipp), $CuphenTh_2$, Cu8AqN, doxorubicin and staurosporine at their individual IC_{80} concentrations. Importantly, the metal complexes and the positive controls did not induce necrosis in these cell lines, indicating intact cellular membranes. MCF-10A mammary cells showed lower sensitivity to the metal complexes, as reflected by higher IC_{50} values compared to MDA-MB-231 breast cancer cells. Due to this, successive apoptotic assays focused on MDA-MB-231breast cancer cells to further assess the anticancer potential of the metal complexes.

3.3 Evaluation of cell death mechanisms in MDA-MB-231 breast cancer cells

Preliminary findings (section 3.2) indicated mainly apoptotic cell death although autophagic cell death could not be ruled out. This section presents the results on apoptosis related assays, such as ROS, annexin V binding, mitochondrial membrane potential, caspase-3/7, caspase-8 and caspase-9 activity in MDA-MB-231 breast cancer cells.

3.3.1 The effects of the metal complexes on reactive oxygen species

Copper and gold complexes have been reported to cause oxidative stress via generation of ROS, and mitochondrial dysfunction. Gold complexes were indicated to cause oxidative stress by inhibiting glutathione, thioredoxin/ thioredoxin reductase enzymes (Arambula *et al.*, 2016; Muenzner *et al.*, 2016; Reddy *et al.*, 2018; Harmse *et al.*, 2019; Zehra *et al.*, 2021). In this study, the ability of the metal complexes to cause oxidative stress was determined by measuring the formation of ROS.

The MDA-MB-231 cells were treated with concentrations equivalent to their IC_{80} values of $AuPPh_3$(trz-Fc-Dipp), $CuThenPh_2$ and Cu8AqN. A well-known ROS inducer, tBHP, was used as a positive control at a concentration of 20 µM in this study. Due to the short half-life of ROS (Griendling *et al.*, 2016; Juan *et al.*, 2021), the assay was done at different treatment periods for 2, 6 and 18 h. ROS was seen as small red punctate fluorescence in the cytoplasm of the cells, the results are shown in Fig. 3.6 and 3.7 .

3.3.1.1 Measurement of ROS in MDA-MB-231 breast cancer cells

MDA-MB-231 untreated control cells had normal morphology with low baseline ROS levels at 2, 6 and 18 h treatment periods, (Fig. 3.6, panels a and b; m and n; y and z; respectively) and Fig. 3.7). At 2 h, the cells treated with $AuPPh_3$(trz-Fc-Dipp) remained adherent to the growth surface, most appeared slightly round with increased red fluorescence indicating ROS formation compared to the control (Fig. 3.6, panel c and d, Fig. 3.7). In $CuPhenTh_2$ treated cells, most maintained normal morphology with few rounded cells on the periphery. Increased ROS formation was present in the rounded cells compared to the monolayered/flattened cells which showed decreased red fluorescence (Fig. 3.6, panel e and f, Fig. 3.7).

Like $AuPPh_3$(trz-Fc-Dipp), Cu8AqN caused the cells to appear round with increased ROS formation (Fig. 3.6, panel g and h; Fig. 3.7) but was less effective than $AuPPh_3$(trz-Fc-Dipp). Doxorubicin treatment changed the shape of the cells and caused the formation of red punctate fluorescence around the nuclei shown by yellow arrows. An increase in red fluorescence in the nuclei of doxorubicin treated cells was attributable to the intrinsic fluorescence of doxorubicin (Fig. 3.6, panel I and j and Fig. 3.7). Positive control, tBHP, caused the cells to assume a round shape, with fewer cells displaying increased ROS levels compared to $AuPPh_3$(trz-Fc-Dipp), $CuPhenTh_2$, and Cu8AqN, suggesting metal complexes as effective ROS producers at this time point (Fig. 3.6, panel k and l; Fig. 3.7).

At 6 h, rounded cells with increased ROS were present in $AuPPh_3$(trz-Fc-Dipp) treated cells (Fig. 3.6, panel o and p; Fig. 3.7). $CuPhenTh_2$ caused granulation and round morphology on the cells with increased ROS levels than at 2 h treatment (Fig. 3.6, panel q and r; Fig. 3.7). Granular and round cells with increased red fluorescence indicative of ROS levels were observed after treatment with Cu8AqN (Fig. 3.6, panel s and t; Fig. 3.7). ROS levels were higher at 6 h then at 2 h treatment. At 6 h, the doxorubicin treated cells maintained a round shape with increased ROS formation in most cells (Fig. 3.6, panel u and v; and Fig. 3.7).

In comparison to the metal complexes, the cells treated with tBHP were elongated with vacuoles and granules possibly indicating cell stress, while some were rounded. Increased ROS formation was observed at 6 h than at 2 h treatment. In some cells, the red fluorescence colocalized with the granules and with the vacuoles in others (Fig. 3.6, panel w and x; Fig. 3.6). Overall, ROS levels were higher at 6 h than at 2 h. At 18 h, the cells treated with $AuPPh_3$(trz-Fc-Dipp) were elongated with poor evidence of red fluorescence, suggestive of decreased ROS levels (Fig. 3.6, panel a' and b', Fig. 3.7). Similar features were observed on the cells treated with $CuPhenTh_2$ (Fig. 3.6, panel

c' and d', Fig. 3.7). Cu8AqN treatment caused the cells to take on a round appearance and they detached from the growth surface and ROS was not present (Fig. 3.6, panel e' and f', Fig. 3.7).

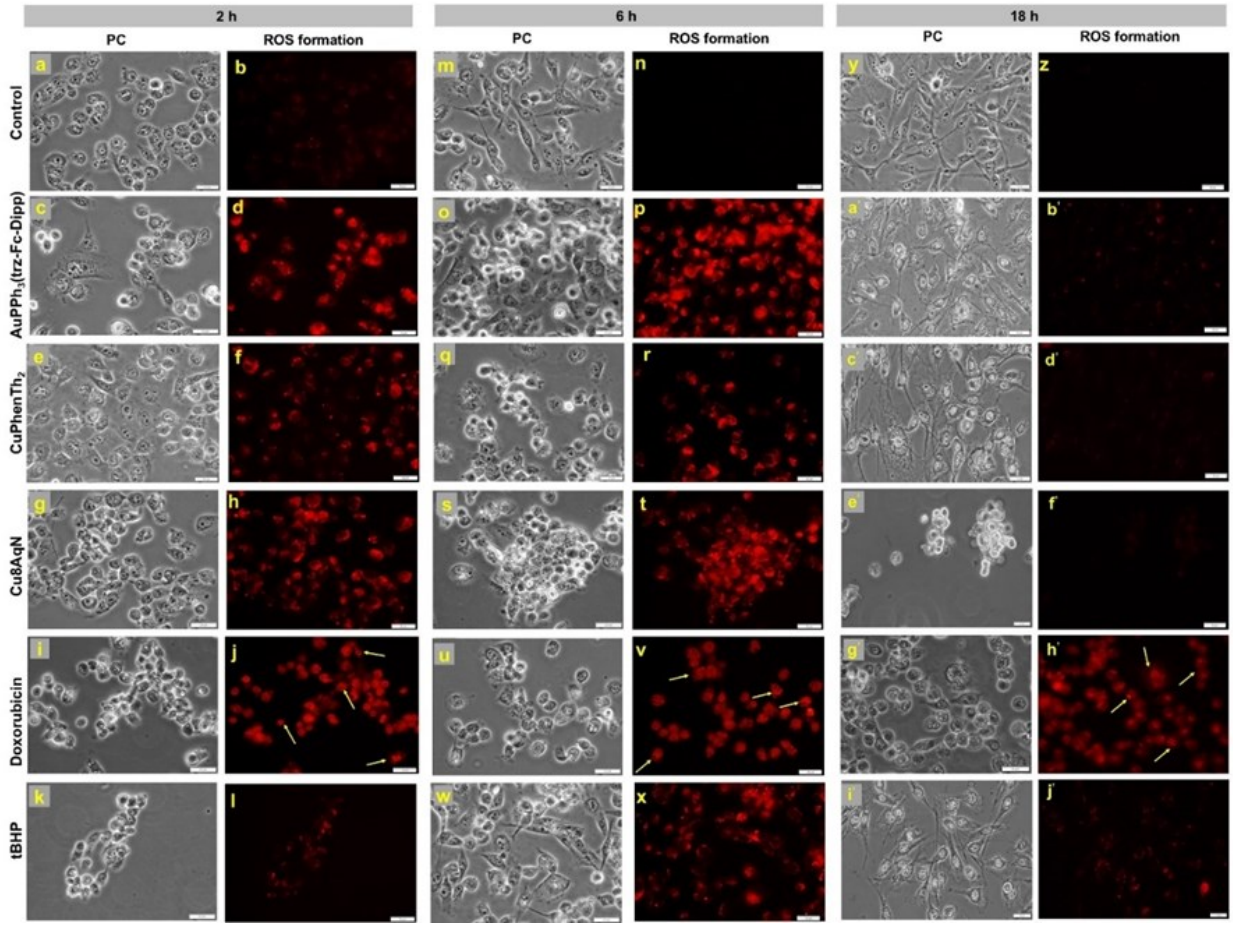


Fig. 3.6 Photomicrographs of MDA-MB-231 breast cancer cells showing ROS formation after treatment with copper and gold complexes. The MDA-MB-231 cells were treated with 5.8 µM of $AuPPh_3$(trz-Fc-Dipp), 5.6 µM of $CuPhenTh_2$, 4.2 µM of Cu8AqN, doxorubicin at 10.0 µM and tBHP at 20 µM for 2, 6, and 18 h. The cells were viewed with an Olympus BX41 epifluorescence microscope at 400 x magnification and were captured with an Olympus DP72 camera using the Olympus U-MWIG2 filter cube for ROS detection. ImageJ software analysed the images. Scalebar: 20 µm. PC=phase contrast, ROS=reactive oxygen species, h=hours.

In doxorubicin treated cells, clusters of red punctate fluorescence were detected around the nuclei indicative of ROS accumulation (Fig. 3.6, panel g' and h', Fig. 3.7). tBHP caused cell elongation and the lack of ROS formation (Fig. 3.6, panel i' and j', Fig. 3.7). ROS levels were decreased across all treatments compared to 2 and 6 h treatment. These results show that gold and copper complexes increased ROS levels, causing oxidative stress in the cells, with the strongest effects observed at 6 h treatment. The metal complexes caused the highest ROS formation than tBHP. Among the metal complexes, the gold complex $AuPPh_3$(trz-Fc-Dipp) was the most effective at generating ROS than the copper complexes.

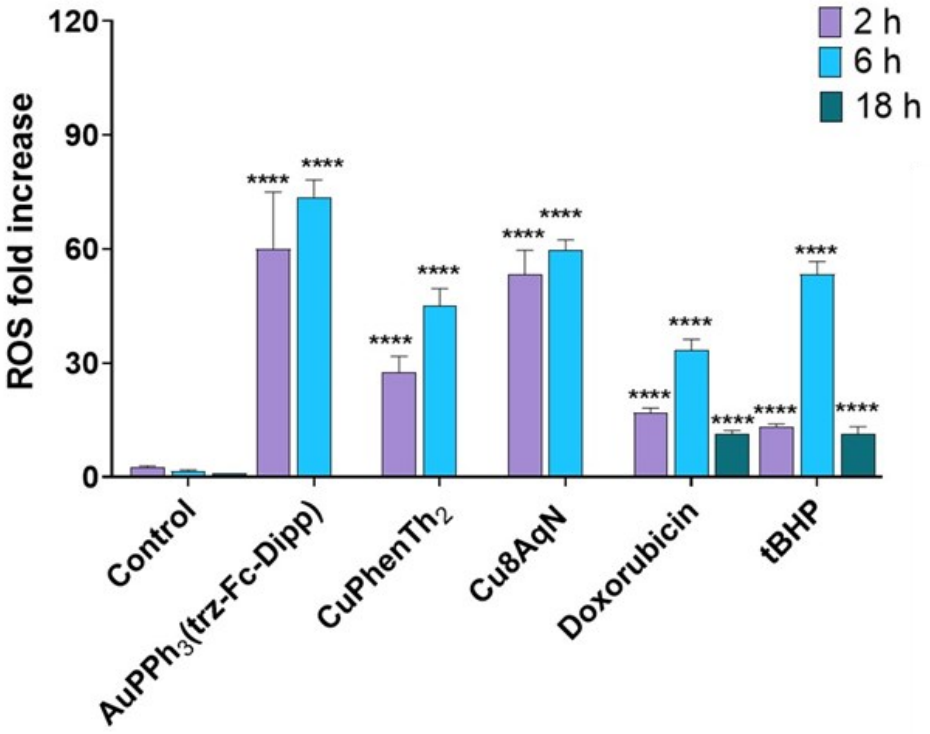


Fig. 3.7 Bar graph showing the fold increase of ROS in MDA-MB-231 breast cancer cells after treatment with the copper and gold metal complexes for 2, 6 and 18 h. Each bar represents the mean ROS fold increase obtained from three independent experiments. Data was analysed in GraphPad prism using one- way ANOVA followed by Dunnett's post-hoc comparison test. (p< 0.05) was considered significant. ROS=reactive oxygen species, h= hours, ns= not significant ****p < 0.0001= highly significant in comparison to the control.

3.3.2 The effects of metal complexes on the exposure of phosphatidyl serine

Phosphatidyl serine (PS) is translocated from the inner leaflet of the membrane to the outer plasma membrane leaflet during apoptosis (Vermes *et al.*, 1995). Annexin conjugated to Alexa-fluor 488 and propidium iodide (PI) differentiated between early apoptotic, late apoptotic, viable and necrotic cells. Annexin V was detected as bright green fluorescence while the red fluorescence indicated PI. Since PS exposure is an early event (Zhong *et al.*, 2017), Annexin V binding to PS was evaluated at 6 and 18 h. The MDA-MB-231 cells were treated with metal complexes and staurosporine at concentrations equivalent to their IC_{80}, while doxorubicin was used at 10 μM. The cells were observed with an Olympus BX41 microscope using the Olympus the U-MNIBA3 filter cube for annexin V and the U-MWIG2 for PI detection. Fluorescent images were captured with an Olympus DP72 camera and representative results are shown in Fig. 3.8 and Table 3.4.

3.3.2.1 The effects of the metal complexes on phosphatidyl serine in MDA-MB-231 breast cancer cells

The untreated control cells had typical MDA-MB-231 cell morphology with no annexin V binding/PI staining at either 6 or 18 h, indicated by the absence of green and red fluorescence in the cells (Fig. 3.8, panel a-d).

At 6 h, cells treated with $AuPPh_3$(trz-Fc-Dipp) remained spindle shaped, some were rounded with increased annexin V-only binding (white arrow) indicative of early apoptotic cells. No PI uptake was detected in the nuclei of the cells, suggesting intact cell membranes (Fig. 3.8, panel e and f). At 18 h, all cells appeared round and stained positive for both annexin V binding and PI in the nuclei indicating late apoptotic stage (red arrows) and cell membrane damage (Fig. 3.8, panel g and h; Table 3.4).

Treatment of the cells with $CuPhenTh_2$ for 6 h, caused the cells to round up and indicated early apoptosis since the cells were positive for annexin V binding only with no PI staining in the nuclei. Annexin V fluorescence was less bright compared to $AuPPh_3$(trz-Fc-Dipp) treated cells at 6 h (Fig. 3.8, panel i and j; Table 3.4).

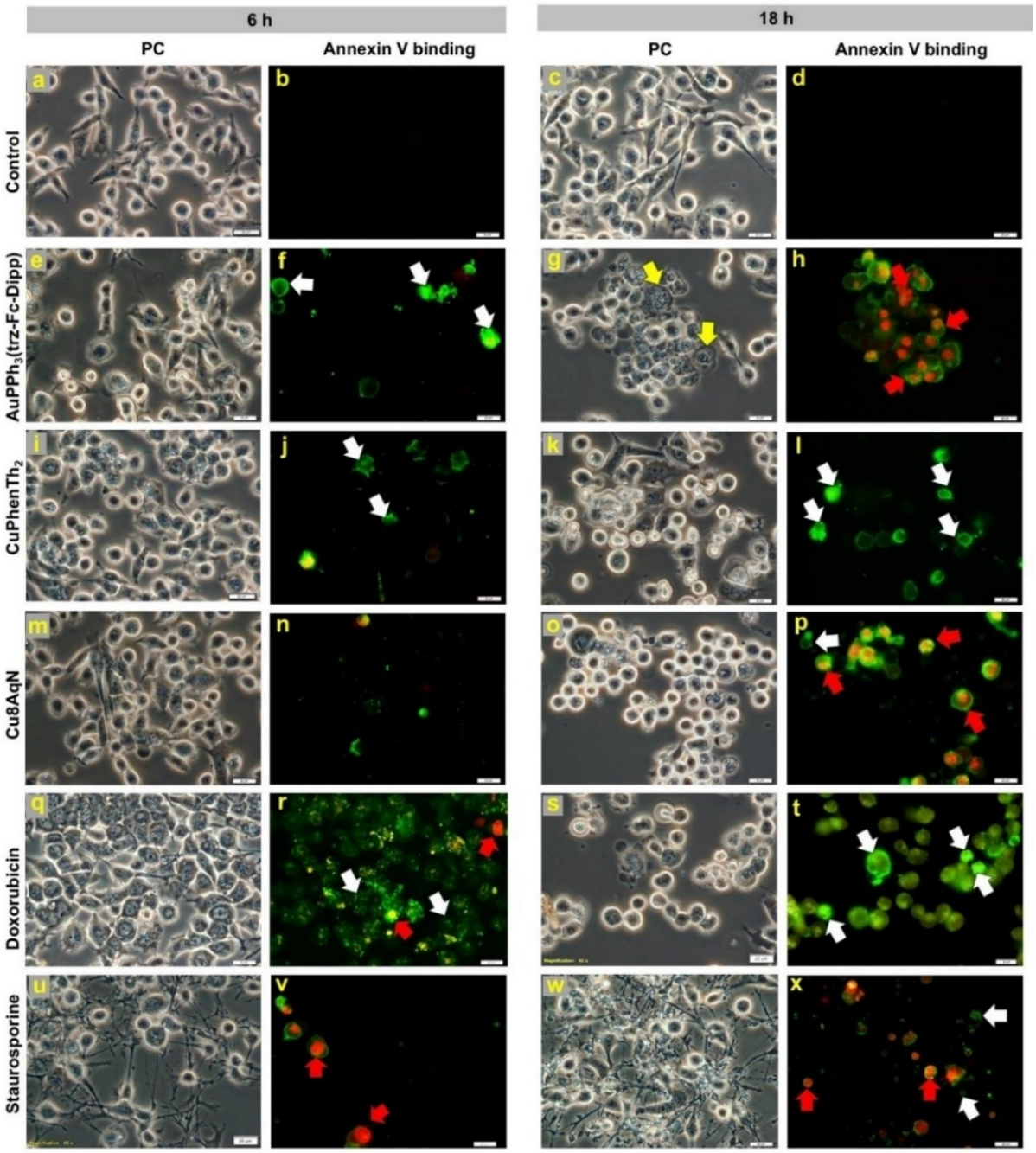


Fig. 3.8 Photomicrographs of MDA-MB-231 breast cancer cells showing annexin-V binding following treatment with metal complexes and positive controls for 6 and 18 h. The cells were treated with 5.8 µM of $AuPPh_3$(trz-Fc-Dipp), 5.6 µM of $CuPhenTh_2$, 4.2 µM of Cu8AqN, 10 µM of doxorubicin, and 0.25 µM of staurosporine. Then viewed with an Olympus BX41 epifluorescence microscope at a 400-x magnification. Images were captured with Olympus DP72 camera and analysed with the Olympus CellSens Software. Scalebar: 20 µm. Legend: white arrow =early apoptotic cells, red arrow=late apoptotic cells, PC=phase contrast, h=hours.

At 18 h, $CuPhenTh_2$ caused cells to assume a round shape in most cells but few of the cells were positive for AV only binding and no cells had PI in the nuclei, indicating early signs of apoptosis as shown by the white arrows (Fig. 3.8, panel k and l; Table 3.4).

The cells treated with Cu8AqN appeared normal with poor indication of AV binding and PI staining in the nuclei compared to $AuPPh_3$(trz-Fc-Dipp) and $CuPhenTh_2$ at 6 h treatment (Fig. 3.8, panel m and n; Table 3.4). After 18 h treatment, Cu8AqN treated cells appeared rounded and most cells had increased annexin V binding and PI staining in the nuclei suggesting late apoptosis as illustrated by the red arrows. Compared to $CuPhenTh_2$, early apoptotic cells were few as indicated by AV-only binding (Fig. 3.8, panel o and p; Table 3.4).

At 6 h, many of the cells treated with doxorubicin were granulated with annexin V only detection suggesting early apoptosis, while few cells were late apoptotic since they were positive for both annexin V binding and PI staining in the nuclei. Rounded cells positive for only annexin V binding (white arrows) were observed at 18 h treatment and indicated early apoptosis (Fig. 3.8, panel q -t; Table 3.4). Staurosporine treated cells had fibrils, assumed a round shape and showed both annexin V binding and PI stain on the nuclei suggestive of late apoptosis in 8.9 % of the cells at 6 h. Similarly, at 18 h, the cells maintained a round shape with increased number of late apoptotic cells (Fig. 3.8, panel u to x; Table 3.4).

These results show that after treatment, some cells were positive for annexin V binding, indicating early apoptosis, while in some were positive for annexin V binding, with PI staining in the nuclei suggesting late apoptotic cell death. This proved that the metal complexes caused the translocation of phosphatidylserine to the outer leaflet of the cell membrane, which is an early event associated with apoptosis. Notably, no cells were positive for PI staining only in the nuclei, suggesting loss of plasma membrane integrity and necrotic cell death.

Table 3.4: Cell percentage of early and late apoptotic MDA-MB-231 cells after treatment with metal complexes and positive controls**.**

	6 h		18 h	
Treatment	**Early apoptotic cells (%)**	**Late apoptotic cells (%)**	**Early apoptotic cells (%)**	**Late apoptotic cells (%)**
$AuPPh_{3(}$trz-Fc-Dipp)	7.00 ± 1.30	0.00 ± 0.00	11.83 ± 0.09	31.88 ± 0.81
$CuPhenTh_2$	7.38 ± 0.40	1.23 ± 0.12	20.60 ± 1.90	1.00 ± 0.99
Cu8AqN	3.37 ± 0.43	1.37 ± 0.10	6.65 ± 0.35	24.89 ± 1.60
Staurosporine	0.00 ± 0.00	8.93 ± 1.61	7.50 ± 0.95	28.09 ± 2.41
Doxorubicin	78.46 ± 0.64	3.83 ± 0.27	91.50 ± 1.50	1.60 ± 0.70

3.3.3 The investigation of effects of the metal complexes on mitochondrial membrane *(ΔΨm)* potential in MDA-MB-231 breast cancer cells

The integrity of the mitochondrial membrane is essential for cell survival and function. Disruption of the mitochondrial function leads to a loss of ΔΨM, which is an early feature of apoptosis (Green and Kroemer, 1998). The cationic dye JC-1 was used to assess the changes in ΔΨM. In healthy cells with high ΔΨM, JC-1 crosses the mitochondrial membrane and forms J-aggregates, which fluoresce red/orange. Conversely, in apoptotic cells with low ΔΨM, the JC-1 dye remains in its green monomeric form, as shown in Fig. 3.9 and 3.10. The MDA-MB-231 cells were treated for 6 and 18 h as described in section 2.5.6.

3.3.3.1 Determination of effects of the metal complexes on ΔΨm in MDA-MB-231 breast cancer cells

Untreated control cells showed an increase in red fluorescence representing JC-1 aggregates at 6 and 18 h, indicating that the cells had a healthy mitochondria and stable mitochondrial membrane potential (Fig. 3. 9 panel a-d and Fig. 3.10A and B). In contrast, the cells treated with $AuPPh_3$ (trz-Fc-Dipp) for 6 and 18 h had a low JC-1 aggregate-to-monomer ratio caused by an increase in green fluorescence and a decrease in red fluorescence, indicating the loss of mitochondrial membrane integrity and ΔΨm. At 18 h, green fluorescence was more intense than at 6 h, suggestive of

progressive mitochondrial membrane dysfunction over time (Fig. 3.9, panel e-h, and Fig. 3.10A and B).

Similarly, $CuPhenTh_2$-treated cells showed mitochondrial depolarization after 6 h, indicated by increased JC-1 monomers and decreased JC-1 aggregates. Few cells showed bright green fluorescence while other cells had poor green fluorescence (Fig. 3.9, panel i and j). At 18 h, most cells were fluorescing bright green, indicating extensive mitochondrial dysfunction and significant loss of $\Delta\Psi m$ (Fig. 3.9, panel k and l; Fig. 3.10A and B).

Cu8AqN treatment caused a significant loss of $\Delta\Psi m$ in the cells. The cells appeared round, showing a moderate green fluorescence at 6 h (Fig. 3.9, panel m and n), and shifted to bright green fluorescence in spindle-shaped cells at 18 h (Fig. 3.9, panel o and p). JC-1 aggregates decreased at both treatment times, suggesting depolarization of the mitochondrial membrane (Fig. 3.9, panel k-n) and Fig. 3.10A and B). Loss of $\Delta\Psi m$ was observed in the cells treated with doxorubicin, shown by a significant increase in JC-1 monomers and a decrease in JC-1 aggregates at 6 and 18 h, signifying mitochondrial membrane interruptions and supporting the apoptotic effect of doxorubicin (Fig. 3.9, panel q-t, and Fig. 3.10A and B).

At 6 h, the cells treated with staurosporine showed an increase in JC-1 monomers but were less bright compared to doxorubicin, but the green fluorescence was significantly increased at 18 h. The JC-1 aggregate-to-monomer ratio decreased, indicating mitochondrial membrane dysfunction (Fig. 3.9, panel u-x, and Fig. 3.10A and B).

Fig. 3.10 A and B show representative bar graphs indicating the percentage of cells with JC-1 monomers (green bars) and aggregates (red bars) at 6 h (A) and 18 h (B). At 6 and 18 h treatment, control cells had increased JC-1 aggregates (90 %), indicating a high $\Delta\Psi m$ and healthy mitochondria. In comparison to the control, the cells treated with $AuPPh_3$(trz-Fc-Dipp), $CuPhenTh_2$, Cu8AqN, doxorubicin, and staurosporine showed a significant shift towards JC-1 monomers (~ 80 – 90 % green bars), suggesting mitochondrial depolarization and a loss of $\Delta\Psi m$, and a significant reduction in JC-1 aggregates (~10- 20 % red fluorescence) was observed, confirming mitochondrial dysfunction at 6 and 18 h.

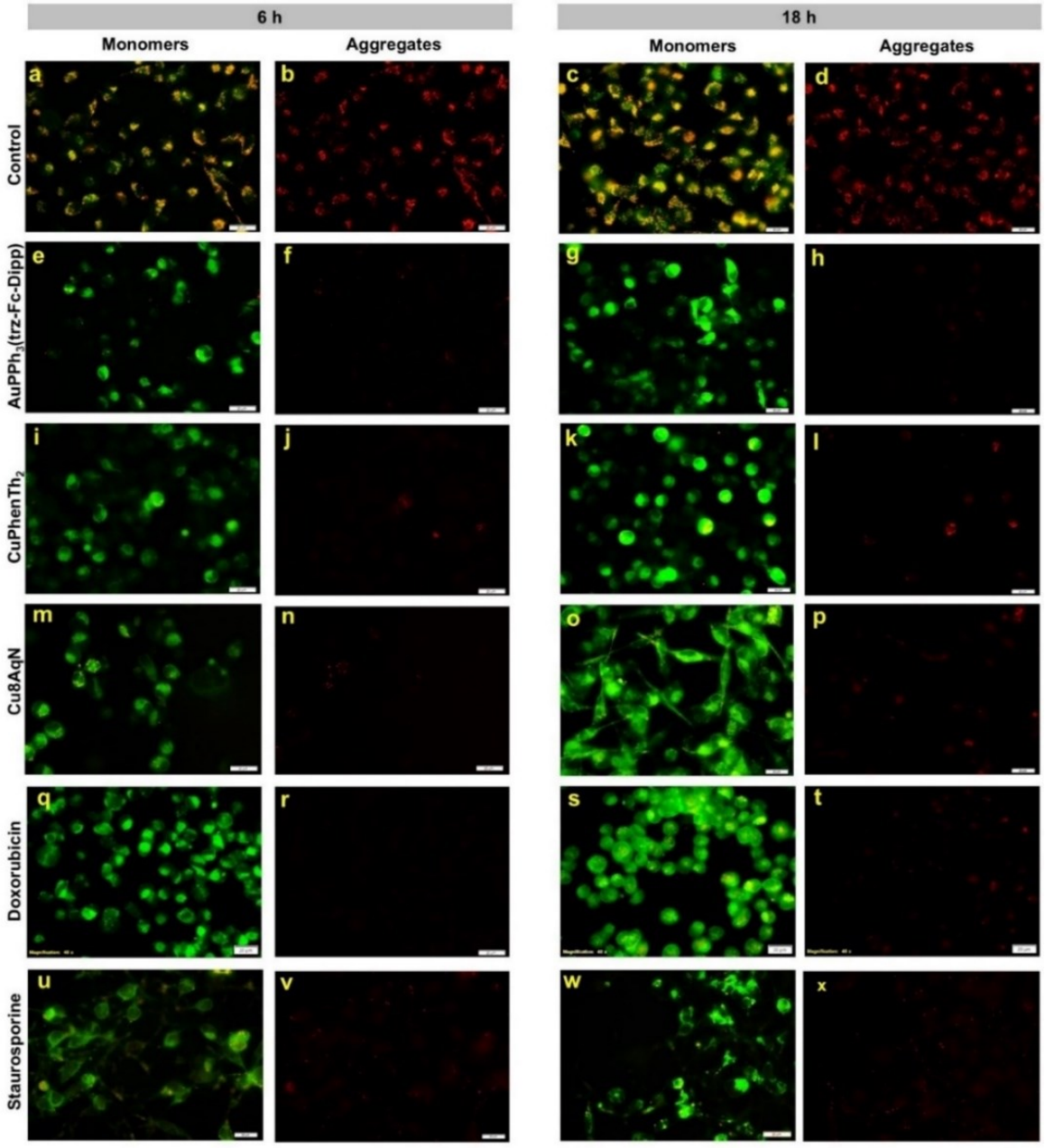


Fig. 3.9 Photomicrographs of MDA-MB-231 cells showing the effects of the metal complexes, doxorubicin and staurosporine on ΔΨm. MDA-MB-231 cells were treated with 5.8 µM of $AuPPh_3$(trz-Fc-Dipp), 5.6 µM of $CuPhenTh_2$, 4.2 µM of Cu8AqN, 10 µM of doxorubicin and 0.25 µM of staurosporine for 6 and 18 h**.** The cells were viewed with Olympus BX41 epifluorescence microscope. Images were captured with an Olympus DP72 camera and analysed with the Olympus CellSens Software. Magnification:400 x, Scalebar=20 µm, h=hours.

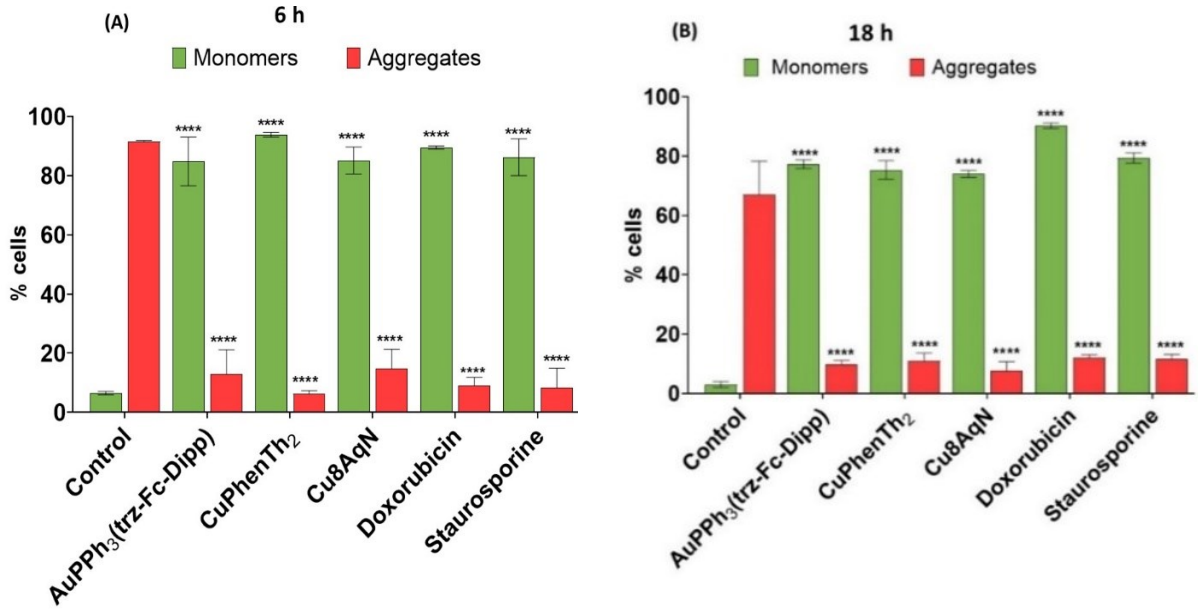


Fig. 3.10 Quantitative analysis of JC-1 aggregates and monomers in MDA-MB-231 cells after treatment with the metal complexes and positive controls for 6 and 18 h. Each bar represents the mean ± SEM of percentage of cells with JC-1 aggregates and monomers obtained from three independent experiments. Cell percentage was obtained by counting the number of cells with positive fluorescence relative to the number of cells in the accompanying phase contrast image. Data was analysed by one-way ANOVA ($p< 0.05$) followed by Dunnett's post-hoc comparison test. (**** $p< 0.0001$ = highly significant in comparison to the untreated control).

3.3.4 Evaluation of the effects of the metal complexes on caspase-9 activity

The activation of caspase-9, which is an essential caspase of the intrinsic apoptotic pathway, was measured to assess the ability of the complexes and positive controls to activate the intrinsic pathway of apoptosis. Caspase-9 inhibitor LEHD-FMK conjugated to FITC detected cells with active caspase-9 and was indicated as bright green fluorescence. Caspase 9 activation was not observed after 18h treatment period, therefore, the experiments were repeated at 24 and 48-h intervals. The cells were treated at concentrations equivalent to their IC_{80} as previously described. The effects of the metal complexes were compared to baseline expression in the untreated control cells, and the results are shown in Fig. 3.11 and Fig. 3.12.

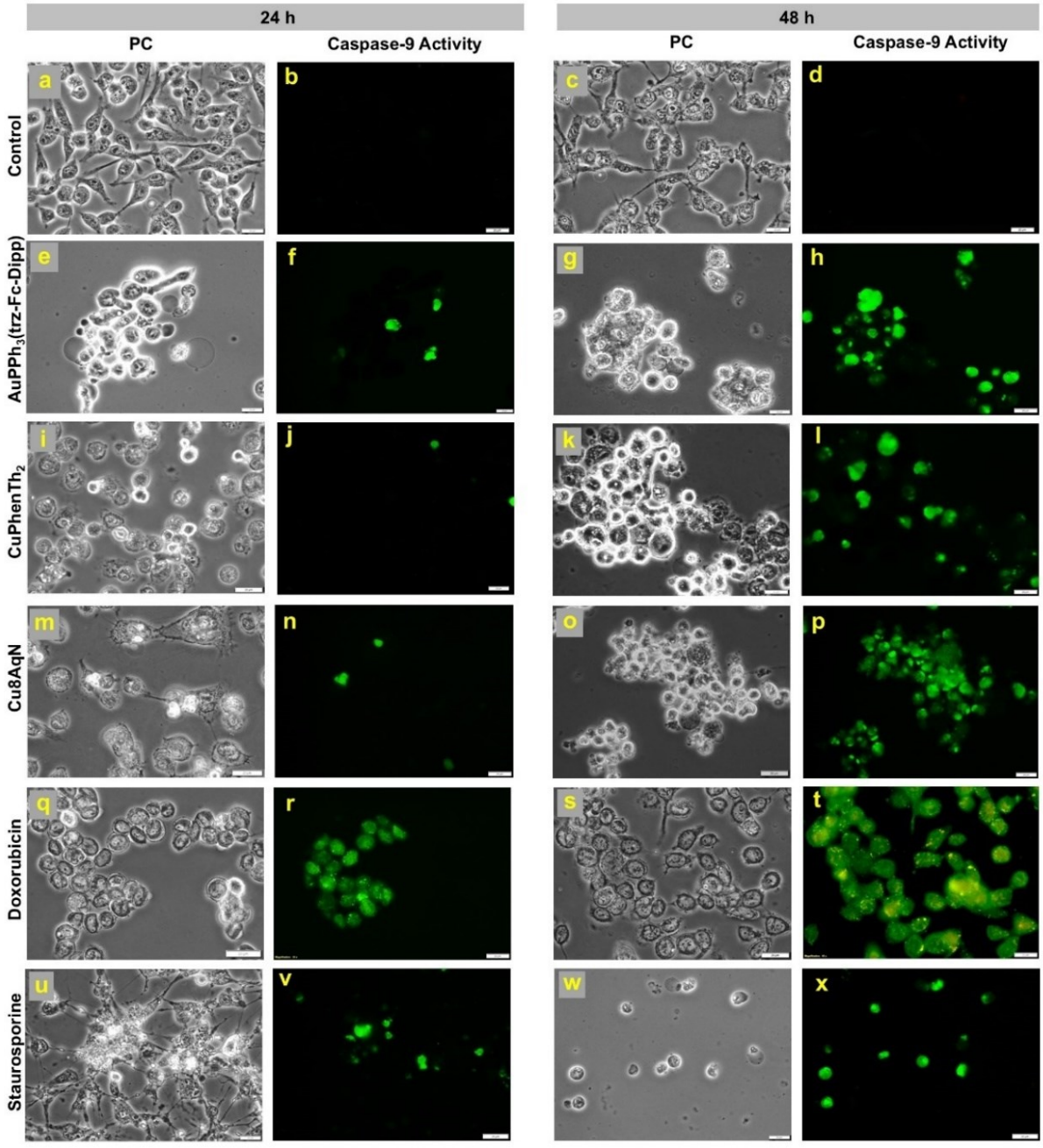


Fig. 3.11 Photomicrographs of MDA-MB-231 cells showing the effects of metal complexes on caspase-9 activity. Cells were treated with 5.8 µM of $AuPPh_3$(trz-Fc-Dipp), 5.6 µM of $CuPhenTh_2$, 4.2 µM of Cu8AqN, 10 µM of doxorubicin, and 0.25 µM of staurosporine for 24 and 48 h and viewed with an Olympus BX41 epifluorescence microscope at 400 x magnification. Images were captured with the Olympus DP72 camera and analysed with the Olympus CellSens Software. Scalebar: 20 µm. Legend: PC=phase contrast, h=hours.

3.3.4.1 Assessment of the effects of the metal complexes on caspase-9 activity in MDA-MB-231 breast cancer cells

In the untreated control cells, the phase contrast images showed cells with normal morphology at both treatment periods, and no green fluorescence was observed indicating the absence of caspase-9 activity (Fig. 3.11, panel a-d, and Fig. 3.12). $AuPPh_3$(trz-Fc-Dipp)-treated cells were rounded and adherent to the growth surface with very few cells positive for active caspase-9 at 24 h (Fig. 3.11, panel e and f, and Fig. 3.12). At 48 h, cells had detached, and caspase-9 activity was significantly increased, as indicated by increased green fluorescence (Fig. 3.11, panel g and h, and Fig. 3.12). At 24 h, $CuPhenTh_2$ caused the cells to round up slightly and only the cells on the periphery had active caspase-9 (Fig. 3.11, panel i and j, and Fig. 3.12). At 48 h, the cells were round and shiny with increased green fluorescence suggesting that caspase-9 activity was increased (Fig. 3.11, panel k and l, and Fig. 3.12).

Some Cu8AqN-treated cells maintained normal morphology but were granulated while others began to round up. Active caspase-9 was present in a few cells at 24 h (Fig. 3.11, panel m and n, and Fig. 3.12). At 48 h, most cells detached the growth surface and were round shaped, with increased green fluorescence intensity indicating the activation of caspase-9 (Fig. 3.11, panel o and p, and Fig. 3.12). Similarly, round cell morphology was present in the cells treated with doxorubicin, this was followed by caspase-9 activation in more than 50 % of the cells at 24 h, which increased to almost 100 % of the cells with active caspase-9 at 48 h (Fig. 3.11, panel q-t, and Fig. 3.12). Staurosporine caused the elongation of most cells and 19 % of cells had active caspase-9 at 24 h (Fig. 3.11, panel u and v, and Fig. 3.12).

At 48 h, all the cells treated with staurosporine had rounded with intense green fluorescence, which indicated an increase in caspase-9 activity (Fig. 3.11, panel w and x, and Fig. 3.12). Fig. 3.12 shows that at 24 h, the metal complexes and staurosporine had few cells with active caspase-9, doxorubicin showed moderate activation of caspase-9 (~55 %). At 48 h, a significant increase was observed for all treatments, with Cu8AqN showing highest caspase-9 activation (~96 %) matching the effects of doxorubicin. These results suggest that metal-complexes caused progressive caspase-9 activation, indicative of intrinsic apoptotic pathway activation and were as effective as doxorubicin.

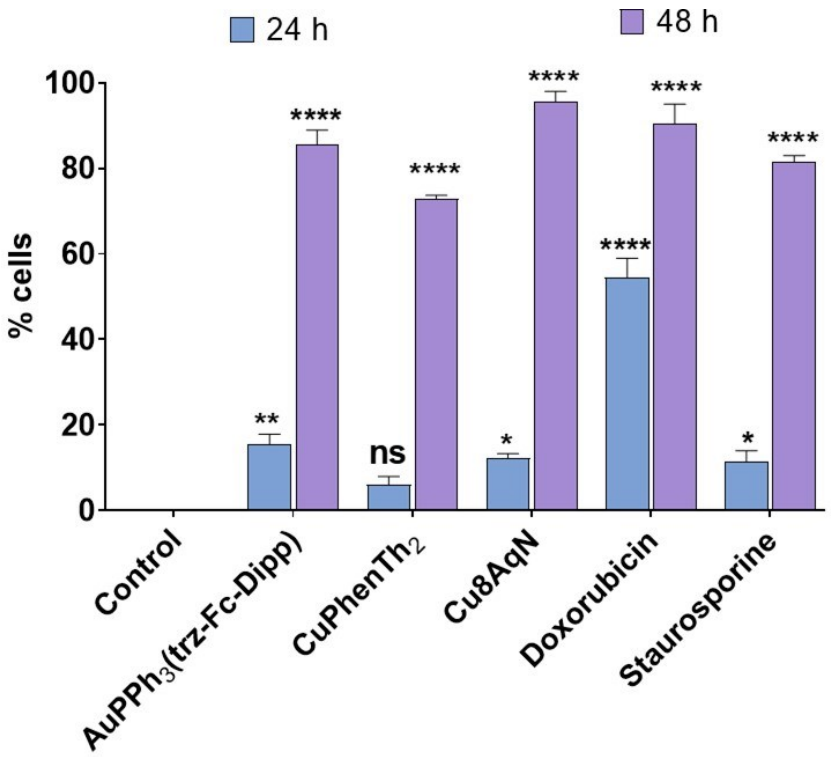


Fig. 3.12 Quantitative presentation of capaspe-9 activity in MDA-MB-231 breast cancer cells after treatment with the metal complexes and positive controls for 24 and 48 h. Each bar represents the mean ± SEM of percentage of cells with active caspase-9 obtained from three independent experiments. Data was analysed by counting % of cells with active caspase-9 relative to the corresponding phase contrast image. One way ANOVA ($p< 0.05$) followed by Dunnett's post-hoc comparison test determined significance. (*$p < 0.05$, ** $p< 0.01$, ***=$p< 0.001$, ****=$p< 0.0001$, ns=not significant in comparison to the control).

3.3.5. Assessment of caspase-8 activity

Caspase-8 assay assessed the ability of the metal complexes to activate the extrinsic apoptotic pathway in MDA-MB-231 cells. Caspase-8 activity was assessed with Red Caspase-8 staining kit. The assay uses caspase-8 inhibitor IETD-FMK conjugated to sulfo-rhodamine (Red-IETD-FMK). Red-IETD-FMK irreversibly binds to activated caspase-8 in apoptotic cells. Caspase-8 activation was observed as bright red fluorescence in the cells. The cells were treated at concentrations equivalent to IC_{80} for 18, 24 and 48 h. For this assay, staurosporine was a positive control since the innate red fluorescence of doxorubicin interfered with the assay. The results were compared to the untreated control and presented in Fig. 3.13 and 3.14.

3.3.5.1 Determination of caspase-8 activity in MDA-MB-231 breast cancer cells

The control cells showed normal morphology with no active caspase-8 at 18, 24, and 48 h (Fig. 3.13, panel a-f). In contrast, $AuPPh_3$(trz-Fc-Dipp) caused progressive apoptosis related to morphological changes in the cells. At 18 h, cells appeared slightly round with minimal fluorescence in a few cells, indicating the activation of caspase- 8 (Fig. 3.13, panel g and h; Fig. 3.14). At 24 h, the cells detached from the growth surface with increased caspase-8 activation in some cells, while, at 48 h, most cells had caspase-8 activated (Fig. 3.13, panel i and l; Fig. 3.14). A similar trend was observed in the cells treated with $CuPhenTh_2$ for 18, 24 and 48 h (Fig. 3.13, panel m-r; Fig. 3.14).

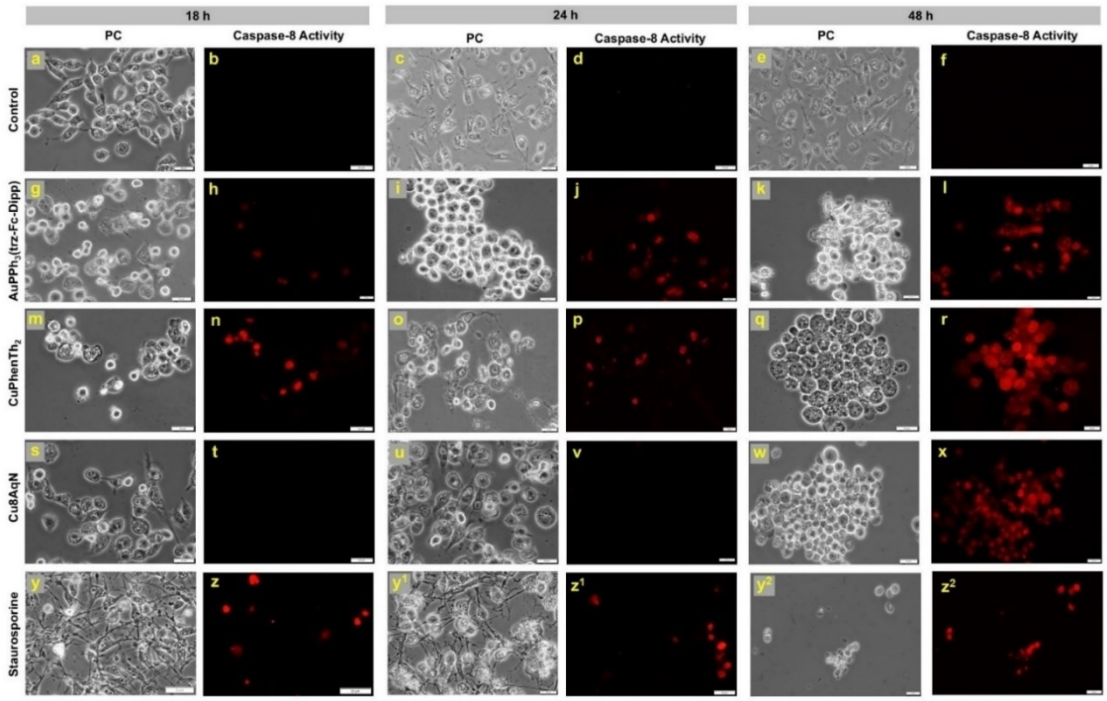


Fig. 3.13 Photomicrographs of caspase-8 positive MDA-MB-231 breast cancer cells after treatment with the metal complexes. Cells were treated with 5.8 µM of $AuPPh_3$(trz-Fc-Dipp), 5.6 µM of $CuPhenTh_2$, 4.2 µM of Cu8AqN, and 0.24 µM of staurosporine. The cells were viewed with an Olympus BX41 epifluorescence microscope at 400 x magnification. Images were captured with an Olympus DP72 camera and analysed with the Olympus CellSens Software. Scalebar: 20 µm. Legend: PC=phase contrast, h=hour

Cu8AqN treated cells were slightly rounded with no activation of caspase-8 at 18 and 24 h treatment (Fig. 3.13, panel s-v; Fig. 3.14). At 48 h, the cells were rounded and detached from the growth surface. Most cells had an intense red fluorescence indicating caspase-8 activation (Fig. 3.13, panel w and x; Fig. 3.14). The cells treated with staurosporine were adherent and elongated with some cells indicating active caspase-8 at 18 and 24 h (Fig. 3.13, panel y-z[1]; Fig. 3.14). At 48 h, all the cells were rounded with active caspase-8 (Fig. 3.13, panel y[2]-z[2]; Fig. 3.14).

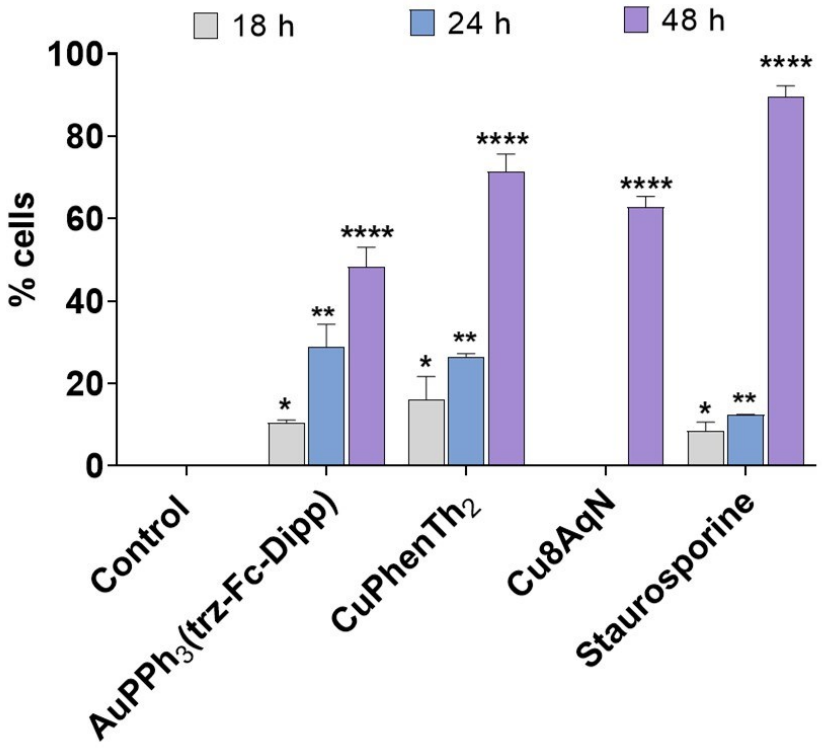


Fig. 3.14 Bar graphs showing percentage of MDA-MB-231 breast cancer cells with caspase-8 activation after treatment with the metal complexes and staurosporine for 18, 24 and 48 h. Each bar represents the percentage mean ± SEM of caspase-8 activity obtained from three independent experiments. Data was analysed by calculating the % of cells with active caspase-8 relative to the phase contrast (PC) of the corresponding image. Statistical significance was determined using GraphPad prism one way ANOVA ($p<0.05$) followed by Dunnett's post-hoc comparison test. (ns=non-significant, *$p < 0.05$, ** $p< 0.01$, ****=$p< 0.0001$ in comparison to the untreated control).

Fig. 3.14 shows bar graphs with percentage of MDA-MB-231 cells positive for caspase-8 activity. At 18 h, $AuPPh_3$(trz-Fc-Dipp), $CuPhenTh_2$ and staurosporine induced caspase-8 activation in less than 20 % of the cells, while Cu8AqN showed no caspase-8 activity in the cells. At 24 h, the cells with active caspase-8 continued to increase after treatment with $AuPPh_3$(trz-Fc-Dipp), $CuPhenTh_2$ and staurosporine (almost 40 %) and the metal complexes were more effective than staurosporine. Cu8AqN treated cells showed no caspase-8 at 24 h. At 48 h treatment, the activation of caspase-8 was significantly increased in all the treated cells, staurosporine had the highest % of cells with caspase-8, followed by $CuPhenTh_2$ then $AuPPh_3$(trz-Fc-Dipp), and lastly Cu8AqN. These results suggest that the metal complexes and staurosporine activate caspase-8 over time, which indicated the activation of the extrinsic apoptotic pathway.

3.3.6 The effect of the metal complexes on caspse-3/7 activity

Caspase-3/7 is responsible for the execution of apoptosis and is typically found in the nucleus (Olsson and Zhivotovsky, 2011). A caspase-3/7 assay was performed to confirm the execution of apoptotic cell death following the treatment with metal complexes and positive controls. A live cell assay using the CellEvent™ Caspase-3/7 green detection reagent assessed caspase-3/7 activity. This is a cell permeable four amino acid peptide-based substrate (DEVD) co-joined to the nucleic acid binding dye. DEVD peptide sequence acts as a cleavage site for caspase-3/7, the conjugated dye is non-fluorescent; it only emits fluorescence once it is separated from the peptide and attached to DNA. In the presence of apoptotic cells with activated caspase-3/7, the DEVD peptide bond is broken down, allowing for the dye to bind to the DNA and produce a bright green fluorescence. The assay was performed on MDA-MB-231 cells for two treatment periods. The results are shown in Fig. 3.15 and 3.16.

3.3.6.1 The effect of the metal complexes on caspase-3/7 activity in MDA-MB-231 cells after treatment

The untreated control cells, maintained a normal morphology and caspase-3/7 was not activated at both time points, shown in Fig. 3.15 (panel a-d) and Fig. 3.16. At 24 h treatment period, all the cells treated with $AuPPh_3$(trz-Fc-Dipp) were round and 65 % of the cells showed caspase-3/7 activation (Fig. 3.15, panel e and f; Fig. 3.16). At 48 h treatment, cell morphology remained the same but the number of cells with activated caspase-3/7 increased to 80 % (Fig. 3.15, panel g and

h; Fig. 3.16). Most $CuPhenTh_2$ treated cells appeared round at 24 h with intense green fluorescence in 20 % of the cells, indicative of caspase-3/7 activation (Fig. 3.15, panel i and j; Fig. 3.16). At 48 h, some cells were elongated while most were round with caspase-3/7 activity, (Fig. 3.15, panel k and l; Fig. 3.16).

At 24 h, the cells treated with Cu8AqN began to assume a round shape and caspase-3/7 activation was only present in the cells that were completely round (Fig. 3.15, panel m and n; Fig. 3.16). At 48 h, all the cells were round, and caspase-3/7 was activated in all of them (Fig. 3.15, panel o and p; Fig. 3.16). Doxorubicin treated cells became round with less green fluorescence after 24 h treatment (Fig. 3.15, panel q and r; Fig. 3.16). At 48 h, the round morphology of the cells treated with doxorubicin was more visible with increased green fluorescence on the cells indicating caspase-3/7 activation (Fig. 3.15, panel s and t; Fig. 3.16).

At 24 and 48 h treatment, the cells treated with staurosporine were rounded. Few cells showed activated caspase-3/7 at 24 h (Fig. 3.15, panel u and v; Fig. 3.16), while 48 h treatment increased the percentage of cells with caspase-3/7 activity, (Fig. 3.15, panel w and x; Fig. 3.16). $AuPPh_3$(trz-Fc-Dipp), and doxorubicin had more than 50 % of the cells with active caspase-3/7 while copper complexes and staurosporine were poor at inducing caspase-3/7 at 24 h treatment. At 48 h treatment all the copper and gold metal complexes increased caspase-3/7 activation on the cells compared to a 24-h treatment, but $CuPhenTh_2$ was less effective when compared to the other metal complexes, staurosporine and doxorubicin. Collectively, the data indicates that the metal complexes and the positive controls trigger the activation of caspase-3/7 in MDA-MB-231 breast cancer cells.

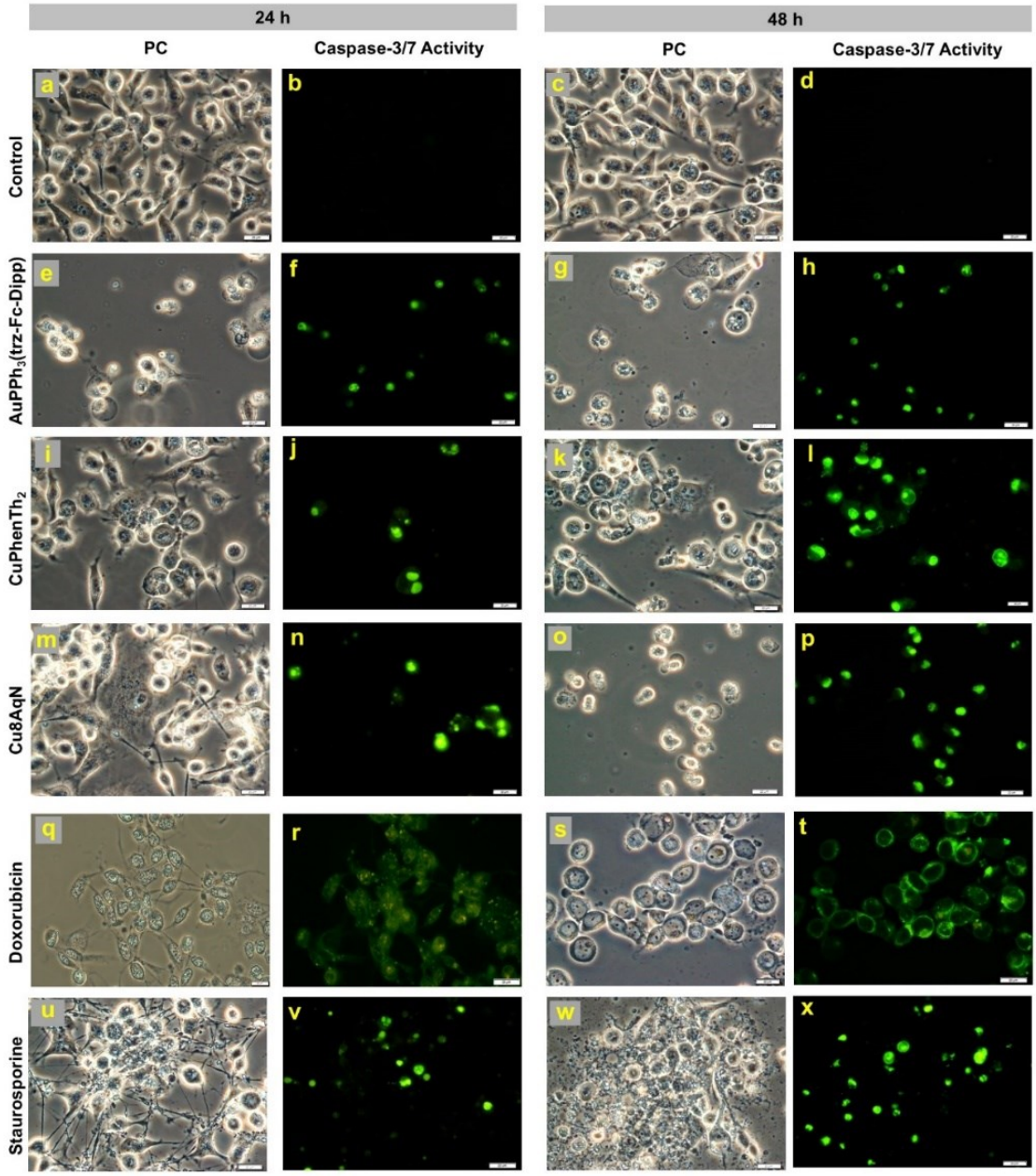


Fig. 3.15 Photomicrographs showing caspase-3/7 activity in MDA-MB-231 breast cancer cells following treatment with the metal complexes and positive controls. Cells were treated with 5.8 µM of AuPPh3(trz-Fc-Dipp), 5.6 µM of $CuPhenTh_2$, 4.2 µM of Cu8AqN, 10 µM of doxorubicin, and 0.25 µM of staurosporine. The Olympus BX41 epifluorescence microscope set at 400 x magnification was used to view the cells. Images were captured with an Olympus DP72 camera and analysed with the Olympus CellSens Software. Scalebar: 20 µm. Legend: PC=phase contrast, h=hour

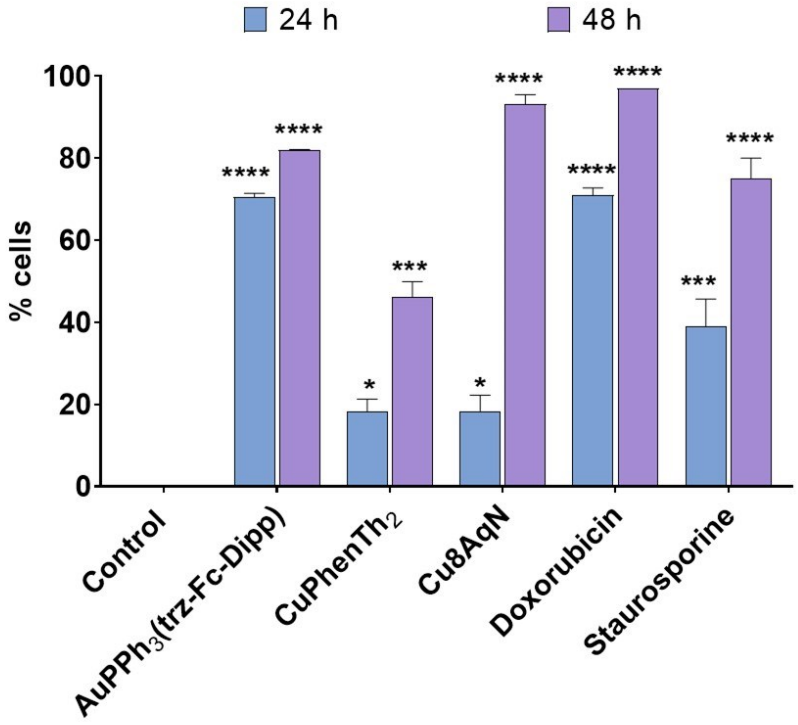


Fig. 3.16 Bar graphs showing percentage of MDA-MB-231 cells positive for active caspase-3/7 after treatment with the metal complexes and positive controls. Each bar represents the percentage mean ± SEM of caspase-3/7 positive cells obtained from three independent experiments. Data was analysed by one way ANOVA ($p< 0.05$) followed by Dunnett's post-hoc comparison test. Comparing the effects of the treated cells to the untreated control. *$p < 0.05$, *** $p< 0.001$, ****$p< 0.0001$ in comparison to the untreated control).

3.4 Proteome profiler human apoptosis array

Following the confirmation that copper complexes cause apoptotic cell death in MDA-MB-231 cells, Cu8AqN and $CuPhenTh_2$ were selected as the lead candidates to evaluate their effects using an apoptosis proteome array. Cu8AqN and $CuPhenTh_2$ had the lowest IC_{50} values of 3.31 ± 0.06 μM and 1.89 ± 0.14 μM respectively, in MDA-MB-231 cancer cells, while showing high IC_{50} values of 9.51 ± 0.03 μM and 5.76 ± 1.96 μM in MCF-10A mammary epithelial cells, indicating some selectivity towards cancer cells. Doxorubicin was selected as the positive control since it is used clinically in the treatment of TNBC.

The Proteome profiler human apoptosis array is an antibody-based array, and useful to evaluate the expression of 35 apoptosis-related proteins simultaneously. The proteome array detects proteins associated with the execution and regulation of apoptosis, thereby providing a better understanding of the effects of the copper complexes on apoptosis. MDAMB-231 cells were treated with Cu8AqN at a concentration of 3.1 μM, $CuPhenTh_2$ at a concentration of 2.3 μM, and doxorubicin at a concentration of 10.0 μM. The concentrations were selected since no obvious changes in the gross morphology of the treated cells were observed in the cells after an 18-h treatment period. At the end of the treatment period, the cells were harvested and lysed, protein concentration of the lysates was determined with the Bradford assay. The whole cell lysates containing 400 μg of protein each were incubated overnight on a rocking platform at 4 ^{0} C with the membrane arrays to detect apoptosis related proteins.

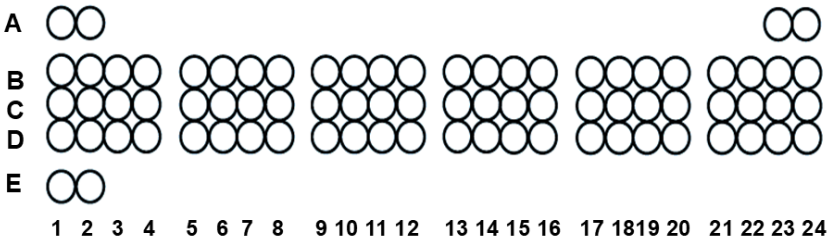


Fig. 3.17 Coordinates for the human apoptosis array, display each apoptosis-related protein with a pair of duplicate spots.

The apoptosis-related proteins were detected as a pair of duplicate spots on the membranes. The orientation of the membranes and the position of each protein is shown in Fig. 3.17 above. The corresponding coordinates are shown in Table 3.5. Relative protein expression levels were determined by measuring the pixel density of each spot on the membrane and calculating the average pixel density of the pair of duplicate spots representing each apoptosis-associated protein. Pixel densities of the proteins were graded and classified as shown in Table 3.6 below. The percentage change in protein expression was obtained by comparing the pixel density of each protein in the treated cells to that of untreated control cells, this is shown in Table 3.7. Due to the semi-quantitative nature of the array, changes in expression levels below 15 % were not considered meaningful. Changes greater than 15 % are shaded in green. Additionally, changes in the expression of poorly expressed proteins, even if statistically significant, were not meaningful.

Table 3.5: Target proteins and their corresponding coordinates on the proteome membrane array.

Target protein/ control	Co-ordinate	Target protein/ control	Co-ordinate
Reference Spots	A1, A2, A23, A24	**HO2/HMOX2**	C13, C14
Bad	B1, B2	**HSP27**	C15, C16
Bax	B3, B4	**HSP60**	C17, C18
Bcl-2	B5, B6	**HSP70**	C19, C20
Bcl-x	B7, B8	**HTRA2/Omi**	C21, C22
Pro-Caspase-3	B9, B10	**Livin**	C23, C24
Cleaved Caspase-3	B11, B12	**PON2**	D1, D2
Catalase	B13, B14	**p21/CIP1/CDKN1A**	D3, D4
cIAP-1	B15, B16	**p27/Kip1**	D5, D6
cIAP-2	B17, B18	**Phospho-p53 (S15)**	D7, D8
Claspin	B19, B20	**Phospho-p53 (S46)**	D9, D10
Clusterin	B21, B22	**Phospho-p53 (S392)**	D11, D12
Cytochrome c	B23, B24	**Phospho-Rad17 (S635)**	D13, D14
TRAIL R1/DR4	C1, C2	**SMAC/Diablo**	D15, D16
TRAIL R2/DR5	C3, C4	**Survivin**	D17, D18
FADD	C5, C6	**TNF RI/TNFRSF1A**	D19, D20
Fas/TNFRSF6/CD95	C7, C8	**XIAP**	D21, D22
HIF-1α	C9, C10	**PBS**	D23, D24
HO1/HMOX1/HSP32	C11, C12	**Reference Spots**	E1, E2

Table 3.6: The grading scale of pixel density was used to classify the expression level.

Pixel density	Expression level grading
50 000- 100 000	Very low
100 000-300 000	Low
300 000- 600 000	Moderate
600 000- 80 000	Moderately high
800 000- 1100 000	High
1100 000-1400 000	Very high

3.4.1 The effects of copper complexes and doxorubicin on apoptotic regulatory proteins in MDA-MB-231 breast cancer cells

MDA-MB-231 control cells expressed various levels of proteins associated with apoptosis as shown in Fig. 3.18. The changes in apoptosis related proteins are reflected in the intensity and the size of the dots. The treatment of the cells with the copper complexes and doxorubicin altered the expression of the proteins as shown in. Fig. 3.18 and Table 3.7 below.

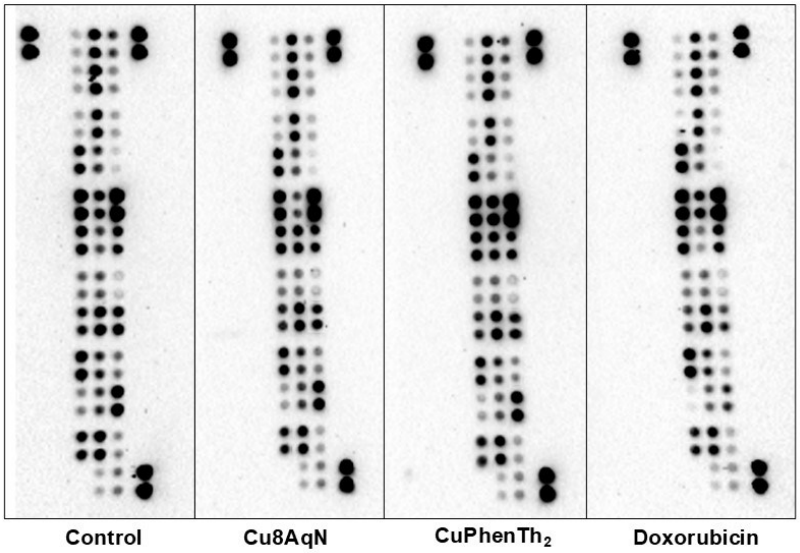


Fig. 3.18 Chemiluminescent signals on nitrocellulose membrane arrays showing the relative expression levels of apoptosis-related proteins in MDA-MB-231 breast cancer cells. MDA-MB-231 cells were treated with 3.1 µM of Cu8AqN, 2.3 µM of $CuPhenTh_2$, and doxorubicin at 10 µM for 18 h. Each membrane was incubated with cell lysate containing 400 µg of protein. Chemiluminescent images were captured using the BIO-RAD ChemiDoc™ MP Imager, analysed using BioRad Image Lab software version V and presented as pixel density.

Table 3.7: Percentage change in the expression of apoptosis related proteins in MDA-MB-231 cells after treatment with copper complexes and doxorubicin for 18 h.

Apoptosis proteins	Baseline expression	Treatment		
		Cu8AqN	$CuPhenTh_2$	Doxorubicin
Bad	Moderate	-47.90	-29.42	-21.74
Bax	Low	-17.66	-2.57	-7.21
Bcl-2	Low	-15.90	-12.43	-42.09
Bcl-X	Low	-58.48	-6.27	-36.17
Pro-caspase-3	Very high	+9.44	+7.87	+6.18
Cleaved Caspase-3	Moderate high	-8.45	-15.79	+5.64
Catalase	Low	-3.51	+3.24	-1.39
cIAP-1	High	-16.19	-23.08	-56.91
cIAP-2	Low	+1.18	-27.74	-42.03
Claspin	Very high	-2.06	-3.14	-69.35
Clusterin	Low	-1.42	-8.11	-10.00
Cytochrome c	Low	+17.60	+10.40	+4.10
Trail R1/DR4	High	-3.05	-11.60	-21.81
Trail R2/DR5	High	-12.32	-9.76	-22.36
FADD	High	-8.50	-12.81	-28.51
Fas/TNFRSF6/CD95	Moderate	-18.05	-35.65	-11.39
HIF-1α	High	-45.85	+97.11	+10.29
HO1/HMOX1	Moderate	+105.92	+78.60	-31.25
HO2/HMOX2	Moderate	-27.88	-14.89	-13.96
HSP27	Very high	+3.46	+4.52	-2.69
HSP60	Moderate	-3.38	-11.08	-1.78
HSP70	Moderate	-2.69	-16.90	-31.11
HtrA2/Omi	High	-13.32	-11.33	-27.73
Livin	Very low	-21.77	-12.07	-7.34
PON2	Low	-20.50	-31.03	-46.66
p21/CIP1CDKN1A	Low	-26.47	-30.29	-18.00
p27/Kip1	Low	-11.30	-30.70	-61.06
Phospho-p53 (S15)	High	-1.21	-7.40	+83.92
Phospho-p53 (S46)	Very high	-3.97	-13.42	+10.12
Phospho-p53 (S392)	High	-1.86	-7.36	+12.34
Phospho-Rad17(S635)	Low	-5.95	-24.61	-7.46
Smac/DIABLO	Moderate	-10.67	-21.22	-23.57
Survivin	High	-33.60	-43.53	+11.64
TNF RI/TNFRSF1A	Low	-25.76	-35.22	-78.82
XIAP	Moderate high	-30.37	-31.66	-33.33

The percentage change shows the change in the expression of the apoptosis-related proteins in the treated cells relative to the untreated control. The negative value indicates a decrease in the proteins, while the positive represents an increase. Green shading =change expression level of protein greater than 15 %.

3.4.2 The effects of copper complexes on the expression levels of phosphorylated p53 species in MDA-MB-231 breast cancer cells

MDA-MB-231 untreated control cells showed high baseline expression of phospho-p53(s15) and phospho-p53(s392) while phospho-p53(s46) was very high as shown in Fig. 3.19A and B, respectively. The treatment of the cells with Cu8AqN and $CuPhenTh_2$ did not change the expression of the three phosphorylated species of p53, in contrast to doxorubicin, which significantly increased the expression levels of phospho-p53(s15), phospho-p53(s46) and phospho-p53(s392).

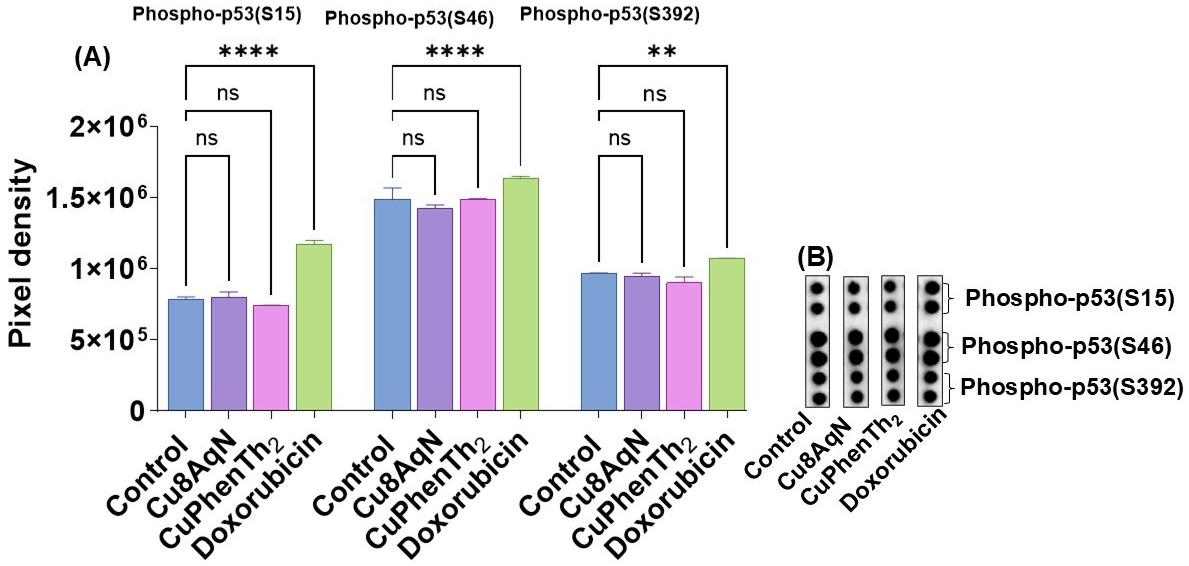


Fig. 3.19 The effects of copper complexes and doxorubicin on the expression levels of phosphorylated p53 species in MDA-MB-231 breast cancer cells. The cells were treated with 3.1 µM of Cu8AqN, $CuPhenTh_2$ at 2.3 µM and 10 µM of doxorubicin for 18 h. **(A)** is a bar graph showing the effects of the copper complexes and doxorubicin on the expression of phospho-p53(s15), phospho-p53(s46) and phospho-p53(s392). **(B)** shows the segment of the nitrocellulose membrane array with the blots for each protein. $^{**}p < 0.01$, $^{****}p < 0.0001$, ns= not significant

3.4.3 The effects of copper complexes on expression levels of the Bcl-2 family proteins in MDA-MB-231 breast cancer cells

The baseline expression of BAD was moderate in MDA-MB-231 untreated control cells (Fig. 3.20A and B), and its expression was decreased by both copper complexes and doxorubicin with Cu8AqN causing the greatest decrease. The baseline expression of Bax was low in the untreated control cells and was not changed after treatment with Cu8AqN, $CuPhenTh_2$ and doxorubicin. The MDA-MB-231 control cells had low baseline expression of Bcl-2 and Bcl-x protein. Treating the cells with Cu8AqN, and $CuPhenTh_2$ caused insignificant changes to Bcl-2 expression, while doxorubicin significantly decreased ($p< 0.01$). Cu8AqN caused a significant reduction ($p< 0.01$) of Bcl-x levels in the cells, in comparison to $CuPhenTh_2$ and doxorubicin which did not cause significant changes. The effects of the Cu8AqN, $CuPhenTh_2$ and doxorubicin were less meaningful since Bcl-2, and Bcl-x proteins were poorly expressed in MDA-MB-231 untreated control cells.

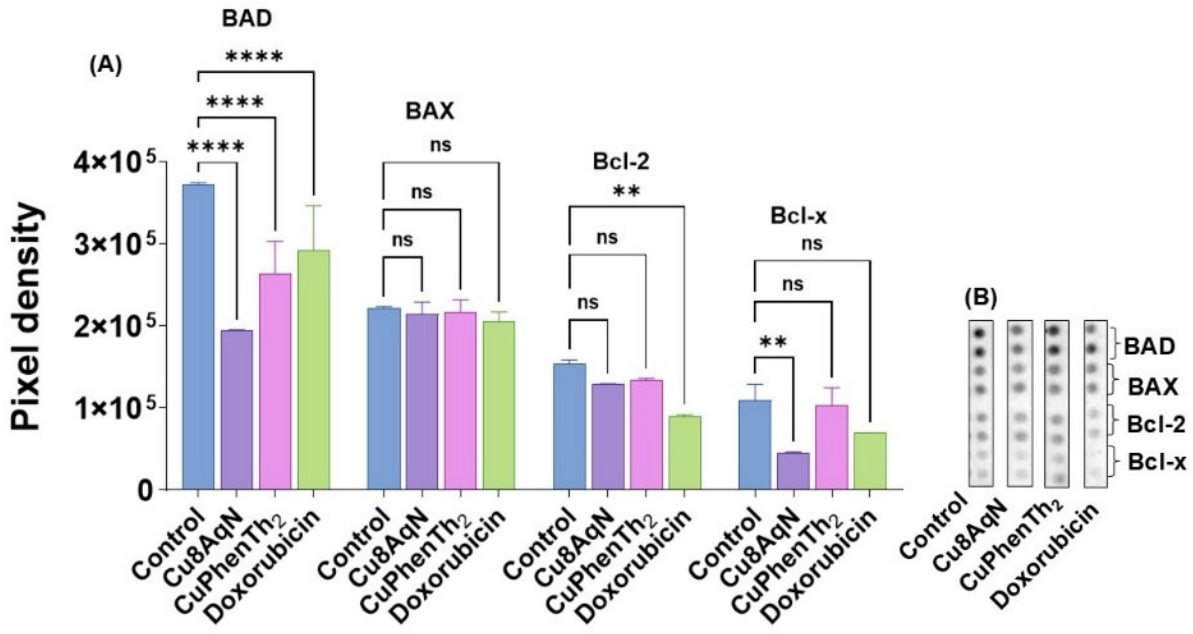


Fig. 3.20 The effects of copper complexes and doxorubicin on Bcl-2 family proteins in MDA-MB-231 breast cancer cells. The cells were treated with 3.1 µM of Cu8AqN, $CuPhenTh_2$ at 2.3 µM and 10 µM of doxorubicin for 18 h. **(A)** shows the effects of copper complexes and doxorubicin on the expression of Bad, Bax, Bcl-2 and Bcl-X **(B)** shows the segment of the nitrocellulose membrane array with the blots for each protein. $^{**}p<0.01$, $^{****}p< 0.0001$, ns= not significant

3.4.4 The effects of the copper complexes and doxorubicin on the expression levels of cytochrome c, Smac/DIABLO and HtrA2 in MDA-MB-231 breast cancer cells

Cytochrome c baseline expression in the control cells was low (Fig. 3.21A and B). Cu8AqN caused a small increase of cytochrome c levels ($p< 0.01$) compared to the control. $CuPhenTh_2$ and doxorubicin did not cause any significant changes to cytochrome c expression after treatment, and this was less meaningful. Basal expression of Smac/DIABLO was moderate and significantly decreased following the treatment of the cells with Cu8AqN, $CuPhenTh_2$, and doxorubicin. In the untreated cells, the baseline expression of HtrA2 was high, but treatment of the cells with Cu8AqN, $CuPhenTh_2$ and doxorubicin significantly reduced ($p< 0.0001$) the expression of HtrA2 in the cells after treatment.

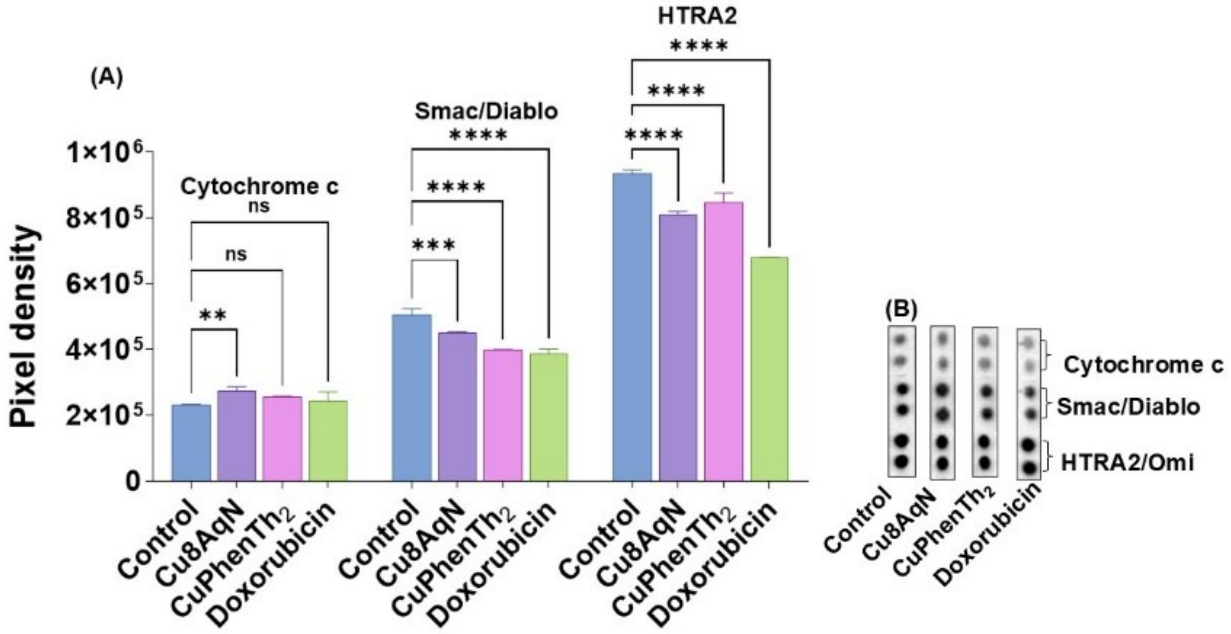


Fig. 3.21 The effects of copper complexes on the levels of cytochrome c, Smac/DIABLO, and HtrA2 in MDA-MB-231 breast cancer cells. The cells were treated with 3.1 µM of Cu8AqN, $CuPhenTh_2$ at 2.3 µM and 10 µM of doxorubicin for 18 h. **(A)** shows the effects of the $CuPhenTh_2$, and doxorubicin on the expression levels cytochrome c, Smac/DIABLO, and HtrA2 **(B)** shows the segment of the nitrocellulose membrane array with the blots for each protein. $^{**}p< 0.01$, $^{***}p< 0.001$, ****, $p< 0.0001$, ns= not significant.

3.4.5 The effects of the copper complexes and doxorubicin on the expression of death receptor proteins in MDA-MB-231 breast cancer cells

Baseline expression levels of TRAIL R1, TRAIL R2 and FADD were high in the control cells, whilst Fas was moderate and TNF-R1 was low as shown in Fig. 3.22A and B. TRAIL R1 expression levels were not changed in the cells after treatment with the copper complexes and doxorubicin. The treatment of the cells with Cu8AqN and doxorubicin marginally reduced the expression levels of TRAIL R2 compared $CuPhenTh_2$ which had no effects on the expression of TRAIL R2. Fas/TNFSF6 baseline expression was moderate in the control cells. Cu8AqN, $CuPhenTh_2$, and doxorubicin decreased the expression of Fas/TNFSF6 ($p< 0.0001$) in the cells, with $CuPhenTh_2$ showing a greater effect ($p< 0.0001$) than Cu8AqN and doxorubicin ($p< 0.01$). Baseline expression of TNF R1 was low and treatment with the copper complexes and doxorubicin ($p< 0.0001$) significantly suppressed TNF R1 levels compared to the control, as shown in Fig. 3.22A and B.

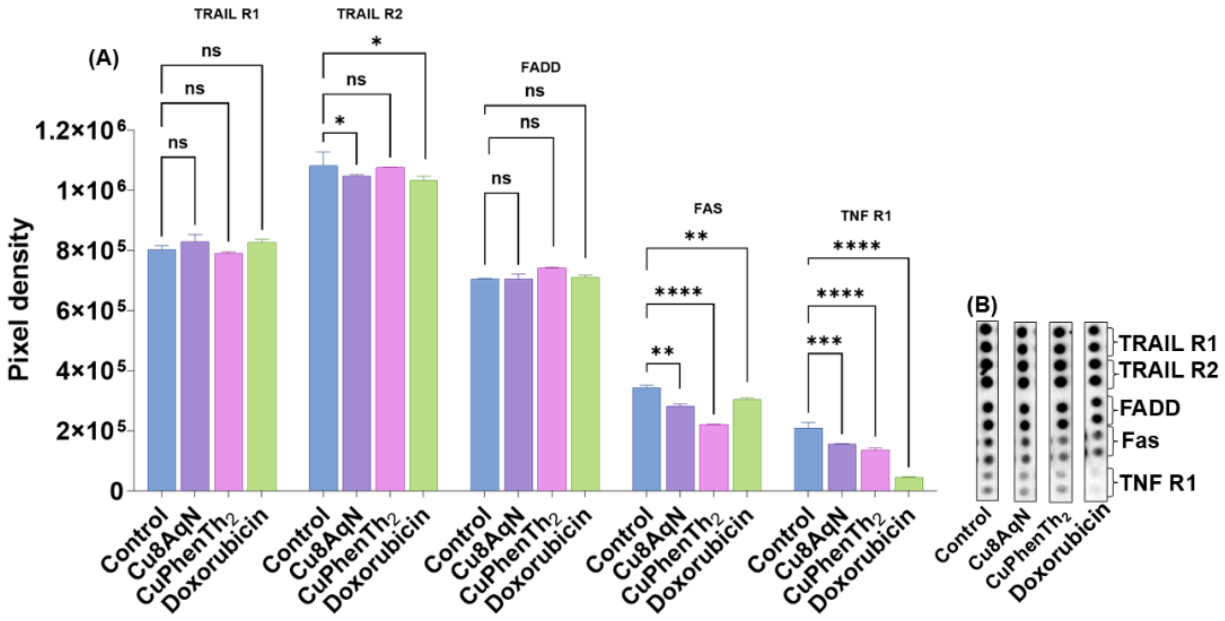


Fig. 3.22 The effects of copper complexes on expression of death receptor proteins in MDA-MB-231 breast cancer cells. The cells were treated with 3.1 µM of Cu8AqN, $CuPhenTh_2$ at 2.3 µM and 10 µM of doxorubicin for 18 h. **(A)** shows the effects of copper complexes and doxorubicin on the expression of TRAIL/DR4, TRAIL/DR5, FADD, Fas and TNF R1 **(B)** shows the segment of the nitrocellulose membrane array with the blots for each protein**$p< 0.01$, ***$p< 0.001$, ****$p< 0.0001$, ns= not significant.

3.4.6 The effects of copper complexes and doxorubicin on the expression levels of p21/Cip1, p27Kip1 and phospho-Rad17 in MDA-MB-231 breast cancer cells

Baseline expression of p21/CIP1 (Fig. 3.23A and B) was low in the control cells, and treatment of the cells with Cu8AqN, $CuPhenTh_2$, and doxorubicin significantly decreased the expression of p21 in the cells ($p< 0.01$). Similarly, baseline expression of p27/KiP1 was low in the control cells. Cu8AqN did not affect its expression, in contrast with $CuPhenTh_2$ and doxorubicin which significantly suppressed p27/KiP1 in the cells ($p< 0.0001$). Although the changes were statistically significant, the changes were less meaningful since both proteins were poorly expressed in the control cells. Baseline expression of phospho-Rad17(s653) was low in the control cells. Cu8AqN suppression was not statistically significant while $CuPhenTh_2$ ($p< 0.0001$), and doxorubicin ($p< 0.05$) significantly decreased the levels of Phospho-Rad17(s653). The results were less meaningful because of the low basal levels.

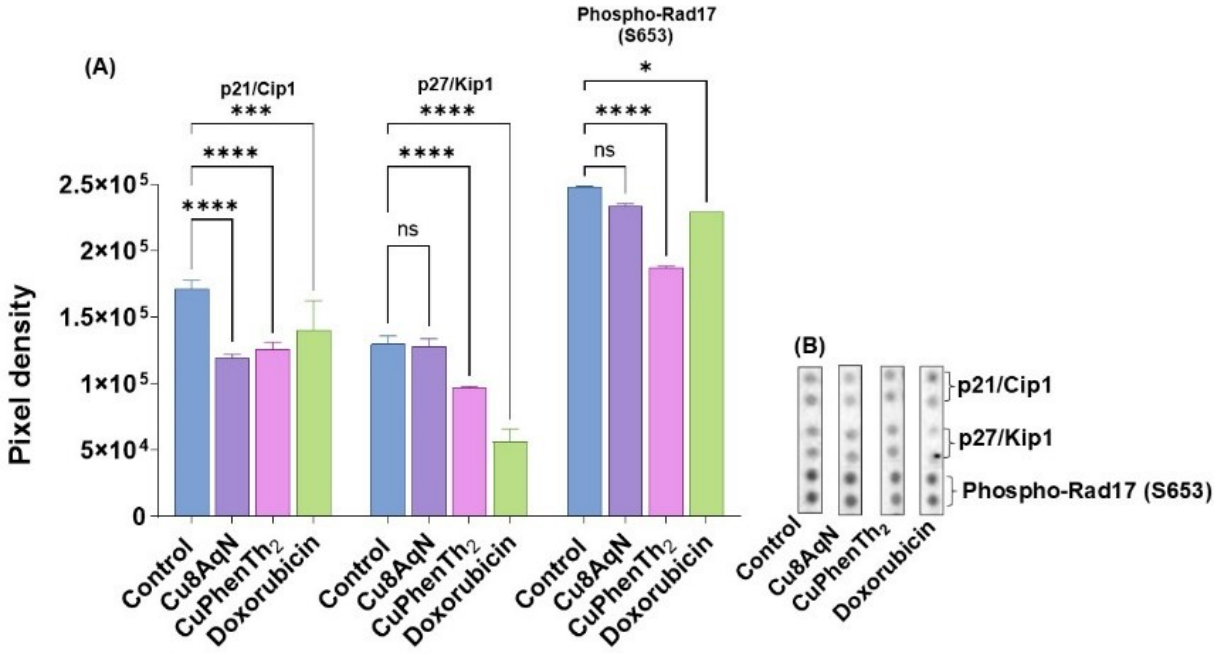


Fig. 3.23 The effects of copper complexes and doxorubicin on the expression levels of p21/Cip1,p27Kip1 and phosho-RAD17 (s653) in MDA-MB-231 breast cancer cells. The cells were treated with Cu8AqN at 3.1 µM, CuPhenTh2 at 2.3 µM and doxorubicin at 10 µM for 18 h. **(A)** shows the effects of the copper complexes and doxorubicin on the expression of p21, p27 and Phospho-Rad 17 (s653). **(B)** show the segment of the nitrocellulose membrane array with the blots for each protein. *$p< 0.05$, ***$p< 0.001$, ****, $p< 0.0001$, ns= not significant.

3.4.7 The effects of copper complexes on the expression levels of IAPs: cIAP-1, cIAP-2, livin, survivin and XIAP in MDA-MB-231 breast cancer cells

The baseline expression level of cIAP-1 was high, while baseline of cIAP-2 was low. The treatment with Cu8AqN, CuPhenTh$_2$, and doxorubicin significantly decreased the level of cIAP1 in the cells, Fig. 3.24A and B. CuPhenTh$_2$ and doxorubicin decreased the expression levels of cIAP-2, while Cu8AqN had no effect. Baseline expression of livin was very low and the observed effects were less meaningful. The baseline expression levels of survivin in the MDA-MB-231 control cells were high and treatment of the cells with Cu8AqN and CuPhenTh$_2$ caused a significant decrease ($p< 0.0001$) in survivin expression levels whilst doxorubicin treatment increased ($p<0.0001$) survivin. In the control cells, XIAP baseline expression was moderately high. The cells treated with Cu8AqN, CuPhenTh$_2$, and doxorubicin had highly significant ($p<0.0001$) and meaningful decrease of XIAP expression.

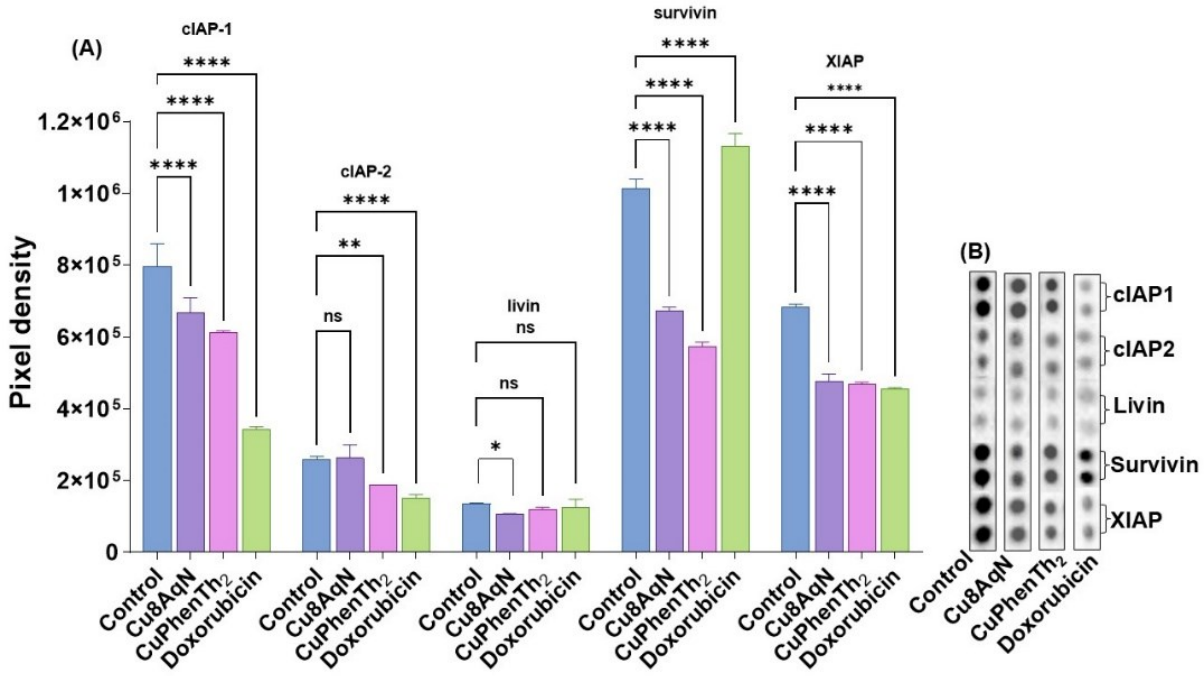


Fig. 3.24 The effects of copper complexes and doxorubicin on the expression levels of IAPs in MDA-MB-231 breast cancer cells. The cells were treated with Cu8AqN at 3.1 µM, CuPhenTh$_2$ at 2.3 µM and doxorubicin at 10 µM for 18 h. **(A)** shows the effects of copper complexes and doxorubicin on the expression of cIAP1, cIAP2, livin, survivin and XIAP **(B)** show the segment of the nitrocellulose membrane array with the blots for each protein. *$p< 0.05$, **$p< 0.01$, ****, $p< 0.0001$, ns= not significant.

3.4.8 The effects of the copper complexes on the expression of heat shock proteins: HSP27, HSP60, HSP70 and PON2 in MDA-MB-231 breast cancer cells

In untreated cells the baseline expression of HSP27 was high, in contrast to the expression of HSP60 and HSP70 which was moderate as shown in Fig. 3.25A and B. The treatment of the cells with Cu8AqN, $CuPhenTh_2$ and doxorubicin caused no significant changes to the expression of HSP27 and HSP60. HSP70 levels were significantly suppressed by $CuPhenTh_2$ and doxorubicin ($p< 0.0001$),whilst Cu8AqN had no effect. PON2 baseline expression levels were low in the control cells. Treatment of the cells with Cu8AqN, $CuPhenTh_2$ and doxorubicin significantly decreased the expression levels of PON2 in the cells but given the low baseline expression levels, the changes were less meaningful.

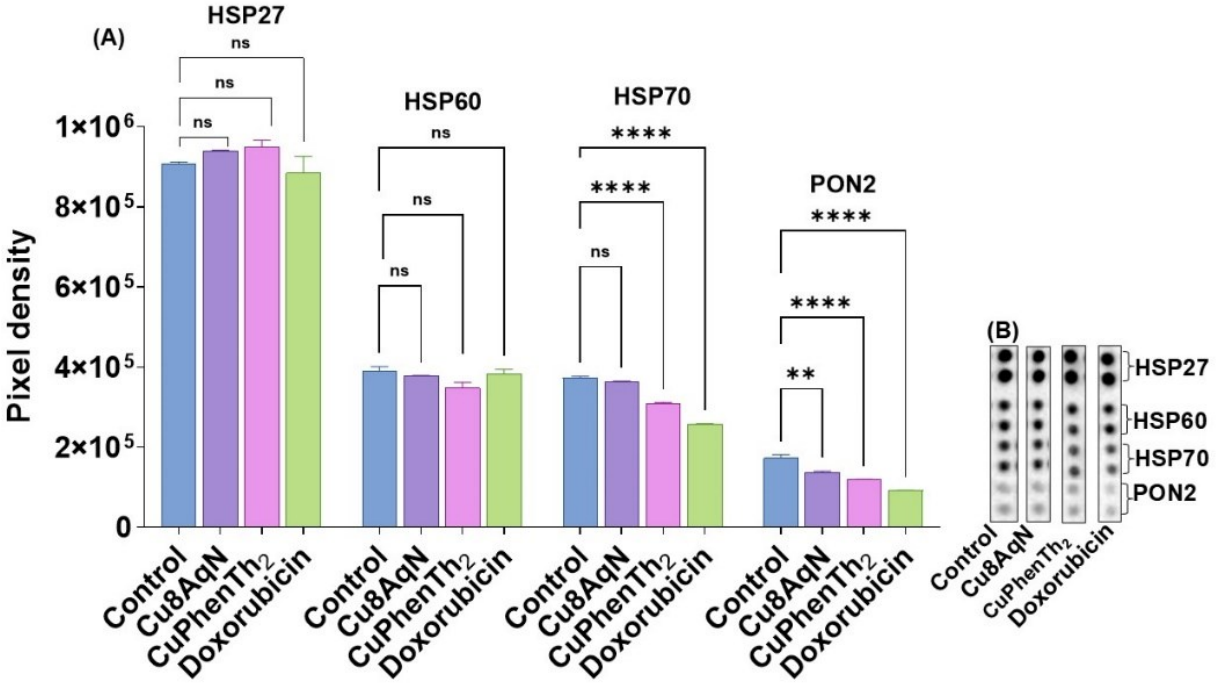


Fig. 3.25 The effects of copper complexes and doxorubicin on the expression levels of HSPs and PON2 in MDA-MB-231 breast cancer cells. The cells were treated with Cu8AqN at 3.1 µM, $CuPhenTh_2$ at 2.3 µM and doxorubicin at 10 µM for 18 h. **(A)** shows the effects of the copper complexes and doxorubicin on the expression levels of HSP27, HSP60, HSP70 and PON2 **(B)** show a segment of the nitrocellulose membrane array with the blots for each protein. **p< 0.01, ****, p< 0.0001, ns= not significant.

3.4.9 The effects of copper complexes on the expression of HIF-1α, HMOX-1, and HMOX-2 in MDA-MB-231 breast cancer cells.

Baseline expression levels of HIF-1α were high and decreased significantly after treatment with Cu8AqN ($p< 0.001$). Treatment with $CuPhenTh_2$ showed a significant increase in the expression levels of HIF-1α ($p< 0.0001$), while doxorubicin poorly increased the expression level of HIF-1α in the cells ($p< 0.05$), Fig. 3.26 A and B. Baseline expression of HMOX-1 was moderate as shown in Fig. 3.26A and B. Cu8AqN and $CuPhenTh_2$ treatment of the cells highly significantly increased the expression of HMOX-1($p< 0.0001$) in contrast to doxorubicin which suppressed its expression ($p< 0.001$). HMOX-2 baseline expression was moderate in the control cells, and the treatment of the cells with Cu8AqN decreased the expression of HMOX-2 significantly ($p< 0.01$), while $CuPhenTh_2$ and doxorubicin did not cause a significant change in HMOX-2 levels in the cells.

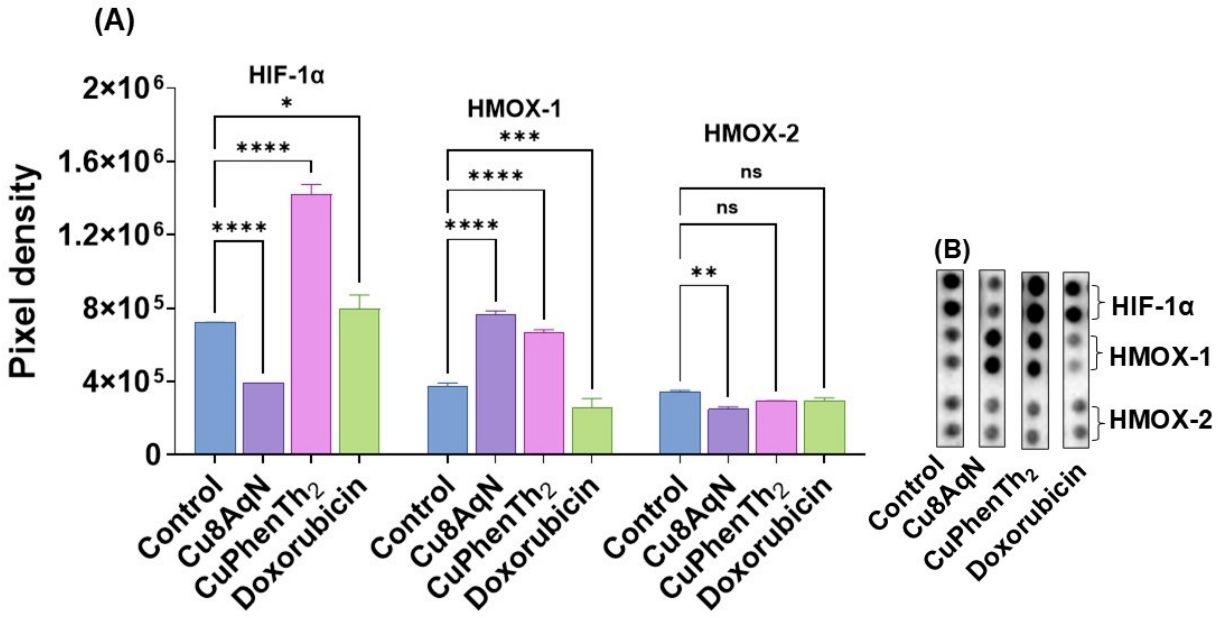


Fig. 3.26 The effects of the copper complexes and doxorubicin on the expression levels of HIF-1 α, HMOX-1 and HMOX-2 in MDA-MB-231 breast cancer cells. The cells were treated with Cu8AqN at 3.1 µM, $CuPhenTh_2$ at 2.3 µM and doxorubicin at 10 µM for 18 h. **(A)** shows the effects of the Cu8AqN, $CuPhenTh_2$ and doxorubicin on the expression of HIF-1α, HMOX-1, and HMOX-2 **(B)** shows a segment of the nitrocellulose membrane array with the blots for each protein. *$p< 0.05$, **$p< 0.01$, ***$p< 0.001$, ****$p< 0.0001$, ns=not significant.

3.5 Detection of NIK, phospho-p53(s15), p21, and HMOX-1 by immunofluorescence

HMOX-1,phospho-p53(s15), p21, and NIK, are regulators of cell stress, survival, and apoptosis and were investigated further to confirm the proteome array results. NIK was assessed since the suppression of cIAP1 may cause an increase of NIK (Lee *et al.,* 2014).

3.5.0 Introduction

Following the identification of changes to apoptosis regulatory proteins, the results were confirmed by immunofluorescent microscopy. Immunofluorescence detected the expression and subcellular localization of NIK, phospho-p53(s15), p21, and HMOX-1 in the cells. Unless indicated otherwise, cells were treated with the copper complexes at concentrations equivalent to their respective IC_{60} values for 18 h. The untreated negative cells incubated without the primary antibody were a negative control for the immunofluorescence assay to determine secondary antibody specificity. The untreated cells incubated with the primary antibody were the fluorescence-negative untreated control to compare with the treated cells. After treatment, the cells were fixed in formaldehyde, permeabilised, blocked in BSA and incubated with primary antibodies on a rocking platform overnight. The signals were detected with Alexa fluor 488 or Alexa fluor 594 conjugated secondary and counterstained with HO, as detailed in section 2.5.3.

The cells were observed with an Olympus BX41 microscope and fluorescent images were captured with an Olympus DP72 camera. Intensity measurement was measured using ImageJ. The plugin "Just another co-localization" (JaCoP) in ImageJ software was used to measure the extend to nuclear colocalization and results are expressed as a Pearson correlation coefficient (PCC). A coefficient of one indicates 100 % nuclear co-localization.

3.5.1 The effects of copper complexes and doxorubicin on the expression of NIK in MDA-MB-231 breast cancer cells.

cIAP-1 was decreased in the cells post treatment with Cu8AqN, $CuPhenTh_2$ and doxorubicin (section 3.4.7). cIAP1 mediates the degradation of NIK to prevent NIK accumulation which activates the non-canonical NFκB signalling pathway and promotes cell survival and chemoresistance (Siegmund *et al.*, 2022).

NIK expression was evaluated by immunofluorescent microscopy to determine if cIAP-1 suppression holds true in this case. NIK was detected as green fluorescence. The results are shown in Fig. 3.27 and 3.28.

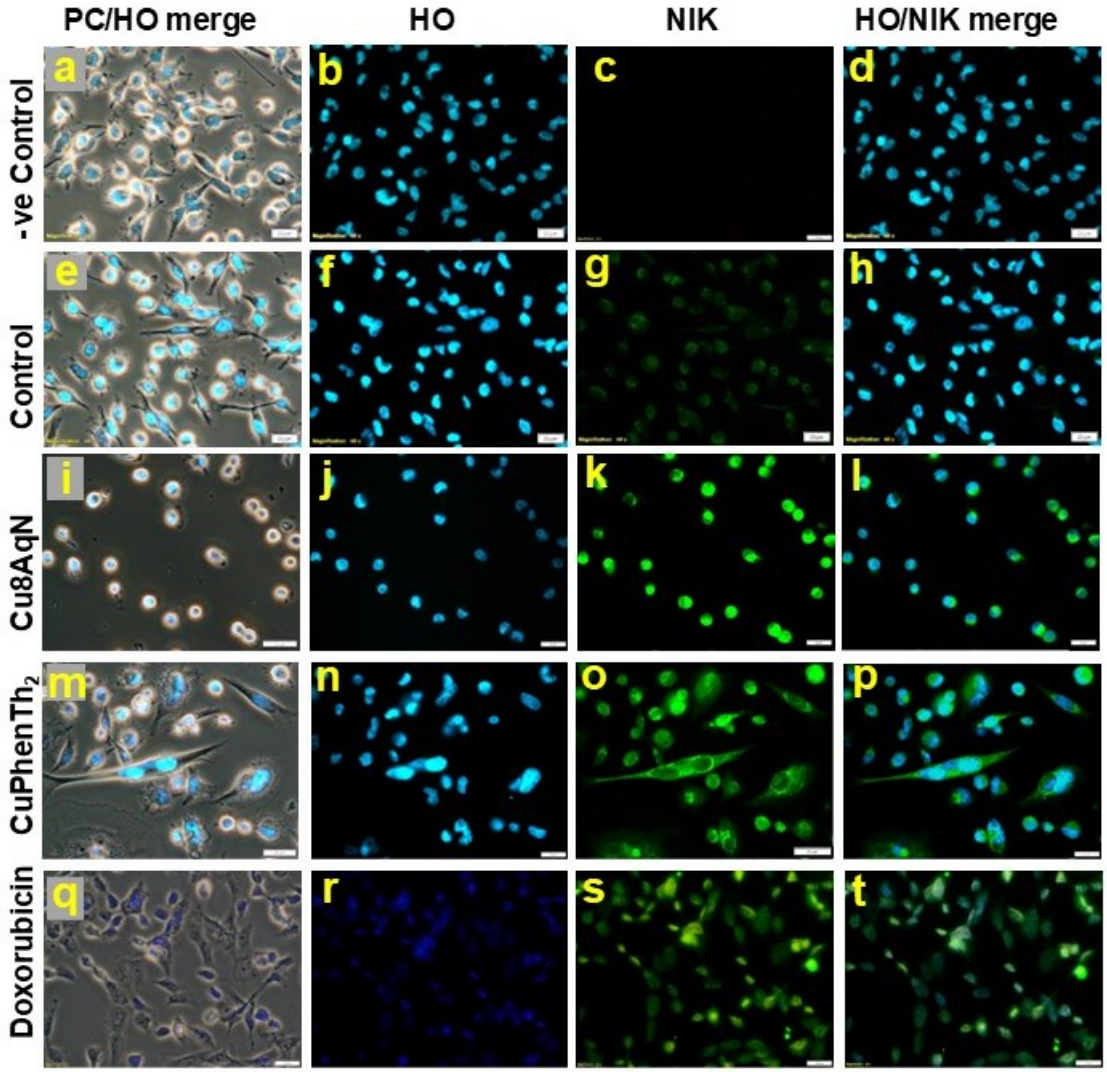


Fig. 3.27 The effects of Cu8AqN, CuPhenTh$_2$, and doxorubicin on the expression of NIK in MDA-MB-231 breast cancer cells. The cells were treated with 3.1 µM of Cu8AqN, 2.3 µM of CuPhenTh$_2$ and 10 µM of doxorubicin for 18 h. Photomicrograph of NIK expression in the control cells, Cu8AqN, CuPhenTh$_2$, and doxorubicin treated cells. The cells were viewed with an Olympus BX41 epifluorescence microscope at 400 x magnification. Images were captured with an Olympus DP72 camera using Olympus U-MWU2 filter cube for HO, and the U-MNIBA3 filter cube for NIK. Images were processed with ImageJ Software. Scalebar: 20 µm. Legend: PC=phase contrast, HO=Hoechst33342; NIK=NFκB inducing kinase.

The negative control cells showed no NIK expression, as shown by the absence of green fluorescence, confirming the specificity of the secondary for NIK (Fig. 3.27, panels a-d). In contrast, the untreated control cells showed typical MDA-MB-231 morphology and with a poor baseline expression of NIK in the nuclei, observed by low green fluorescence intensity and a PCC of 0.65 Fig. 3.27, panel e-h and Fig. 3.28 A and B.

All treated cells showed increased NIK expression compared to the untreated control. In Cu8AqN-treated cells, the cells appeared rounded with bright blue fluorescence and high intensity green fluorescence, proving increased NIK expression. The green fluorescence was observed in the nucleus, as it overlapped with the blue HO dye, suggesting NIK localization in the nucleus. This was confirmed by a PCC of 0.83 (Fig. 3.27, panels i–l; Fig. 3.28 A, B).

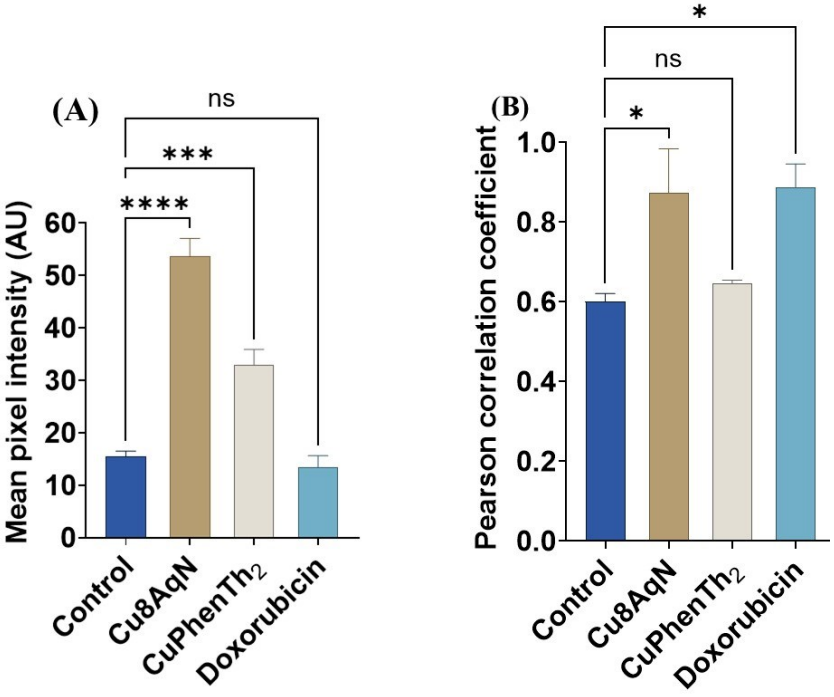


Fig. 3.28 NIK intensity and correlation measurement in MDA-MB-231 breast cancer cells treated with Cu8AqN, CuPhenTh$_2$, and doxorubicin. **(A)** shows the fluorescence intensity of NIK expression of two independent experiments**.** Intensity was measured using basic ImageJ package by using analyse tool > Set measurements. **(B)** shows PCC of the treated cells relative to the untreated control. Statistical significance was determined using GraphPad Prism ANOVA, followed with Dunnett's multiple comparison test compared to the control. * $p < 0.05$, *** $p < 0.001$, **** $p < 0.0001$, ns not significant. AU=arbitrary units.

Some $CuPhenTh_2$ treated cells remained elongated while others were round shaped. NIK expression was increased in all the cells, green fluorescence was detected in the nucleus in the rounded cells, while green intensity was high around the nucleus and in the cytoplasm in the elongated cells which was supported by the PCC value of 0.65 in these cells (Fig. 3.27, panels m-p and Fig. 3.28A and B).

In the cells treated with doxorubicin, morphological changes were observed along with increased green fluorescence in the nuclei, indicating increased NIK expression. The PCC was 0.85, confirming NIK localization in the nucleus (Fig. 3.27, panels q – t; Fig. 3.28 A, B). These results suggest that both copper complexes and doxorubicin increased nuclear NIK expression in response to cIAP1 suppression.

3.5.2 The effects of copper complexes on the expression levels of phospho-p53(s15) in MDA-MB-231 breast cancer cells

The phospho-p53(s15) is a primary response to DNA damage and cellular stress. MDA-MB-231 cells harbour mutant p53 protein, contributing to poor survival and chemoresistance (Curtis *et al.,* 2012; Meric-Bernstam *et al*., 2018). Due to the intrinsic fluorescent nature of doxorubicin, staurosporine was used as an additional positive control for phospho-p53(s15). Phospho-p53(s15) was evaluated to assess whether the complexes and positive controls degraded mutant Phospho-p53(s15). The results are presented in Fig. 3.29 and 3.30.

The negative untreated control and the untreated control cells had a normal morphology and showed no detectable expression of phospho-p53(s15) indicated by the lack of red fluorescence in Fig. 3.29, panels a-d, and e-h respectively, and Fig. 3.30A. This showed that the secondary antibody was specific to phospho-p53(s15) and that the untreated control cells lacked baseline expression of phospho-p53(s15). Cu8AqN (Fig. 3.29, panels i-l), treated cells were rounded with increased phospho-p53(s15) in the nuclei, Nuclear phospho-p53(s15) was confirmed with PCC values of 0.85 in the nuclei of the cells (Fig. 3.29, panels i-l, and 3.30 A and B).

In the cells treated with $CuPhenTh_2$, the morphology was changed and the cells had increased expression of nuclear phospho-p53(s15) which was shown by PCC value of 0.78, (Fig. 3.29, panels m-p, and 3.30 A and B)

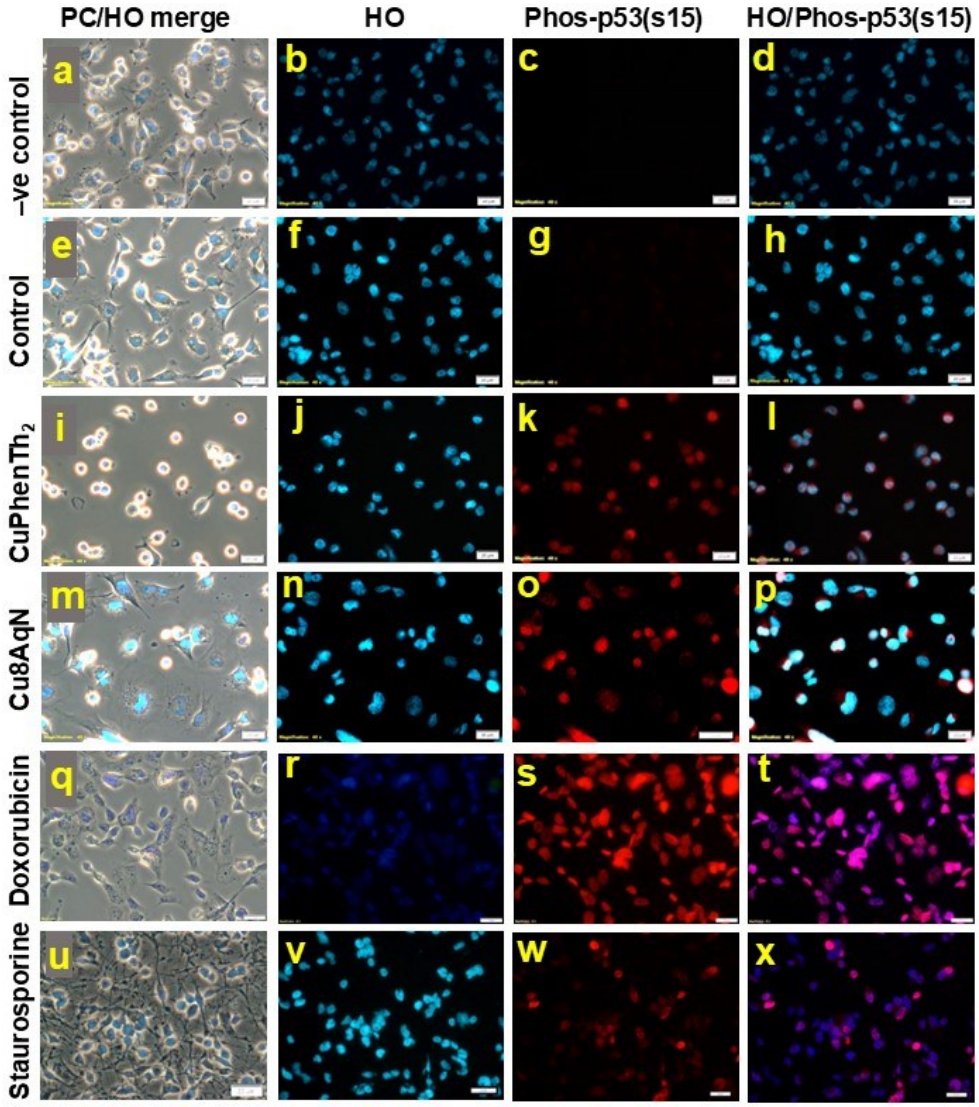


Fig. 3.29 The effects of copper complexes and doxorubicin on phospho-p53(s15) expression in MDA-MB-231 breast cancer cells. Cu8AqN at 3.1 µM, 2.3 µM of $CuPhenTh_2$,10 µM of doxorubicin, and 0.09 µM of staurosporine was used to treat the cells for 18 h. Photomicrograph of phospho-p53(s15) expression in the control and treated cells. The cells were viewed with an Olympus BX41 epifluorescence microscope at 400 x magnification. Images were captured with an Olympus DP72 camera and analysed with ImageJ Software. Scalebar: 20 µm. Legend: PC=phase contrast, Phospho-p53(s15) =serine 15 phosphorylated p53,HO=Hoechst33342.

The cells treated with doxorubicin had increased red fluorescence this is shown in (Fig. 3.29, panel q -t; Fig. 3.30) probably due to the innate fluorescence of doxorubicin since it was co-localised to the nucleus and the PCC for doxorubicin treated cells was 0.92 (Fig. 3.30B). Staurosporine caused the cells to round up with apoptotic nuclei.

An increased in red fluorescence was observed on the cells, in some cells the fluorescence was highly intense while others showed low red fluorescence intensity, indicating low and high expression of phospho-p53(s15) (Fig. 3.29, panel u-x; Fig. 3.30). The phospho-p53(s15) expression was in the nuclei with PCC of 0.71. These results show that the copper complexes increased the expression levels of phospho-p53(s15), and it was co-localised to the nucleus, while doxorubicin results were not conclusive. Staurosporine increased nuclear expression of phospho-p53(s15).

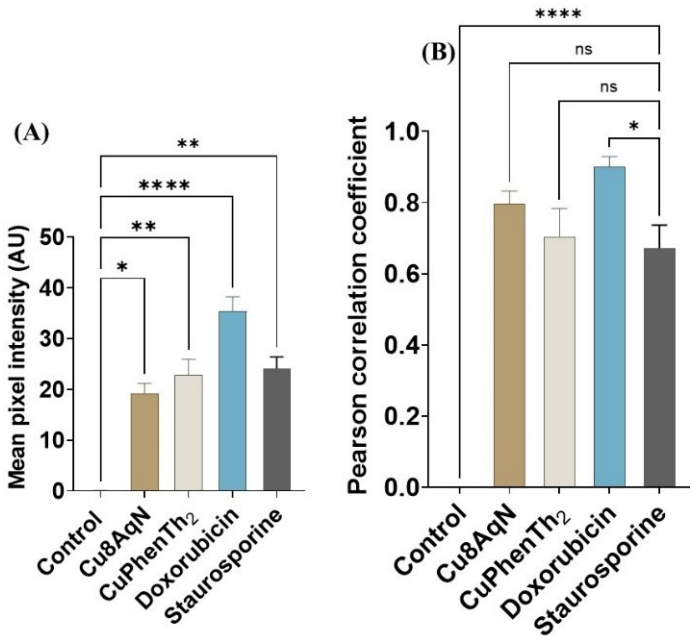


Fig. 3.30 Bar graphs showing phospho-p53(s15) expression in MDA-MB-231 breast cancer cells after treatment with the copper complexes. **(A)** is the measurement of intensity of phospho-p53(s15) in the control and in the cells treated with Cu8AqN, $CuPhenTh_2$ and doxorubicin of two independent experiments. **(B)** shows co-localization quantification using the Pearson correlation coefficient. ** $p< 0.01$, ***$p< 0.001$, ns= not significant. AU=arbitrary units

3.5.3 The effects of copper complexes and doxorubicin on the expression levels of p21 in MDA-MB-231 breast cancer cells

The tumour suppressor protein, p21 is induced upon cellular stress and DNA damage then regulates the cell cycle arrest (Kreis *et al.*, 2019). In this study, p21 expression was studied as an indicator of DNA damage or cellular stress and was visible as green fluorescence in p21 positive cells. Doxorubicin was used as a positive control for comparison. The results are shown in Fig. 3.31 and Table 3.8.

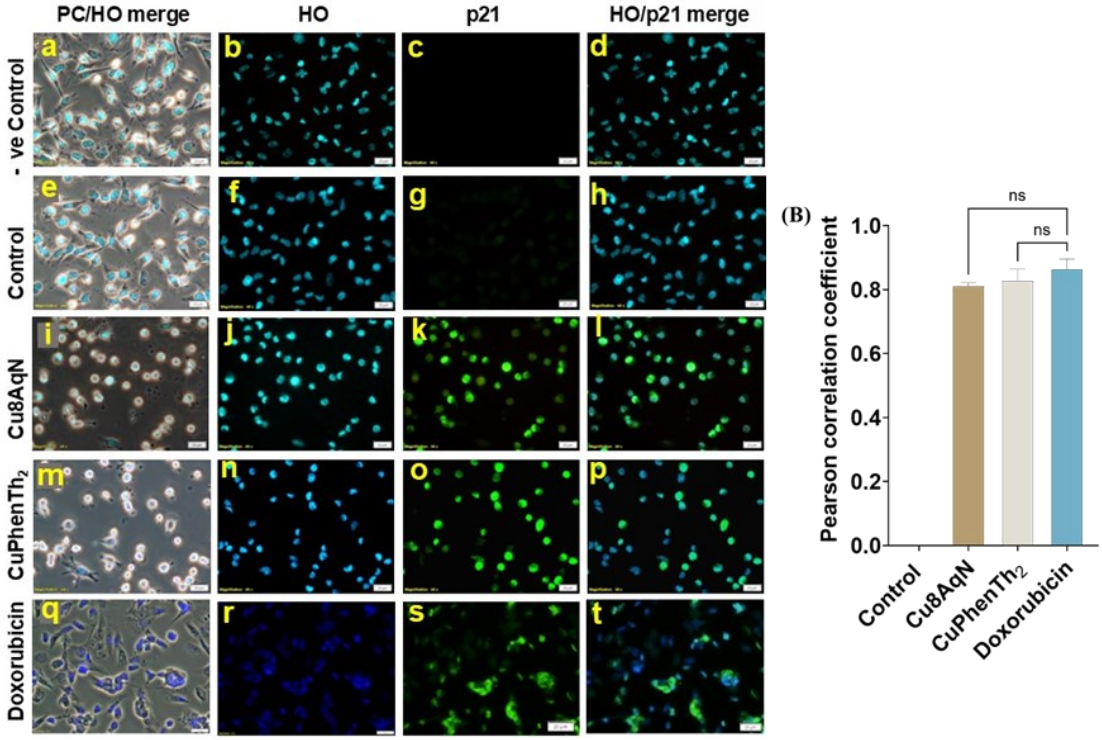


Fig. 3.31 The effects of copper complexes and doxorubicin on p21 expression in MDA-MB-231 breast cancer cells. The cells were treated with 3.1 µM of Cu8AqN, 2.3 µM of $CuPhenTh_2$ and 10.0 µM of doxorubicin for 18 h. **(A)** Photomicrograph of p21 expression in the treated cells**.** The cells were viewed with an Olympus BX41 epifluorescence microscope at 400 x magnification. Images were captured with an Olympus DP72 camera and analysed with the Olympus CellSens Software. Scalebar: 20 µm. **(B)** PCC was determined using (JACoP) in ImageJ software in three separate fields. A coefficient of one indicates 100 % nuclear co-localization. Statistical significance was determined using GraphPad Prism ANOVA, followed with Dunnett's multiple comparison test compared to doxorubicin. Legend: PC=phase contrast, HO=Hoechst33342, p21=cyclin dependent kinase inhibitor.

The absence of green fluorescence in the negative control, and the fluorescence control indicated the absence of p21 expression, and the specificity of the secondary antibody as shown in Figure 3.31A, panel c. Expression of p21 was not detected in the negative untreated control cells (Table 3.8 and Fig. 3.31A, panel g).

Treatment of the cells with the copper complexes and doxorubicin induced p21 and was observed as high or low expression observed as low/ bright green fluorescence. Cells treated with Cu8AqN had a round shape with p21 in 80.3 % of the cells, among these, 40 % were bright green fluorescent (Fig. 3.31, panels i-l, and Table 3.8). In all the cells, p21 was observed in the nucleus, having PCC of 0.8 for Cu8AqN. $CuPhenTh_2$ altered the morphology of the cells and increased p21 expression in 89 % of the cells, 76 % had a high expression (bright green fluorescence) while 13 % of cells displayed low expression (low green fluorescence), Fig. 3.31A, panels m -p, and Table 3.8 (below). The PCC for $CuPhenTh_2$ treated cells was 0.8 indicative of nuclear co-localization.

In doxorubicin treated cells, 38 % of the cells had high p21 expression and poor p21 expression was observed in 62 % of the cells, (Fig. 3.31, panels q-t s, and Table 3.8). The expression of p21 was primary in the nucleus and was confirmed by a PCC of 0.8, Fig. 3.32B. These results indicate that the copper complexes and doxorubicin increased nuclear p21 in the cells.

Table 3.8: Percentage of MDA-MB-231 cells expressing p21 following treatment with copper complexes and doxorubicin for 18 h.

MDA-MB-231 cells			
Treatment	**High p21 expression (% cells)**	**Low p21 expression (% cells)**	**Total p21 expression (% cells)**
Control	0.00	0.00	0.00
Cu8AqN	40.0 ± 4.7	43.3 ± 6.0	83.3 ± 10.70
$CuPhenTh_2$	76.0 ± 12.0	13.3 ± 3.28	89.3 ± 15.30
Doxorubicin	38.0 ± 2.30	62.0 ± 3.80	100.0 ± 6.10

3.5.4 The effects of the copper complexes on the expression levels of HMOX-1 in MDA-MB-231 breast cancer cells

In breast cancer, increased HMOX-1 expression is associated with poorer prognosis, angiogenesis and cancer cell survival (Wu *et al.*, 2021). Immunofluorescence confirmed the increased expression of HMOX-1 in the cells. The results are shown in Fig. 3.33 and 3.34A and B.

The secondary antibody was specific to the primary antibody as shown by the absence of green signal on the negative untreated control cells, (Fig. 3.32, panels a-d). In untreated control MDA-MB-231 cells (Fig. 3.32, panel e-h, Fig. 3.33A), green fluorescence indicative of HMOX-1 expression was observed in both the nucleus and cytoplasm of the cells, but with decreased fluorescence intensity compared to the treated cells. The PCC was 0.95 which indicated 95 % co-localization to the nucleus.

Treatment of the cells with the Cu8AqN (Fig. 3.32, panel i-l and Fig. 3.33A) caused most cells to appear slightly rounded while some were elongated. An increase in HMOX-1 fluorescence expression was observed in all the cells. The rounded cells showed HMOX-1 expression in their nuclei while it was both in the nucleus and cytoplasm in the elongated cells. Nuclear HMOX-1 expression was confirmed by PCC of 0.87 (Fig.3.33B). Cu8AqN showed the highest HMOX-1 expression compared to the other treatments. $CuPhenTh_2$ (Fig. 3.32 panel m-p, Fig. 3.33A) caused all the cells to assume a round shape with high expression in their nuclei suggestive of HMOX-1 expression. PCC of $CuPhenTh_2$ treated cells was 0.87 which indicated high extend of HMOX-1 nuclear expression. The cells treated with doxorubicin were slightly rounded and showed low intensity green fluorescence compared to the copper complexes and the untreated cells. The green fluorescence was in the nuclei suggesting nuclear expression of HMOX-1. The PCC of 0.85 proved HMOX-1 nuclear localization. The results show that the untreated control cells had low baseline expression of HMOX-1 in the nuclei. The HMOX-1 expression was increased in the cells upon treatment with the copper complexes, while doxorubicin did not change the expression levels of HMOX-1 in the cells. In all the cells HMOX-1 was co-localized to the nucleus.

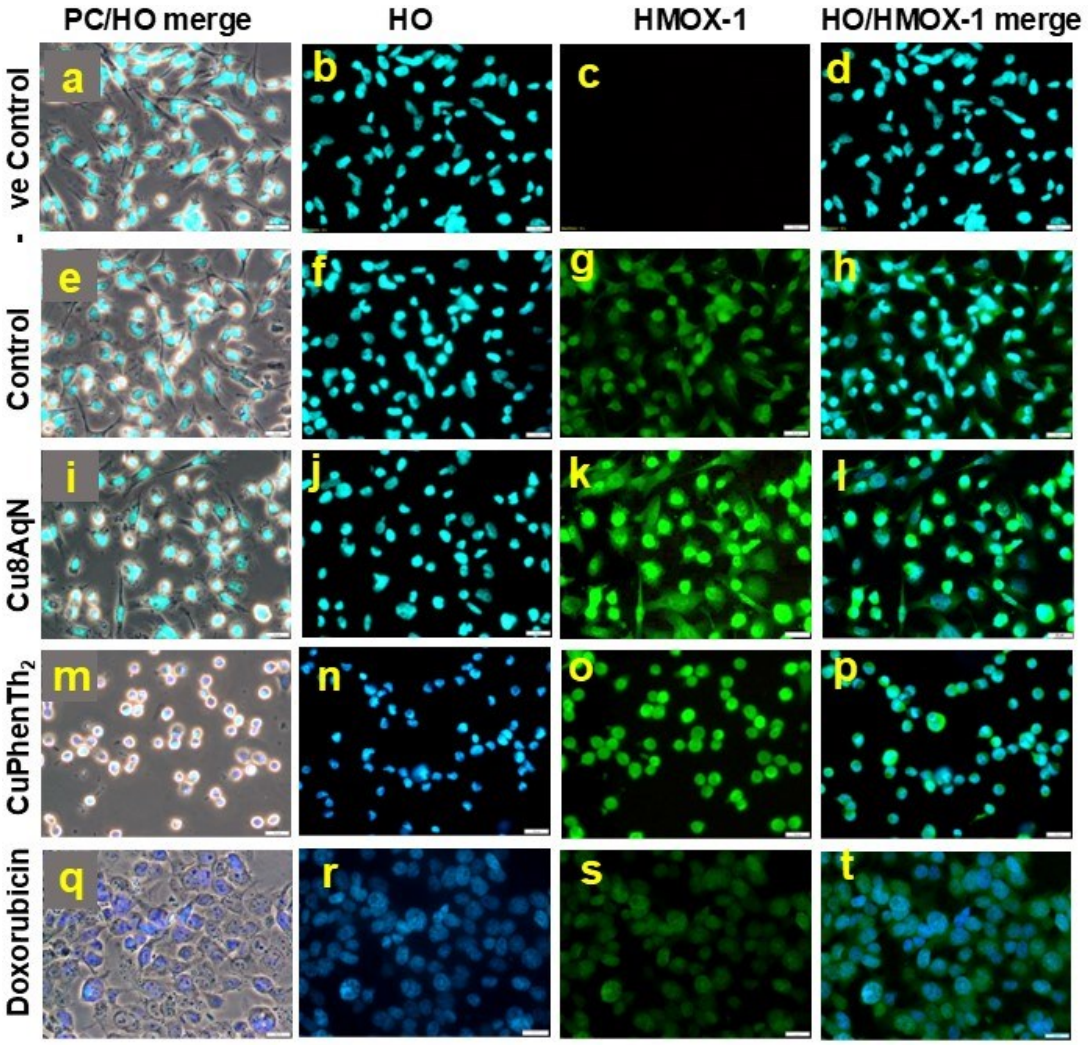


Fig. 3.32 Photomicrograph showing HMOX-1 expression levels in MDA-MB-231 breast cancer cells after treatment with copper complexes and doxorubicin. The cells were treated with 3.1 µM of Cu8AqN, $CuPhenTh_2$ at 2.3 µM and 10.0 µM of doxorubicin for 18 h. The cells were viewed with an Olympus BX41 epifluorescence microscope at 400 x magnification and captured with an Olympus DP72 camera. The analysis was performed with the Olympus CellSens Software. Scalebar: 20 µm. Legend: PC=phase contrast, HO=Hoechst3342, HMOX-1=haemoxygenase-1.

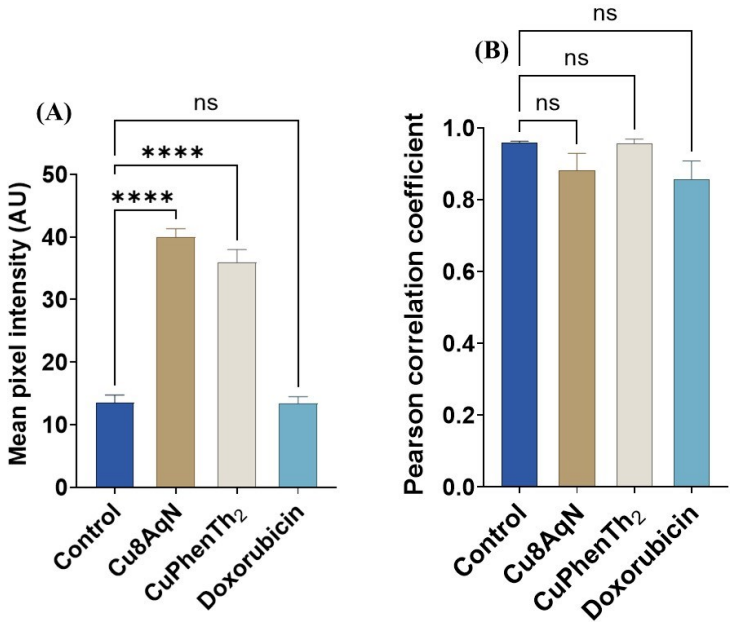


Fig. 3.33 Quantification of HMOX-1 expression and correlation in MDA-MB-231 breast cancer cells. **(A)** illustrates the HMOX-1 mean pixel intensity measured in arbitrary units. **(B)** Shows Pearson correlation co-efficient (PCC) values. Statistical significance was determined using GraphPad Prism ANOVA, followed with Dunnett's multiple comparison test compared to the control. ns=not significant, ****p<0.0001. AU=arbitrary units.

3.6 Determination of HMOX-1 expression using the western blot assay

After confirming HMOX-1 expression with the proteome array and immunofluorescence, the western blot assay was used to determine the molecular weight of HMOX-1 and whether the expressed HMOX-1 was truncated. MDA-MB-231 cells were treated with Cu8AqN at a concentration of 3.1 µM, $CuPhenTh_2$ at a concentration of 2.3 µM, and doxorubicin at a concentration of 10.0 µM. After treatment, the cells were harvested and lysed, protein concentration of the lysates was determined with the Bradford assay. The whole lysates with 16. 32 µg of protein each, were denatured in Laemmli sample buffer. On separate lanes, the samples, and molecular weight markers were added on 12 % SDS discontinuous gels and separated via electrophoresis, followed by the transfer of the proteins from the gels to the PVF membranes. Thereafter, the membranes with the proteins were blocked in BSA and incubated with the primary antibody on a rocking platform overnight at 4 ^{0}C to detect HMOX-1 and β-tubulin (control). HMOX-1 and β-tubulin expression was detected as bands on the PVF membranes.

The membranes incubated with the primary antibody were for HMOX-1 detection and the membranes incubated without the primary antibody confirmed the specificity of the secondary antibody. Relative protein expression levels were determined by measuring the pixel density of each band on the membrane and calculating the fold increase relative to the control. Molecular weight was determined by measuring the RF value of the molecular weight markers and extrapolating the HMOX-1 and β-tubulin molecular weight from the log MW value using a standard curve (Appendix D2). Results are shown in Fig. 34.

3.6.1 Assessing molecular weight of HMOX-1 in MDA-MB-231 breast cancer cells

In Figure 3.34 A and B, the control cells (lane 3) and treated cells (lane 5, 7, and 9) displayed bands at 32 kDa (Red arrow) which correlates with the published molecular weight of HMOX-1. Cu8AqN and CuPhenTh$_2$ caused a marked increase in the size and intensity of the bands at 32 kDa suggesting an increase in HMOX-1 levels and expression of full length HMOX-1. Cu8AqN caused a higher increase (3.2-fold increase) than CuPhenTh$_2$ which caused a 2.8-fold increase.

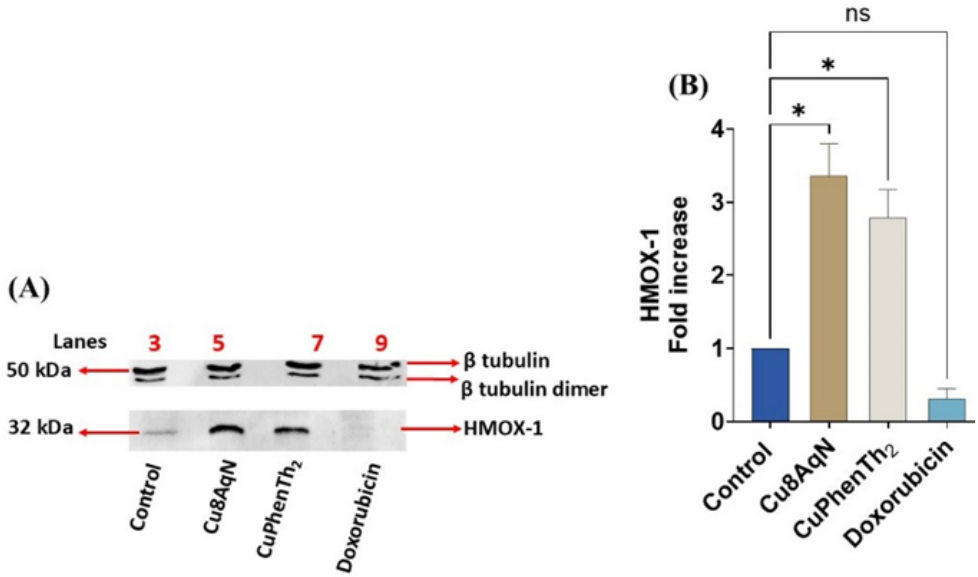


Fig. 3.34 Western blots and bar graphs showing HMOX-1 expression on MDA-MB-231 breast cancer cells. The cells were treated with 3.1 µM of Cu8AqN, CuPhenTh$_2$ at 2.3 µM and 10.0 µM of doxorubicin for 18 h and lysed. Gels were loaded with 16.32 µg of protein from each treatment. **(A)** shows a membrane with β tubulin and HMOX-1 bands in the control and treated cells. **(B)** shows the fold increase of HMOX-1 levels in the treated cells compared to the control. Band intensity was measured using the BioRad Image Lab software. *p< 0.05, ns=not significant. Legend: kDa=kiloDalton,HMOX-1=haemoxygenase-1

Treatment of the cells with doxorubicin showed significantly reduced band intensity indicative of decreased HMOX-1 expression compared to the copper complexes and the control. Additionally, the results show equal bands at 50 kDa suggesting that the treatments did not affects the β-tubulin expression.

3.6.2 Assessing the efficacy of Cu8AqN and CuPhenTh$_2$ in the presence of HMOX-1 inhibitor in MDA-MB-231 breast cancer cells

OB24,(1-[[2-[2-(4-Bromophenyl)ethyl]-1,3-dioxolan-2-yl]methyl]-1H-imidazole hydrochloride) is a selective inhibitor of HMOX-1, with an IC_{50} value of 1.9 ± 0.2 μM for HMOX-1 enzyme, obtained by performing an enzyme assay on rat spleen extracts. The IC_{50} values for HMOX-2 were greater than 100 μM indicating its specificity for HMOX-1 (Alaoui-Jamali *et al.*, 2009). The cytotoxic effect of OB24 by itself was tested at 20, 40, and 60 μM in MDA-MB-231 cells. At 20 and 40 μM, OB24 had no significant effect on MDA-MB-231 cell viability. At 60 μM, OB24 reduced cell viability to 80 % (Fig. 3.35 below), indicating poor cytotoxicity at higher concentrations.

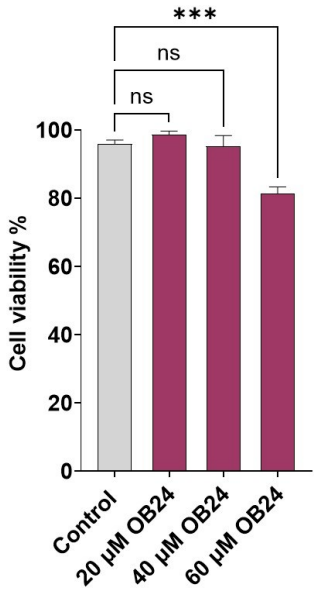


Fig. 3.35 The effects of OB24 on MDA-MB-231 breast cancer cell viability. The cells were treated with 20, 40 and 60 μM of OB24 for 48 h. MTT assay was used to measure cytotoxicity. The control cells were given culture media. OB24= (1-[[2-[2-(4-Bromophenyl)ethyl]-1,3-dioxolan-2-yl]methyl]-1H-imidazolehydrochloride),ns=non-significant. *** p< 0.001.

A concentration of 20 μM OB24 did not significantly affect cell viability, and it was selected as the concentration for combination studies with Cu8AqN and $CuPhenTh_2$ since, Cu8AqN and $CuPhenTh_2$ increased HMOX-1 expression, whereas doxorubicin had no effects on HMOX-1 expression. When combined with 20 μM OB24, Cu8AqN significantly reduced ($p< 0.0001$) the IC_{50} value from 3.31 ± 0.06 μM to 0.30 ± 0.09 μM, indicating that inhibiting HMOX-1 sensitized the cells to Cu8AqN. In contrast, $CuPhenTh_2$ significantly increased ($p = 0.0195$) its IC_{50} value from 1.89 ± 0.14 μM to 3.81 ± 0.77 μM after 48-h treatment (Table 3.9) suggesting that OB24 potentially may have interfered with and reduced the cytotoxic activity of $CuPhenTh_2$.

Table 3.9: IC_{50} values of Cu8AqN and $CuPhenTh_2$ individually and in combination with 20 μM of OB24 in MDA-MB-231 breast cancer cells after 48 h.

Treatment	IC_{50} values (μM)		
	Without OB24	With OB24	*p* value
Cu8AqN	3.31 ± 0.06	0.30 ± 0.09	< 0.0001
$CuPhenTh_2$	1.89 ± 0.14	3.81 ± 0.77	0.0195

Chapter Four: Discussion

4.0 Brief overview of the study

This study investigated the potential anti-cancer effects of copper and gold complexes as well as their individual ligands against MDA-MB-231 triple negative breast cancer cells and MCF-10 normal mammary epithelial cells. Gemcitabine and doxorubicin were evaluated as positive controls and the kinase inhibitor staurosporine was used as a positive control for apoptotic assays. An initial investigation using the MTT cytotoxicity assay was used to identify the active copper and gold metal complexes that caused cell viability below 50 % at 5 μM in the MDA-MB-231 cells. These complexes were considered to be active according to (Liston and Davis, 2017), and were studied further.

Further evaluation determined the IC_{50} values of the active copper and gold metal complexes in the MDA-MB-231 cells. Thereafter, the copper and gold complexes that had IC_{50} values below 5 μM were evaluated for their cytotoxicity against the MCF-10A mammary epithelial cells, and their mechanism of cell death were investigated in the MDA-MB-231 breast cancer cells. The copper and gold metal complexes showed some selectivity towards the breast cancer cells indicated by higher IC_{50} values in the MCF-10A cells than in the MDA-MB-231 breast cancer cells.

In all the experiments, the cells were treated with copper and gold metal complexes at concentrations that were equivalent to their respective IC_{80} values. Although the *in vitro* IC_{80} values do not directly translate to clinical dosing because of the differences in pharmacokinetics, tissue distribution, and tumour microenvironment, the IC_{80} value was chosen to represent a high efficacy concentration as observed in the previous studies (Harmse *et al.,* 2019; Ismail *et al.,* 2022), which provides a better understanding of how these copper and gold complexes induce cell death. In addition, clinical dosing of chemotherapeutic agents is calculated to cause a 100 % cell death rate of cancer cells or the maximal dose that the patient can tolerate (Wellstein, 2023).

Preliminary investigation of the mechanism of cell death of the copper and gold metal complexes in the MDA-MB-231 cells and the MCF-10A cells was determined with cell morphology assays using fluorescent microscopy and vital dyes , HO, AO and PI. MDA-MB-231 and MCF-10A cells

showed morphological changes associated with apoptotic cell death. Exploratory experiments on the MCF-10A cells treated with concentrations equivalent to IC_{80} values obtained for MDA-MB-231 cells, which was lower than IC_{80} obtained for MCF-10A, showed no significant effects on the morphology of the MCF-10A cells (Appendix C). Since the copper and gold metal complexes were partially selective towards the cancer cells, successive experiments evaluated the potential of the copper and gold metal complexes to induce apoptosis in MDA-MB-231 TNBC cells.

After the copper and gold metal complexes were shown to cause apoptotic cell death in MDA-MB-231 cells, the copper complexes, $CuPhenTh_2$ and Cu8AqN were selected as lead candidates to study their effects on apoptosis-related proteins in MDA-MB-231 cells using an apoptosis proteome array, immunofluorescent microscopy, and western blot analysis.

4.1 Copper and gold complexes preferentially inhibit the proliferation of MDA-MB-231 cells compared to MCF-10A cells

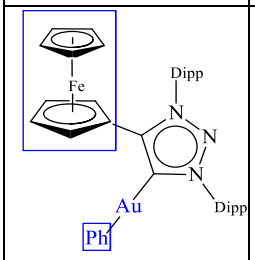
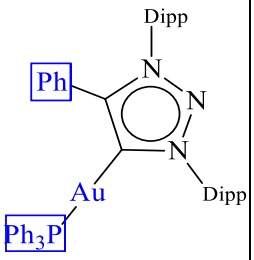
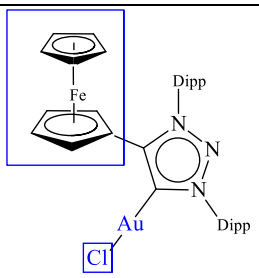
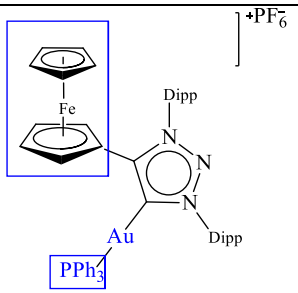
4.1.1 Cytotoxicity of the gold(I) complexes and 1,2,3-triazolylidene (trz) ligand

The 1,2,3-triazolylidene (trz) ligand was poorly active at both tested screening concentrations, suggesting that the coordination to the gold(I) centre is essential for biological efficacy.

Among the evaluated gold complexes, those incorporating both a ferrocenyl (Fc) substituent and a triphenylphosphine (PPh_3) ligand, such as $AuPPh_3$(trz-Fc-Dipp) (Dipp: diisopropylphenyl) showed superior potency (Table 4.1). This suggests that ligand co-ordination is essential for the cytotoxic potential, with the PPh_3 ligand likely enhancing the cytotoxic activity, as observed in related gold(I) phosphine complexes (Muenzner *et al.,* 2016; Kim *et al*., 2019). The presence of the ferrocenyl moiety at the C5 position in all active complexes may contribute to redox cycling and ROS generation, aligning with literature reports on ferrocenyl-substituted gold(I) N-heterocyclic carbene complexes showing significant antiproliferative activity (Arambula *et al.,* 2016). Despite structural similarities, the IC_{50} values in MDA-MB-231 cells in the present study were higher than those reported in lung (A549, H1975) and colon (HCT-116) cancer cell lines (Aucamp *et al.,* 2018; Muenzner *et al.,* 2016).

The IC_{50} values vary since each cell line represents a different type of cancer and have different molecular characteristics, including differences in driver oncogenes and activation of proliferative signal transduction pathways in MDA-MB-231 cells.

Table 4.1: Structure activity relationship of the gold-1,2,3-triazolylidene complexes

Gold complexes			
AuPh(trz-Fc-Dipp) Inactive	**$AuPPh_3$(trz-Ph-Dipp)** Inactive	**AuCl(trz-Fc-Dipp)** Active (IC_{50} value= 7.75 ± 0.70 µM)	**$AuPPh_3$(trz-Fc-Dipp)** Active (IC_{50} value= 2.00 ± 0.39 µM)
			

While $AuPPh_3$(trz-Fc-Dipp) had modest selectivity over MCF-10A non-cancer cells based on the criteria by (Olar *et al.*, 2022), the selectivity index (1.67) suggests a narrow therapeutic window, warranting further structural optimisation. Its cytotoxic activity aligns with related gold(I) complexes that were more active than cisplatin in some studies (Magherini *et al.,* 2018), reinforcing the therapeutic potential of the trz-ferrocenyl scaffold. The current findings contribute to growing evidence of growth inhibitory effects of the gold(I)-trz-ferrocenyl complexes in MDA-MB-231, triple negative breast cancer cells.

4.1.2 Cytotoxicity of the copper complexes and ligands

In this study, copper complexes that had more than 50 % cell viability at 5 µM were identified as clinically irrelevant as outlined by Liston and Davis (2017) and no further studies were performed on them. The 1,10-phenanthroline ligand, showed poor activity at 5 µM, suggesting limited cytotoxicity as a standalone ligand.

Theophylline, a xanthine derivative, and a co-ligand in $CuPhenTh_2$, lacked cytotoxic activity at both tested concentrations. The coordination of copper ($CuTh_2$) or manganese ($MnTh_2$) to theophylline maintained poor cytotoxic activity at 5 µM, further proving limited potency of theophylline ligand alone. But the addition of 1,10-phenanthroline ligand to $CuTh_2$ yielded $CuPhenTh_2$ with improved cytotoxic activity at both screening concentrations.

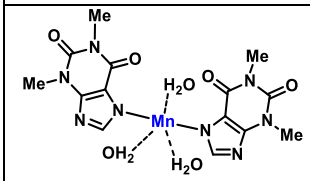
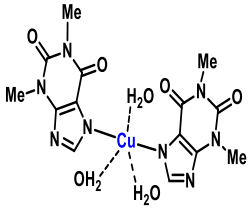
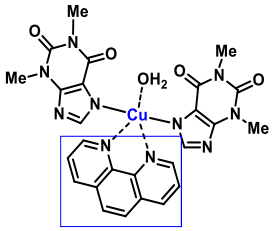
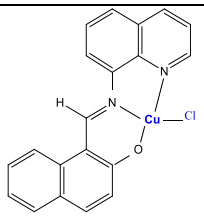
The $CuPhenTh_2$ complex, containing 1,10-phenanthroline, and theophylline as part of its structure had potent cytotoxicity against MDA-MB-231 cells with an IC_{50} value of 1.89 ± 0.14 µM and had a threefold higher IC_{50} value in non-cancerous MCF-10A cells, yielding a selectivity index of 3.04, indicating selectivity towards the cancer cells. This suggests that 1,10-phenanthroline contributes to stabilizing the Cu(II) complex and promoting intracellular copper accumulation. The planar structure of 1,10-phenanthroline likely facilitates DNA intercalation, further improving anticancer activity (Sigman *et al.,* 1979; McGivern *et al.,* 2018).

The copper complex, Cu8AqN, based on the 8-aminoquinoline ligand which alone had limited activity, showed selective cytotoxicity with an IC_{50} value of 3.31 ± 0.06 µM in MDA-MB-231 cells and 9.51 ± 0.03 µM in MCF-10A cells. Previous work from our group showed differential sensitivity to Cu8AqN among breast cancer cell lines, with greater potency in MCF-7 compared to MDA-MB-231 cells, while the ligand alone remained poorly cytotoxic. This confirms the importance of copper coordination to the organic scaffold for cytotoxic activity (Myeza *et al.,* 2024). Comparative analysis showed that Cu8AqN was more active than doxorubicin in MDA-MB-231 cells, whereas doxorubicin was more effective in MCF-7 cells. This shows how cell specific molecular characteristics activate cell death pathways. Supporting evidence from the literature corroborates these findings.

Jhetam *et al*. (2025) reported IC_{50} values below 5 µM for $CuPhenTh_2$, Cu8AqN, and related copper-aromatic-isoindoline complexes in pancreatic cancer cell lines, with copper-aromatic-isoindoline complexes showing superior potency relative to doxorubicin, although cytotoxicity was cell line-dependent. Santini *et al.* (2011) identified $[Cu(thp)_4][PF_6]$ as a highly potent copper phosphine complex with an IC_{50} value of 2.00 ± 0.03 µM against HCT-15 cells, significantly more active than cisplatin.

A study by Li *et al.* (2019) described Cu(II) complexes containing phenanthroline derivatives as cytotoxic complexes against breast cancer cell lines, with better activity than carboplatin, and attributed it to structural differences impacting on their efficacy.

Table 4.2: Structure activity relationship of the copper complexes and ligands

Copper complexes			
$MnTh_2$	**$CuTh_2$**	**$CuPhenTh_2$**	**Cu8AqN**
Inactive	Inactive	Active (IC_{50} value= 1.89 ± 0.14 µM)	Active (IC_{50} value= 3.31 ± 0.06 µM)
			

In the present study, doxorubicin showed moderate activity against MDA-MB-231 cells (IC_{50} value of 8.75 ± 0.88 µM) and limited selectivity (IC_{50} value 2.99 ± 0.88 µM, SI= 0.34) in MCF-10A, showing the superior potency and selectivity of the tested copper and gold complexes. While staurosporine was the most cytotoxic with the lowest IC_{50} value, its nonspecific kinase inhibition causes serious off-target toxicity and limits clinical use (Ōmura *et al.,* 2018). Although doxorubicin remains a valuable chemotherapeutic agent, its clinical use is accompanied by cardiotoxicity, including cardiomyopathy and arrhythmias (Jones *et al.,* 2006; Octavia *et al.,* 2012; van der Zanden *et al.,* 2021; Morelli *et al.,* 2022). Emerging therapeutic strategies, such as dexrazoxane administration, mitigate these adverse effects (Morelli *et al.,* 2022). This encourages a continued exploration of copper- and gold-based complexes as promising candidates for triple-negative breast cancer therapy, where targeted treatment is needed.

4.2 Copper and gold metal complexes caused changes to the morphology of MDA-MB-231 breast cancer and MCF-10A mammary epithelial cells

$AuPPh_3$(trz-Fc-Dipp), $CuPhenTh_2$, and Cu8AqN had the lowest IC_{50} values in MDA-MB-231 cells with marginally high IC_{50} values in MCF-10A cells, and they were studied further to determine their mechanisms of cell death, compared to staurosporine and doxorubicin. Cell morphology was investigated at concentrations equivalent to the IC_{80} value of each cell line. These experiments provided a preliminary indication of the possible mechanism of cell death and importantly, indicated if the copper and gold metal complexes caused necrotic cell death.

Necrosis is a form of cell death marked by cytoplasmic swelling (oncosis), rupture of the plasma membrane, and organelle swelling, resulting in the uncontrolled release of intracellular contents. This can activate an inflammatory response, as the body recognises the released cellular components as a sign of injury (Galluzzi *et al.*, 2018). In cancer treatment, necrotic cell death is undesirable due to the potential of severe inflammation and tumour lysis syndrome (TLS). TLS is a collection of metabolic disorders that are a result of the rapid release of intracellular components, such as potassium, phosphates, nucleic acids, proteins, and their metabolites, into the bloodstream because of an abrupt cancer cell death. If not diagnosed and treated promptly, the condition may be fatal. Inflammation may exacerbate the tumour and damage the neighbouring cells/ tissues (Wells, 2009; Vaidya and Acevedo, 2015).

The morphology of MDA-MB-231 cancer cells (Fig. 3.4) and MCF-10A mammary epithelial cells (Fig. 3.5) changed after being treated with copper and gold metal complexes and the positive controls. Phase contrast microscopy, showed that the complexes caused cytoplasmic vacuolization which is associated with endoplasmic reticulum stress, and stress-induced apoptosis (Sperandio *et al.*, 2004; Shubin *et al.*, 2016). AO staining of MDA-MB-231 cells treated with $AuPPh_3$(trz-Fc-Dipp) and Cu8AqN, as well as the MCF-10A cells treated with $CuPhenTh_2$, doxorubicin, and staurosporine showed lysosomal formation. Excessive lysosomal formation is a preliminary indicator of autophagy (Aits and Jäättelä, 2013). However additional experiments are required to confirm the role of autophagy in response to the complexes evaluated in this study.

HO staining showed cells with apoptotic nuclei having features such as nuclear condensation and fragmentation (Earnshaw, 1995; Hacker, 2000; Martelli *et al.*, 2001). Chromatin condensation is an early event in apoptosis, followed by nuclear fragmentation where the nucleus is cleaved into fragments to be encased in apoptotic bodies. These nuclear changes signify the activation of caspases, particularly caspase-3 and caspase-7 which are responsible for degrading DNA indicative of the induction of apoptosis (Tait and Green, 2010; Galluzzi *et al.*, 2018). In both cell lines, PI staining was not observed in the nuclei suggesting that the nuclear membranes were intact and necrosis was not the primary mode of cell death.

This work parallels that of Aucamp *et al*. (2018) on $AuPPh_3$(trz-Fc-Dipp), who showed that the $AuPPh_3$(trz-Fc-Dipp) complex induced autophagic, parapoptotic and apoptotic, like morphological changes in A549 and H1975 lung cancer cells without causing necrosis. Reddy and colleagues reported on nuclear changes consistent with apoptosis indicated by Hoechst staining of the nuclei after treating the HeLa cells with gold phosphine complexes for 48 h. Similarly, results from this study on copper complexes align with the findings from (Dam *et al.*, 2017; Harmse *et al.*, 2019; Ismail *et al.*, 2022; Jhetam *et al.*, 2025) which reported that copper complexes cause morphological changes associated with apoptosis rather than necrosis in cancer cells.

In MCF-10A cells, the copper and gold metal complexes caused cell morphological changes consistent with apoptosis, such as nuclear fragmentation. This suggests that MCF-10A, while immortalized, they retain some sensitivity to apoptotic stimuli, unlike cancer cells, which often acquire resistance to cell death signals (Soule *et al.*, 1973; Martin and Leder, 2001). The MCF-10A cells have deletion of locus containing p16 which is inhibitor of cyclin-dependent kinase 4a (INK4a), p14, alternate reading frame protein (ARF), and gain of MYC proto-oncogene, bHLH transcription factor (MYC) (Soule *et al.*, 1990; Debnath *et al.*, 2003). Cyclin-dependent kinase inhibitor p16 (INK4a) and p14 (ARF), both encoded by the CDKN2A locus, function as tumour suppressors through cell cycle regulation in the p53 and retinoblastoma pathways (Brown *et al.*, 2004), while, the MYC gene, is an oncogenic transcription factor that drives proliferation, and primes the cells for apoptosis under stressful conditions. It may be possible that the loss of these tumour suppressors and gain of MYC make MCF-10A more vulnerable to apoptosis under stress conditions.

This warrants for future investigations to assess apoptotic pathways/caspase activity involved. While apoptotic morphological changes were observed in MCF-10A mammary epithelial cells, no further experiments were conducted to fully confirm the exact mechanism of cell death or to explore additional apoptotic markers in these cells.

4.3 Copper and gold metal complexes caused the accumulation of reactive oxygen species (ROS) in MDA-MB-231 breast cancer cells

Reactive oxygen species like superoxide anion ($O_2^{\bullet -}$), hydroxyl radical (•OH), hydrogen peroxide (H_2O_2) are generated as byproducts of normal mitochondrial cellular metabolism during oxidative phosphorylation and by enzymatic reactions involving NADPH oxidases, like xanthine oxidase in cell membranes (Reczek and Chandel, 2017).

In this study, the potential of copper and gold metal complexes to cause ROS accumulation was assessed and compared to the effects of doxorubicin and tert butyl hydroperoxide (tBHP) at 2, 6 and 18 h (Fig. 3.6 and 3.7). Low levels of ROS were detected in the untreated control MDA-MB-231 cells. In cancer cells, ROS have a dual role, at low levels, ROS promotes cell proliferation, invasion and metastasis (Xiang Li *et al.*, 2022). All three copper and gold metal complexes increased ROS in MDA-MB-231 cells at 2 h and 6 h, in addition, the assay was performed at 18 h and no ROS formation was observed proving ROS accumulation as an early event occurring before activation of apoptosis. At increased levels, ROS cause oxidative stress, and mitochondrial dysfunction (Nagdas and Kashatus, 2017; Ježek *et al.*, 2018).

Among the copper and gold metal complexes, ferrocene bearing gold complex, $AuPPh_3$(trz-Fc-Dipp) was the most effective at increasing intracellular ROS. Gold(I) complexes with redox-active ligands like ferrocene strongly disrupt redox homeostasis (Perez *et al.*, 2015). The ferrocene substituent in $AuPPh_3$(trz-Fc-Dipp) further increase ROS through Fenton-like reactions or undergo a one-electron oxidation, forming the ferrocenium cation (Fc^{2+}/Fc^{3+}), a process linked to its cytotoxic effects, (McKeage, 2002; Gimeno *et al.*, 2011; Perez *et al.*, 2015), which may explain why the gold complex may have caused the highest ROS accumulation. Similarly, Arambula *et al.* (2016) reported that gold(I)-ferrocenylated N-heterocyclic carbene complexes significantly increased ROS levels in A549 lung cancer cells, as detected using DCFDA staining.

However, some studies suggest that gold complexes may potentially reduce oxidative stress rather than exacerbate it. For instance, Belza *et al.*(2024) reported that gold(I) N-heterocyclic carbene complexes with 7-azaindoles did not increase ROS in A2780 ovarian cancer cells. The present work provides evidence that gold complexes may increase ROS accumulation and cause oxidative stress.

Copper complexes have been widely studied for their ability to induce oxidative stress through the generation of ROS, a mechanism that has been linked to their cytotoxic effects in cancer cells (Ng *et al.*, 2014; Sîrbu *et al.*, 2017; Harmse *et al.*, 2019; Li *et al.*, 2019). However, some studies suggest that certain copper(II) complexes may exert cytotoxicity independent of ROS production, as observed with bis(pyrazol-1-yl)- and bis(triazol-1-yl)-acetate heteroscorpionate ligands (Pellei *et al.*, 2019). In the present study, Cu8AqN and $CuPhenTh_2$ induced significant ROS accumulation, reinforcing the role of copper complexes in oxidative stress-mediated cytotoxicity. The ability of copper(II) complexes to undergo redox cycling from Cu(II) to Cu(I) in the presence of cellular reductants is a well-documented source of ROS generation (Valko *et al.*, 2016; Ribeiro *et al.*, 2023).

The formation of ROS has been demonstrated in various copper complexes, including Cu(sal)(Phen), which triggered ROS production in colorectal cancer cells (Liu *et al.*, 2023), and copper(II) mixed-ligand complexes containing phenanthroline and quinoline-, quinoxaline-, or quinazoline-derived ligands, which showed ROS-mediated cytotoxicity in A549 lung cancer cells (Radhakrishnan *et al.*, 2021). These findings are consistent with the results on Cu8AqN and $CuPhenTh_2$ copper complexes, despite differences in the cell lines used, further supporting the efficacy of copper complexes as potent ROS-inducing agents.

The positive controls in this study, doxorubicin and tBHP, both induced ROS accumulation, with doxorubicin being more potent than tBHP. In doxorubicin treated cells, ROS was observed in the perinuclear, indicating that it was not associated with doxorubicin innate fluorescence since it was not in the nuclei. Doxorubicin induces ROS through redox cycling, by undergoing enzymatic reduction from quinone form, to a semiquinone radical, which reacts with molecular oxygen to produce superoxide anions (O_2^-) and hydrogen peroxide (H_2O_2).

This process generates ROS and causes oxidative stress and apoptosis in doxorubicin treated cells (Kalantar *et al.*, 2016; Zhong *et al.*, 2017; Jafari *et al.*, 2022). On the other hand, tBHP generates ROS via direct decomposition into alkoxyl and peroxyl radicals, resulting in oxidative damage (Mansara *et al.*, 2015; Farhan *et al.*, 2016). In MDA-MB-231 and other cancer cell lines, both doxorubicin and tBHP have been shown to disrupt redox homeostasis and cause oxidative stress (Heni di *et al.*, 2020; Jafari *et al.*, 2022; Ayachi *et al.*, 2024). Similarly, in this study, the copper and gold metal complexes induced ROS accumulation in MDA-MB-231 cells, confirming that they, like the positive controls, cause oxidative stress. This ROS accumulation was strongly associated with apoptosis, as evidenced by nuclear condensation and fragmentation.

4.4 Copper and gold metal complexes disrupt mitochondrial membrane potential ($\Delta\Psi m$) in MDA-MB-231 breast cancer cells

As highlighted before, excessive ROS cause oxidative stress and disrupt mitochondrial function, playing a crucial role in activating the intrinsic apoptotic pathway and this is controlled by the mitochondrial membrane permeability (Tait and Green, 2010; Redza-Dutordoir and Averill-Bates, 2016). The mitochondrial permeability transition pore (PTP) consists of the voltage-dependent anion channel (VDAC), mitochondrial benzodiazepine receptor, and the inner membrane adenine nucleotide translocase (ANT), which is linked to cyclophilin D. All these proteins have been shown to regulate the mitochondrial membrane permeability and maintain ΔΨm gradient (Bernadi and Forte, 2007; Bernadi *et al*., 2021).

Under normal conditions, ΔΨm is tightly maintained to drive adenosine triphosphate (ATP) synthesis and oxidative phosphorylation, and the PTP remains in a closed state to preserve mitochondrial integrity. Apoptotic stimuli such as oxidative stress, or treatment with cytotoxic agents can trigger conformational changes in PTP components, shifting the pore from a closed or low-conductance state to a high-conductance state (Bernadi *et al*., 2021). This transition results in a loss of ΔΨm due to the change in the electrochemical gradient across the inner mitochondrial membrane. The loss of the ΔΨm impairs ATP generation and facilitates the swelling of the mitochondrial matrix, rupture of the outer membrane, and subsequent release of apoptogenic

factors such as cytochrome *c*, AIF, and Smac/DIABLO from the intermembrane space into the cytosol (Bernadi *et al.,* 2007; Zorova *et al.,* 2018).

In the cytoplasm cytochrome *c*, ATP and Apaf-1 forms an apoptosome and cause the activation of caspase-9, leading to caspase-3 activation and execution of apoptosis, while AIF translocate to the nucleus where it promotes chromatin condensation and DNA fragmentation (Galluzi e*t al.,* 2018). In the case of MDA-MB-231 cells treated with copper and gold complexes (Fig. 3.9 and Fig. 3.10), the observed ΔΨm depolarization suggests mitochondrial dysfunction that facilitates both caspase-dependent death pathways and each pathway will be explained in the subsequent sections. Mitochondrial membrane depolarization has been reported in other cells treated with gold complexes (Reddy *et al.*, 2018; Olelewe *et al.*, 2022) and copper complexes (Periasamy *et al.*, 2020; Ismail *et al.*, 2022; Li *et al.*, 2024; Jhetam *et al.*, 2025). The data from this study provides evidence that copper and gold metal complexes cause mitochondrial membrane depolarization leading to mitochondrial dysfunction and activation of the intrinsic apoptotic pathway.

4.5 Copper and gold metal complexes induced apoptotic cell death by increasing annexin V binding and activating caspase-3/7 in MDA-MB-231 breast cancer cells

4.5.1 Annexin V binding

Changes in the cell membrane are among the earliest indicators of apoptosis (Demchenko, 2013; Zhang *et al.*, 2018). During early apoptosis, phosphatidylserine translocate from the inner to the outer leaflet of the plasma membrane. This externalization is recognized by phagocytic cells, which engulfs and remove the apoptotic cells, preventing inflammation (Zhang *et al.*, 2018). Phosphatidylserine exposure was assessed with annexin V(AV)/ propidium iodide (PI) double staining, allowing differentiation between early apoptotic (AV^+/PI^-) and late apoptotic (AV^+/PI^+) /necrotic (AV^-/PI^+) cells. Annexin V is a phospholipid dye with a high affinity for PS (Balasubramanian and Schroit, 2003). PI intercalates into DNA and stains the nucleus of cells with a compromised cell membranes (Vermes *et al.*, 1995; Riccardi and Nicoletti, 2006). AV binding was measured at 6 h and 18 h, (Fig. 3.8 and Table 3.4).

The significant increase in AV+/PI− cells after treatment with $AuPPh_3$(trz-Fc-Dipp) at 6 h, indicates early apoptosis as indicated by annexin-V binding to phosphatidylserine an increase in AV^+/PI^+ cells at 18 h, suggests progression to late apoptosis or secondary necrosis as indicated by the presence of PI in the nuclei. This aligns with previous reports demonstrating that gold-based complexes can trigger apoptosis by increasing AV binding (Ott *et al.*, 2009; Zarić *et al.*, 2021).

Copper complexes, $CuPhenTh_2$, and Cu8AqN also caused phosphatidylserine externalization. The cells treated with $CuPhenTh_2$ maintained a prolonged early apoptotic events with intact cell membranes at 6 h and 18 h, as observed by AV+ only. Cu8AqN was poor at causing phosphatidylserine exposure at 6 h. At 18 h, Cu8AqN caused phosphatidylserine exposure evidenced by increased percentage of cells with annexin V binding and PI staining in their nuclei, indicating a progression to late-stage apoptosis with compromised cell membranes. These findings support what was reported by (Salimi *et al.*, 2015; Foo *et al.*, 2018; Lee *et al.*, 2021; Radhakrishnan *et al.*, 2021).

Doxorubicin maintained annexin V only staining on the cells indicating early apoptotic events. This is consistent with its mechanism of action, which involves DNA intercalation and the generation of oxidative stress, leading to apoptotic cell death. Conversely, staurosporine treated cells showed both annexin V binding and PI staining of the nuclei at both times, suggesting early onset of late apoptotic events and the loss of cell membrane integrity. The early and late apoptotic events align with the morphological changes such as round shape, vacuolization, nuclear condensation, and fragmentation which are observed in early and late apoptotic cells. Importantly, the treatments did not again show PI-staining only on the nuclei of the cells, which proved that the copper and gold metal complexes did not cause necrotic cell death.

4.5.2 Caspase-3/7 activation

Apoptosis induction by the complexes and the positive controls was further confirmed by the activation of executioner caspases-3/7. Caspase-3/7 are central executioner proteases in the apoptotic pathway and increased caspase-3/7 activity indicate apoptosis (Porter and Jänicke, 1999; Lamkanfi and Kanneganti, 2010; Galluzzi *et al.*, 2018). CellEvent Caspase-3/7 live cell green detection reagent was used to detect caspase-3 or caspase-7.

The assay cannot distinguish between caspase-3 and caspase-7 because it uses the DEVD peptide sequence which acts as a cleavage site for caspase-3 and caspase-7. In this study, caspase-3/7 activation was assessed at 24 and 48 h (Fig. 3.15 and 3.16). Caspase-3/7 cleaves the inhibitor of caspase-activated DNase (ICAD), releasing caspase-activated DNase (CAD), which translocate to the nucleus where it degrades chromosomal DNA, causes nuclear fragmentation and condensation (Jänicke *et al.*, 1998; Porter and Jänicke, 1999; Olsson and Zhivotovsky, 2011). Additionally, caspase-3/7 cleaves cytoskeletal and nuclear proteins like poly (ADP-ribose) polymerase (PARP), vimentin, and lamin A/C, contributing to chromatin condensation and nuclear envelope breakdown (Slee *et al.*, 2001; Walsh *et al.*, 2008).

While apoptotic features such as membrane blebbing and cell shrinkage are regulated by Rho-associated kinase (ROCK1), these processes are initiated by caspase-3-mediated cleavage of key regulatory proteins such as α-fodrin, gelsolin and p21-activated kinases (Pak2)(Coleman *et al.*, 2001; Sebbagh *et al.*, 2001). Thus, caspase-3/7 activation is a hallmark of apoptotic execution, orchestrating a cascade of proteolytic events leading to cellular dismantling and eventual phagocytic clearance. Copper and gold metal complexes have been reported to cause apoptosis (López-Hernández *et al.*, 2023). Accordingly, the results indicate that $AuPPh_3$(trz-Fc-Dipp) caused caspase-3/7 activation at 24 h, with a further increase at 48 h, suggesting rapid and sustained apoptotic induction. This is align with what was reported by (Reddy *et al.*, 2018; Pian *et al.*, 2022).

The ability of copper complexes to induce apoptosis in various cancer cells is well documented (Ma *et al.*, 2012; Salimi *et al.*, 2015; Harmse *et al.*, 2019; Li *et al.*, 2019, 2024; Ismail *et al.*, 2022; Jhetam *et al.*, 2025). However, (Gandin *et al.*, 2012) indicated that copper(I) phosphine complexes caused paraptosis in LoVo colon cancer cells which is a non-apoptotic cell death. Another study reported high levels of lactate dehydrogenase and the presence of ethidium bromide nuclei of A549 lung cancer cells treated with copper(II) pyrazole complex which indicated necrosis (Vyas *et al.*, 2015). In the current study, copper complexes showed a time dependant caspase-3/7 activation indicating apoptosis.

This suggests that the MDA-MB-231 cells may have a delayed response to copper complexes which could possibly results from delayed cellular uptake of the copper complexes. Copper-based complexes have been reported to exert apoptosis via oxidative stress, but their rate of caspase activation can vary depending on ligand composition and redox activity.

Doxorubicin and staurosporine, which are well-known apoptotic inducers, triggered caspase-3/7 activation at 24 h and 48 h. It was encouraging to observe the copper and gold metal complexes to have the same effects as doxorubicin. Overall, these findings confirm that the copper and gold metal complexes induce apoptosis via caspase-3/7 activation, and this was consistent with the cell morphology changes, ROS accumulation and phosphatidylserine externalization.

4.6 The copper and gold metal complexes activate both caspase-8 and caspase-9 in MDA-MB-231 breast cancer cells

The activation of initiator caspases determines the dominant apoptotic pathway. Caspase-8 activation is associated with the extrinsic apoptotic pathways, while the activation of caspase-9 indicates for the intrinsic apoptotic pathway. Simultaneous activation of both initiator caspases suggests potential crosstalk between these pathways.

4.6.1 Caspase-9 activation

Caspase-9 activation occurs when cytochrome *c* is released from the mitochondria to the cytosol to form an apoptosome complex with Apaf-1, dATP and procaspase-9. In the apoptosome complex, procaspase-9 dimerizes and forms a long length caspase-9 which activates executioner caspase-3/7 and trigger intrinsic apoptotic pathway (Tait and Green, 2010; Galluzzi *et al.*, 2012, 2018). In this study, caspase-9 was not observed at 18 h in the treated cells, as a result the experiment was repeated at 24 and 48 h. At 24 h, only a few cells treated with the copper and gold metal complexes and staurosporine were positive for active caspase-9, with a marked increase at 48 h. This suggests that the copper and gold metal complexes have a delayed activation of caspase-9 compared to doxorubicin which had more than 50 % cells with active caspase-9 at 24 h. These results indicate that the intrinsic apoptotic pathway is being triggered, consistent with the mitochondrial membrane depolarization as explained in section 4.4.

Comparable findings have been reported in the literature. Rackham *et al.*(2007) demonstrated that gold(I) phosphine complexes induce apoptosis in MDA-MB-468 breast cancer cells via caspase-9 activation as shown by western blot analysis. Similarly, Gorini *et al.*(2021) observed that gold(III) complexes, Au2phen and Auoxo trigger apoptosis in A270 ovarian cancer cells through caspase-9 activation, as determined by fluorescence-activated cell sorting. In addition, fluorescent microscopy studies have shown that copper complexes with an imidazole pyridine scaffold induce apoptotic cell death in leukemic (K562 and HL-60) and HT29 colorectal cancer cells by activating caspase-9 (Harmse *et al.*, 2019; Ismail *et al.*, 2022). Lee *et al.* (2021) reported similar caspase-9 activation in MCF-7 and MDA-MB-231 breast cancer cells treated with [Cu(phen)(L-tyr)Cl]·3H_2O. The consistent activation of caspase-9 across various metal-based complexes indicates their potential as promising agents capable of triggering apoptosis via mitochondrial/ intrinsic pathways.

4.6.2 Caspase-8 activation

Unexpectedly caspase-8 was activated. The percentage of cells with active caspase-8 was very low at 18 h but increased at 24 and 48 h in the cells treated with $AuPPh_3$(trz-Fc-Dipp), $CuPhenTh_2$ and staurosporine, likely indicating the early and maintained activity of the copper and gold metal complexes in activating caspase-8. In contrast, Cu8AqN activated caspase-8 after 48 h treatment only, indicating late activation of caspase-8. Active caspase-8 was observed in rounded and detached cells while adherent cells showed low/ no caspase-8 activation. Caspase-8 activation indicated the induction of the extrinsic/ death receptor driven apoptotic pathway.

Caspase-8 is activated when death receptors like Fas, TNFR, or TRAIL on the cell surface bind their specific ligands, this triggers the formation of DISC. Within DISC, adaptor proteins like FADD are recruited, which in turn bind to procaspase-8 (Elmore, 2007). Procaspase-8 molecules dimerize and undergo autocatalytic cleavage into active caspase-8. Active caspase-8 directly cleaves and activates the executioner caspases, caspase-3 and caspase-7 in the extrinsic apoptotic pathway (Elmore, 2007; Galluzzi *et al.*, 2018). Active caspase-8 may cleave pro-apoptotic protein Bid, to truncated Bid (tBID). The resulting tBid translocate to the mitochondria, promoting mitochondrial outer membrane permeabilization (MOMP) and thereby linking the extrinsic and intrinsic pathways of apoptosis (Galluzzi *et al.*, 2018).

The results on the gold complex $AuPPh_3$(trz-Fc-Dipp) concur with what was reported by (Magherini *et al.*, 2018; Gorini *et al.*, 2021). Caspase-8 activation in these cells by the copper complexes contrasts with what was previously reported by Harmse *et al.*(2019) and Ismail *et al.*(2022) who could not demonstrate the activation of caspase-8 in leukemic and colorectal cancer cells after treatment with the imidazole pyridine copper complexes. In another study, mononuclear copper(II) complexes with chiral Schiff-base were reported to cause a time dependent activation of both caspase-8 and caspase-9 in MDA-MB-231 cells (Zhou *et al.*, 2016). Data from the present study show that in MDA-MB-231 cells, the copper complexes activate both the intrinsic and the extrinsic pathways of apoptosis. In summary, the gold complex and copper complexes cause cell morphology changes consistent with apoptosis, ROS accumulation, mitochondrial dysfunction, PS exposure, activate caspase-3/7, and induce apoptosis via activation of the intrinsic and the extrinsic apoptotic pathways indicated by cleavage of caspase-3/7, caspase-8 and -9 activity, $\Delta\Psi m$ depolarization, and ROS accumulation in MDA-MB-231 cells. Despite the promising results observed for $AuPPh_3$(trz-Fc-Dipp) in the MDA-MB-231 cells, the complex had the lowest IC_{50} value in the MCF-10A cells indicative of poor selectivity compared to the copper complexes, due to this, the complex was not investigated further.

4.7 Copper complexes cause changes to apoptosis regulatory proteins

Following the confirmation that copper complexes cause apoptotic cell death in MDA-MB-231 cells, Cu8AqN and $CuPhenTh_2$ were selected as the lead candidates to evaluate their effects on proteome array. Cu8AqN and $CuPhenTh_2$ caused the lowest IC_{50} values of 3.31 ± 0.06 μM and 1.89 ± 0.14 μM respectively, in MDA-MB-231 cancer cells, while showing partially high IC_{50} values of 9.51 ± 0.03 μM and 5.76 ± 1.96 μM in MCF-10A mammary epithelial cells, indicating some selectivity towards cancer cells, compared to the gold complex. Doxorubicin was selected as the positive control since it is used clinically in the treatment of TNBC. The human apoptosis proteome array is an antibody-based array and determined the expression level of 35 apoptosis-related proteins simultaneously. The proteome array detected proteins associated with the execution and regulation of apoptosis, thereby providing a comprehensive understanding of the effects of the copper complexes on apoptosis and identify specific molecular targets to enhance our understanding of the mechanism of action and therapeutic potential of these copper complexes.

4.7.1 The effect of the copper complexes and doxorubicin on phosphorylated p53 species

Tumour suppressor, p53, is a transcription factor that regulates DNA repair, cell cycle arrest, senescence, and apoptosis in response to stress-induced DNA damage (Helton and Chen, 2007; Dolan *et al.*, 2015; Marvalim *et al.*, 2023). The p53 protein is activated by diverse intra and extracellular stress including hypoxia, ROS, DNA damage and therapeutic agents (Madan *et al.,* 2019; Wang *et al.,* 2019; Mancikova *et al.,* 2023). Mutations in the *TP53* gene are common in cancers, including breast cancer, leading to loss of its tumour-suppressive functions (Dumay *et al.*, 2013; Yue *et al.*, 2016, 2017; Ungerleider *et al.*, 2018).

The MDA-MB-231 cells harbour missense mutation in the *TP53* gene, resulting in the arginine (R) to lysine (K) substitution at codon 280 (R280K) within the DNA-binding domain and this mutation is characterized as a gain-of-function (GOF) mutation (Olivier *et al.*, 2002; Leroy *et al.*, 2014; Amirtharaj *et al.*, 2022; Marvalim *et al.*, 2023). This mutation confers new oncogenic properties, enabling mutant p53 to interact with transcription factors and modulate genes that promote tumour progression, metastasis, chemoresistance, and cell survival (Leroy *et al.*, 2014; Muller and Vousden, 2014).

The proteome array included 3 forms of phosphorylated p53 proteins at the specific serine residues, phospho-p53(s15), phospho-p53(s46) and phospho-p53(s392). Proteome array data showed high baseline expression levels of phospho-p53(s15), and phospho-p53(s392), while phospho-p53(s46) was very high in the untreated control cells. Phosphorylation is required for p53 stabilization, accumulation, and translocation to the nucleus, where it activate or regress its target genes. Phosphorylation of p53 at serine 15 (s15) residues is an early response to DNA damage (Loughery *et al.*, 2014). In p53 protein, serine 15 is phosphorylated by the ataxia telangiectasia mutated (ATM) in response to double strand DNA strand breaks (Balmer *et al.*, 2014). This stabilizes p53 by preventing its interaction with MDM2 via subsequent threonine 18 phosphorylation allowing for the release of p53 from MDM2, facilitating p53 accumulation and nuclear translocation, where it modulates the transcription of target genes involved in DNA repair and apoptosis (Loughery *et al.*, 2014).

Upon excessive oxidative stress leading to genotoxicity, p53 is phosphorylated at serine 46 mediated by the homeodomain interacting protein kinase2 (HIPK2) and dual specificity tyrosine regulated kinase 2 (DYRK2). Phosphorylation at serine 46 directs p53 towards activation of apoptotic genes like Puma, Noxa, and apoptosis inducing protein 1, leading to intrinsic apoptosis over cell cycle arrest thereby preventing cancer cell progression (Smeenk *et al.*, 2011; Hernandez-Valencia *et al.*, 2018). Phospho-p53(s392) is phosphorylated by casein kinase-2 (CK2) and p38 mitogen-activated protein kinase (MAPK) to enhance the transcriptional function of p53 by increasing structural stability and the ability to bind to DNA (Bar *et al.*, 2009). Moreover, Phospho-p53(s392) regulates p53 mitochondrial translocation, independent of it transcription role in the nucleus (Castrogiovanni *et al.*, 2018).

The high expression of phospho-p53 species in the untreated cells in this study was due to gain of function- mutant p53 (Muller and Vousden, 2014), and the phosphorylation of mutant p53 protein at serine 15, serine 46 and serine 392 may suggest stabilization of mutant p53 , and support gain-of-function activities, thereby contributing to cancer progression and survival, leading to tumorigenesis and chemoresistance, a phenomenon observed in MDA-MB-231 TNB cancer cells (Olivier *et al.*, 2002; Hui *et al.*, 2006; Curtis *et al.*, 2012; Meric-Bernstam *et al.*, 2018). Unlike wild-type p53, mutant p53 escape MDM2 degradation, by being stabilized by heat shock chaperone protein 90 (Hsp90), which interact with mutant p53 to prevent ubiquitination and degradation of mutant p53 (Peng *et al.*, 2001).

The copper complexes Cu8AqN and $CuPhenTh_2$ showed no effects on phospho-p53(s15), phospho-p53(s46) and phospho-p53(s392), suggesting that the copper complexes could not cause the degradation GOF-mutant p53 in these cells. In a parallel study, our group found that copper complex Cu8AqN, increased the levels of all three phosphorylated wild type p53 species in MCF-7 breast cancer cells (Myeza *et al.,* 2024). Ismail *et al.* (2022) reported that copper-imidazo[1,2-a]pyridine complexes induced intrinsic apoptosis in leukemic cells (HL-60 and K562) without wild type p53 accumulation. In contrast, another study from our group using similar complexes, reported a high expression of phospho-p53(s15), phospho-p53(s46) and phospho-p53(s392) in HT-29 colorectal cancer cells due to GOF-mutant p53. But the copper complexes decreased GOF-mutant p53 in these cells, triggering intrinsic apoptosis (Harmse *et al*., 2019).

In the present study, apoptosis was induced regardless of mutant p53 degradation, suggesting that the role of mutant p53 in apoptotic cell death and its susceptibility to degradation may vary depending on the specific copper complexes. Doxorubicin upregulated all three phosphorylated p53 species, indicating failure to degrade GOF-mutant p53 in MDA-MB-231 cells. While doxorubicin effectively induces wild-type p53 accumulation in MCF-7 breast cancer cells (Balmer *et al.*, 2014; Myeza *et al.*, 2024), the inability to degrade GOF-mutant p53 in MDA-MB-231 cells reduces its effectiveness in triple negative breast cancer. This has been observed in other studies, where doxorubicin was less effective MLN120B in p53-mutant tumours (Dalmases *et al.*, 2013). Unlike wild type p53, which mediates apoptosis via transcriptional activation, mutant p53 confers chemoresistance. The inability of $CuPhenTh_2$ and Cu8AqN to facilitate the degradation of mutant p53 suggests that the complexes induce apoptosis via p53-independent pathways, potentially making them effective in p53-mutant TNBC subtype.

4.7.2 Copper complexes decreased the expression of Bad in MDA-MB-231 breast cancer cells

The Bcl-2 protein family plays an important role in regulating the intrinsic apoptotic pathway, balancing pro-apoptotic and anti-apoptotic signals to determine whether the cells proliferates or die (Singh *et al.*, 2019). Anti-apoptotic members such as Bcl-2 and Bcl-x suppress apoptosis by inhibiting pro-apoptotic proteins, including Bax and Bad, which are required for MOMP to the cytosol (Tait and Green, 2010; Czabotar *et al.*, 2014).

The baseline expression of Bad was moderate in the untreated control cells and decreased after treatment as indicated in the proteomes array results, Fig. 3.20. The regulation of Bad by phosphorylation plays a pivotal role in its apoptotic activity. Phosphorylation at serine residues s112, and s136 promotes Bad interaction with 14-3-3 proteins, leading to its deactivation and enhanced cell survival (Xing *et al.*, 2000). Dephosphorylated Bad binds to Bcl-2/Bcl-xL, facilitating apoptosis (Galluzzi *et al.*, 2018). The findings suggest that the copper complexes modulate Bad activity, probably by targeting phosphorylated Bad to restore apoptotic function. Further studies on how the copper complexes and doxorubicin affect various phosphorylated forms of Bad may help elucidate the underlying mechanisms of these complexes.

Bcl-2 is a prognostic marker and low levels are associated with poor prognosis in TNBC (Eom *et al.*, 2016). The proteome array results showed low baseline expression of Bcl-2, which correlates with poor prognosis observed in TNBC. Elevated levels of Bcl-xL in breast cancer cells have been linked to increased metastatic potential and resistance to chemotherapy (Nocquet *et al.*, 2024). In the current study, basal expression of Bcl-xL in the untreated cells was low, this warrants further investigation on the role of Bcl-xL in TNBC. Cancer cells express low levels of Bax to evade apoptosis (Guttà *et al.*, 2020). The baseline expression of Bax in the untreated control cells was low, which could possibly indicate that this cell line is resistance to apoptosis. The changes caused by the treatment were considered not to be meaningful due to low basal expression.

4.7.3 Copper complexes decreased the inhibitor of apoptosis proteins (IAPs) in MDA-MB-231 breast cancer cells

The high expression levels of IAPs is associated with apoptosis inhibition, cancer progression, chemoresistance and increased morbidity (Fulda, 2014; Finlay *et al.*, 2017). Proteomic analysis showed that the basal expression level of XIAP was moderate high in the untreated control cells, Fig. 3.24. XIAP is commonly overexpressed in cancer, contributing to chemoresistance (Pluta *et al.*, 2015). The treatment of the cells with the copper complexes (Cu8AqN and $CuPhenTh_2$) and doxorubicin significantly ($p< 0.0001$) decreased the expression of XIAP. XIAP exert anti-apoptotic functions by binding to and inhibiting caspase-3, -7, and -9 through IAP BIR domains, thereby inhibiting the intrinsic pathway of apoptosis. BIR domains are conserved protein interaction modules found in IAPs. These domains play important roles in regulating apoptosis by binding to and inhibiting caspases, particularly caspase-3, caspase-7, and caspase-9 (Gill *et al.*, 2009; Cheung *et al.*, 2020; Albadari and Li, 2023).

These results suggest that Cu8AqN, $CuPhenTh_2$ and doxorubicin target XIAP to promote apoptosis signalling and this is consistent with the activation of caspase-3/7 and caspase-9 observed in the present study. Similarly, our recent work, showed that Cu8AqN caused a decrease in XIAP levels in MCF-7 cells, and this was consistent with the activation of caspase-7 and caspase-9 in the MCF-7(Myeza *et al.*, 2024). Harmse *et al.*(2019) reported a significant decrease of XIAP levels in HT-29 colorectal cancer cells after treatment with JD46(27), JD47(29) and JD88(21) copper-imidazo[1,2-a] pyridines.

The activation of caspase-3/7 and caspase-9 further supported the apoptotic signals in these cells. In contrast, Ismail *et al.*(2022) indicated that in HL-60 leukaemia cells a copper-imidazo[1,2-a] pyridine complex, JD88(21) increased the expression of XIAP which was associated with pro-survival response in these cells, but the same complex when was used in K562, caused a decrease in XIAP levels contributing to the execution of apoptosis. This shows that the effect of JD88(21) in XIAP is cell line dependant. The present study reports on the pro-apoptotic activity of the copper complexes by decreasing XIAP.

Survivin baseline expression levels were high in the untreated control cells, survivin is a marker for poor prognosis and chemoresistance (Yong-Gang *et al.*, 2010), which is observed in TNBC. Survivin was decreased by the copper complexes and increased by doxorubicin, suggesting chemoresistance. By binding to the pro-apoptotic proteins Smac/DIABLO, which are released from mitochondria during intrinsic apoptosis, survivin prevents them from neutralizing IAPs, thus maintaining the inhibition of the caspases (Johnson and Howerth, 2004; Chen *et al.*, 2016). At physiological concentrations, survivin functions as a weak apoptosis inhibitor and may primarily exert its anti-apoptotic effects by stabilizing XIAP (Rathore *et al.*, 2017). Survivin directly binds to and inhibits initiator caspase-9 thereby blocking the execution of apoptosis, but the effects of survivin in binding with effector caspases-3 and -7 is controversial (Johnson and Howerth, 2004). This suggests that the copper complexes caused apoptosis by decreasing survivin, thereby promoting caspase-9 activation. In MCF-7 cells, Cu8AqN and doxorubicin caused a decrease in survivin levels and promoted intrinsic apoptosis (Myeza *et al.*, 2024). The current study shows that the copper complexes promote apoptosis by attenuating the inhibitory effects of survivin and XIAP.

In the untreated control cells, the baseline expression of cIAP-2 and livin was low, and the changes in the expression levels of these proteins in the cells were considered less meaningful because of low basal expression. The untreated control cells had high basal expression of cellular inhibitor of apoptosis protein 1 (cIAP1), and this was significantly decreased by the copper complexes and doxorubicin. cIAP1 regulate apoptosis through their BIR domains and RING (Really Interesting New Gene) domains, which have distinct roles in inhibiting caspases. The BIR domains in cIAP1 facilitate protein-protein interactions, allowing them to bind and inhibit apoptotic proteins like

caspase-8 activation, thereby blocking the extrinsic apoptosis pathway before it can initiate downstream caspase cascades like caspase-3/-7 (Finlay *et al.*, 2017). The RING domain in cIAP1 gives these proteins E3 ubiquitin ligase activity, allowing them to tag target proteins with ubiquitin chains, marking them for proteasomal degradation. By promoting proteasomal degradation of caspase-3 and caspase-7, cIAP1 inhibits the execution of apoptosis (Lalaoui and Vaux, 2018).

4.7.3.1 cIAP1 expression prevents caspase-8 activation

cIAP1 modulates apoptosis and TNF receptor signalling, then function as E3 ubiquitin ligases due to their RING domains. They are recruited to TNFR signalling complexes through their interaction with TNFR-associated factor 2 (TRAF2). In TNF-related apoptosis-inducing ligand (TRAIL) signalling (Siegmund *et al.*, 2022; Dumétier *et al.*, 2023), cIAP1 binds to TNFR-associated factor 2 (TRAF2) and get recruited to the TNFR signalling complexes. Because cIAP1 has a poor affinity for the caspases, they function as E3 ubiquitin ligases. These enzymes cause the ubiquitination of target proteins like TRAIL R1/ TRAIL R2 in the TRAIL receptor complex. Ubiquitination targets proteins for proteasomal degradation. This prevents the formation of an active death inducing signalling complex (DISC) thereby blocking the activation of caspase-8 (Varfolomeev *et al.*, 2007, 2008). Thus, cIAP1 inhibition caused an unexpected activation of caspase-8 suggesting that decreasing cIAP1, cause extrinsic apoptosis in the cells.

4.7.3.2 cIAP1 supressed the canonical nuclear factor kappa B pathway

Apart from caspase inhibition, cIAP1 controls both the canonical and non-canonical NF-κB pathways and is regulated by TNF R1. In the canonical pathway, cIAP1 controls NF-κB pathway, this occurs when TNF binds to TNF R1, causing the formation of Complex 1 which consists of TNFR1-associated death domain protein (TRADD), Receptor-Interacting Serine/Threonine-Protein Kinase 1(RIPK1), TRAF2 and cIAP1.

cIAP1 ubiquinates RIPK1 which activates IKK. Subsequently, IKK phosphorylates and degrade IκBα via proteasome leading to it dissociation form the NF-κB (p50, p65). NFκB translocate to the nucleus and stimulate the transcription of survival genes like cIAP1, cIAP2 and XIAP (Cetraro *et al.*, 2022; Siegmund *et al.*, 2022). The decrease in cIAP1 in this study, indicate that the copper complexes may have suppressed the canonical NF-κB pathway.

The copper complex, Cu8AqN was reported to inhibit cIAP1 in MCF-7 breast cancer cells, which promoted intrinsic apoptosis and possibly blocked the stimulation of the canonical NF-κB pathway (Myeza *et al.*, 2024), HT-29 colorectal cancer cells treated with the imidazole pyridine copper complexes were reported to have decreased cIAP1 expression (Harmse *et al.*, 2019), likely inhibiting the canonical NF-κB pathway. This study indicate that the copper complexes potentially inhibit the activation of the canonical NF-κB pathway by decreasing cIAP1 and TNFR, but further studies on the expression of individual kinases involved in NF-κB is warranted to validate these results.

4.7.4 Copper complexes decreased the expression of Smac /DIABLO, and HtrA2/Omi in MDA-MB-231 breast cancer cells

Cytochrome *c*, Smac/DIABLO, and HtrA2/Omi, key mediators of intrinsic apoptosis, were investigated. Smac/DIABLO and HtrA2 (also known as Omi) are mitochondrial proteins that are essential for the regulation of intrinsic apoptosis by neutralising inhibitor of apoptosis proteins (IAPs) (Maas *et al.*, 2010). Smac/DIABLO is released into the cytosol, where it bonds to IAPs such as XIAP, cIAP1, and cIAP2, neutralising their inhibitory effect on caspases and thereby promoting apoptosis, in response to apoptotic stimuli (Paul *et al.*, 2018). Copper complexes has been shown to increase Smac/DIABLO expression in HL-60 leukemic cells and triggering apoptosis in the cells as indicated by the proteomic array data (Ismail *et al.*, 2022). Our proteome array results showed moderate basal levels of Smac/DIABLO expression in untreated control cells Fig. 3.21, which was unexpected in the absence of apoptotic signals. This observation suggests potential alternative roles for Smac/DIABLO in cancer cells, possibly as a biomarker or regulator involved in processes beyond apoptosis.

HtrA2/Omi is a mitochondrial serine protease that is released into the cytosol during apoptosis, where it contributes to the degradation of IAPs. It contains an Alanine-Valine-Proline-Serine (AVPS) motif, a well-characterized IAP-binding tetrapeptide responsible for interacting with and inactivating IAPs such as cIAP1, thereby promoting caspase activation and apoptosis. This mechanism reduces the ability of IAPs to ubiquitylate and inhibit caspases, thus facilitating apoptotic progression (Fulda, 2014).

Beyond its pro-apoptotic role, HtrA2/Omi has been implicated in tumour-promoting functions, particularly in aggressive malignancies such as colon, liver, and cervical cancers (Mao *et al.*, 2014; Hirschfeld *et al.*, 2015; Wang *et al.*, 2018). Interestingly, studies in pancreatic cancer cells demonstrated that inhibition of HtrA2/Omi led to apoptosis, suggesting that its function may be context-dependent and potentially linked to tumour survival in specific cancer types (Gmeiner *et al.*, 2015). In the present study, basal levels of HtrA2/Omi were significantly high in untreated control cells, possibly due to tumour promoting functions.

The significant decrease of Smac/DIABLO and HtrA2/Omi after treatment with the copper complexes and doxorubicin possibly suggests increased ubiquitination and proteasomal degradation. Given that Smac/DIABLO and HtrA2/Omi are proteins and are subjected to protein folding for their proper physiological function, it is likely that the copper complexes and doxorubicin may have caused misfolding of these proteins leading to their rapid proteasomal degradation. Additionally, the HSP were highly expressed, they may have facilitated the degradation of Smac/DIABLO and HtrA2/Omi. However, future studies are required to clarify the role of Smac/DIABLO and HtrA2/Omi in TNBC cancer cells. In the array data, the baseline expression of cytochrome *c* was low in the untreated control cells, since the basal expression was low, the changes were less meaningful.

4.7.5 Copper complexes caused insignificant changes in the highly expressed cleaved caspase-3 in MDA-MB-231 breast cancer cells

Caspase-3 and caspase-7 are key executioner proteases in apoptotic cell death, with their cleavage serving as a definitive marker of apoptosis execution. These proteases are synthesized as inactive precursors (procaspases) and require cleavage by upstream initiator caspases, such as caspase-8 (extrinsic pathway) or caspase-9 (intrinsic pathway), to become fully active and drive apoptotic cell death (Porter and Jänicke, 1999; Lamkanfi and Kanneganti, 2010; Galluzzi *et al.*, 2018). In the present study, proteome array analysis demonstrated very high baseline levels of procaspase-3 in untreated MDA-MB-231 cells, indicating that these cells are primed for apoptosis but have not activated caspase-3.

Following treatment with the copper complexes, procaspase-3 levels remained unchanged, indicating that the copper complexes did not significantly alter the expression of executioner caspase-3. This prompted for the investigation of cleaved caspase-3.

The baseline expression of cleaved caspase-3 was moderately high in the untreated control cells. Treatment with the copper complexes or doxorubicin did not alter this expression, suggesting that the observed apoptotic activity was not mediated through caspase-3 activation. It is possible that caspase-7 contributed to the apoptosis observed; however, this cannot be confirmed, as the proteome array used was specific only to cleaved caspase-3. In contrast, the fluorogenic probe employed in section 3.3.6.1 detects both cleaved caspase-3 and caspase-7 due to its lack of specificity. Therefore, the apoptotic signal detected by the fluorogenic assay may have originated from cleaved caspase-7, which would explain the absence of cleaved caspase-3 detection in the proteome array. Copper complexes have been reported to activate caspase-3 in various cancer cells (Salimi *et al.*, 2015; Harmse *et al.*, 2019; Periasamy *et al.*, 2020; Ismail *et al.*, 2022).

4.7.6 Copper complexes decreased the expression of the Fas/ CD95 receptor in MDA-MB-231 breast cancer cells

The extrinsic apoptosis pathway is initiated by binding of Fas ligand (FasL) to Fas receptor (FasR). Binding of FasL to Fas R, recruits Fas-associated death domain (FADD) and procaspase-8, forming the DISC complex. Caspase-8 is activated and triggers execution of apoptosis. Proteome array results indicate that the basal expression of Fas in the untreated control cells was moderate. Fas R expression is associated with aggressive (prognostic marker), poorly differentiated tumours, particularly in invasive ductal carcinomas, where it may promote breast cancer cell invasiveness, metastasis and chemoresistance (Zheng *et al.,* 2014; Saigusa *et al.,* 2015; Papadaki *et al.,* 2024). Fas, when circulating in cancer cells, shifts from an apoptotic function to one that supports tumour survival. This role is mediated through the activation of key signalling pathways, such as NF-κB via cIAP1, promoting the transcription of genes that drive cancer cell proliferation, survival, and resistance to apoptosis (Cipriano *et al.,* 2013; Devanaboyina *et al.,* 2022). The decrease of Fas by the copper complexes and doxorubicin observed in this study supported the inhibition of canonical NF-κB pathway. The basal expression of TNFR 1 was low in the untreated cells as a result, the changes caused by the copper complexes and doxorubicin were less meaningful.

The baseline expression of the death receptor proteins, TRAIL R1, TRAIL R2 and FADD was high in the control cells, indicating the potential of extrinsic apoptotic cell death. The treatment of the cells with the copper complexes and doxorubicin did not change the expression of these death receptors, suggesting the complexes do not target these receptors directly, but decreasing cIAP1 levels may have an important factor driving the late activation of caspase-8.

4.7.7 Copper complexes decreased the expression of cell cycle regulators, p21, p27 and phospho-RAD179 (s635) in MDA-MB-231 breast cancer cells

Proteome array profiler detected the expression levels of p21, p27 and phospho-RAD179 (s635) and immunofluorescence was used to further investigate changes to p21 expression. Cyclin-dependent kinase inhibitors, p21 and p27 have important roles in regulating cell cycle progression (Katner *et al.*, 2002; Abbas and Dutta, 2010). Proteome array data indicated low basal expression of p21, p27 and phospho-RAD179 (s635) in the untreated control cells, as a result the changes caused by the complexes on the expression levels in the cells were less meaningful.

The expression of p21 was decreased and validated with immunofluorescent microscopy to confirm the results. Previous studies in our research group reported on the expression of p21 in lung and colorectal cancer cells after being treated with novel metallodrugs (Peega *et al.*, 2021), this prompted for an evaluation of the effects of copper complexes on p21 expression in MDA-MB-231 cells. Untreated control MDA-MB-231 cells lacked the expression of p21, but all the treated cells showed an increase in nuclear expression of p21, an indicator for DNA damage. This confirmed the DNA damaging activity of doxorubicin (Cao *et al.*, 2021) and align with our previous work where Cu8AqN treatment led to p21 overexpression in MCF-7 breast cancer cells (Myeza *et al.*, 2024).

In the nucleus, p21 is an indicator to DNA damage via p53 tumour suppressor protein and regulates cell cycle arrest in G1 and G2/mitotic phase (Denicourt *et al.,* 2007; Dolan *et al.,* 2015). In contrast, cytoplasmic p21 prevents apoptosis by binding and preventing the activation of pro-caspase-3, and caspase-8 there by inhibiting Fas mediated apoptosis (Kreis *et al.*, 2019). The cyclin-dependent kinase inhibitor p21 binds to proliferating cell nuclear antigen (PCNA) and inhibits PCNA-dependent DNA replication and repair processes, ensuring a strong gatekeeping action to prevent

uncontrolled cell division (Georgakilas *et al*., 2017). These results suggest that the copper complexes caused and increase in the nuclear p21 localisation which is an indicator of DNA damage in response to cellular stress. Albeit a decrease in total amount of p21 in the lysates.

4.7.8 Copper complexes decreased paraoxonase-2 and heat shock proteins in MDA-MB-231 breast cancer cells

Paraoxonase-2 (PON2), a member of the paraoxonase gene family, promotes cancer cell survival by acting as an antioxidant, reducing intracellular ROS levels, and inhibiting oxidative stress-induced apoptosis. The basal expression levels of PON2 were low in the untreated control cells as a result, the changes caused by the complexes in cellular expression of PON2 were less meaningful.

Heat shock proteins (HSPs) are molecular chaperones activated upon oxidative stress to promote cell survival or cell death (Zhang and Bi, 2024). HSP27 basal levels were very high in untreated control cells. High levels of HSP27 in breast cancer cells are associated with proliferation, invasion and drug resistance (Wang *et al.*, 2020; Bi *et al.*, 2023). Knockdown of HSP27 sensitized MDA-MB-231 cells to chemotherapy and potentiated cleavage of caspase-3/7 and triggered apoptosis (Peng *et al.*, 2013). Treatment of the cells with the copper complexes and doxorubicin caused no changes to the expression of HSP27 suggesting that this protein was not a therapeutic target.

Proteome array analysis indicated that the basal expression of HSP60 was moderate in the untreated control cells. The role of HSP60 in the cells is dependent on the location. In the mitochondria, HSP60 inhibit apoptosis by binding to mitochondrial p53 and promote cell survival (Ghosh *et al.*, 2008). When expressed in the endoplasmic reticulum, HSP60 inhibit the expression of XIAP and allow for apoptosis to occur (Arya *et al.*, 2015). Expression of HSP60 on the cell membranes promotes breast cancer metastasis by interacting with alpha-three beta- one (α3β) integrin (Cappello *et al.*, 2014). The expression of HSP60 was not changed in the cells post treatment with the copper complexes, indicating poor interaction with this protein.

The basal levels of HSP70 in the untreated cells were moderate. HSP70 is a molecular chaperone that facilitates protein folding, inhibits the aggregation of misfolded proteins, and stabilises proteins during physiological stress (Chanteloup *et al.,* 2020). HSP70 is a marker of prognosis in

many cancers, protects cells from apoptosis and promotes tumour aggressiveness (Murphy, 2013; Vostakolaei, *et al.,* 2021). HSP70 promotes survival by binding to and inhibiting apoptotic mediators like Apaf-1 and AIF, therefore blocking the apoptosome formation and caspase activation (Park *et al.,* 2017). It stabilises lysosomal membranes, inhibits cathepsin release, and interacts with IκB kinase (IKK) to sustain NF-κB signalling, hence enhancing cell survival and inflammatory responses (Mawatari *et al.,* 2015; Chanteloup *et al.,* 2020; Fusella *et al.,* 2020). These pathways contribute to cancer cell proliferation, migration, and survival (Mawatari *et al.*, 2015; Chanteloup *et al.*, 2020).

The current study showed that treatment with the copper complex Cu8AqN did not alter HSP70 expression levels, suggesting that Cu8AqN does not interfere with HSP70-mediated cytoprotection. Conversely, $CuPhenTh_2$ and doxorubicin significantly reduced HSP70 expression, indicating that the downregulation of HSP70 may be a mechanism through which they exert their cytotoxic effects and alleviate cancer cell progression. By lowering HSP70 levels, $CuPhenTh_2$ and doxorubicin may attenuate the anti-apoptotic and pro-proliferative roles of HSP70, thereby promoting mitochondrial apoptotic signalling and impairing cancer cell survival. This supports the idea that HSP70 inhibition can enhance the sensitivity of tumour cells to treatment.

4.7.9 Copper complexes increased the expression of haem oxygenase-1 in MDA-MB-231 breast cancer cells

Haem oxygenase-1 (HMOX-1) is an inducible oxidative stress response protein expressed in many cancers, including breast cancer (Podkalicka *et al.,* 2018; Gandini *et al.,* 2019; Mascaró *et al.,* 2021). The expression of HMOX-1 is upregulated by several stimuli, including oxidative stress, UV irradiation, infections, heavy metals, cytokines (Vanella *et al.*, 2016). The enzyme contributes to cellular defence by degrading haem into bilirubin and carbon monoxide (CO), which are potent antioxidants that neutralize ROS and reduce oxidative damage/stress. By mitigating oxidative stress, HMOX-1 have an important role in promoting cell survival under oxidative conditions (Chen *et al.*, 2022). Proteome array analysis showed moderate baseline expression of HMOX-1 in the untreated control cells (section 3.4.4; Fig. 3.26). HMOX-1 expression has been reported in many cancer cell lines, and its expression is associated with cancer cell proliferation and chemoresistance (Was *et al.*, 2006; Consoli *et al.*, 2024).

HMOX-1 was significantly increased ($p< 0.0001$) after treatment with Cu8AqN and $CuPhenTh_2$, suggesting that these copper complexes induce oxidative stress, which is consistent with their redox activity and ROS-generating potential. Copper imidazole pyridine complexes were reported to cause an increase of HMOX-1 expression in HT-29 colorectal cancer cells (Harmse *et al.,* 2019), which was observed in the present study. The transcription of the HMOX-1 gene is regulated by multiple transcription factors, including hypoxia-inducible factor-1α (HIF-1α), nuclear factor erythroid 2-related factor-2 (Nrf2), NF-κB and activator protein-1 and 2 (AP-1 and AP-2) (Loboda *et al.,* 2016; Singhabahu *et al.,* 2024), as a result the expression of (HIF-1α) was evaluated. Proteome array indicated high basal expression of HIF-1α levels in the untreated control cells. Solid tumours are characterised by oxygen deprivation, which is a significant factor in the progression of solid breast malignancies (Nejad *et al.,* 2021). Cancer cells activate survival-associated genes that contain hypoxia-responsive elements (HREs) in such hypoxic conditions. These genes are regulated by the hypoxia-inducible factor-1 (HIF-1) transcription factor (Parks *et al.,* 2016). The active HIF-1 heterodimer initiates adaptive responses, including increased anaerobic glycolysis, angiogenesis, resistance to apoptosis, and autophagy, upon binding to these promoter sequences. These responses facilitate the growth and progression of tumours (Zhong *et al.,* 1999; Parks *et al.,* 2016).

Cu8AqN significantly decreased HIF-1α expression, suggesting that this complex reduced hypoxic stress and attenuated cancer cell progression. HMOX-1 was increased in Cu8AqN treated cells suggesting that other transcription factors, such as Nrf2 or AP-1, independent of HIF-1α may have contributed to the increased levels of HMOX-1 (Mehta *et al.*, 2007; Loboda *et al.*, 2016). Conversely, $CuPhenTh_2$ significantly increased HIF-1α suggestive of increased hypoxic stress and possibly chemoresistance, this was correlated with high HMOX-1 in the cells treated with this complex. The differences suggest that the copper complexes exert their cytotoxic effects through distinct molecular mechanisms, modulating transcriptional pathways that regulate oxidative and hypoxic stress. Under hypoxic conditions, HIF-1α accumulates in the cytoplasm and translocate to the nucleus, where it pairs with HIF-1β to initiate transcriptional activity (Galanis *et al.*, 2008; Azimi, 2018; Singhabahu *et al.*, 2024). The direct interaction between Hypoxia Response Elements (HREs) in the HMOX-1 promoter region recruits transcriptional coactivators, such as

p300/CBP (CREB-binding protein), steroid receptor coactivator-1 (SRC-1), and transcriptional intermediary factor-2 (TIF-2), which promotes transcriptional activity and increases HMOX-1. Increased HMOX-1 expression then triggers cytoprotective effects, by reducing oxidative stress (Galanis *et al.*, 2008; Azimi, 2018). Doxorubicin marginally increased HIF-1α expression while HMOX-1 was poorly expressed in doxorubicin treated cells. This suggested dissociation between hypoxic stress signalling, antioxidant defence and chemoresistance. Doxorubicin is known to generate ROS and cause DNA damage, which can stabilize HIF-1α (Ahmadpour *et al.,* 2021). However, the concomitant downregulation of HMOX-1, a cytoprotective enzyme regulated by Nrf2, indicated an impaired antioxidant response.

HMOX-2 basal levels were moderate in the untreated control cells. HMOX-2 is constitutively expressed in the small endoplasmic reticulum (sER) and brain tissue, where it plays a role in maintaining basal haem homeostasis, ensuring continuous production of protective byproducts like CO and bilirubin (Su *et al.*, 2022). HMOX-2 levels decreased across all the treated cells, indicating a diminished cytoprotective function of HMOX-2 by the copper complexes and doxorubicin. The ability of the copper complexes to increase HMOX-1 and decrease HMOX-2 expression reinforces their cytotoxic effects via oxidative stress-mediated apoptotic cell death.

4.8 Immunofluorescence of NIK, phospho-p53(s15) and HMOX-1

After the changes caused by the copper complexes on the apoptosis related proteins were identified, the results of select proteins were confirmed by immunofluorescent microscopy. Immunofluorescence detected the expression and subcellular localization of NF-κB-inducing kinase (NIK), phospho-p53(s15), and HMOX-1.

4.8.1 Copper complexes caused nuclear expression of NF-κB-inducing kinase (NIK) in MDA-MB-231 breast cancer cells

NIK is a key regulatory kinase that regulates mainly the non-canonical NF-κB signalling pathway. NIK is an unstable protein, and it is tightly controlled through ubiquitination by a TRAF2, TRAF3, and cIAP1/2 in the cytoplasm, notably, ubiquitination is mediated by cIAP1/2. In unstimulated cells, cIAP1/2, TRAF2 and TRAF3 mark NIK for ubiquination and proteasomal degradation, thereby preventing the accumulation of NIK and activation of the non-canonical NFκB pathway

in the nucleus (Minicozzi *et al.*, 2021; Siegmund *et al.*, 2022). Low cIAP1/2, TRAF2, and TRAF3 levels stabilizes cytosolic NIK, and cause the activation of inhibitor of nuclear factor kappa-B kinase-alpha (IKKα) by phosphorylation. Subsequently, IKKα activates p100, which triggers proteolysis giving rise to p52, which dimerizes with RelB (Coope *et al.*, 2002; Gambhir *et al.*, 2015; Siegmund *et al.*, 2022). This allows for the translocation of p52/RelB dimer to the nucleus and activation of NF-κB target genes involved in cell survival and proliferation (Rovillain *et al.*, 2011; Gambhir *et al.*, 2015; Minicozzi *et al.*, 2021). In the present study, immunofluorescent microscopy results showed poor basal expression of nuclear NIK in the untreated control cells. NIK shuttles between the cytosol and the nucleus (Birbach *et al.*, 2002), in many cell types, NIK is predominantly localized in the cytoplasm but in MDA-MB-231 breast cancer cells, NIK localizes to the nucleus, this suggests that nuclear NIK may play a role in maintaining NF-κB activity, potentially contributing to the aggressiveness of this subtype (Birbach *et al.*, 2004).

The cIAP1 expression levels were decreased after treatment with the copper complexes and doxorubicin. Consequently, NIK accumulated and was highly expressed in the nucleus of the cells treated with the copper complexes and doxorubicin, indicating the important role of cIAP1 in NIK degradation. In the nucleus, NIK activates IKK, which has been shown to shuttle between the nucleus and the cytoplasm (Birbach *et al.*, 2002), and is essential for NF-κB pathway activation. Nuclear NIK was reported to be responsible for a direct activation of p65 NF-κB via phosphorylation (Jiang *et al.*, 2003). But, Reporter gene assays, showed that non-shuttling cytosolic NIK had a highest NF-κB activation compared to the nuclear NIK (Birbach *et al.*, 2004). While inhibition of cIAP1 suppresses the canonical NF-κB pathway as observed before, the observed increase in NIK suggests an activation of non-canonical NF-κB, which may contribute to chemoresistance and cancer cell progression. This warrants further studies to determine consequences of NIK activation in TNBC.

4.8.2 Copper complexes increased the expression of nuclear phospho-p53(s15) in MDA-MB-231 breast cancer cells

Immunofluorescence of phospho-p53(s15) confirmed proteome array results. Phosphorylation of p53 at serine 15 (s15) by ATM in wild p53 is an early cellular response to DNA damage, and is required for p53 stabilization an accumulation in the nucleus. (Balmer *et al.*, 2014; Loughery *et*

al., 2014). MDA-MB-231 cells have mutated TP53, which impairs normal p53 function (Olivier *et al.*, 2002; Leroy *et al.*, 2014; Amirtharaj *et al.*, 2022). The results show that phospho-p53(s15) was not expressed in the untreated control cells, indicating absence of DNA damage in the untreated cells. Treatment with copper complexes, doxorubicin, and staurosporine caused nuclear phospho-p53(s15) expression. Suggesting that the copper complexes and doxorubicin may cause DNA damage that may trigger phosphorylation of mutant p53 at serine 15 via gain of function activity. This post-translational modification may contribute to the stabilization of the aberrant p53 protein. Although consistent with the proteome array, the results from doxorubicin treated cells were inconclusive since doxorubicin has red innate fluorescence in the nucleus, staurosporine circumvented this, as a positive control for phospho-p53(s15).

The results obtained for copper complexes differed from the results obtained in the proteome array. Likely because the IF provides localization of proteins, allowing detection of phospho-p53(s15) within specific cellular compartments. It can identify phosphorylated p53, even if the total protein levels remain low, in contrast, the proteome array measure total cellular protein levels, detecting changes in the entire cell lysate. If phospho-p53(s15) is increased only in certain cellular compartments (e.g. nucleus) or only in a subset of cells, the average expression across the population may remain unchanged, leading to what was observed here. This study report that the copper complexes cause DNA damage and leading to phosphorylation of mutant phospho-p53(s15).

4.8.3 Copper complexes increased the expression of nuclear HMOX-1 in MDA-MB-231 breast cancer cells

Immunofluorescence confirmed HMOX-1 expression in the treated cells as observed in the proteome array. Basal expression of HMOX-1 was low in the untreated control cells and was present in the nucleus. In the treated cells, HMOX-1 expression was highly increased and was also located in the nucleus. Nuclear HMOX-1, is a truncated form known to be enzymatically inactive (no cell protection roles). It is associated with aggressive tumours and function as a cofactor in the transcription of genes involved in regulation of oxidative stress responses, hypoxia, tumour progression and survival (Biswas *et al.*, 2014; Hsu *et al.*, 2015). In addition to immunofluorescence staining experiments of HMOX-1, western blot analysis of HMOX-1 to confirm the molecular

weight of HMOX-1 and determine whether it is a truncated or full length (not truncated) form were conducted. Western blot analysis indicated poor expression of HMOX-1 in the untreated control cells and in the cells treated with doxorubicin, while confirming a molecular weight of 32 kDa in the cells treated with the copper complexes, suggesting the expression of full length HMOX-1 in the nucleus. These results confirm that copper complexes are potent inducers of oxidative stress via ROS accumulation, this aligns with the findings of Jhetam *et al*(2025).

4.8.4 The efficacy of copper complexes in the presence of HMOX-1 inhibitor, OB24.

Since HMOX-1 is implicated in cancer cell survival, this study investigated the effect of HMOX-1inhibition on the efficacy of the copper complexes. The cells were treated with the copper complexes in combination with 20 μM OB24, which is specific at inhibiting HMOX-1 enzymatic activity (cell protection roles inhibited). The results showed that the effects of HMOX-1 inhibition were complex dependant. HMOX-1 inhibition significantly decreased the IC_{50} value of Cu8AqN from 3.31 ± 0.06 μM to 0.30 ± 0.09 μM while the IC_{50} of $CuPhenTh_2$ was increased from 1.89 ± 0.14 μM to 3.81 ± 0.77 μM.

HMOX-1 inhibition had varied response on the efficacy of Cu8AqN and $CuPhenTh_2$ treatment showing the implication of HMOX-1 in chemotherapy response. HMOX-1 high expression is associated with chemoresistance and cancer cell survival (Mascaró *et al.,* 2021). In the presence of HMOX-1, Cu8AqN was less cytotoxic (IC_{50} value 3.31 ± 0.06 μM), the inhibition of HMOX-1 enzymatic activity sensitized MDA-MB-231 cells to Cu8AqN (IC_{50} value decreased more than 10-fold), indicating that HMOX-1 over expression supported resistance to treatment with Cu8AqN in these cells. This was further supported by a decreased expression of HIF-1α observed in the proteome array. This implies that the tumours with high expression of HMOX-1 could benefit from Cu8AqN treatment in combination with HMOX-1 inhibitor, OB24, as previously reported by Jhetam *et al.,* 2025. In other studies, HMOX-1 inhibition with zinc and tin protoporphyrin (ZnPP and SnPP) sensitized pancreatic ductal adenocarcinoma cells to albumin bound paclitaxel and gemcitabine (NPG) induced cytotoxicity and triggered apoptosis (Ahmad *et al.,* 2021). The knockdown of HMOX-1 using short interfering (si)RNA in MDA-MB-231 and BT549 increased doxorubicin cytotoxicity and apoptosis, indicating that HMOX-1 expression supports chemoresistance in these breast cancer cell lines (Zhu *et al.,* 2015). In contrast, $CuPhenTh_2$

showed increased IC_{50} values (less active) when HMOX-1 was inhibited, suggesting that alterative pro-survival mechanisms were activated when HMOX-1 was inhibited. One possibility could be the shift towards the HIF-1α signalling since it was increased in the cells treated with $CuPhenTh_2$. HIF-1α is upregulated in TNBC and linked to chemotherapy resistance (Nejad *et al.,* 2021). HIF-1α drives hypoxia-induced survival, thus, in high-HIF-1α tumours, blocking HMOX-1 may favour these alternative pathways. Jhetam *et al.*(2025) reported that the inhibition of HMOX-1 using OB24 in the pancreatic ductal adenocarcinoma sensitized the cells to $CuPhenTh_2$ and decreased the IC_{50} values (from 4.0 μM to 1.8 μM) in the cells treated with the combination of $CuPhenTh_2$ and OB24, which did not corroborate the findings from the present study.

Another cell survival mechanism could be the involvement of the Nrf2. Nrf2 activity can promote cancer cell progression and drug resistance in cancer cells (Ji *et al.,* 2013; Wu *et al.,* 2015; Zuo *et al.,* 2025), and it is a widely known transcription factor of HMOX-1 (Loboda *et al.*, 2016). The inhibition of Nrf2 with Nrf2 inhibitor, ML385, sensitized cisplatin resistant lung cancer cells to cisplatin, and triggered ferroptosis in these cells by blocking the Nrf2-HMOX-1 pathway (Zuo *et al.,* 2025). Nrf2-HMOX-1 signalling pathway presents a promising therapeutic approach worth exploring to improve therapeutic outcomes in TNBC. The HMOX-1 modulation by Nrf2 requires further investigation. Collectively, these results identify HMOX-1 as a potential therapeutic target and highlight the implication of HMOX-1 in cell survival, and treatment response. HMOX-1 expression requires further evaluation using mRNA to evaluate gene profile of oxidative stress regulators.

4.9 Study limitations

While this study provides valuable data on the cytotoxicity and apoptotic effects of these copper and gold metal complexes, several limitations must be acknowledged. The experiments were conducted *in vitro*, and the findings may not fully translate to *in vivo* conditions due to potential differences in bioavailability, and tumour microenvironment interactions. Although the complexes demonstrated selectivity toward MDA-MB-231 TNBC cells, further validation in an additional TNBC cell line and or organoids would provide more comprehensive results. While the proteome array provided valuable data, its limitation in distinguishing between protein isoforms must be considered when interpreting the results.

Chapter Five: Conclusion

TNBC is a clinically aggressive breast cancer subtype defined by the absence of ER, PR, and HER2 expression. This receptor-negative profile significantly limits targeted therapeutic options and contributes to a poor prognosis. The five-year survival rate for TNBC patients is approximately 65 % for non-metastatic TNBC but decreases to 11 % in metastatic cases (Denkert *et al.,* 2017; Gonçalves *et al.,* 2018). The absence of effective targeted treatments and high rates of recurrence warrants for the development of novel therapeutic agents with improved efficacy and selectivity. This study showed that the copper and gold complexes represent a promising class of metallodrugs capable of selectively inhibiting the proliferation of MDA-MB-231 cells.

Organic metal complexes containing gold ($AuPPh_3$(trz-Fc-Dipp), and copper ($CuPhenTh_2$; Cu8AqN) complexes were cytotoxic against MDA-MB-231 cells, with IC_{50} values below 5 μM. In comparison to $AuPPh_3$(trz-Fc-Dipp), the copper complexes, $CuPhenTh_2$ and Cu8AqN showed partial selectivity toward MDA-MB-231 breast cancer cells compared to normal mammary epithelial cells, represented by MCF-10A cells. Fluorescent microscopy indicated that all the metal complexes caused the MDA-MB-231 cells to shrink with nuclear condensation and fragmentation, which were morphological features consistent with apoptosis (Fig 5.1). There was no evidence of necrotic cell death, supporting the conclusion that cell death occurred primarily through apoptosis rather than necrosis. Additional experiments indicated that the copper and gold complexes induced oxidative stress by increasing intracellular ROS (Fig 5.1).

The externalization of phosphatidylserine, evidenced by annexin V binding, indicated early and late apoptotic events. The presence of active caspase-3/7 confirmed apoptosis as the primary mechanism of cell death. Active caspase-8 and caspase-9 (Fig 5.1) indicated the respective activation of both the extrinsic and intrinsic apoptotic pathways. Mitochondrial membrane depolarization further supported the involvement of the intrinsic pathway of apoptosis as shown in Fig 5.1. The activation of apoptosis as the main mode of cell death by copper complexes and gold complex provided a therapeutic advantage over necrosis. Apoptosis is a programmed cell death process that prevent inflammatory responses, in contrast to necrosis, which causes uncontrolled inflammation and damage to the adjacent healthy tissue (Kroemer *et al.,* 2005, 2009;

Su *et al.,* 2015). In addition, apoptosis improves the tolerability of chemotherapy treatment by reducing tissue damage and the accompanying adverse effects associated with a high burden of cell death (Tait *et al.*, 2014; Lopez and Tait, 2015).

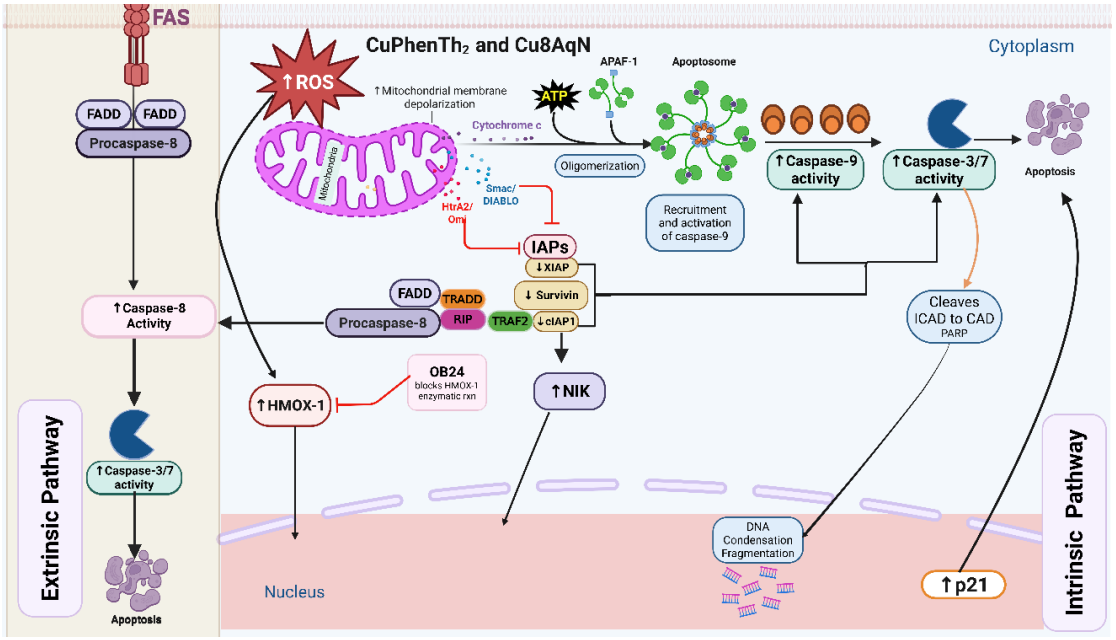


Fig 5.1 Mechanism of cell death of $CuPhenTh_2$ and Cu8AqN in MDA-MB-231 cells. Summary of the effects of Cu8AqN and $CuPhenTh_2$ copper complexes on MDA-MB-231cells. Apoptotic proteins affected by the copper complexes triggering apoptosis in MDA-MB-231 cells. Black arrows represent positive response/activation; red arrows with flat head=inhibition; orange arrow= cleaves/release. FAS ligand and receptor, ROS=reactive oxygen species, ATP=adenosine triphosphate, SmaC=second mitochondria-derived activator of caspases, HtrA2=mitochondrial serine protease, APAF-1=apoptotic protease-activating factor-1, IAPs=inhibitor of apoptosis proteins, XIAP=X-linked inhibitor of apoptosis protein, cIAP1=cellular Inhibitor of apoptosis1/ 2, TRADD=TNF-associated death domain, TRAF2= TNF receptor-associated factors2, RIP=receptor interacting proteins, FADD=Fas-associated death domain, OB24=(1-[[2-[2-(4-Bromophenyl)ethyl]-1,3-dioxolan-2-yl]methyl]-1H-imidazolehydrochloride),HMOX-1= haemoxygenase-1, rxn=reaction, p21=cyclin-dependant kinase inhibitor, ICAD=inhibitor of caspase-activated DNase, DNA=deoxyribose nucleic acid. Created in https://BioRender.com.

The data from this study indicated some selectivity of the metal complexes towards cancer cells and highlights their therapeutic potential in TNBC. Despite the promising results of the gold(I) complex, $AuPPh_3$(trz-Fc-Dipp) was more toxic to the normal cells than the copper complexes and caused excessive ROS which could potentially cause mitochondrial damage. For this reason,

$CuPhenTh_2$ and Cu8AqN were selected as lead candidates for further evaluation using an apoptosis proteome array profiler. Analysis of the apoptotic proteome array showed that copper complexes modulate the expression of key apoptosis-regulatory proteins. The decreased expression of IAPs such as XIAP, cIAP1, and survivin facilitated caspase activation and promoted apoptosis (Fig 5.1). The decrease in Fas/CD95 and cIAP1 expression was linked to the modulation of NF-κB signalling, which is an important pathway in cancer cell survival and progression (Rovillain *et al.*, 2011; Gambhir *et al.*, 2015; Siegmund *et al.*, 2022). The suppression of cIAP1 inhibited the canonical NFκB pathway and triggered the non-canonical pathway (Meyerovich *et al.,* 2024) as seen by the increase of NIK in the treated cells.

Since MDA-MB-231 cells have mutant, functionally inactive p53 (Curtis *et al.,* 2012; Marvalim *et al.,* 2023; Olivier *et al.,* 2002), the unchanged levels of phosphorylated p53 species indicated that apoptosis was induced via p53-independent pathways. This is significant because p53 mutations contribute to chemoresistance in TNBC (Meric-Bernstam *et al.,* 2018), and to circumvent this resistance mechanism supports their therapeutic efficacy in TNBC. Tumour suppressor p53 regulates the expression of p21 through p53-response element in its promoter, and phosphorylation of p53 in serine 15/ serine 20 (Katner *et al.*, 2002; Abbas and Dutta, 2010; Loughery *et al.,* 2014; Hernandez-Valencia *et al.,* 2018). In this study, p21 was increased independent of p53. The potential of copper complexes to increase p21 was an indicator for oxidative stress. Cyclin-dependent kinase inhibitor, p21 can also be induced independently of p53 via oxidative-stress–responsive Nrf2, which is important here given the ROS response in the treated cells (Villeneuve *et al.,* 2009; Chen *et al.,* 2009).

Immunofluorescence experiments indicated an increase in phospho-p53(s15) and p21, which suggested DNA damage. Oxidative stress markers further validated oxidative stress-mediated cytotoxicity in the cells after treatment with the copper complexes. The upregulation of HMOX-1 expression (Fig 5.1), with a concomitant decrease in HSP70 and HMOX-2 further supplied evidence for oxidative stress mediated apoptosis. The varied expression of HIF-1α suggested that the expression of HMOX-1 may involve other transcription factors like Nrf2, a well-known transcription factor for HMOX-1 (Mehta *et al.*, 2007; Loboda *et al.*, 2016) which may require exploration. The inhibition of HMOX-1 enzyme activity by OB24 differentially affected the

response to different copper complex treatments highlighting the important role of HMOX-1 in chemoresistance. HMOX-1 requires further exploration using oxidative stress proteome profiler and mRNA to evaluate gene profile of oxidative stress regulators. These findings support copper-induced oxidative stress which promoted apoptosis in TNBC cells.

Future recommendations

Despite the promising findings, future studies to fully understand the mechanism of action of the metal complexes are recommended. The cytotoxic effects of $CuPhenTh_2$, Cu8AqN, and $AuPPh_3$(trz-Fc-Dipp) should be further validated using 3D culture systems and xenograft tumour models like nude mice, to assess efficacy, systemic toxicity, and investigate preliminary pharmacokinetics. Structural modifications of these complexes could be explored to enhance selectivity toward cancer cells. Additionally, the development of drug delivery systems enabling controlled and sustained release could further optimize therapeutic outcomes and limit toxicity to the normal cells. To confirm oxidative stress-mediated cytotoxicity, ROS formation and the expression of HMOX-1 should be evaluated in the presence of antioxidants and HMOX-1 inhibitors. Moreover, assessing HMOX-1 gene expression at the mRNA level using quantitative PCR (qPCR) would provide comprehensive evidence for HMOX-1 regulation by transcription factors like Nrf2, AP-1/2 and NF-κB. Future studies could explore proteome profiling for $AuPPh_3$(trz-Fc-Dipp). Finally, proteome array data should be validated using immunofluorescence, western blotting, and qPCR to confirm changes in both protein and /or the transcription genes.

In conclusion, these copper complexes represent promising alternatives to conventional chemotherapy warranting further preclinical evaluation. This body of work contributes to the growing evidence supporting metallodrugs as apoptosis inducers and innovative candidates for addressing therapeutic challenges in aggressive breast cancer subtypes, like TNBC.

References

Abbas, T. and Dutta, A. (2010) p21 in Cancer, *Nature reviews Cancer*, 9(6), pp. 400–414. https://doi.org/10.1038/nrc2657.p21.

Abuetabh, Y., Wu, H.H., Chai, C., Al Yousef, H., Persad, S., Sergi, C.M. and Leng, R. (2022) DNA damage response revisited: the p53 family and its regulators provide endless cancer therapy opportunities, *Experimental and Molecular Medicine*, 54(10), pp. 1658–1669.

Ahmad, I. M., Dafferner, A. J., O'Connell, K. A., Mehla, K., Britigan, B. E., Hollingsworth, M. A., & Abdalla, M. Y. (2021) Haem Oxygenase-1 Inhibition Potentiates the Effects of Nab-Paclitaxel-Gemcitabine and Modulates the Tumor Microenvironment in Pancreatic Ductal Adenocarcinoma. *Cancers*, 13(9), pp. 2264. https://doi.org/10.3390/cancers13092264.

Ahmadpour, S. T., Desquiret-Dumas, V., Yikilmaz, U., Dartier, J., Domingo, I., Wetterwald, C., Orre, C., Gueguen, N., Brisson, L., Mahéo, K., & Dumas, J.-F. (2021) Doxorubicin-Induced Autophagolysosome Formation Is Partly Prevented by Mitochondrial ROS Elimination in DOX-Resistant Breast Cancer Cells. *International Journal of Molecular Sciences*, *22*(17), pp. 9283. https://doi.org/10.3390/ijms22179283.

Aits, S. and Jäättelä, M. (2013) Lysosomal cell death at a glance, *Journal of Cell Science*, 126(9), pp. 1905–1912. https://doi.org/10.1242/jcs.091181.

Alaoui-Jamali, M. A., Bismar, T. A., Gupta, A., Szarek, W. A., Su, J., Song, W., Xu, Y., Xu, B., Liu, G., Vlahakis, J. Z., Roman, G., Mansure, J. J., & Schipper, H. M. (2009) A novel experimental heme oxygenase-1-targeted therapy for hormone-refractory prostate cancer. *Cancer Research, 69*(20), pp. 8017–8024. https://doi.org/10.1158/0008-5472.CAN-09-0419.

Ali, A., Sepay, Nasim, Afzal, M., Sepay, Nayim, Alarifi, A., Shahid, M. and Ahmad, M. (2021) Molecular designing, crystal structure determination and in silico screening of copper(II) complexes bearing 8-hydroxyquinoline derivatives as anti-COVID-19, *Bioorganic Chemistry*, 110(1), pp. 104772. https://doi.org/https://doi.org/10.1016/j.bioorg.2021.104772.

Albadari, N. and Li, W. (2023) Survivin Small Molecules Inhibitors: Recent Advances and Challenges, *Molecules*, 28(3), pp. 1376. https://doi.org/10.3390/molecules28031376.

Almansour, N.M. (2022) Triple-Negative Breast Cancer: A Brief Review About Epidemiology, Risk Factors, Signaling Pathways, Treatment and Role of Artificial Intelligence, *Frontiers in Molecular Biosciences*, 2(1), pp. 1–15. https://doi.org/10.3389/fmolb.2022.836417.

Amirtharaj, F., Venkatesh, G.H., Wojtas, B., Nawafleh, H.H., Mahmood, A.S., Nizami, Z.N., Khan, M.S., Thiery, J. and Chouaib, S. (2022) p53 reactivating small molecule PRIMA-1MET/APR-246 regulates genomic instability in MDA-MB-231 cells, *Oncology reports*, 47(4), pp. 1–9. https://doi.org/10.3892/or.2022.8296.

Arambula, J.F., McCall, R., Sidoran, K.J., Magda, D., Mitchell, N.A., Bielawski, C.W., Lynch, V.M., Sessler, J.L. and Arumugam, K. (2016) Targeting antioxidant pathways with ferrocenylated N-heterocyclic carbene supported gold(i) complexes in A549 lung cancer cells, *Chemical Science*, 7(2), pp. 1245–1256. https://doi.org/10.1039/c5sc03519h.

Arya, R. K., Kumar, S., Bisht, B., Bhatt, M. L. B., Nair, S., & Datta, D. (2015) Anti-breast tumor activity of *Eclipta* extract in-vitro and in-vivo: Novel evidence of endoplasmic reticulum specific localization of Hsp60 during apoptosis. *Scientific Reports, 5*, pp. 18457. https://doi.org/10.1038/srep18457.

Aucamp, D., Kumar, S. V., Liles, D.C., Fernandes, M.A., Harmse, L. and Bezuidenhout, D.I. (2018) Synthesis of heterobimetallic gold(i) ferrocenyl-substituted 1,2,3-triazol-5-ylidene complexes as potential anticancer agents, *Dalton Transactions*, 47(45), pp. 16072–16081. https://doi.org/10.1039/C8DT03116A.

Augello, G., Azzolina, A., Rossi, F., Prencipe, F., Mangiatordi, G.F., Saviano, M., Ronga, L., Cervello, M. and Tesauro, D. (2023) New Insights into the Behavior of NHC-Gold Complexes in Cancer Cells, *Pharmaceutics*,15(2), pp.1–12 https://doi.org/10.3390/pharmaceutics15020466.

Ayachi, A., Boy, G., Samet, S., Téné, N., Bouzayani, B., Treilhou, M., Mezghani-Jarraya, R. and Billet, A. (2024) Isolation, NMR Characterization, and Bioactivity of a Flavonoid Triglycoside

from Anthyllis henoniana Stems: Antioxidant and Antiproliferative Effects on MDA-MB-231 Breast Cancer Cells, *Antioxidants,* 13(7), pp. 793 https://doi.org/10.3390/antiox13070793.

Azimi, I. (2018) The interplay between HIF-1 and calcium signalling in cancer, International Journal of Biochemistry and Cell Biology, (97), pp. 73–77. https://doi.org/10.1016/j.biocel.2018.02.001.

Badve, S., Dabbs, D. J., Schnitt, S. J., Baehner, F. L., Decker, T., Eusebi, V., Fox, S. B., Ichihara, S., Jacquemier, J., Lakhani, S. R., Palacios, J., Rakha, E. A., Richardson, A. L., Schmitt, F. C., Tan, P. H., Tse, G. M., Weigelt, B., & Reis-Filho, J. S. (2011) Basal-like and triple-negative breast cancers: A critical review with an emphasis on the implications for pathologists and oncologists. *Modern Pathology*, 24(2), pp. 157–167. https://doi.org/10.1038/modpathol.2010.200.

Bae, Y.H., Shin, J.M., Park, H.J., Jang, H.O., Bae, M.K. and Bae, S.K. (2014) Gain-of-function mutant p53-R280K mediates survival of breast cancer cells, *Genes and Genomics*, 36(2), pp. 171–178. https://doi.org/10.1007/s13258-013-0154-9.

Balasubramanian, K. and Schroit, A.J. (2003) Aminophospholipid Asymmetry: A Matter of Life and Death, *Annual Review of Physiology*, 65, pp. 701–734. https://doi.org/10.1146/annurev.physiol.65.092101.142459.

Balmer, M.T., Katz, R.D., Liao, S., Goodwine, J.S. and Gal, S. (2014) Doxorubicin and 5-fluorouracil induced accumulation and transcriptional activity of p53 are independent of the phosphorylation at serine 15 in MCF-7 breast cancer cells, *Cancer Biology and Therapy*, 15(8), pp. 1000–1012. https://doi.org/10.4161/cbt.29112.

Balsa, L.M., Rodriguez, M.R., Ferraresi-Curotto, V., Parajón-Costa, B.S., Gonzalez-Baró, A.C. and León, I.E. (2023) Finding New Molecular Targets of Two Copper(II)-Hydrazone Complexes on Triple-Negative Breast Cancer Cells Using Mass-Spectrometry-Based Quantitative Proteomics, *International Journal of Molecular Sciences*, 24(8). pp. 7531 https://doi.org/10.3390/ijms24087531.

Bar, J.K., Saomska, I., Rabczyńki, J., Noga, L. and Grybov, M. (2009) Expression of p53 protein phosphorylated at serine 20 and serine 392 in malignant and benign ovarian neoplasms correlation with clinicopathological parameters of tumors, *International Journal of Gynecological Cancer*, 19(8), pp. 1322–1328. https://doi.org/10.1111/IGC.0b013e3181b70465.

Barnes, P.J. (2013) Theophylline, *American Journal of Respiratory and Critical Care Medicine*, 188(8), pp. 901–906. https://doi.org/10.1164/rccm.201302-0388PP.

Batra, H., Mouabbi, J. A., Ding, Q., Sahin, A. A., & Raso, M. G. (2023) Lobular Carcinoma of the Breast: A Comprehensive Review with Translational Insights. *Cancers*, *15*(22), pp. 5491. https://doi.org/10.3390/cancers15225491.

Bebber, C.M., Müller, F., Clemente, L.P., Weber, J. and von Karstedt, S. (2020) Ferroptosis in cancer cell biology, *Cancers*, 12(1), pp. 164. https://doi.org/10.3390/cancers12010164.

Belza, J., Trávníček, Z., Vančo, J., Čajan, M., Hošek, J. and Dvořák, Z. (2024) Gold(I) N-Heterocyclic Carbene Complexes with 7-Azaindoles Demonstrates *In Vitro* Antiproliferative Effects on Ovarian Cancer Cells and Anti-inflammatory Activity, *Organometallics*, 43(I), pp. 1155–1164. https://doi.org/10.1021/acs.organomet.4c00093.

Bernardi, P., & Forte, M. (2007) The mitochondrial permeability transition pore. In *Mitochondrial Biology: New Perspectives: Novartis Foundation Symposium 287* (287), pp. 157-169. https://doi.org/10.1002/9780470725207.ch11.

Bernardi, P., Carraro, M. and Lippe, G. (2022) The mitochondrial permeability transition: Recent progress and open questions. The *Federal of European Biochemical Societies Journal*, 289, pp. 7051-7074. https://doi.org/10.1111/febs.16254.

Bencsik, P., Bartekova, M., Görbe, A., Kiss, K., Pálóczi, J., Radosinska, J., Szűcs, G. and Ferdinandy, P. (2017) MMP Activity Detection in Zymograms BT - Zymography: Methods and Protocols, in J. Wilkesman and L. Kurz (eds). New York, NY: Springer New York, pp. 53–70. https://doi.org/10.1007/978-1-4939-7111-4_6.

Bi, X., Zhang, M., Zhou, J., Yan, X., Cheng, L., Luo, L., Huang, C. and Yin, Z. (2023) Phosphorylated Hsp27 promotes adriamycin resistance in breast cancer cells through regulating

dual phosphorylation of c-Myc, *Cellular Signalling*, 112(112) pp. 110913. https://doi.org/10.1016/j.cellsig.2023.110913.

Bianchini, G., Balko, J.M., Mayer, I.A., Sanders, M.E. and Gianni, L. (2016) Triple-negative breast cancer: challenges and opportunities of a heterogeneous disease, *Nature Reviews Clinical Oncology*, 13(11), pp. 674–690. https://doi.org/10.1038/nrclinonc.2016.66.

Birbach, A., Gold, P., Binder, B.R., Hofer, E., de Martin, R. and Schmid, J.A. (2002) Signaling Molecules of the NF-κB Pathway Shuttle Constitutively between Cytoplasm and Nucleus, *Journal of Biological Chemistry*, 277(13), pp. 10842–10851. https://doi.org/10.1074/jbc.M112475200.

Birbach, A., Bailey, S.T., Ghosh, S. and Schmid, J.A. (2004) Cytosolic, nuclear and nucleolar localization signals determine subcellular distribution and activity of the NF-κB inducing kinase NIK, *Journal of Cell Science*, 117(16), pp. 3615–3624. https://doi.org/10.1242/jcs.01224.

Biswas, C., Shah, N., Muthu, M., La, P., Fernando, A.P., Sengupta, S., Yang, G. and Dennery, P.A. (2014) Nuclear heme oxygenase-1 (HO-1) modulates subcellular distribution and activation of Nrf2, impacting metabolic and antioxidant defenses, *Journal of Biological Chemistry*, 289(39), pp. 26882–26894. https://doi.org/10.1074/jbc.M114.567685.

Brown, V.L., Harwood, C.A., Crook, T., Cronin, J.G., Kelsell, D.R. and Proby, C.M. (2004) p16INK4a and p14ARF tumor suppressor genes are commonly inactivated in cutaneous squamous cell carcinoma, *Journal of Investigative Dermatology*, 122(5), pp. 1284–1292. https://doi.org/10.1111/j.0022-202X.2004.22501.x.

Brunton, L.L. and Knollmann, C.B. (2023) Goodman and Gilman's The Pharmacological Basis of Therapeutics. 14th edition. Edited by L.L. Brunton, J.S. Lazo, and K.L. Parker. McGraw-Hill. https://doi.org/10.1036/0071422803.

Cairrao, F. and Domingos, P.M. (2010) Apoptosis : Molecular Mechanisms Apoptosis : Molecular Mechanisms, *Encyclopedia of Life Sciences*, pp. 1–8. https://doi.org/10.1002/9780470015902.a0001150.pub2.

Cao, L., Zhao, S., Yang, Q., Shi, Z., Liu, J., Pan, T., Zhou, D. and Zhang, J. (2021) Chidamide Combined with Doxorubicin Induced p53-Driven Cell Cycle Arrest and Cell Apoptosis Reverse Multidrug Resistance of Breast Cancer, *Frontiers in Oncology*, 11(11), pp. 1–12. https://doi.org/10.3389/fonc.2021.614458.

Cappello, F., Gammazza, A.M., Piccionello, A.P., Campanella, C., Pace, A., De Macario, E.C. and Macario, A.J.L. (2014) Hsp60 chaperonopathies and chaperonotherapy: Targets and agents, *Expert Opinion on Therapeutic Targets*, 18(2), pp. 185–208. https://doi.org/10.1517/14728222.2014.856417.

Castrogiovanni, C., Waterschoot, B., De Backer, O. and Dumont, P. (2018) Serine 392 phosphorylation modulates p53 mitochondrial translocation and transcriptionindependent apoptosis, *Cell Death and Differentiation*, 25(1), pp. 190–203. https://doi.org/10.1038/cdd.2017.143.

Cavalcante, G.C., Schaan, A.P., Cabral, G.F., Santana-Da-Silva, M.N., Pinto, P., Vidal, A.F. and Ribeiro-Dos-Santos, Â. (2019) A cell's fate: An overview of the molecular biology and genetics of apoptosis, *International Journal of Molecular Sciences*, 20(17), pp. 1–20. https://doi.org/10.3390/ijms20174133.

Cetraro, P., Plaza-Diaz, J., Mackenzie, A. and Abadía-Molina, F. (2022) A Review of the Current Impact of Inhibitors of Apoptosis Proteins and Their Repression in Cancer, *Cancers*, 14(7), pp. 1–25. https://doi.org/10.3390/cancers14071671.

Chang, Y. L., Hsu, Y. J., Chen, Y., Wang, Y. W., & Huang, S. M. (2017) Theophylline exhibits anti-cancer activity via suppressing SRSF3 in cervical and breast cancer cell lines. *Oncotarget*, 8(60), pp. 101461–101474. https://doi.org/10.18632/oncotarget.21464.

Chanteloup, G., Cordonnier, M., Isambert, N., Bertaut, A., Marcion, G., Garrido, C., & Gobbo, J. (2020) Monitoring HSP70 exosomes in cancer patients' follow-up: A clinical prospective pilot study. *Journal of Extracellular Vesicles*, 9(1), 1766192. https://doi.org/10.1080/20013078.2020.1766192.

Chapdelaine, A.G. and Sun, G. (2023) Challenges and Opportunities in Developing Targeted Therapies for Triple Negative Breast Cancer, *Biomolecules,* 13(8), pp. 1207 https://doi.org/10.3390/biom13081207.

Chen, B., Zhang, L., Zhou, H., Ye, W., Luo, C., Yang, L., Fang, N. and Tang, A. (2022) HMOX1 promotes lung adenocarcinoma metastasis by affecting macrophages and mitochondrion complexes, Frontiers in Oncology, 12(8), pp. 1–19. https://doi.org/10.3389/fonc.2022.978006.

Chen, J. (2016) The Cell-Cycle Arrest and Apoptotic Functions of p53 in Tumor Initiation and Progression, *Cold Spring Harbor Perspectives in Medicine,* 6(5), pp. 1–16. https://doi: 10.1101/cshperspect.a026104.

Chen, L. and Han, X. (2015) Anti–PD-1/PD-L1 therapy of human cancer: past, present, and future, *The Journal of clinical investigation*, 125(9), pp. 3384–3391. https://doi.org/10.1172/JCI80011.

Chen, X., Duan, N., Zhang, C. and Zhang, W. (2016) Survivin and Tumorigenesis : *Molecular Mechanisms and Therapeutic Strategies*, 7(3), pp. 314 https://doi.org/10.7150/jca.13332.

Cheung, C.H.A., Chang, Y.C., Lin, T.Y., Cheng, S.M. and Leung, E. (2020) Anti-apoptotic proteins in the autophagic world: An update on functions of XIAP, Survivin, and BRUCE, *Journal of Biomedical Science*, 27(1), pp. 1–10. https://doi.org/10.1186/s12929-020-0627-5.

Coleman, M.L., Sahai, E.A., Yeo, M., Bosch, M., Dewar, A. and Olson, M.F. (2001) Membrane blebbing during apoptosis results from caspase-mediated activation of ROCK I Mathew, *Nature Cell Biology*, 3(3), pp. 339–346. https://doi.org/https://doi.org/10.1038/35070019.

Consoli, V., Fallica, A.N., Sorrenti, V., Pittalà, V. and Vanella, L. (2024) Novel Insights on Ferroptosis Modulation as Potential Strategy for Cancer Treatment: When Nature Kills, *Antioxidants and Redox Signaling,* 40(1), pp. 40–85. https://doi.org/10.1089/ars.2022.0179.

Coope, H.J., Atkinson, P.G.P., Huhse, B., Belich, M., Janzen, J., Holman, M.J., Klaus, G.G.B., Johnston, L.H. and Ley, S.C. (2002) CD40 regulates the processing of NF-kB2 p100 to p52*,* *EMBO Journal*, 21(20), pp. 5375–5385. https://doi.org/10.1093/emboj/cdf542.

Crowley, L.C., Marfell, B.J., Scott, A.P. and Waterhouse, N.J. (2016) Quantitation of apoptosis and necrosis by annexin V binding, propidium iodide uptake, and flow cytometry, *Cold Spring Harbor Protocols*, 2016(11), pp. 953–957. https://doi.org/10.1101/pdb.prot087288.

Curtis, C., Shah, S. P., Chin, S.-F., Turashvili, G., Rueda, O. M., Dunning, M. J., Speed, D., Lynch, A. G., Samarajiwa, S., Yuan, Y., Gräf, S., Ha, G., Haffari, G., Bashashati, A., Russell, R., McKinney, S., Langerød, A., Green, A., Provenzano, E., and Caldas, C. (2012) The genomic and transcriptomic architecture of 2,000 breast tumours reveals novel subgroups. *Nature, 486*(7403), pp. 346–352. https://doi.org/10.1038/nature10983.

Czabotar, P.E., Lessene, G., Strasser, A. and Adams, J.M. (2014) Control of apoptosis by the BCL-2 protein family: Implications for physiology and therapy, *Nature Reviews Molecular Cell Biology*, 15(1), pp. 49–63. https://doi.org/10.1038/nrm3722.

D'Aguanno, S. and Del Bufalo, D. (2020) Inhibition of Anti-Apoptotic Bcl-2 Proteins in Preclinical and Clinical Studies: Current Overview in Cancer, *Cells*, 9(5). https://doi.org/10.3390/cells9051287.

Dalmases, A., Villanueva, A., Martínez, A., Hernández-Argudo, M., Pantoja, S., Pantano, E., Ferreres, J. C., Tusquets, I., Rovira, A., Gil-Martín, M., Gomis, R. R., Grana, B., Ramon y Cajal, S., & Rojo, F. (2013) Deficiency in p53 is required for doxorubicin-induced transcriptional activation of NF-κB target genes in human breast cancer. *Oncotarget, 5*(1), pp. 196–210. https://doi.org/10.18632/oncotarget.1556.

Dam, J., Ismail, Z., Kurebwa, T., Gangat, N., Harmse, L., Marques, H.M., Lemmerer, A., Bode, M.L. and de Koning, C.B. (2017) Synthesis of copper and zinc 2-(pyridin-2-yl)imidazo[1,2-a]pyridine complexes and their potential anticancer activity, *European Journal of Medicinal Chemistry*, 126(1), pp. 353–368. https://doi.org/10.1016/j.ejmech.2016.10.041.

Datta, S.R., Katsov, A., Hu, L., Petros, A., Fesik, S.W., Yaffe, M.B. and Greenberg, M.E. (2000) 14-3-3 proteins and survival kinases cooperate to inactivate BAD by BH3 domain phosphorylation, *Molecular Cell,* 6(1), pp. 41–51.https://doi.org/10.1016/S1097-2765(05)00012-2.

Debnath, J., Muthuswamy, S.K. and Brugge, J.S. (2003) Morphogenesis and oncogenesis of MCF-10A mammary epithelial acini grown in three-dimensional basement membrane cultures, *Methods*, 30(3), pp. 256–268. https://doi.org/10.1016/S1046-2023(03)00032-X.

Del Bello, F., Bonsignore, R., Bartoli, S., Di Pietro, S., Marchini, C., Andreucci, E., Arcovito, A., Bucci, C., Severi, M., Sanna, T., Contino, M., Marchetti, L., Biffi, S., La Rocca, L., Gianferrara, T., Marzano, C., & Gandin, V. (2022) Cu(I) and Cu(II) complexes based on lonidamine-conjugated ligands designed to promote synergistic antitumor effects. *Inorganic Chemistry*, 61(12), pp.4919–4937. https://doi.org/10.1021/acs.inorgchem.1c03658.

Demchenko, A.P. (2013) Beyond annexin V: Fluorescence response of cellular membranes to apoptosis, *Cytotechnology*, 65(2), pp. 157–172. https://doi.org/10.1007/s10616-012-9481-y.

Denkert, C., Liedtke, C., Tutt, A. and von Minckwitz, G. (2017) Molecular alterations in triple-negative breast cancer—the road to new treatment strategies, *The Lancet*, 389(10087), pp. 2430–2442. https://doi.org/10.1016/S0140-6736(16)32454-0.

DeSantis, C.E., Fedewa, S.A., Goding Sauer, A., Kramer, J.L., Smith, R.A. and Jemal, A. (2016) Breast cancer statistics, 2015: Convergence of incidence rates between black and white women, CA: *A Cancer Journal for Clinicians*, 66(1), pp. 31–42. https://doi.org/10.3322/caac.21320.

Dixon, S. J., Lemberg, K. M., Lamprecht, M. R., Skouta, R., Zaitsev, E. M., Gleason, C. E., Patel, D. N., Bauer, A. J., Cantley, A. M., Yang, W. S., Morrison, B., & Stockwell, B. R. (2012) Ferroptosis: An iron-dependent form of nonapoptotic cell death. *Cell, 149*(5), pp. 1060–1072. https://doi.org/10.1016/j.cell.2012.03.042.

Dolan, D.W.P., Zupanic, A., Nelson, G., Hall, P., Miwa, S., Kirkwood, T.B.L. and Shanley, D.P. (2015) Integrated Stochastic Model of DNA Damage Repair by Non-homologous End Joining and p53/p21- Mediated Early Senescence Signalling, *PLoS Computational Biology,* 11(5), pp. 1–19. https://doi.org/10.1371/journal.pcbi.1004246.

Douglas, H.(2022) Hallmarks of Cancer: New Dimensions. *Cancer Discov*ery,12(1), pp. 31–46. https://doi.org/10.1158/2159-8290.CD-21-1059.

Duffy, M.J., Synnott, N.C., O'Grady, S. and Crown, J. (2022) Targeting p53 for the treatment of cancer, *Seminars in Cancer Biology*, 79(5), pp. 58–67. https://doi.org/10.1016/j.semcancer.2020.07.005.

Dumay, A., Feugeas, J. P., Wittmer, E., Lehmann-Che, J., Bertheau, P., Espié, M., Plassa, L. F., Cagnard, N., Ricci, F., Letourneur, F., Laplace-Marie, X., & De Thé, H. (2013). Distinct tumor protein p53 mutants in breast cancer subgroups. *International Journal of Cancer*, 132(5), pp. 1227–1231. https://doi.org/10.1002/ijc.27767.

Dumétier, B., Montfort, A., Szymczak, W., Berthelet, J., Torre, C., Micheau, O., & Dubrez, L. (2023) cIAP1/TRAF2 interplay promotes tumor growth through the activation of STAT3. *Oncogene, 42*(3), pp. 198–208. https://doi.org/10.1038/s41388-022-02544-y.

Earnshaw, W.C. (1995) Nuclear changes in apoptosis, *Current Opinion in Cell Biology*, 7(3), pp. 337–343. https://doi.org/10.1016/0955-0674(95)80088-3.

Elmore, S. (2007) Apoptosis: A Review of Programmed Cell Death, *Toxicologic Pathology*, 35(4), pp. 495–516. https://doi.org/10.1080/01926230701320337.

Eom, Y.H., Kim, H.S., Lee, A., Song, B.J. and Chae, B.J. (2016) BCL2 as a subtype-specific prognostic marker for breast cancer, *Journal of Breast Cancer*, 19(3), pp. 252–260. https://doi.org/10.4048/jbc.2016.19.3.252.

Facchetti, G., Neva, F., Coffetti, G., & Rimoldi, I. (2023) Chiral 8-amino-5, 6, 7, 8-tetrahydroquinoline derivatives in metal catalysts for the asymmetric transfer hydrogenation of 1-aryl substituted-3, 4-dihydroisoquinolines as alkaloids precursors. *Molecules*, 28(4), 1907. https://doi.org/10.3390/molecules28041907.

Farhan, M., Khan, H.Y., Oves, M., Al-Harrasi, A., Rehmani, N., Arif, H., Hadi, S.M. and Ahmad, A. (2016) Cancer therapy by catechins involves redox cycling of copper ions and generation of reactive oxygen species, *Toxins*, 8(2), pp. 37 https://doi.org/10.3390/toxins8020037.

Feng, Y., Yang, Z., Wang, J. Zhao, H. (2024) Cuproptosis: unveiling a new frontier in cancer biology and therapeutics, *Cell Communication and Signaling,* 22(249), pp. 249. https://doi.org/10.1186/s12964-024-01625-7.

Finlay, D., Teriete, P., Vamos, M., Cosford, N.D.P. and Vuori, K. (2017) Inducing death in tumor cells: Roles of the inhibitor of apoptosis proteins, *F1000Research*, 6, pp. 1–18. https://doi.org/10.12688/f1000research.10625.1.

Foo, J. B., Looi, C. Y., Omar, A. R., Kadir, H. A., Rahman, N. A., Indumathy, S., & Saiful Yazan, L. (2018) Copper complex derived from S-benzyldithiocarbazate and 3-acetylcoumarin induced apoptosis in breast cancer cells. *BioMetals, 31*(4), pp. 505–515. https://doi.org/10.1007/s10534-018-0096-4

Fouad, Y.A. and Aanei, C. (2017) Revisiting the hallmarks of cancer, *American journal of cancer research*, 7(5), pp. 1016-1036. PMID: 28560055; PMCID: PMC5446472.

Friedmann Angeli, J. P., Schneider, M., Proneth, B., Tyurina, Y. Y., Tyurin, V. A., Hammond, V. J., Herbach, N., Aichler, M., Walch, A., Eggenhofer, E., Basavarajappa, D., Rådmark, O., Kobayashi, S., Seibt, T., Beck, H., Neff, F., Esposito, I., Wanke, R., Förster, H., Conrad, M. (2014). Inactivation of the ferroptosis regulator Gpx4 triggers acute renal failure in mice. *Nature Cell Biology*, 16(12), 1180–1191. https://doi.org/10.1038/ncb3064

Fulda, S. (2014) Molecular pathways: Targeting inhibitor of apoptosis proteins in cancer-from molecular mechanism to therapeutic application, *Clinical Cancer Research*, 20(2), pp. 289–295. https://doi.org/10.1158/1078-0432.CCR-13-0227.

Fusella, F., Seclì, L., Cannata, C. (2020) The one thousand and one chaperones of the NF-κB pathway, *Cellular Molecular Life Sciences*, 77, pp. 2275–2288. https://doi.org/10.1007/s00018-019-03402-z

Galanis, A., Pappa, A., Giannakakis, A., Lanitis, E., Dangaj, D. and Sandaltzopoulos, R. (2008) Reactive oxygen species and HIF-1 signalling in cancer, *Cancer Letters*, 266(1), pp. 12–20. https://doi.org/10.1016/j.canlet.2008.02.028.

Galluzzi, L., Maiuri, M.C., Vitale, I., Zischka, H., Castedo, M., Zitvogel, L. and Kroemer, G. (2007) Cell death modalities: Classification and pathophysiological implications*, Cell Death and Differentiation*, 14(7), pp. 1237–1243. https://doi.org/10.1038/sj.cdd.4402148.

Galluzzi, L., Vitale, I., Abrams, J. M., Alnemri, E. S., Baehrecke, E. H., Blagosklonny, M. V., Dawson, T. M., Dawson, V. L., El-Deiry, W. S., Fulda, S., Gottlieb, E., Green, D. R., Hengartner, M. O., Kepp, O., Knight, R. A., Kumar, S., Lipton, S. A., Lu, X., Madeo, F., Kroemer, G. (2012). Molecular definitions of cell death subroutines: Recommendations of the Nomenclature Committee on Cell Death 2012. *Cell Death and Differentiation, 19*(1), 107–120. https://doi.org/10.1038/cdd.2011.96.

Galluzzi, L., Vitale, I., Aaronson, S. A., Abrams, J. M., Adam, D., Agostinis, P., Alnemri, E. S., Altucci, L., Amelio, I., Andrews, D. W., Annicchiarico-Petruzzelli, M., Antonov, A. V., Ashkenazi, A., Baehrecke, E. H., Barlev, N. A., Bazan, N. G., Bernassola, F., Bertrand, M. J. M., Bianchi, K., Kroemer, G. (2018). Molecular mechanisms of cell death: Recommendations of the Nomenclature Committee on Cell Death 2018. *Cell Death and Differentiation, 25*(3), 486–541. https://doi.org/10.1038/s41418-017-0012-4.

Gambhir, S., Vyas, D., Hollis, M., Aekka, A. and Vyas, A. (2015) Nuclear factor kappa B role in inflammation associated gastrointestinal malignancies, *World Journal of Gastroenterology*, 21(11), pp. 3174–3183. https://doi.org/10.3748/wjg.v21.i11.3174.

Gandin, V., Pellei, M., Tisato, F., Porchia, M., Santini, C. and Marzano, C. (2012) A novel copper complex induces paraptosis in colon cancer cellsviathe activation of ER stress signalling, *Journal of Cellular and Molecular Medicine*, 16(1), pp. 142–151. https://doi.org/10.1111/j.1582-4934.2011.01292.x.

Gandin, V., Tisato, F., Dolmella, A., Pellei, M., Santini, C., Giorgetti, M., Marzano, C. and Porchia, M. (2014) *In vitro* and *in vivo* anticancer activity of copper(I) complexes with homoscorpionate tridentate tris(pyrazolyl)borate and auxiliary monodentate phosphine ligands, *Journal of Medicinal Chemistry*, 57(11), pp. 4745–4760. https://doi.org/10.1021/jm500279x.

Gandini, N. A., Fermento, M. E., Salomón, D. G., Obiol, D. J., Andrés, N. C., Zenklusen, J. C., López Romero, A., Blasco, J., & Facchinetti, M. M. (2019). Heme oxygenase-1 has an antitumor role in breast cancer. *Antioxidants & Redox Signaling*, 30(18), pp. 2030–2049. https://doi.org/10.1089/ars.2018.7554.

Gao, M., Yi, J., Zhu, J., Minikes, A.M., Monian, P., Thompson, C.B. and Jiang, X. (2019) Role of Mitochondria in Ferroptosis, *Molecular Cell*, 73(2), pp. 354-363.e3. https://doi.org/10.1016/j.molcel.2018.10.042.

Georgakilas, A.G., Martin, O.A. and Bonner, W.M. (2017) p21: A Two-Faced Genome Guardian, *Trends in Molecular Medicine*, 23(4), pp. 310–319. https://doi.org/10.1016/j.molmed.2017.02.001.

Ghosh, J.C., Dohi, T., Byoung, H.K. and Altieri, D.C. (2008) Hsp60 regulation of tumor cell apoptosis, *Journal of Biological Chemistry*, 283(8), pp. 5188–5194. https://doi.org/10.1074/jbc.M705904200.

Gill, C., Dowling, C., O'Neill, A.J. and Watson, R.W.G. (2009) Effects of cIAP-1, cIAP-2 and XIAP triple knockdown on prostate cancer cell susceptibility to apoptosis, cell survival and proliferation*, Molecular Cancer*, 8(1), pp. 1–12. https://doi.org/10.1186/1476-4598-8-39.

Gimeno, M.C., Goitia, H., Laguna, A., Luque, M.E., Villacampa, M.D., Sepúlveda, C. and Meireles, M. (2011) Conjugates of ferrocene with biological compounds. Coordination to gold complexes and antitumoral properties*, Journal of Inorganic Biochemistry*, 105(11), pp. 1373–1382. https://doi.org/10.1016/j.jinorgbio.2011.07.015.

Gmeiner, W.H., Boyacioglu, O., Stuart, C.H., Jennings-Gee, J. and Balaji, K.C. (2015) The cytotoxic and pro-apoptotic activities of the novel fluoropyrimidine F10 Towards prostate cancer cells are enhanced by Zn2+-chelation and inhibiting the serine protease Omi/HtrA2, *Prostate*, 75(4), pp. 360–369. https://doi.org/10.1002/pros.22922.

Gonçalves, H., Guerra, M.R., Duarte Cintra, J.R., Fayer, V.A., Brum, I.V. and Bustamante Teixeira, M.T. (2018) Survival Study of Triple-Negative and Non–Triple-Negative Breast

Cancer in a Brazilian Cohort, Clinical Medicine Insights: *Oncology*, 12. https://doi.org/10.1177/1179554918790563.

Gorini, G., Magherini, F., Fiaschi, T., Massai, L., Becatti, M., Modesti, A., Messori, L. and Gamberi, T. (2021) Au2phen and auoxo6, two dinuclear oxo-bridged gold(III) compounds, induce apoptotic signaling in human ovarian a2780 cancer cells, *Biomedicines*, 9(8), pp. 871. https://doi.org/10.3390/biomedicines9080871.

Griendling, K.K., Touyz, R.M., Zweier, J.L., Dikalov, S., Chilian, W., Chen, Y.-R., Harrison, D.G. and Bhatnagar, A. (2016) Measurement of reactive oxygen species, reactive nitrogen species, and redox-dependent signaling in the cardiovascular system: a scientific statement from the American Heart Association, *Circulation research*, 119(5), pp. e39–e75. https://doi.org/10.1161/RES.0000000000000110.

Guan, X., Ma, F., Fan, Y., Zhu, W., Hong, R. and Xu, B. (2015) Platinum-based chemotherapy in triple-negative breast cancer: a systematic review and meta-analysis of randomized-controlled trials, *Anti-cancer drugs*, 26(8), pp. 894–901. https://doi.org/10.1097/CAD.0000000000000260.

Guttà, C., Varga, M., Szebényi, K., Vértesy, Á., Mán, I., Tóvári, J., Barbai, T., Váncza, L., Hegedűs, B., Márk, Á., Rásó, E., Kenessey, I., & Rehm, M. (2020). Low expression of pro-apoptotic proteins Bax, Bak and Smac indicates prolonged progression-free survival in chemotherapy-treated metastatic melanoma. *Cell Death and Disease*. Advance online publication. 11(2), pp. 124. https://doi.org/10.1038/s41419-020-2309-3.

Hacker, G. (2000) The morphology of apoptosis. Cell Tissue Res, *Cell Tissue Res*, 301(5), pp. 5–17. https://doi.org/10.1007/s004410000193.

Hanahan, D. (2022) Hallmarks of Cancer: New Dimensions, *Cancer Discovery*, 12(1), pp. 31–46. https://doi.org/10.1158/2159-8290.CD-21-1059.

Hanahan, D. and Weinberg, R.A. (2011) Hallmarks of cancer: The next generation, *Cell*, 144(5), pp. 646–674. https://doi.org/10.1016/j.cell.2011.02.013.

Harmse, L., Gangat, N., Martins-Furness, C., Dam, J. and de Koning, C.B. (2019) Copper-imidazo[1,2-a]pyridines induce intrinsic apoptosis and modulate the expression of mutated p53,

haem-oxygenase-1 and apoptotic inhibitory proteins in HT-29 colorectal cancer cells, *Apoptosis*, 24(7–8), pp. 623–643. https://doi.org/10.1007/s10495-019-01547-7.

Hatem, E., Berthier, C., Menard, J. A., Zhenjiang, L., Mellottée, L., Masson, C., El Banna, N., Radosevic-Robin, N., Boby, F., Jilkova, Z., Piechaczyk, M., Gratas, C., Penault-Llorca, F., Al-Daccak, R., & Huang, M. E. (2019) Auranofin/Vitamin C: A novel drug combination targeting triple-negative breast cancer. *Journal of the National Cancer Institute, 111*(6), pp. 597–608. https://doi.org/10.1093/jnci/djy149.

Haupt, Y., Maya, R., Kazaz, A. and Moshe, O. (1997) Mdm2 promote the rapid degradation of p53, *Nature*, 387(1), pp. 296–299. https://doi.org/https://doi.org/10.1038/387296a0.

Helton, E.S. and Chen, X. (2007) p53 modulation of the DNA damage response, *Journal of Cellular Biochemistry*, 100(4), pp. 883–896. https://doi.org/10.1002/jcb.21091.

Henidi, H.A., Al-Abbasi, F.A., El-Moselhy, M.A., El-Bassossy, H.M., Al-Abd, A.M. and Gil, G. (2020) Despite Blocking Doxorubicin-Induced Vascular Damage, Quercetin Ameliorates Its Antibreast Cancer Activity, *Oxidative Medicine and Cellular Longevity*, 2020(1), pp. 8157640. https://doi.org/10.1155/2020/8157640.

Hernandez-Valencia, J., Garcia-Villa, E., Arenas-Hernandez, A., Garcia-Mena, J., Diaz-Chavez, J. and Gariglio, P. (2018) Induction of p53 phosphorylation at serine 20 by resveratrol is required to activate p53 target genes, restoring apoptosis in MCF-7 cells resistant to cisplatin, *Nutrients*, 10(9), pp.1148. https://doi.org/10.3390/nu10091148.

Hirschfeld, M., Ouyang, Y.Q., Jaeger, M., Erbes, T., Orlowska-Volk, M., zur Hausen, A. and Stickeler, E. (2015) HNRNP G and HTRA2-BETA1 regulate estrogen receptor alpha expression with potential impact on endometrial cancer*, BMC Cancer*, 15(1), pp. 1–11. https://doi.org/10.1186/s12885-015-1088-1.

Howlader, N. , Altekruse, S. F. , Li, C. I. , Chen, V. W. , Clarke, C. A. , Ries, L. A. & Cronin, K. A. (2014). US Incidence of Breast Cancer Subtypes Defined by Joint Hormone Receptor and HER2 Status, *Journal of the National Cancer Institute*, 106 (5), 1-8. doi: 10.1093/jnci/dju055.

Hsu, F.F., Yeh, C.T., Sun, Y.J., Chiang, M.T., Lan, W.M., Li, F.A., Lee, W.H. and Chau, L.Y. (2015) Erratum: Signal peptide peptidase-mediated nuclear localization of heme oxygenase-1 promotes cancer cell proliferation and invasion independent of its enzymatic activity, *Oncogene*, 34(18), pp. 2410–2411. https://doi.org/10.1038/onc.2014.464.

Huang, Z., Yu, P. and Tang, J. (2020) Characterization of triple-negative breast cancer MDA-MB-231 cell spheroid model, *OncoTargets and Therapy*, 13, pp. 5395–5405. https://doi.org/10.2147/OTT.S249756.

Hui, L., Zheng, Y., Yan, Y., Bargonetti, J. and Foster, D.A. (2006) Mutant p53 in MDA-MB-231 breast cancer cells is stabilized by elevated phospholipase D activity and contributes to survival signals generated by phospholipase D, *Oncogene*, 25(55), pp. 7305–7310. https://doi.org/10.1038/sj.onc.1209735.

Hwang, H.W., Lee, J.R., Chou, K.Y., Suen, C.S., Hwang, M.J., Chen, C., Shieh, R.C. and Chau, L.Y. (2009) Oligomerization is crucial for the stability and function of heme oxygenase-1 in the endoplasmic reticulum, *Journal of Biological Chemistry*, 284(34), pp. 22672–22679. https://doi.org/10.1074/jbc.M109.028001.

Iacopetta, D., Rosano, C., Sirignano, M., Mariconda, A., Ceramella, J., Ponassi, M., Saturnino, C., Sinicropi, M.S. and Longo, P. (2020) Is the way to fight cancer paved with gold? Metal-based carbene complexes with multiple and fascinating biological features, *Pharmaceuticals*, 13(5), pp. 91. https://doi.org/10.3390/ph13050091.

Ismail, Z., Dam, J., Penny, C., de Koning, C.B. and Harmse, L. (2022) Copper-imidazo[1,2-a]pyridines differentially modulate pro- and anti-apoptotic protein and gene expression in HL-60 and K562 leukaemic cells to cause apoptotic cell death, *Biochimica et Biophysica Acta - Molecular Cell Research*, 1869(1), pp. 119160. https://doi.org/10.1016/j.bbamcr.2021.119160.

Jafari, M., Sriram, V., Premnauth, G., Merino, E. and Lee, J.Y. (2022) Modified peroxamide-based reactive oxygen species (ROS)-responsive doxorubicin prodrugs, *Bioorganic Chemistry*, 127(4), pp. 105990. https://doi.org/10.1016/j.bioorg.2022.105990.

Jänicke, R.U., Sprengart, M.L., Wati, M.R. and Porter, A.G. (1998) Caspase-3 is required for DNA fragmentation and morphological changes associated with apoptosis, *Journal of Biological Chemistry*, 273(16), pp. 9357–9360. https://doi.org/10.1074/jbc.273.16.9357.

Ježek, J., Cooper, K.F. and Strich, R. (2018) Reactive oxygen species and mitochondrial dynamics: The yin and yang of mitochondrial dysfunction and cancer progression, *Antioxidants*, 7(1), pp. 13. https://doi.org/10.3390/antiox7010013.

Jhetam, Z., Martins-Furness, C., Slabber, C., Munro, O.Q., Nel, M. and Harmse, L. (2025) Copper complexes induce haem oxygenase-1 (HMOX1) and cause apoptotic cell death in pancreatic cancer cells, *Journal of Inorganic Biochemistry*, 264(12), pp. 112815. https://doi.org/10.1016/j.jinorgbio.2024.112815.

Jiang, X., Takahashi, N., Ando, K., Otsuka, T., Tetsuka, T. and Okamoto, T. (2003) NF-κB p65 transactivation domain is involved in the NF-κB-inducing kinase pathway, *Biochemical and Biophysical Research Communications*, 301(2), pp. 583–590. https://doi.org/https://doi.org/10.1016/S0006-291X(03)00011-1.

Ji, L., Li, H., Gao, P., Shang, G., Zhang, D. D., Zhang, N., & Jiang, T. (2013) Nrf2 pathway regulates multidrug-resistance-associated protein 1 in small cell lung cancer. *PloS one*, 8(5), pp. e63404. https://doi.org/10.1371/journal.pone.0063404.

Johnson, M.E. and Howerth, E.W. (2004) Survivin: A bifunctional inhibitor of apoptosis protein, *Veterinary Pathology*, 41(6), pp. 599–607. https://doi.org/10.1354/vp.41-6-599.

Jones, R., Swanton, C. and Ewer, M. (2006) Anthracycline cardiotoxicity, *Expert Opinion on Drug Safety*, 5(6), pp. 791–809. https://doi.org/https://doi.org/10.1517/14740338.5.6.791.

Juan, C.A., Pérez de la Lastra, J.M., Plou, F.J. and Pérez-Lebeña, E. (2021) The chemistry of reactive oxygen species (ROS) revisited: outlining their role in biological macromolecules (DNA, lipids and proteins) and induced pathologies, *International Journal of Molecular Sciences*, 22(9), pp. 4642.

Kalantar, H., Rajabi, S., Seyedabadi, M., & Moini-Zanjani, T. (2016). The effect of rapamycin on oxidative stress in MCF-7 and MDA-MB-231 human breast cancer cell lines. *Jundishapur*

Journal of Natural Pharmaceutical Products, 11(3), pp. 3–8. https://doi.org/10.17795/jjnpp-38177.

Kathryn, J.C., Sireesha V, G. and Stanley, L. (2012) Triple Negative Breast Cancer Cell Lines: One Tool in the Search for Better Treatment of Triple Negative Breast Cancer, *Breast Dis*, 32(1), pp. 35–48. https://doi.org/10.3233/BD-2010-0307.Triple.

Katner, A.L., Hoang, Q.B.L., Gootam, P., Jaruga, E., Ma, Q., Gnarra, J. and Rayford, W. (2002) Induction of cell cycle arrest and apoptosis in human prostate carcinoma cells by a recombinant adenovirus expressing p27Kip1*, Prostate,* 53(1), pp. 77–87. https://doi.org/10.1002/pros.10124.

Kean, W.F. and Kean, I.R.L. (2008) Clinical pharmacology of gold, *Inflammopharmacology*, 16(3), pp. 112–125. https://doi.org/10.1007/s10787-007-0021-x

Kim, J.H., Reeder, E., Parkin, S. and Awuah, S.G. (2019) Gold(I/III)-Phosphine Complexes as Potent Antiproliferative Agents, *Scientific Reports*, 9(1), pp. 1–18. https://doi.org/10.1038/s41598-019-48584-5.

Kreis, N. N., Louwen, F., & Yuan, J. (2019) The Multifaceted p21 (Cip1/Waf1/*CDKN1A*) in Cell Differentiation, Migration and Cancer Therapy. *Cancers*, *11*(9), pp. 1220. https://doi.org/10.3390/cancers11091220.

Kroemer, G. and Jäättelä, M. (2005) Lysosomes and autophagy in cell death control, *Nature Reviews Cancer*, 5(11), pp. 886–897. https://doi.org/10.1038/nrc1738.

Kroemer, G., Galluzzi, L., Vandenabeele, P., Abrams, J., Alnemri, E. S., Baehrecke, E. H., Blagosklonny, M. V., El-Deiry, W. S., Golstein, P., Green, D. R., Hengartner, M., Knight, R. A., Kumar, S., Lipton, S. A., Malorni, W., Nuñez, G., Peter, M. E., Tschopp, J., Yuan, J., Melino, G. (2005) Classification of cell death: Recommendations of the Nomenclature Committee on Cell Death. *Cell Death and Differentiation,* 12(1), pp. 1463–1467. https://doi.org/10.1038/sj.cdd.4401724.

Kroemer, G., Galluzzi, L., Vandenabeele, P., Abrams, J., Alnemri, E. S., Baehrecke, E. H., Blagosklonny, M. V., El-Deiry, W. S., Golstein, P., Green, D. R., Hengartner, M., Knight, R. A., Kumar, S., Lipton, S. A., Malorni, W., Nuñez, G., Peter, M. E., Tschopp, J., Yuan, J., Melino, G.

(2009) Classification of cell death: Recommendations of the Nomenclature Committee on Cell Death. *Cell Death and Differentiation, 16*(1), pp. 3–11. https://doi.org/10.1038/cdd.2008.150.

Kuchenbaecker, K. B., Hopper, J. L., Barnes, D. R., Phillips, K. A., Mooij, T. M., Roos-Blom, M. J., Jervis, S., van Leeuwen, F. E., Milne, R. L., Andrieu, N., & the CIMBA Consortium. (2017) Risks of breast, ovarian, and contralateral breast cancer for BRCA1 and BRCA2 mutation carriers. *Journal of American Medical Association, 317*(23), pp. 2402–2416. https://doi.org/10.1001/jama.2017.7112.

Lalaoui, N. and Vaux, D.L. (2018) Recent advances in understanding inhibitor of apoptosis proteins, *F1000Research*, 7(0), pp. 1–15. https://doi.org/10.12688/f1000research.16439.1.

Lamkanfi, M. and Kanneganti, T.D. (2010) Caspase-7: A protease involved in apoptosis and inflammation, *International Journal of Biochemistry and Cell Biology,* 42(1), pp. 21–24. https://doi.org/10.1016/j.biocel.2009.09.013.

Lamouille, S., Xu, J. and Derynck, R. (2014) Molecular mechanisms of epithelial–mesenchymal transition., *Nature Reviews Molecular Cell Biology*, 15(3), pp. 178–196. https://doi.org/10.1038/nrm3758.Molecular.

Lee, Z. Y., Looi, C. Y., Yusoff, K., Yow, Y. Y., Lim, W. M., Abdullah, R., Kadir, H. A., & Foo, J. B. (2021) Induction of apoptosis and autophagy by ternary copper complex towards breast cancer cells. *Anti-Cancer Agents in Medicinal Chemistry, 22*(6), pp. 1159–1170. https://doi.org/10.2174/1871520621666210726132543.

Lehmann, B.D., Bauer, J.A., Chen, X., Sanders, M.E., Chakravarthy, A.B., Shyr, Y. and Pietenpol, J.A. (2011) Identification of human triple-negative breast cancer subtypes and preclinical models for selection of targeted therapies, *Journal of Clinical Investigation*, 121(7), pp. 2750–2767. https://doi.org/10.1172/JCI45014.

Lehmann, B.D., Jovanović, B., Chen, X., Estrada, M. V., Johnson, K.N., Shyr, Y., Moses, H.L., Sanders, M.E. and Pietenpol, J.A. (2016) Refinement of Triple-Negative Breast Cancer Molecular Subtypes: Implications for Neoadjuvant Chemotherapy Selection, *PloS one*, 11(6), p. e0157368. https://doi.org/10.1371/journal.pone.0157368.

Leroy, B., Girard, L., Hollestelle, A., Minna, J.D., Gazdar, A.F. and Soussi, T. (2014) Analysis of TP53 mutation status in human cancer cell lines: A reassessment, *Human Mutation*, 35(6), pp. 756–765. https://doi.org/10.1002/humu.22556.

Li, D., Wang, H., Tan, C., Dai, L., Zhi, S. and Yang, Z. (2024) Design, Synthesis, and biological evaluation of copper(II) complexes with phenanthroline-based ligands as potential anticancer agents, *Journal of Coordination Chemistry*, 77(6), pp. 2175–2191. https://doi.org/10.1080/00958972.2024.2400169.

Li, D.D., Yagüe, E., Wang, L.Y., Dai, L.L., Yang, Z.B., Zhi, S., Zhang, N., Zhao, X.M. and Hu, Y.H. (2019) Novel Copper Complexes That Inhibit the Proteasome and Trigger Apoptosis in Triple-Negative Breast Cancer Cells, *ACS Medicinal Chemistry Letters*, 10(9), pp. 1328–1335. https://doi.org/10.1021/acsmedchemlett.9b00284.

Li, H., Liu, ZY., Wu, N. (2020) PARP inhibitor resistance: the underlying mechanisms and clinical implications. *Molecular Cancer,* 19(9), pp.107. https://doi.org/10.1186/s12943-020-01227-0.

Li, J., Cao, F., Yin, H.L. (2020) Ferroptosis: past, present and future. Cell Death and Disease, 11(2), pp. 88. https://doi.org/10.1038/s41419-020-2298-2.

Li, Xiang, Wang, Y., Li, M., Wang, H. and Dong, X. (2022) Metal Complexes or Chelators with ROS Regulation Capacity: Promising Candidates for Cancer Treatment, *Molecules*, 27(1), pp. 1–15. https://doi.org/10.3390/molecules27010148.

Li, X., & Zhu, J. (2022) Regulation of p53 signaling in breast cancer by the E3 ubiquitin ligase RNF187. *Cell Death and Disease, 13*(2), pp.1–11. https://doi.org/10.1038/s41419-022-04604-3.

Lim, B., Miller, E., Lee, H.J., Lulla, A., Hernandez, L. and Gokare, P. (2014) Current treatment of early breast cancer: Adjuvant and neoadjuvant therapy, *F1000Research,* 3(0), pp. 1–14. https://doi.org/10.12688/f1000research.4340.1.

Liston, D.R. and Davis, M. (2017) Clinically relevant concentrations of anticancer drugs: A guide for nonclinical studies, *Clinical Cancer Research*, 23(14), pp. 3489–3498. https://doi.org/10.1158/1078-0432.CCR-16-3083.

Litière, S., Werutsky, G., Fentiman, I.S., Rutgers, E., Christiaens, M.-R., Van Limbergen, E., Baaijens, M.H.A., Bogaerts, J. and Bartelink, H. (2012) Breast conserving therapy versus mastectomy for stage I–II breast cancer: 20 year follow-up of the EORTC 10801 phase 3 randomised trial, *The Lancet Oncology*, 13(4), pp. 412–419. https://doi.org/10.1016/S1470-2045(12)70042-6.

Liu, H., Su, Y., Zhang, W., Wang, M., Li, W., Cao, X., Zhang, L., Zhang, Y., Bao, Y., & Xu, W. (2017). Improvement of pharmacokinetic profile of TRAIL via trimer-tag enhances its antitumor activity *in vivo*. *Scientific Reports, 7*(1), pp. 8953. https://doi.org/10.1038/s41598-017-09303-4.

Li, X., Li, Y., Yang, X., Shao, F., Liu, J., Wang, J., Liu, F., Zhang, H., Li, C., Zhang, R., Zhou, Y., Li, X., & Zhu, J. (2022) Regulation of p53 signaling in breast cancer by the E3 ubiquitin ligase RNF187. *Cell Death and Disease, 13*(2), pp. 1–11. https://doi.org/10.1038/s41419-022-04604-3.

Liu, Z., Fan, L., Niu, D., Chen, M., Zhang, W., Liu, Y., Xu, J. and Wang, D. (2023) Copper (II) complex of salicylate phenanthroline induces the apoptosis of colorectal cancer cells, including oxaliplatin-resistant cells, *Oncology Reports*, 50(3), pp. 1–12. https://doi.org/10.3892/or.2023.8607.

Loboda, A., Damulewicz, M., Pyza, E., Jozkowicz, A. and Dulak, J. (2016) Role of Nrf2/HO-1 system in development, oxidative stress response and diseases: an evolutionarily conserved mechanism, *Cellular and Molecular Life Sciences,* 73(17), pp. 3221–3247. https://doi.org/10.1007/s00018-016-2223-0.

López-Hernández, J.E., Nayeem, N., Cerón-Carrasco, J.P., Ahad, A., Hafeez, A., León, I.E. and Contel, M. (2023) Platinum(IV)–Gold(I) Agents with Promising Anticancer Activity: Selected Studies in 2D and 3D Triple-Negative Breast Cancer Models, *Chemistry - A European Journal*, 29(59). https://doi.org/10.1002/chem.202302045.

Lopez, J. and Tait, S.W.G. (2015) Mitochondrial apoptosis: killing cancer using the enemy within, *British journal of cancer*, 112(6), pp. 957–962. https://doi.org/10.1038/bjc.2015.85

Lord, C.J. and Ashworth, A. (2017) PARP inhibitors: Synthetic lethality in the clinic, *Science*, 355(6330), pp. 1152–1158. https://doi.org/10.1126/science.aam7344.

Loughery, J., Cox, M., Smith, L.M. and Meek, D.W. (2014) Critical role for p53-serine 15 phosphorylation in stimulating transactivation at p53-responsive promoters, *Nucleic Acids Research*, 42(12), pp. 7666–7680. https://doi.org/10.1093/nar/gku501.

Lv, Y., Ma, X., Du, Y. and Feng, J. (2021) Understanding patterns of brain metastasis in triple-negative breast cancer and exploring potential therapeutic targets, *OncoTargets and Therapy*, 14(1), pp. 589–607. https://doi.org/10.2147/OTT.S293685.

Ma, Z.Y., Qiao, X., Xie, C.Z., Shao, J., Xu, J.Y., Qiang, Z.Y. and Lou, J.S. (2012) Activities of a novel Schiff Base copper(II) complex on growth inhibition and apoptosis induction toward MCF-7 human breast cancer cells via mitochondrial pathway, *Journal of Inorganic Biochemistry*, 117(6), pp. 1–9. https://doi.org/10.1016/j.jinorgbio.2012.08.007.

Maas, C., Verbrugge, I., De Vries, E., Savich, G., Van De Kooij, L.W., Tait, S.W.G. and Borst, J. (2010) Smac/DIABLO release from mitochondria and XIAP inhibition are essential to limit clonogenicity of Type i tumor cells after TRAIL receptor stimulation*, Cell Death and Differentiation*, 17(10), pp. 1613–1623. https://doi.org/10.1038/cdd.2010.39.

Madan, E., Prasad, S., Roy, P., George, J., Mukhopadhyay, S., Hussain, T., Datt, M., Banerjee, D., Sharma, A., Chander, H., & Gogna, R. (2019) HIF-transcribed p53 chaperones HIF-1α. *Nucleic Acids Research, 47*(19), pp. 10212–10234. https://doi.org/10.1093/nar/gkz766.

Ma, H., Ursin, G., Xu, X., (2017) Reproductive factors and the risk of triple-negative breast cancer in white women and African American women: a pooled analysis. *Breast Cancer Research,* (19), pp. 6. https://doi.org/10.1186/s13058-016-0799-9.

Magherini, F., Modesti, A., Bini, L., Nediani, C., Massai, L., Messori, L., & Gamberi, T. (2018). Antiproliferative effects of two gold(I)-N-heterocyclic carbene complexes in A2780 human ovarian cancer cells: A comparative proteomic study. *Oncotarget, 9*(46), 28042–28068. https://doi.org/10.18632/oncotarget.25556.

Makki, J. (2015) Diversity of breast carcinoma: Histological subtypes and clinical relevance, Clinical Medicine Insights: *Pathology*, 8(1), pp. 23–31. https://doi.org/10.4137/CPath.s31563.

Mancikova, V., Smardova, J., Vasinek, M., Bouchalova, P., Kralova, K., Muller, P., Pavlova, S., Doubek, M., & Pospisilova, S. (2023). Distinct p53 phosphorylation patterns in chronic lymphocytic leukemia patients are reflected in the activation of circumjacent pathways upon DNA damage. *Molecular Oncology, 17*(1), pp. 82–97. https://doi.org/10.1002/1878-0261.13337.

Mansara, P.P., Deshpande, R.A., Vaidya, M.M. and Kaul-Ghanekar, R. (2015) Differential ratios of omega fatty acids (AA/EPA+DHA) modulate growth, lipid peroxidation and expression of tumor regulatory MARBPs in breast cancer cell lines MCF7 and MDA-MB-231, *PLoS ONE*, 10(9), pp. 1–22. https://doi.org/10.1371/journal.pone.0136542.

Mao, G., Zhang, Y., Mo, W., Yu, Y., Lu, H., & Ni, R. (2014). The expression levels and prognostic value of high temperature required A2 (HtrA2) in NSCLC. *Pathology Research and Practice, 210*(12), pp. 939–943. https://doi.org/10.1016/j.prp.2014.06.030.

Marei, H.E., Althani, A., Afifi, N., Hasan, A., Caceci, T., Pozzoli, G., Morrione, A., Giordano, A. and Cenciarelli, C. (2021) P53 Signaling in Cancer Progression and Therapy, *Cancer Cell International*, 21(1), pp. 1–15. https://doi.org/10.1186/s12935-021-02396-8.

Martelli, A.M., Zweyer, M., Ochs, R.L., Tazzari, P.L., Tabellini, G., Narducci, P. and Bortul, R. (2001) Nuclear apoptotic changes: An overview, *Journal of Cellular Biochemistry*, 82(4), pp. 634–646. https://doi.org/10.1002/jcb.1186.

Martin, S.S. and Leder, P. (2001) Human MCF10A Mammary Epithelial Cells Undergo Apoptosis following Actin Depolymerization That Is Independent of Attachment and Rescued by Bcl-2, 21(19), pp. 6529–6536. https://doi.org/10.1128/MCB.21.19.6529.

Marvalim, C., Datta, A., Lee, S.C. (2023) Role of p53 in breast cancer progression: An insight into p53 targeted therapy. *Theranostics*, 13(4), pp. 1421-1442. https://doi.org/10.7150/thno.81847.

Marzano, C., Pellei, M., Tisato, F. and Santini, C. (2012) Copper Complexes as Anticancer Agents, *Anti-Cancer Agents in Medicinal Chemistry*, 9(2), pp. 185–211. https://doi.org/10.2174/187152009787313837.

Mascaró, M., Alonso, E.N., Alonso, E.G., Lacunza, E., Curino, A.C. and Facchinetti, M.M. (2021) Nuclear localization of heme oxygenase-1 in pathophysiological conditions: Does it explain the dual role in cancer? *Antioxidants*, 10(1), pp. 1–15. https://doi.org/10.3390/antiox10010087.

Mawatari, T., Ninomiya, I., Kajiwara, H., Fushida, S., Fujimura, T., Oyama, K., Hirata, K., Tajima, H., Kinami, S., Tanaka, C., Nishizawa, T., Takamura, H., & Ohta, T. (2015) Valproic acid inhibits proliferation of HER2-expressing breast cancer cells by inducing cell cycle arrest and apoptosis through Hsp70 acetylation. *International Journal of Oncology, 47*(6), pp. 2073–2081. https://doi.org/10.3892/ijo.2015.3213.

McCarthy, A. M., Friebel, T. M., Ehsan, S., Armstrong, N., Bradbury, A. R., & Armstrong, K. (2021) Relationship of established risk factors with breast cancer subtypes. *Cancer Medicine, 10*(18), pp. 6456–6467. https://doi.org/10.1002/cam4.4158.

McGivern, T.J.P., Afsharpour, S. and Marmion, C.J. (2018) Copper complexes as artificial DNA metallonucleases: From Sigman's reagent to next generation anti-cancer agent? *Inorganica Chimica Acta*, 472, pp. 12–39. https://doi.org/10.1016/j.ica.2017.08.043.

McKeage, M.J. (2002) Gold opens mitochondrial pathways to apoptosis, *British Journal of Pharmacology*, 136(8), pp. 1081–1082. https://doi.org/10.1038/sj.bjp.0704822.

Medina, M.A., Oza, G., Sharma, A., Arriaga, L.G., Hernández, J.M.H., Rotello, V.M. and Ramirez, J.T. (2020) Triple-negative breast cancer: A review of conventional and advanced therapeutic strategies, *International Journal of Environmental Research and Public Health*, 17(6), pp. 1–32. https://doi.org/10.3390/ijerph17062078.

Mehta, S.A., Christopherson, K.W., Bhat-Nakshatri, P., Goulet, R.J., Broxmeyer, H.E., Kopelovich, L. and Nakshatri, H. (2007) Negative regulation of chemokine receptor CXCR4 by tumor suppressor p53 in breast cancer cells: Implications of p53 mutation or isoform expression

on breast cancer cell invasion, *Oncogene*, 26(23), pp. 3329–3337. https://doi.org/10.1038/sj.onc.1210120.

Menon, G., Alkabban, F.M., Ferguson, T., Breast Cancer. (2024) Feb 25. In: StatPearls. Treasure Island (FL): StatPearls Publishing. http://europepmc.org/abstract/MED/29493913

Meyerovich, K., Fukaya, M., Terra, L.F., Ortis, F., Eizirik, D.L., Cardozo, A.K. (2016) The non-canonical NF-κB pathway is induced by cytokines in pancreatic beta cells and contributes to cell death and proinflammatory responses *in vitro. Diabetologia*, 59(3), pp. 512-521. doi: 10.1007/s00125-015-3817-z.

Meric-Bernstam, F., Frampton, G. M., Ferrer-Lozano, J., Yelensky, R., Pérez-Fidalgo, J. A., Wang, Y., Palmer, G. A., Sun, J., Kang, Y.-K., García-Sáenz, J. Á., Cortés, J., Dienstmann, R., Verma, C., Martínez-Bueno, A., Rodríguez-Lescure, A., Calvo, E., & Chen, K. (2018) Survival outcomes by TP53 mutation status in metastatic breast cancer. *JCO Precision Oncology, 2*, pp. 1–15. https://doi.org/10.1200/PO.17.00245.

Miah, S., Goel, R. K., Dai, C., Kalra, N., Beaton-Brown, E., & Lukong, K. E. (2019). Estrogen receptor signaling regulates the expression of the breast tumor kinase in breast cancer cells. *BMC Cancer, 19*(1), pp. 1–12. https://doi.org/10.1186/s12885-018-5186-8.

Minicozzi, V., Almerinda, D.V., Eleonora, N., Alessandro, G., Anna Maria, C., Luisa, D.P. and and Mei, G. (2021) Non-symmetrical structural behavior of a symmetric protein: the case of homo-trimeric TRAF2 (tumor necrosis factor-receptor associated factor 2), *Journal of Biomolecular Structure and Dynamics*, 39(1), pp. 319–329. https://doi.org/10.1080/07391102.2020.1719202.

Momose, I., Onodera, T. and Kawada, M. (2021) Potential anticancer activity of auranofin, *Yakugaku Zasshi*, 141(3), pp. 315–321. https://doi.org/10.1248/yakushi.20-00179-2.

Morelli, M.B., Bongiovanni, C., Da Pra, S., Miano, C., Sacchi, F., Lauriola, M. and D'Uva, G. (2022) Cardiotoxicity of Anticancer Drugs: Molecular Mechanisms and Strategies for Cardioprotection, *Frontiers in Cardiovascular Medicine*, 9(4), pp. 847012 https://doi.org/10.3389/fcvm.2022.847012.

Mosmann, T. (1983) Rapid colorimetric assay for cellular growth and survival: application to proliferation and cytotoxicity assays*, Journal of immunological methods*, 65(2), pp. 55–63. https://doi.org/10.1016/0022-1759(83)90303-4.

Muenzner, J. K., Stojanovic, A., Iordanov, V., Simeonova, R., Wenzel, M. N., Sigel, R. K. O., & Schobert, R. (2016). Ferrocenyl-coupled N-heterocyclic carbene complexes of gold(I): A successful approach to multinuclear anticancer drugs. *Chemistry – A European Journal, 22*(52), pp. 18953–18962. https://doi.org/10.1002/chem.201604246.

Muller, P.A.J. and Vousden, K.H. (2014) Mutant p53 in cancer: New functions and therapeutic opportunities, *Cancer Cell*, 25(3), pp. 304–317. https://doi.org/10.1016/j.ccr.2014.01.021.

Murphy, M. E.(2013) The HSP70 family and cancer, *Carcinogenesis*, 34(6), pp. 1181–1188. https://doi.org/10.1093/carcin/bgt111.

Myeza, N., Slabber, C., Munro, O.Q., Sookai, S., Zacharias, S.C., Martins-Furness, C. and Harmse, L. (2024) An 8-aminoquinoline-naphthyl copper complex causes apoptotic cell death by modulating the expression of apoptotic regulatory proteins in breast cancer cells, *European Journal of Pharmacology*, 978(6), pp. 176764. https://doi.org/10.1016/j.ejphar.2024.176764.

Nagdas, S. and Kashatus, D.F. (2017) The interplay between oncogenic signalling networks and mitochondrial dynamics, *Antioxidants*, 6(2), pp. 33 https://doi.org/10.3390/antiox6020033.

Nejad, A. E., Najafgholian, S., Rostami, A., Sistani, A., Shojaeifar, S., Esparvarinha, M., Ahmadlou, M.(2021) The role of hypoxia in the tumour microenvironment and development of cancer stem cell: A novel approach to developing treatment*., Cancer Cell International*, 21(62), pp. 1719. https://doi. org/10.1186/s12935-020-01719-5, 62.

Ng, C.H., Kong, S.M., Tiong, Y.L., Maah, M.J., Sukram, N., Ahmad, M. and Khoo, A.S.B. (2014) Selective anticancer copper(ii)-mixed ligand complexes: Targeting of ROS and proteasomes, *Metallomics*, 6(4), pp. 892–906. https://doi.org/10.1039/c3mt00276d.

Nicotera, P. and Melino, G. (2004) Regulation of the apoptosis–necrosis switch, *Oncogene*, 23(16), pp. 2757–2765. https://doi.org/10.1038/sj.onc.1207559.

Nocquet, L., Roul, J., Lefebvre, C.C., Duarte, L., Campone, M., Juin, P.P. and Souazé, F. (2024) Low BCL - xL expression in triple - negative breast cancer cells favor chemotherapy efficacy , and this effect is limited by cancer - associated fibroblasts, *Scientific Reports*, 14(1), pp. 1–10. https://doi.org/10.1038/s41598-024-64696-z.

Noh, S. J., Bae, J. S., Jamiyandorj, U., Park, H. S., Jang, K. Y., Chung, M. J., Moon, W. S., Lee, D. G., Lee, Y. S., & Kang, M. J. (2013). Expression of nerve growth factor and heme oxygenase-1 predict poor survival of breast carcinoma patients. *BMC Cancer, 13*, pp. 516. https://doi.org/10.1186/1471-2407-13-516.

Oesterreich, S., Nasrazadani,A., Zou, J., Carleton, N., Onger,T., Wright, M. D., Li, Y., Demanelis, K., Ramaswamy, B., Tseng, G Lee, A. V., Williams, N., Kruse, M., (2022) Clinicopathological Features and Outcomes Comparing Patients With Invasive Ductal and Lobular Breast Cancer, *Journal of the National Cancer Institute*, 114 (11), pp. 1511–1522, https://doi.org/10.1093/jnci/djac157.

Octavia, Y., Tocchetti, C.G., Gabrielson, K.L., Janssens, S., Crijns, H.J. and Moens, A.L. (2012) Doxorubicin-induced cardiomyopathy: From molecular mechanisms to therapeutic strategies, *Journal of Molecular and Cellular Cardiology*, 52(6), pp. 1213–1225. https://doi.org/10.1016/j.yjmcc.2012.03.006.

Olar, R., Maxim, C., Badea, M., Bacalum, M., Raileanu, M., Avram, S., Korošin, N.Č., Burlanescu, T. and Rostas, A.M. (2022) Antiproliferative Copper(II) Complexes Bearing Mixed Chelating Ligands: Structural Characterization, ROS Scavenging, In Silico Studies, and Anti-Melanoma Activity, *Pharmaceutics*, 14(8), pp. 1692. https://doi.org/10.3390/pharmaceutics14081692.

Olelewe, C., Kim, J.H., Ofori, S., Mertens, R.T., Gukathasan, S. and Awuah, S.G. (2022) Gold(III)-P-chirogenic complex induces mitochondrial dysfunction in triple-negative breast cancer, *iScience*, 25(5), pp. 104340. https://doi.org/10.1016/j.isci.2022.104340.

Olivier, M., Eeles, R., Hollstein, M., Khan, M.A., Harris, C.C. and Hainaut, P. (2002) The IARC TP53 database: New online mutation analysis and recommendations to users, *Human Mutation*, 19(6), pp. 607–614. https://doi.org/10.1002/humu.10081.

Olsson, M. and Zhivotovsky, B. (2011) Caspases and cancer, *Cell Death and Differentiation*, 18(9), pp. 1441–1449. https://doi.org/10.1038/cdd.2011.30.

Ōmura, S., Asami, Y. and Crump, A. (2018) Staurosporine: new lease of life for parent compound of today's novel and highly successful anti-cancer drugs, *Journal of Antibiotics*, 71(8), pp. 688–701. https://doi.org/10.1038/s41429-018-0029-z.

Ott, I., Kircher, B., Schumacher, P., Wenzel, M., & Bagowski, C. P. (2009). A gold(I) phosphine complex containing a naphthalimide ligand functions as a TrxR inhibiting antiproliferative agent and angiogenesis inhibitor. *Journal of Medicinal Chemistry, 52*(3), pp. 763–770. https://doi.org/10.1021/jm8012135.

Oun, R., Moussa, Y.E. and Wheate, N.J. (2018) The side effects of platinum-based chemotherapy drugs: a review for chemists, *Dalton transactions*, 47(19), pp. 6645–6653. https://doi.org/10.1039/C8DT00838H.

Paul, A., Krelin, Y., Arif, T., Jeger, R. and Shoshan-Barmatz, V. (2018) A New Role for the Mitochondrial Pro-apoptotic Protein SMAC/Diablo in Phospholipid Synthesis Associated with Tumorigenesis, *Molecular Therapy*, 26(3), pp. 680–694. https://doi.org/10.1016/j.ymthe.2017.12.020.

Park, Y.H., Seo, J.H., Park, J., Lee, H.S., & Kim, K. (2017). Hsp70 acetylation prevents caspase-dependent/independent apoptosis and autophagic cell death in cancer cells. *International Journal of Oncology*, 51(2), pp. 573-578. https://doi.org/10.3892/ijo.2017.4039.

Parks, S.K., Cormerais, Y., Marchiq, I. and Pouyssegur, J. (2016) Hypoxia optimises tumour growth by controlling nutrient import and acidic metabolite export, *Molecular Aspects of Medicine*, 47(8), pp. 3–14. https://doi.org/https://doi.org/10.1016/j.mam.2015.12.001.

Peega, T., Magwaza, R.N., Harmse, L. and Kotzé, I.A. (2021) Synthesis and evaluation of the anticancer activity of [Pt(diimine)(N,N-dibutyl-N′-acylthiourea)]+complexes, *Dalton Transactions*, 50(34), pp. 11742–11762. https://doi.org/10.1039/d1dt01385h.

Pellei, M., Gandin, V., Marchiò, L., Marzano, C., Bagnarelli, L. and Santini, C. (2019) Syntheses and biological studies of Cu(II) complexes bearing bis (pyrazol-1-yl)- And Bis(triazol-1-yl)-acetato heteroscorpionate ligands, *Molecules,* 24(9), pp. 1–18. https://doi.org/10.3390/molecules24091761.

Pendergrass, W., Wolf, N. and Pool, M. (2004) Efficacy of MitoTracker GreenTM and CMXRosamine to measure changes in mitochondrial membrane potentials in living cells and tissues, *Cytometry Part A*, 61(2), pp. 162–169. https://doi.org/10.1002/cyto.a.20033.

Peng, C.Y., Fong, P.C., Yu, C.C., Tsai, W.C., Tzeng, Y.M. and Chang, W.W. (2013) Methyl antcinate a suppresses the population of cancer stem-like cells in MCF7 human breast cancer cell line, *Molecules*, 18(3), pp. 2539–2548. https://doi.org/10.3390/molecules18032539.

Peng, Y., Chen, L., Li, C., Lu, W. and Chen, J. (2001) Inhibition of MDM2 by hsp90 Contributes to Mutant p53 Stabilization, *Journal of Biological Chemistry*, 276(44), pp. 40583–40590. https://doi.org/10.1074/jbc.M102817200.

Pérez, W., Soto, Y., Ortiz, C., Matta, J., & Melendez, E. (2015) Ferrocenes as potential chemotherapeutic drugs: Synthesis, cytotoxic activity, reactive oxygen species production and micronucleus assay. *Bioorganic & Medicinal Chemistry*, 23(3), pp. 471–479. https://doi.org/10.1016/j.bmc.2014.12.023.

Periasamy, V.S., Riyasdeen, A., Rajendiran, V., Palaniandavar, M., Krishnamurthy, H., Alshatwi, A.A. and Akbarsha, M.A. (2020) Induction of redox-mediated cell death in ER-positive and ER-negative breast cancer cells by a copper(II)-phenolate complex: An *in vitro* and in silico study, *Molecules*, 25(19), pp. 4504 https://doi.org/10.3390/molecules25194504.

Pian, A.K., Foong, C.P. and Hamid, R.A. (2022) S-phase arrest and apoptosis in human breast adenocarcinoma MCF-7 cells via mitochondrial dependent pathway induced by

tricyclohexylphosphine gold (I) n-mercaptobenzoate complexes, *Life Sciences*, 311(PB), pp. 121161. https://doi.org/10.1016/j.lfs.2022.121161.

Pierzyńska-Mach, A., Janowski, P.A. and Dobrucki, J.W. (2014) Evaluation of acridine orange, LysoTracker Red, and quinacrine as fluorescent probes for long-term tracking of acidic vesicles, *Cytometry Part A*, 85(8), pp. 729–737. https://doi.org/10.1002/cyto.a.22495.

Pimentel, J.M., Zhou, J.Y. and Wu, G.S. (2023) The Role of TRAIL in Apoptosis and Immunosurveillance in Cancer, *Cancers*, 15(10), pp. 1–18. https://doi.org/10.3390/cancers15102752.

Pluta, P., Jeziorski, A., Pluta, A., Cebula-obrzut, B., Wierzbowska, A., Piekarski1, J. And Smolewski, P. (2015) Expression of IAP family proteins and its clinical importance in breast cancer patients P., *Neoplasma*, 60(5), pp. 607–616. https://doi.org/10.4149/neo.

Podkalicka, P., Mucha, O., Józkowicz, A., Dulak, J. and Łoboda, A. (2017) Heme oxygenase inhibition in cancers: Possible tools and targets, *Wspolczesna Onkologia*, 2(1A), pp. 23–32. https://doi.org/10.5114/wo.2018.73879.

Pogoda, K., Niwińska, A., Sarnowska, E., Nowakowska, D., Jagiełło-Gruszfeld, A., Siedlecki, J. and Nowecki, Z. (2020) Effects of BRCA Germline Mutations on Triple-Negative Breast Cancer Prognosis, *Journal of Oncology*, 2020(1), pp. 8545643. https://doi.org/10.1155/2020/8545643.

Porchia, M., Pellei, M., Marinelli, M., Tisato, F., Del, F. and Santini, C. (2018) New insights in Au-NHCs complexes as anticancer agents, *European Journal of Medicinal Chemistry*, 146(1), pp. 709–746. https://doi.org/10.1016/j.ejmech.2018.01.065.

Porter, A.G. and Jänicke, R.U. (1999) Emerging roles of caspase-3 in apoptosis, *Cell Death and Differentiation*, 6(2), pp. 99–104. https://doi.org/10.1038/sj.cdd.4400476.

Radhakrishnan, K., Khamrang, T., Sambantham, K., Sali, V.K., Chitgupi, U., Lovell, J.F., Mohammad, A.A. and Venugopal, R. (2021) Identification of cytotoxic copper(II) complexes with phenanthroline and quinoline, quinoxaline or quinazoline-derived mixed ligands, *Polyhedron*, 194(1), pp. 114886. https://doi.org/10.1016/j.poly.2020.114886.

Rathore, R., McCallum, J.E., Varghese, E., Florea, A.M. and Büsselberg, D. (2017) Overcoming chemotherapy drug resistance by targeting inhibitors of apoptosis proteins (IAPs), *Apoptosis*, 22(7), pp. 898–919. https://doi.org/10.1007/s10495-017-1375-1.

Reczek, C.R. and Chandel, N.S. (2017) The two faces of reactive oxygen species in cancer, *Annual Review of Cancer Biology*, 1(1), pp. 79–98. https://doi.org/10.1146/annurev-cancerbio-041916-065808.

Reddy, T., Privér, S.H., Rao, V. V., Mirzadeh, N. and Bhargava, S.K. (2018) Gold(i) and gold(iii) phosphine complexes: synthesis, anticancer activities towards 2D and 3D cancer models, and apoptosis inducing properties, *Dalton Transactions*, 47(43), pp. 15312–15323. https://doi.org/10.1039/C8DT01724G.

Redza-Dutordoir, M. and Averill-Bates, D.A. (2016) Activation of apoptosis signalling pathways by reactive oxygen species, Biochimica et Biophysica Acta - *Molecular Cell Research*, 1863(12), pp. 2977–2992. https://doi.org/10.1016/j.bbamcr.2016.09.012.

Reers, M., Smiley, S., Mottola-Hartshorn, C., Chen, A., Lin, M. and Chen, L. (1995) Mitochondrial Membrane Potential Monitored by JC- 1 Dye, *Biophysical Methods*, 260(1), pp. 406-417. https://doi.org/10.1016/0076-6879(95)60154-6.

Ribble, D., Goldstein, N.B., Norris, D.A. and Shellman, Y.G. (2005) A simple technique for quantifying apoptosis in 96-well plates, *BMC biotechnology*, 5(1), pp. 1–7. https://doi.org/10.1186/1472-6750-5-12.

Ribeiro, N., Santos, A. M., Valente, A., Marques, F., Félix, V., & Correia, I. (2023) Promising anticancer agents based on 8-hydroxyquinoline hydrazone copper(II) complexes. *Frontiers in Chemistry, 11(1)*, Article 1106349. https://doi.org/10.3389/fchem.2023.1106349.

Riccardi, C. and Nicoletti, I. (2006) Analysis of apoptosis by propidium iodide staining and flow cytometry, *Nature Protocols*, 1(3), pp. 1458–1461. https://doi.org/10.1038/nprot.2006.238.

Rick, W. (1974) Trypsin, *Methods of enzymatic analysis.* Elsevier, pp. 1013–1024. https://doi.org/10.1016/B978-0-12-091302-2.50099-2

Ritter, J., Lewis, L., Mant, T., & Ferro, A. (2008). A Textbook of Clinical Pharmacology and Therapeutics, 5Ed (5th ed.). CRC Press. https://doi.org/10.1201/b13234

Robles-Bañuelos, B., Romo-Perez, A., Dominguez-Gomez, G., Chavez-Blanco, A., Gonzalez-Fierro, A. and Duenas-Gonzalez, A. (2024) Selection of clinically relevant drug concentrations for *in vitro* studies of candidates drugs for cancer repurposing: a proposal, *Clinical and Translational Oncology*, 26(5), pp. 1077–1088. https://doi.org/10.1007/s12094-023-03352-w.

Robson, M. E., Tung, N., Conte, P., Im, S. A., Senkus, E., Xu, B., Masuda, N., Delaloge, S., Li, W., Armstrong, A., Wu, W., Goessl, C., Runswick, S., & Domchek, S. M. (2019) OlympiAD final overall survival and tolerability results: Olaparib versus chemotherapy treatment of physician's choice in patients with a germline BRCA mutation and HER2-negative metastatic breast cancer. *Annals of oncology : official Journal of the European Society for Medical Oncology*, *30*(4), 558–566. https://doi.org/10.1093/annonc/mdz012

Rovillain, E., Mansfield, L., Caetano, C., Alvarez-Fernandez, M., Caballero, O.L., Medema, R.H., Hummerich, H. and Jat, P.S. (2011) Activation of nuclear factor-kappa B signalling promotes cellular senescence, *Oncogene*, 30(20), pp. 2356–2366. https://doi.org/10.1038/onc.2010.611.

Rugo, H.S., Tolaney, S.M., Loirat, D.(2011) Safety analyses from the phase 3 ASCENT trial of sacituzumab govitecan in metastatic triple-negative breast cancer. *Breast Cancer*, (8), pp. 98. https://doi.org/10.1038/s41523-022-00467-1.

Salimi, M., Abdi, K., Kandelous, H.M., Hadadzadeh, H., Azadmanesh, K., Amanzadeh, A. and Sanati, H. (2015) Antiproliferative effects of copper(II)-polypyridyl complexes in breast cancer cells through inducing apoptosis, *BioMetals*, 28(2), pp. 267–278. https://doi.org/10.1007/s10534-015-9820-5.

Sánchez-González, Á., & Gil, A. (2021a) Elucidating the intercalation of methylated 1, 10-phenanthroline with DNA: the important weight of the CH/H interactions and the selectivity of CH/π and CH/n interactions. *Royal Society of Chemistry Advances*, 11(3), pp. 1553-1563. https://doi.org/10.1039/D0RA07646E.

Sánchez-González, Á., Bandeira, N. A. G., Ortiz de Luzuriaga, I., Martins, F. F., Elleuchi, S., Jarraya, K., Lanuza, J., Lopez, X., Calhorda, M. J., Gil, A. (2021b) New Insights on the Interaction of Phenanthroline Based Ligands and Metal Complexes and Polyoxometalates with Duplex DNA and G-Quadruplexes. *Molecules*, 26(16), pp. 4737. https://doi.org/10.3390/molecules26164737.

Sankunny, M. and Eng, C. (2018) KLLN-mediated DNA damage-induced apoptosis is associated with regulation of p53 phosphorylation and acetylation in breast cancer cells, *Cell Death Discovery*, 4(1). https://doi.org/10.1038/s41420-018-0094-x.

Santini, C., Pellei, M., Gandin, V., Porchia, M., Tisato, F., & Marzano, C. (2011). *In vitro* antitumour activity of water-soluble Cu(I), Ag(I) and Au(I) complexes supported by hydrophilic alkyl phosphine ligands. *Journal of Inorganic Biochemistry, 105*(2), pp. 232–240. https://doi.org/10.1016/j.jinorgbio.2010.10.016.

Santini, C., Pellei, M., Gandin, V., Porchia, M., Tisato, F. and Marzano, C. (2014) Advances in copper complexes as anticancer agents, *Chemical Reviews*, 114(1), pp. 815–862. https://doi.org/10.1021/cr400135x.

Sariego, Jack (2010) Breast Cancer in the Young Patient, *The American SurgeonTM*, 76(12), pp. 1397–1400. https://doi.org/10.1177/000313481007601226.

Sebbagh, M., Renvoizé, C., Hamelin, J., Riché, N., Bertoglio, J. and Bréard, J. (2001) Caspase-3-mediated cleavage of ROCK I induces MLC phosphorylation and apoptotic membrane blebbing, *Nature Cell Biology*, 3(2), pp. 1148–1159. https://doi.org/https://doi.org/10.1038/35070009.

Shaath, H., Elango, R. and Alajez, N.M. (2021) Molecular classification of breast cancer utilizing long non-coding rna (Lncrna) transcriptomes identifies novel diagnostic lncrna panel for triple-negative breast cancer, *Cancers*, 13(21), pp. 5350 https://doi.org/10.3390/cancers13215350.

Shah, R., Rosso, K. and David Nathanson, S. (2014) Pathogenesis, prevention, diagnosis and treatment of breast cancer, *World Journal of Clinical Oncology*, 5(3), pp. 283–298. https://doi.org/10.5306/wjco.v5.i3.283.

Shubin, A. V., Demidyuk, I. V., Komissarov, A.A., Rafieva, L.M. and Kostrov, S. V. (2016) Cytoplasmic vacuolization in cell death and survival, *Oncotarget*, 7(34), pp. 55863–55889. https://doi.org/10.18632/oncotarget.10150.

Siegmund, D., Wagner, J., & Wajant, H. (2022). TNF Receptor Associated Factor 2 (TRAF2) Signaling in Cancer. *Cancers*, *14*(16), 4055. https://doi.org/10.3390/cancers14164055.

Sigman, D.S., Graham, D.R., D'Aurora, V. and Stern, A.M. (1979) Oxygen-dependent cleavage of DNA by the 1,10-phenanthroline.cuprous complex. Inhibition of Escherichia coli DNA polymerase I, *Journal of Biological Chemistry*, 254(24), pp. 12269–12272. https://doi.org/10.1016/s0021-9258(19)86305-6.

Silver, D. P., Richardson, A. L., Eklund, A. C., Wang, Z. C., Szallasi, Z., Li, Q., Juul, N., Leong, C. O., Calza, S., Buraimoh, A., Maruyama, R., Biswas, S., Fatima, A., Bergamaschi, A., Natrajan, R., Lamb, J., Ganesan, S., Ellis, M. J., Larsen, M., and Garber, J. E. (2010). Efficacy of neoadjuvant cisplatin in triple-negative breast cancer. *Journal of Clinical Oncology, 28*(7), pp. 1145–1153. https://doi.org/10.1200/JCO.2009.22.4725.

Singh, R., Letai, A. and Sarosiek, K. (2019) Regulation of apoptosis in health and disease: the balancing act of BCL-2 family proteins, *Nature Reviews Molecular Cell Biology*, 20(3), pp. 175–193. https://doi.org/10.1038/s41580-018-0089-8.

Singhabahu, R., Kodagoda Gamage, S.M. and Gopalan, V. (2024) Pathological significance of heme oxygenase-1 as a potential tumor promoter in heme-induced colorectal carcinogenesis, *Cancer Pathogenesis and Therapy*, 2(2), pp. 65–73. https://doi.org/10.1016/j.cpt.2023.04.001.

Sîrbu, A., Grosu, A. L., Oniga, O., Zglimbea, L., Leopold, L. F., Jurj, A., Diaconeasa, Z., Stiufiuc, R., Florea, A., Tăbăran, F., Lucaciu, C. M., Muntean, D., Braicu, C., Berindan-Neagoe, I., & Arion, V. B. (2017). Copper(II) thiosemicarbazone complexes induce marked ROS

accumulation and promote Nrf2-mediated antioxidant response in highly resistant breast cancer cells. *Dalton Transactions, 46*(12), pp. 3833–3847. https://doi.org/10.1039/c7dt00283a.

Slee, E.A., Adrain, C. and Martin, S.J. (2001) Executioner Caspase-3, -6, and -7 Perform Distinct, Non-redundant Roles during the Demolition Phase of Apoptosis, *Journal of Biological Chemistry*, 276(10), pp. 7320–7326. https://doi.org/10.1074/jbc.M008363200.

Smeenk, L., van Heeringen, S.J., Koeppel, M., Gilbert, B., Janssen-Megens, E., Stunnenberg, H.G. and Lohrum, M. (2011) Role of p53 Serine 46 in p53 target gene regulation, *PLoS ONE*, 6(3). pp. e0017574. https://doi.org/10.1371/journal.pone.0017574.

Soleimanpour, E. and Babaei, E. (2015) Survivin as a potential target for cancer therapy, *Asian Pacific Journal of Cancer Prevention*, 16(15), pp. 6187–6191. https://doi.org/10.7314/APJCP.2015.16.15.6187.

Soule, H.D., Vazquez, J., Long, A., Albert, S. and Brennan, M. (1973) A human cell line from a pleural effusion derived from a breast carcinoma1,2, *Journal of the National Cancer Institute*, 51(5), pp. 1409–1416. https://doi.org/10.1093/jnci/51.5.1409.

Soule, H.D., Maloney, T.M., Wolman, S.R., Brenz, R., Russo, J., Pauley, R.J., Jones, R.F., Brooks, S.C. and McGrath, C.M. (1990) Isolation and Characterization of a Spontaneously Immortalized Human Breast Epithelial Cell Line, MCF-10, *Cancer Research*, 50(18), pp. 6075–6086.https://aacrjournals.org/cancerres/article/50/18/6075/495814/Isolation-and-Characterization-of-a-Spontaneously

Sperandio, S., Poksay, K., de Belle, I., Lafuente, M.J., Liu, B., Nasir, J. and Bredesen, D.E. (2004) Paraptosis: Mediation by MAP kinases and inhibition by AIP-1/Alix, *Cell Death and Differentiation*, 11(10), pp. 1066–1075. https://doi.org/10.1038/sj.cdd.4401465.

Starita, L.M. and Parvin, J.D. (2003) The multiple nuclear functions of BRCA1: transcription, ubiquitination and DNA repair, *Current opinion in cell biology*, 15(3), pp. 345–350. https://doi.org/10.1016/S0955-0674(03)00042-5.

Su, S.-C., Chen, Y.-T., Hsieh, Y.-H., Yang, W.-E., Su, C.-W., Chiu, W.-Y., Yang, S.-F. and Lin, C.-W. (2022) Gambogic Acid Induces HO-1 Expression and Cell Apoptosis through p38

Signaling in Oral Squamous Cell Carcinoma, *The American Journal of Chinese Medicine*, 50(06), pp. 1663–1679. https://doi.org/10.1142/S0192415X22500707.

Su, Z., Yang, Z., Xu, Y., Chen, Y. and Yu, Q. (2015) Apoptosis, autophagy, necroptosis, and cancer metastasis, *Molecular cancer*, 14, pp. 1–14. https://doi.org/10.1186/s12943-015-0321-5

Sun, Z., Fourcade, J., Pagliano, O., Chauvin, J.-M., Sander, C., Kirkwood, J.M. and Zarour, H.M. (2015) IL10 and PD-1 cooperate to limit the activity of tumor-specific CD8+ T cells, *Cancer research*, 75(8), pp. 1635–1644. https://doi.org/10.1158/0008-5472.CAN-14-3016.

Tait, S.W.G. and Green, D.R. (2010) Mitochondria and cell death: Outer membrane permeabilization and beyond, *Nature Reviews Molecular Cell Biology*, 11(9), pp. 621–632. https://doi.org/10.1038/nrm2952.

Tait, S.W.G., Ichim, G. and Green, D.R. (2014) Die another way–non-apoptotic mechanisms of cell death, *Journal of cell science*, 127(10), pp. 2135–2144. https://doi.org/10.1242/jcs.093575.

Tallis, M., Morra, R., Barkauskaite, E., & Ahel, I. (2014). Poly(ADP-ribosyl)ation in regulation of chromatin structure and the DNA damage response. *Chromosoma,* 123(1-2), pp.79–90. https://0-doi-org.innopac.wits.ac.za/10.1007/s00412-013-0442-9

Tenhunen, R., Marver, H.S. and Schmid, R. (1968) The enzymatic conversion of heme to bilirubin by microsomal heme oxygenase., *Proceedings of the National Academy of Sciences of the United States of America*, 61(2), pp. 748–755. https://doi.org/10.1073/pnas.61.2.748.

Tennant, J.R. (1964) Evaluation of the trypan blue technique for determination of cell viability, Transplantation, 2(6), pp. 685–694. https://journals.lww.com/transplantjournal/abstract/1964/11000/evaluation_of_the_trypan_blue_technique_for.1.aspx.

Tisato, F., Marzano, C., Porchia, M., Pellei, M. and Carlo, S. (2010) Copper in Diseases and Treatments, and Copper-Based Anticancer Strategies, *Medicinal Research Reviews*, 30(4), pp. 708–749. https://doi.org/DOI 10.1002/med.20174.

Topalian, S.L., Taube, J.M., Anders, R.A. and Pardoll, D.M. (2016) Mechanism-driven biomarkers to guide immune checkpoint blockade in cancer therapy, *Nature Reviews Cancer*, 16(5), pp. 275–287. https://doi.org/10.1038/nrc.2016.36.

Tsvetkov, P., Coy, S., Petrova, B., Dreishpoon, M., Verma, A., Abdusamad, M., Rossen, J., Joesch-Cohen, L., Humeidi, R., Spangler, R. D., Eaton, J. K., Frenkel, E., Kocak, M., Corsello, S. M., Lutsenko, S., Kanarek, N., Santagata, S., & Golub, T. R. (2022) Copper induces cell death by targeting lipoylated TCA cycle proteins. *Science, 375*(6586), pp. 1254–1261. https://doi.org/10.1126/science.abf0529.

Turner, N. C., Telli, M. L., Rugo, H. S., Mailliez, A., Ettl, J., Grischke, E. M., Mina, L. A., Balmana, J., Castrellon, A., Hammad, N., Swaby, R. F., Roche, H., Curigliano, G., Thompson, D., Domchek, S. M., Tung, N. M., Laney, J. A., Surovtseva, Y., & Robson, M. E. (2019) A phase II study of talazoparib after platinum or cytotoxic nonplatinum regimens in patients with advanced breast cancer and germline BRCA1/2 mutations (ABRAZO). *Clinical Cancer Research, 25*(9), pp. 2717–2724. https://doi.org/10.1158/1078-0432.CCR-18-1891.

Travis, R. C., & Key, T. J. (2003) Oestrogen exposure and breast cancer risk. *Breast cancer research*, *5*(5), pp. 239–247. https://doi.org/10.1186/bcr628.

Ungerleider, N.A., Rao, S.G., Shahbandi, A., Yee, D., Niu, T., Frey, W.D. and Jackson, J.G. (2018) Breast cancer survival predicted by TP53 mutation status differs markedly depending on treatment, *Breast Cancer Research*, 20(1), pp. 1–8. https://doi.org/10.1186/s13058-018-1044-5.

Vaidya, G.N. and Acevedo, R. (2015) Tumor lysis syndrome in metastatic breast cancer after a single dose of paclitaxel, *American Journal of Emergency Medicine*, 33(2), pp. 308.e1-308.e2. https://doi.org/10.1016/j.ajem.2014.07.039.

Valko, M., Jomova, K., Rhodes, C.J., Kuča, K. and Musílek, K. (2016) Redox- and non-redox-metal-induced formation of free radicals and their role in human disease, *Archives of Toxicology*, 90(1), pp. 1-37. https://doi.org/10.1007/s00204-015-1579-5.

Vanella, L., Barbagallo, I., Tibullo, D., Forte, S., Zappalà, A. and Li Volti, G. (2016) The non-canonical functions of the heme oxygenases, *Oncotarget,* 7(42), pp. 69075–69086. https://doi.org/10.18632/oncotarget.11923.

Varfolomeev, E., Blankenship, J. W., Wayson, S. M., Fedorova, A. V., Kayagaki, N., Garg, P., Zobel, K., Dynek, J. N., Elliott, L. O., Wallweber, H. J. A., Flygare, J. A., Fairbrother, W. J., Deshayes, K., Dixit, V. M., & Vucic, D. (2007) IAP antagonists induce autoubiquitination of c-IAPs, NF-κB activation, and TNFα-dependent apoptosis. *Cell, 131*(4), pp. 669–681. https://doi.org/10.1016/j.cell.2007.10.030.

Varfolomeev, E., Goncharov, T., Fedorova, A. V., Dynek, J.N., Zobel, K., Deshayes, K., Fairbrother, W.J. and Vucic, D. (2008) c-IAP1 and c-IAP2 are critical mediators of tumor necrosis factor α (TNFα)-induced NF-κB activation*, Journal of Biological Chemistry*, 283(36), pp. 24295–24299. https://doi.org/10.1074/jbc.C800128200.

Vermes, I., Haanen, C. and Steffens-Nakken, H. (1995) A novel assay for apoptosis Flow cytometric detection of phosphatidylserine early apoptotic cells using fluorescein labelled expression on Annexin V, *Journal of Immunological Methods*, 184(1–4), pp. 39–51. https://doi.org/https://doi.org/10.1016/0022-1759(95)00072-I.

Villeneuve, N. F., Sun, Z., Chen, W., & Zhang, D. D. (2009) Nrf2 and p21 regulate the fine balance between life and death by controlling ROS levels. *Cell cycle,* 8(20), pp 3255-3256. https://doi.org/10.4161/cc.8.20.9565.

Vostakolaei, M.A., Hatami-Baroogh, L., Babaei, G., Molavi, O., Kordi, S., Abdolalizadeh, J. (2021) Hsp70 in cancer: A double agent in the battle between survival and death. *Journal of Cell Physiology,* 236, pp. 3420–3444. https://doi.org/10.1002/jcp.30132.

Vyas, K.M., Devkar, R. V., Prajapati, A. and Jadeja, R.N. (2015) Pyrazolone incorporating bipyridyl metallointercalators as effective DNA, protein and lung cancer targets: Synthesis, characterization and *in vitro* biocidal evaluation, *Chemico-Biological Interactions*, 240(1), pp. 250–266. https://doi.org/10.1016/j.cbi.2015.08.022.

Wahba, H.A. and El-Hadaad, H.A. (2015) Current approaches in treatment of triple-negative breast cancer, *Cancer Biology and Medicine*, 12(2), pp. 106–116. https://doi.org/10.7497/j.issn.2095-3941.2015.0030.

Walsh, J.G., Cullen, S.P., Sheridan, C., Lüthi, A.U., Gerner, C. and Martin, S.J. (2008) Executioner caspase-3 and caspase-7 are functionally distinct proteases, *Proceedings of the National Academy of Sciences of the United States of Americ*a, 105(35), pp. 12815–12819. https://doi.org/10.1073/pnas.0707715105.

Wang, J., Li, B., Luo, M., Huang, J., Zhang, K., Zheng, S., Zhang, S., Zhou, J., (2024) Progression from ductal carcinoma in situ to invasive breast cancer: molecular features and clinical significance. *Signal Transduction and Targeted Therapy,* 9(1), pp. 83 https://doi.org/10.1038/s41392-024-01779-3.

Wang, H., Jiang, F., Hao, F. and Ju, R. (2018) The expression of HtrA2 and its diagnostic value in patients with hepatocellular carcinoma, *Medicine (United States),* 97(14), pp. 2016–2019. https://doi.org/10.1097/MD.0000000000010128.

Wang, P., Guan, D., Zhang, X.P., Liu, F. and Wang, W. (2019) Modeling the regulation of p53 activation by HIF-1 upon hypoxia, *FEBS Letters*, 593(18), pp. 2596–2611. https://doi.org/10.1002/1873-3468.13525.

Wang, S., Zhang, X., Wang, H., Wang, Y., Chen, P. and Wang, L. (2020) Heat Shock Protein 27 Enhances SUMOylation of Heat Shock Protein B8 to Accelerate the Progression of Breast Cancer, *American Journal of Pathology*, 190(12), pp. 2464–2477. https://doi.org/10.1016/j.ajpath.2020.04.012.

Was, H., Cichon, T., Smolarczyk, R., Rudnicka, D., Stopa, M., Chevalier, C., Przybytkowski, T., Weigel, G., Glynos, G., Dulak, J., & Jozkowicz, A. (2006). Overexpression of heme oxygenase-1 in murine melanoma: Increased proliferation and viability of tumor cells, decreased survival of mice, *American Journal of Pathology, 169*(6), p.p 2181–2198. https://doi.org/10.2353/ajpath.2006.051365.

Watkins, Elyse J. DHSc, PA-C, DFAAPA. (2019) Overview of breast cancer. *Journal of the American Academy of Physician Assistants*, 32(10), pp.13-17. https://doi.org/10.1097/01.JAA.0000580524.95733.3d.

Weinlich, R., Oberst, A., Dillon, C. P., Janke, L. J., Milasta, S., Lukens, J. R., Rodríguez, D. A., Gurung, P., Savage, C., Kimmey, J. M., Kang, T. B., Hung, J., Ortiz, S., Dillon, M. T., Green, D. R. (2013) Protective roles for caspase-8 and cFLIP in adult homeostasis. *Cell Reports, 5*(2), pp. 340–348. https://doi.org/10.1016/j.celrep.2013.08.045.

Wells, R. (2009) Tumour lysis syndrome, *Australian Journal of Medical Science*, 30(4), pp. 123–126. https://doi.org/10.1016/j.medcle.2019.03.006.

Wellstein, A, & Sausville, E., A. (2023). Cytotoxics and antimetabolites. Brunton L.L., & Knollmann B.C.(Eds.), *Goodman & Gilman's: The Pharmacological Basis of Therapeutics, 14th Edition.* McGraw-Hill Education. https://0-accessmedicine-mhmedical-com.innopac.wits.ac.za/content.aspx?bookid=3191&sectionid=269730494

Wellstein A (2023). General principles in the pharmacotherapy of cancer. Brunton L.L., & Knollmann B.C.(Eds.), *Goodman & Gilman's: The Pharmacological Basis of Therapeutics, 14th Edition.* McGraw-Hill Education. https://0-accessmedicine-mhmedical-com.innopac.wits.ac.za/content.aspx?bookid=3191&sectionid=266700746

Wellstein A, & Giaccone G (2023). Protein kinase inhibitors and pathway-targeted small molecules. Brunton L.L., & Knollmann B.C.(Eds.), *Goodman & Gilman's: The Pharmacological Basis of Therapeutics, 14th Edition*. McGraw-Hill Education. https://0-accesspharmacy-mhmedical-com.innopac.wits.ac.za/content.aspx?bookid=3191&sectionid=269309724

Wen, M., Ding, L., Zhang, L., Zhang, T., Terzaghi, L., Sun, G., Zhu, R., Liu, J., Wang, W., Yu, L., & Cheng, Y. (2019). Identification of a novel Bcl-2 inhibitor by ligand-based screening and investigation of its anti-cancer effect on human breast cancer cells. *Frontiers in Pharmacology,* 10(391), pp. 1–14. https://doi.org/10.3389/fphar.2019.00391.

Whelan, T. J., Olivotto, I. A., Parulekar, W. R., Ackerman, I., Chua, B. H., Nabid, A., Pierce, L. J., Fu, T., Choan, E., Simmons, C., Fyles, A., Schneider, K., Gelmon, K., Robidoux, A.,

Pritchard, K. I., Vallis, K. A., Panet-Raymond, V., Joy, A. A., Proulx, M. A., and Levine, M. N. (2015) Regional nodal irradiation in early-stage breast cancer. *New England Journal of Medicine, 373*(4), pp. 307–316. https://doi.org/10.1056/nejmoa1415340.

Wright, N., Rida, P., Rakha, E., Agboola, A. and Aneja, R. (2018) Panoptic overview of triple-negative breast cancer in Nigeria: Current challenges and promising global initiatives*, Journal of Global Oncology*, 2018(4). https://doi.org/10.1200/JGO.17.00116.

Wu, J., Li, S., Li, C., Cui, L., Ma, J. and Hui, Y. (2021) The non-canonical effects of heme oxygenase-1, a classical fighter against oxidative stress, *Redox Biology*, 47(1), pp. 102170. https://doi.org/10.1016/j.redox.2021.102170.

Wu, T., Harder, B. G., Wong, P. K., Lang, J. E., and Zhang, D. D. (2015) Oxidative stress, mammospheres and Nrf2–new implication for breast cancer therapy? *Molecular carcinogenesis*, *54*(11), pp.1494-1502. https://doi.org/10.1002/mc.22202.

Xie, J., Yang, Y., Gao, Y. and He, J. (2023) Cuproptosis: mechanisms and links with cancers, *Molecular Cancer*, 22(1), pp. 1–30. https://doi.org/10.1186/s12943-023-01732-y.

Xing, H., Zhang, S., Weinheimer, C., Kovacs, A. and Muslin, A.J. (2000) 14-3-3 Proteins block apoptosis and differentially regulate MAPK cascades, *European Molecular Biology Organization Journal*, 19(3), pp. 349–358. https://doi.org/10.1093/emboj/19.3.349.

Xiong, N., Wu, H. and Yu, Z. (2024) Advancements and challenges in triple-negative breast cancer: a comprehensive review of therapeutic and diagnostic strategies, *Frontiers in Oncology*, 14(5), pp. 1–11. https://doi.org/10.3389/fonc.2024.1405491.

Yao, Y., Chu, Y., Xu, B., Hu, Q. and Song, Q. (2019) Risk factors for distant metastasis of patients with primary triple-negative breast cancer, *Bioscience Reports*, 39(6), pp. 1–10. https://doi.org/10.1042/BSR20190288.

Yong-Gang, L., Fang, Y., Qing, Y., Jiang-Hao, C. and Ling, W. (2010) The role of survivin in diagnosis, prognosis and treatment of breast cancer., *Journal of thoracic disease*, 2(2), pp. 100-10. PMID: 22263027; PMCID: PMC3256445. https://pmc.ncbi.nlm.nih.gov/articles/PMC3256445/.

Yousefi, M., Nosrati, R., Salmaninejad, A., Dehghani, S., Shahryari, A. and Saberi, A. (2018) Organ-specific metastasis of breast cancer: molecular and cellular mechanisms underlying lung metastasis, *Cellular Oncology*, 41(2), pp. 123–140. https://doi.org/10.1007/s13402-018-03766.

Yue, X., Zhao, Y., Huang, G., Li, J., Zhu, J., Feng, Z. and Hu, W. (2016) A novel mutant p53 binding partner BAG5 stabilizes mutant p53 and promotes mutant p53 GOFs in tumorigenesis, *Cell Discovery*, 2, pp. 1–15. https://doi.org/10.1038/celldisc.2016.39.

Yue, X., Zhao, Y., Xu, Y., Zheng, M., Feng, Z. and Hu, W. (2017) Mutant p53 in Cancer: Accumulation, Gain-of-Function, and Therapy, *Journal of Molecular Biology*, 429(11), pp. 1595–1606. https://doi.org/10.1016/j.jmb.2017.03.030.

van der Zanden, S.Y., Qiao, X. and Neefjes, J. (2021) New insights into the activities and toxicities of the old anticancer drug doxorubicin, *Federation of European Biochemical Societies Journal*, 288(21), pp. 6095–6111. https://doi.org/10.1111/febs.15583.

Zarić, M. M., Mladenović, M., Milenković, D., Matić, I. Z., Stanojković, T. P., Radanović, D., & Simović, A. R. (2021). New gold pincer-type complexes induce caspase-dependent apoptosis in human cancer cells *in vitro*. *Vojnosanitetski Pregled, 78*(8), pp. 865–873. https://doi.org/10.2298/VSP190507002Z.

Zehra, S., Cirilli, I., Silvestri, S., Gómez-Ruiz, S., Tabassum, S. and Arjmand, F. (2021) Structure elucidation, *in vitro* binding studies and ROS-dependent anti-cancer activity of Cu(II) and Zn(II) phthaloylglycinate(phen) complexes against MDA-MB-231 cells, Metallomics, 13(11),pp. mfab064. https://doi.org/10.1093/mtomcs/mfab064.

Zhang, M. and Bi, X. (2024) Heat Shock Proteins and Breast Cancer, *International Journal of Molecular Sciences*, 25(2), pp. 876. https://doi.org/10.3390/ijms25020876.

Zhang, H. Y., Han, L. L., Wu, H. Y., Xu, X. X., Yu, M. B., Chen, G. Y., & Qi, X. L. (2024) Research Progress on Structure-Activity Relationship of 1,8-Naphthalimide DNA Chimeras Against Tumor. *Technology in cancer research & treatment*, 23, 15330338231225861. https://doi.org/10.1177/15330338231225861.

Zhang, Y., Chen, X., Gueydan, C. and Han, J. (2018) Plasma membrane changes during programmed cell deaths, *Cell Research*, 28(1), pp. 9–21. https://doi.org/10.1038/cr.2017.133.

Zhao, X., Zhang, Y., Deng, J., Zhang-Negrerie, D. and Du, Y. (2017) TBHP/TBAI-mediated oxidative cascade reaction consisting of dimerization, cyclization, and 1, 2-aryl migration: metal-free synthesis of pyrrolin-4-ones and highly substituted pyrroles, *The Journal of Organic Chemistry*, 82(23), pp. 12682–12690. https://doi.org/10.1021/acs.joc.7b02491.

Zheng, C., Kabaleeswaran, V., Wang, Y., Cheng, G. and Wu, H. (2010) Crystal Structures of the TRAF2: cIAP2 and the TRAF1: TRAF2: cIAP2 Complexes: Affinity, Specificity, and Regulation, *Molecular Cel*l, 38(1), pp. 101–113. https://doi.org/10.1016/j.molcel.2010.03.009.

Zhong, Z.F., Tan, W., Tian, K., Yu, H., Qiang, W.A. and Wang, Y.T. (2017) Combined effects of furanodiene and doxorubicin on the migration and invasion of MDA-MB-231 breast cancer cells *in vitro*, *Oncology Reports*, 37(4), pp. 2016–2024. https://doi.org/10.3892/or.2017.5435.

Zhong, H., De Marzo, A. M., Laughner, E., Lim, M., Hilton, D. A., Zagzag, D., Simons, J. W. (1999) Overexpression of hypoxia-inducible factor 1α in common human cancers and their metastases. *Cancer research*, *59*(22), pp. 5830-5835. https://aacrjournals.org/cancerres/article/59/22/5830/505651/Overexpression-of-Hypoxia-inducible-Factor-1-in.

Zhou, X.Q., Li, Y., Zhang, D.Y., Nie, Y., Li, Z.J., Gu, W., Liu, X., Tian, J.L. and Yan, S.P. (2016) Copper complexes based on chiral Schiff-base ligands: DNA/BSA binding ability, DNA cleavage activity, cytotoxicity and mechanism of apoptosis, *European Journal of Medicinal Chemistry,* 114, pp. 244–256. https://doi.org/10.1016/j.ejmech.2016.02.055.

Zhu, X. F., Li, W., Ma, J. Y., Shao, N., Zhang, Y. J., Liu, R. M., Wu, W. B., Lin, Y., & Wang, S. M. (2015) Knockdown of heme oxygenase-1 promotes apoptosis and autophagy and enhances the cytotoxicity of doxorubicin in breast cancer cells. *Oncology letters*, 10(5), pp. 2974–2980. https://doi.org/10.3892/ol.2015.3735.

Ziegler, S., Sievers, S. and Waldmann, H. (2021) Morphological profiling of small molecules, *Cell chemical biology*, 28(3), pp. 300–319. https://doi.org/10.1016/j.chembiol.2021.02.012.

Zorova, L.D., Popkov, V, A., Plotnikov, E. Y., Zorov, D.B. (2018) Mitochondrial membrane potential, *Analytical Biochemistry*, 552(1), pp. 50–59. https://doi.org/10.1016/j.ab.2017.07.009.

Zuo, L., Zou, X., Ge, J. (2025) The Nrf2-HMOX1 pathway as a therapeutic target for reversing cisplatin resistance in non-small cell lung cancer via inhibiting ferroptosis. *Cell Death Discovery.* 11, 287. https://doi.org/10.1038/s41420-025-02564-z

Appendix A: Ethics waiver certificate

UNIVERSITY OF THE WITWATERSRAND, JOHANNESBURG

HUMAN RESEARCH ETHICS COMMITTEE (MEDICAL)

Human Research Ethics Committee (Medical)

Research Office Secretariat:
Faculty of Health Sciences, Phillip Tobias Health Sciences Building, 3rd Floor, Office 301/2/4, 29 Princess of Wales Terrace, Parktown, 2193
Private Bag 3, Wits 2050
Office email: HREC-Medical.ResearchOffice@wits.ac.za
Website: www.wits.ac.za/research/about-our-research/ethics-and-research-integrity/

Ref: W-CBP-190923-01 23/09/2019

TO WHOM IT MAY CONCERN:

Waiver:	This certifies that the following research does not require clearance from the Human Research Ethics Committee (Medical)
Investigator:	Miss Nonzuzo Praiseworth Myeza (Student no. 1038710)
Supervisor:	Dr Leonie Harmse
Department:	Pharmacy and Pharmacology
Project title:	An evaluation of the effects of metal complexes on cell death signalling networks in breast cancer cell lines
Reason:	*In vitro* laboratory study. Using two breast cell lines MDA-MB-231 and SKRB-3. No human participants will be involved in the study.

CB Penny

Dr CB Penny

Chairperson: Human Research Ethics Committee (Medical)

Copy – HREC (Medical) Secretariat: Zanele Ndlovu, Mapula Ramaila, Josh Ndlangamandla and Rhulani Mkansi

Appendix B: Doxorubicin concentration selection supplementary images

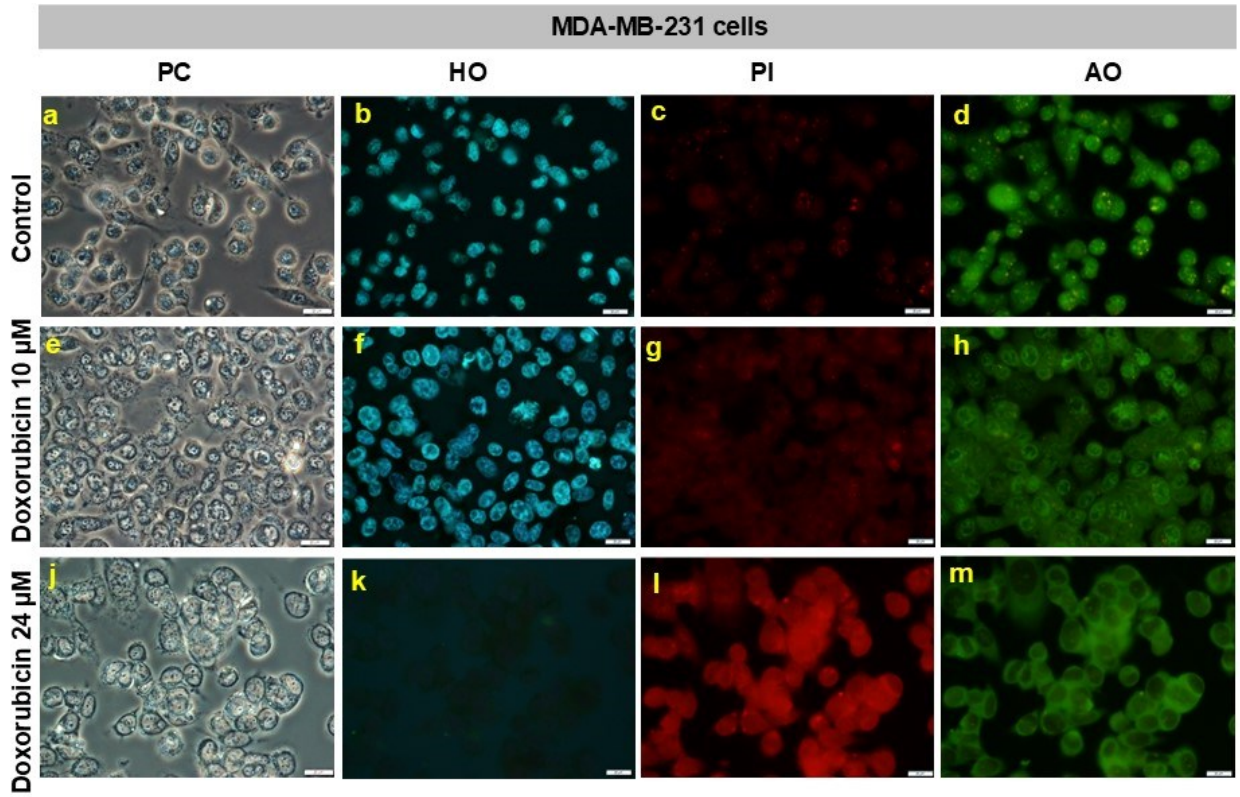


Fig. B1 Photomicrographs showing the MDA-MB-231 cell morphology after treatment with doxorubicin. The MDA-MB-231 cells were treated with 10 µM of doxorubicin and 24 µM of doxorubicin for 18 h. Cell were viewed with an Olympus BX41 epifluorescence microscope at 400x magnification. Images captured with an Olympus DP72 camera and analyzed with the Olympus CellSens Software. Scalebar: 20 µm.

Appendix C: MCF-10A cell morphology supplementary image

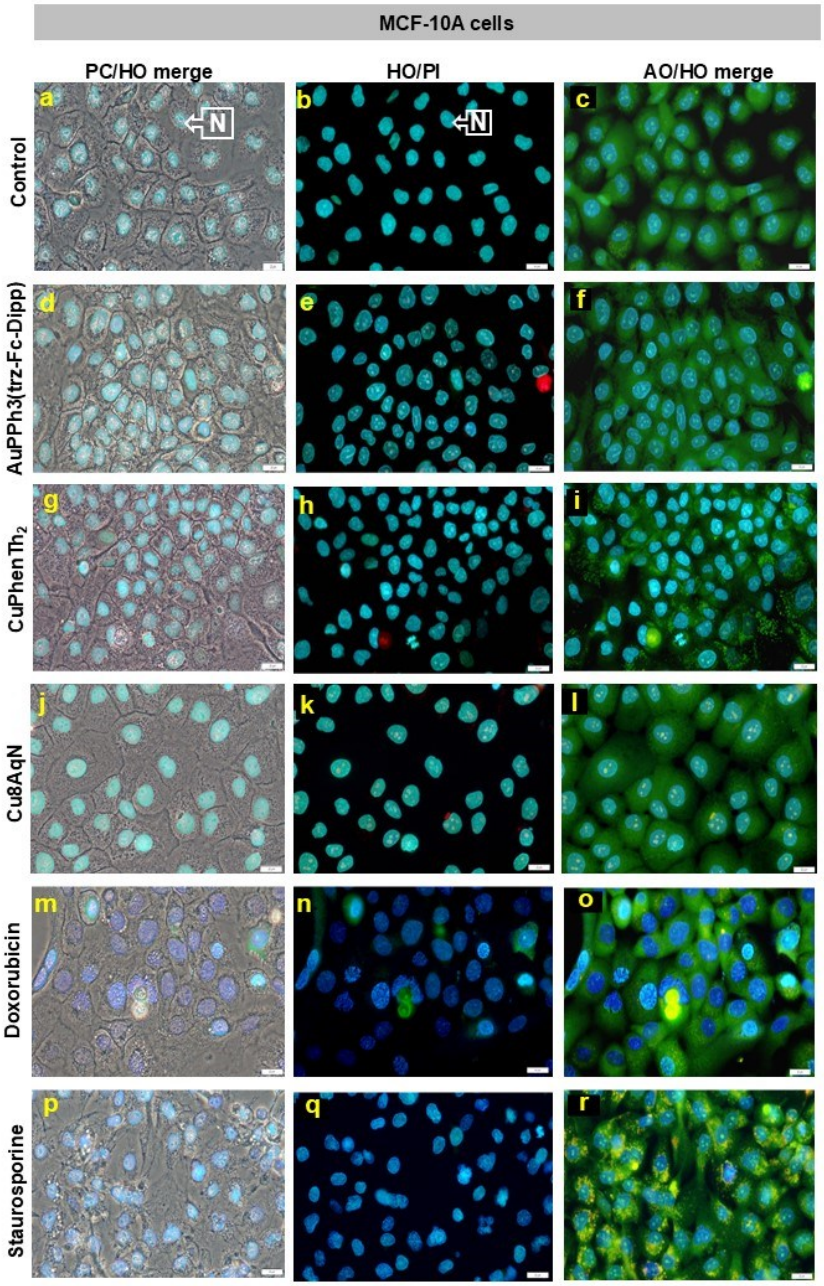


Figure C1 Photomicrographs showing the effects of metal complexes and positive controls on MCF-10A cell morphology. The MCF-10 cells were treated with 5.8 µM of $AuPPh_3$(trz-Fc-Dipp), 5.6 µM $CuPhenTh_2$, 4.2 µM Cu8AqN, doxorubicin at 10 µM and 0.25 µM of staurosporine for 18 h. Cell were viewed with an Olympus BX41 epifluorescence microscope at 400x magnification. Images captured with an Olympus DP72 camera and analyzed with the Olympus CellSens Software. Scalebar: 20 µm.

Appendix D: Standard curves

D1 Standard curve for proteome array and western blot assay

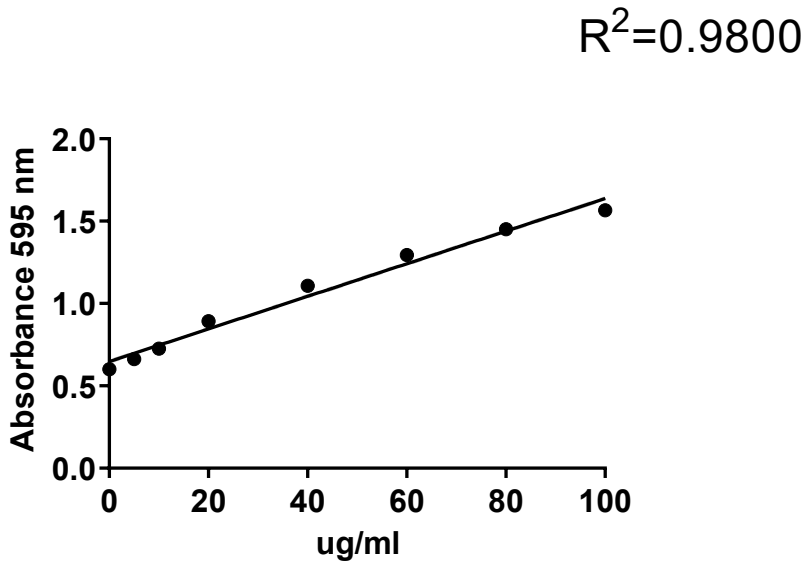


Fig. D1 Standard curve for proteome array and western blot assay

D2 Standard curve for molecular weight markers

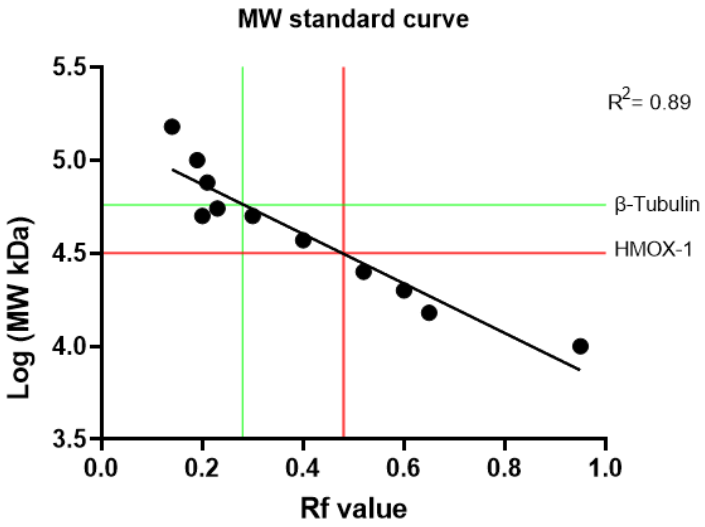


Fig. D2 Standard curve for HMOX-1 MW estimation.

Appendix E: Western blot membranes

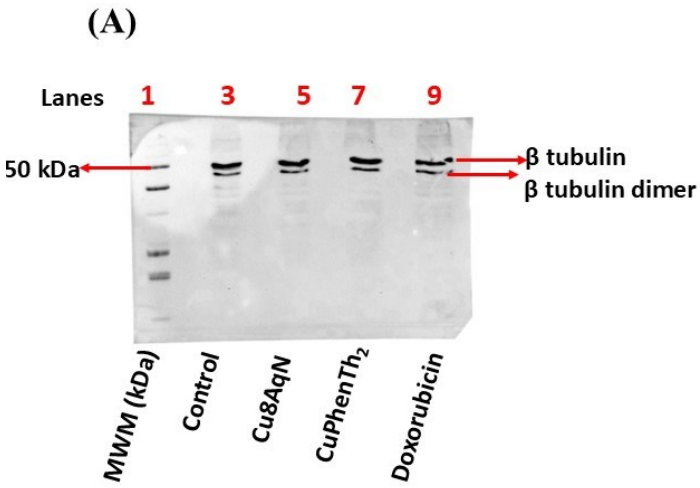


Fig. E1 Secondary antibody specificity membrane

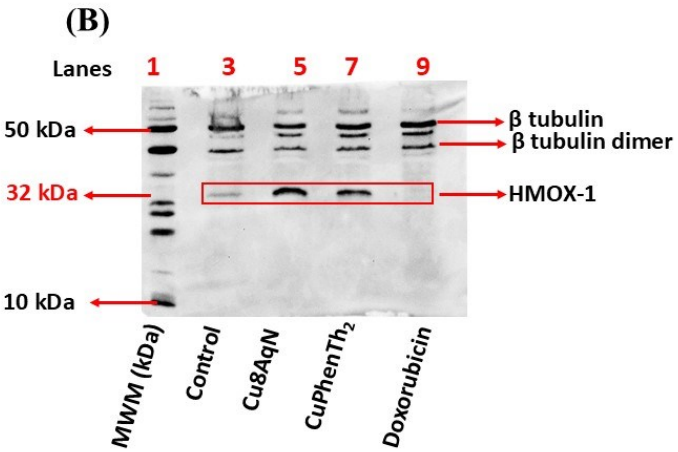


Fig. E2 Experimental membrane

Appendix F: Turn-It-In report

NONZUZO MYEZA FULL thesis v02 TURNITTIN.docx

ORIGINALITY REPORT

12%	9%	14%	%
SIMILARITY INDEX	INTERNET SOURCES	PUBLICATIONS	STUDENT PAPERS

PRIMARY SOURCES

1	eprints.whiterose.ac.uk Internet Source	5%
2	wiredspace.wits.ac.za Internet Source	2%
3	Nonzuzo Myeza, Cathy Slabber, Orde Q. Munro, Sheldon Sookai, Savannah C. Zacharias, Carla Martins-Furness, Leonie Harmse. "An 8-aminoquinoline-naphthyl copper complex causes apoptotic cell death by modulating the expression of apoptotic regulatory proteins in breast cancer cells.", European Journal of Pharmacology, 2024 Publication	1%
4	Ismail, Zeenat. "The Apoptotic Effect of Copper-Imidazo[1,2-a]Pyridine Complexes on Leukaemic Cells", University of the Witwatersrand, Johannesburg (South Africa), 2025 Publication	1%
5	Gangat, Nadia. "The Effect of Copper-Imidazo[1,2-a]Pyridine Complexes on HT-29 and DLD-1 Colorectal Cancer Cells", University of the Witwatersrand, Johannesburg (South Africa), 2025 Publication	1%
6	Systems Biology of Free Radicals and Antioxidants, 2014. Publication	1%
7	www.science.gov Internet Source	

Appendix G: Figure copyright permission

This Agreement between Nonzuzo Myeza ("You") and American Association for Cancer Research ("American Association for Cancer Research") consists of your license details and the terms and conditions provided by American Association for Cancer Research and Copyright Clearance Center.

License Number	6093000188204
License date	Aug 20, 2025
Licensed Content Publisher	American Association for Cancer Research
Licensed Content Publication	Cancer Discovery
Licensed Content Title	Hallmarks of Cancer: New Dimensions
Licensed Content Author	Hanahan, Douglas
Licensed Content Date	Jan 12, 2022
Licensed Content Volume	12
Licensed Content Issue	1
Type of Use	Thesis/Dissertation
Requestor type	academic/educational
Format	print and electronic
Portion	figures/tables/illustrations
Number of figures/tables/illustrations	1

G1= Licence for figure 1.1 in chapter 1.

This Agreement between Nonzuzo Myeza ("You") and John Wiley and Sons ("John Wiley and Sons") consists of your license details and the terms and conditions provided by John Wiley and Sons and Copyright Clearance Center.

License Number	6093001483503
License date	Aug 20, 2025
Licensed Content Publisher	John Wiley and Sons
Licensed Content Publication	Wiley Books
Licensed Content Title	Apoptosis: Molecular Mechanisms
Licensed Content Author	Pedro M Domingos, Fátima Cairrão
Licensed Content Date	Jan 15, 2010
Licensed Content Pages	8
Type of use	Dissertation/Thesis
Requestor type	University/Academic
Format	Print and electronic
Portion	Figure/table
Number of figures/tables	1
Will you be translating?	No

G2= Licence for figure 1.2 in chapter 1.